# Investigation in Pulse Compression Techniques for radar systems

Universidad Politécnica de Cartagena

**Author:** Santiago Egea Gómez.

**Director:** Alejandro Álvarez Melcón.

| | |
|---|---|
| **Author** | Santiago Egea Gómez |
| **Author´s email** | santiago.egea.gomez@gmail.com |
| **Director** | Alejandro Álvarez Melcón |
| **Director´s email** | Alejandro.alvarez@upct.es |
| **Title** | Investigation in Pulse Compression Techniques for Radar systems |
| **Spanish Title** | Estudio de técnicas de compresión de pulsos<br>en sistemas radar |
| **Summary** | This work deals with pulse compression techniques. These techniques are often used in radar systems. The study is focused on pulse compression using Frequency Modulation techniques.<br><br>In this work, we have reviewed the important concepts and tested them carrying out numerical simulations via Matlab. The main techniques investigated are pulse compression using CHIRP pulses, mismatched filtering and pulse compression using other FM laws. We have studied the limitations and the benefits of these techniques.<br><br>Additionally, a novel approach is presented to correct undesired effects due to moving targets. |
| **Degree** | Telecommunications Engineer |
| **Department** | Tecnologías de la Información y las Comunicaciones |
| **Submission date** | 30th September 2014 |


Universidad Politécnica de Cartagena

# *Acknowledgements*

*I would like to acknowledge the support which I have received from my relatives, close friends and close classmates. I would like to do special mention to my couple; mother and father; and Alejandro Álvarez Melcón, who has directed this work, managed to motivate me, demonstrating a strong commitment with me and this work.*

*I do not forget thanking all my teachers, from primary school to the university, who have demonstrated me that the public education is a great education model.*

# Contents

1. Introduction ..... 1
1.1. Radar Systems ..... 1
1.2. Energy and power of signal ..... 4
1.3. Basic radar performances ..... 6

2. Radar´s Signals and Networks ..... 11
2.1. Real Radar Signals ..... 11
2.1.1 Spectrum ..... 12
2.1.2 Energy ..... 13
2.1.3 Autocorrelation function ..... 14
2.2. Complex Radar Signals ..... 14
2.2.1 Spectrum ..... 15
2.2.2 Autocorrelation function ..... 16
2.3. Analytic Radar Signals ..... 16
2.3.1 Spectrum and Waveform ..... 17
2.3.2 Hilbert Transform ..... 17
2.3.3 Relationship to Complex signal ..... 19
2.3.4 Energy in Analytic Signal ..... 19
2.3.5 Properties of Analytic Signal ..... 20
2.4. Interesting parameters: Signal Duration and Frequency ..... 21
2.4.1 Relationships from Parseval´s theorem ..... 21
2.4.2 Mean Time and RMS Duration ..... 22
2.4.3 Mean Frequency and RMS Bandwidth ..... 23
2.5. Transmissions of Signals through networks ..... 25
2.5.1 Real Signals through Real Networks ..... 26
2.5.2 Analytic Signal through Real Networks ..... 26
2.5.3 Analytic Signal though Analytic Networks ..... 27

3. Matched Filter and Ambiguity function ..... 30
3.1. Matched Filter for Nonwhite Noise ..... 30
3.2. Matched Filter for White Noise ..... 33
3.3. Ambiguity Function ..... 37
3.3.1 Properties of Matched Filter Response ..... 39
3.3.2 Properties of Ambiguity Function ..... 40
3.3.3 Examples ..... 41

**4. Pulse Compression ..... 46**
4.1. Basic Concept ..... 46
4.2. The Chirp pulse ..... 47
4.3. Sidelobes suppression ..... 54
4.3.1 Mismatched filtering ..... 55
4.3.2 Signal Design by using FM laws ..... 58
4.3.3 Adaptive Pulse Compression algorithms ..... 68
4.4. Other Pulse Compression Techniques ..... 70
4.4.1 Pulse Compression by Costas FM ..... 70
4.4.2 Pulse Compression by Phase Coding ..... 72

**5. Results and Conclusions ..... 76**
5.1. Considerations ..... 76
5.2. Linear FM pulse (CHIRP) ..... 79
5.2.1 $\Delta fT$-product dependency for CHIRP pulse ..... 79
5.2.2 CHIRP pulse compression for moving targets ..... 85
5.2.3 Small Target hidden by bigger target ..... 89
5.3. Sidelobes suppression. Mismatching Filtering ..... 91
5.3.1 Truncated Taylor´s Filter ..... 91
5.3.2 Taylor´s Filter ..... 102
5.4. Sidelobes suppression. FM laws ..... 110
5.4.1 $\Delta fT$-product dependency for FM laws ..... 110
5.4.2 FM laws pulse compression for moving targets ..... 114
5.4.3 Discovering a hidden target by using FM laws ..... 117
5.5. Conclusions ..... 121

**6. Doppler Compensation in CHIRP Pulse Compression ..... 123**
6.1. Basic concept ..... 123
6.2. Results ..... 128
6.2.1 Verification of Compensation System functionality ..... 128
6.2.2 Compensated Ambiguity Function ..... 129
6.2.3 Doppler Compensation in presence of noise ..... 143
6.3. Conclusions ..... 149

**7. Conclusions and Future Work ..... 150**
7.1. Conclusions ..... 150
7.2. Future Work ..... 151

**Appendix ..... 152**
A. Guide: Pulse Compression Matlab´s Gui ..... 153
B. Matlab´s Functions description ..... 164

**Bibliography ..... 167**

# List of figures

Fig 1.-1: Basic principle of radar systems ..... 1
Fig 1.-2.1: CW-Radar transmitted signal ..... 3
Fig 1.-2.2: CW-Radar transmitted signal ..... 3
Fig 1.-3: Thevenin´s equivalent circuit ..... 4
Fig 1.-4: Pulsed radar. Transmitted signal & Rejected signal from targets ..... 6
Fig 1.-5: Scenario with a Target in motion ..... 7
Fig 1.-6: Transmitted Waveform. Doppler Effect ..... 8
Fig 1.-7: Back to radar Waveform. Doppler Effect ..... 9

Fig 2.-1: Real Radar Signal Spectrum ..... 13
Fig 2.-2: Complex Radar Signal Spectrum ..... 15
Fig 2.-3: Analytic Radar Signal Spectrum ..... 16
Fig 2.-4.1: Phase of $s(t)$ ..... 18
Fig 2.-4.2: Phase of $\left(s(t)\right)$ ..... 18
Fig 2.-4.3: Phase of $\left(\hat{s}(t)\right)$ ..... 18
Fig 2.-5.1: $\psi_2(t)$ Spectrum ..... 20
Fig 2.-5.2: $\psi_1^*(t)$ Spectrum ..... 20
Fig 2.-6: Real Signal across Real Network ..... 26
Fig 2.-7: Analytic Signal across Real Network ..... 26
Fig 2.-8: Analytic Signal across Analytic Network ..... 27

Fig 3.-1: Received Signal and Noise Signal across Real Filter ..... 30
Fig 3.-2.1 Original received signal ..... 35
Fig 3.-2.2 -t0 Shifting ..... 35
Fig 3.-2.3 Folding about the origin ..... 35
Fig 3.-3 Graphical convolution ..... 36
Fig 3.-4 Ambiguity Function of Square Pulse,$\tau = -T + \Delta t$ ..... 42
Fig 3.-5 Ambiguity Function of Square Pulse, $\tau = 0$ ..... 43
Fig 3.-6 Ambiguity Function of Square Pulse. Cut $|x(0, \omega_d)|$ ..... 44
Fig 3.-7 Ambiguity Function of Square Pulse. Cut $|x(\tau, 0)|$ ..... 44

Fig 4.-2 Transmitted Signal. Pulse Compression Basic Concept ..... 46
Fig 4.-3: Block Diagram. Pulse Compression Basic Concept ..... 47
Fig 4.-4: Instantaneous Frequency for various values of $\mu$. $\mu_1 < \mu_2 < \mu_3$ ..... 48
Fig 4.-5: Cuts of Ambiguity Function of CHIRP Pulse ..... 50
Fig 4.-6: Contour of Ambiguity Function of CHIRP Pulse ..... 50
Fig 4.-7: 3D Ambiguity Function of CHIRP Pulse ..... 51

Fig 4.-8: Fresnell Integral Functions ..... 52
Fig 4.-9: CHIRP Pulse Spectrum. $\Delta fT = 23.3$ ..... 53
Fig 4.-10: CHIRP Pulse Spectrum. $\Delta fT = 133.3$ ..... 54
Fig 4.-11: Small target masked by another bigger one ..... 54
Fig 4.-12: Even Quadratic FM law ..... 66
Fig 4.-13: Odd Quadratic FM law ..... 66
Fig 4.-14: Even Vee FM law ..... 66
Fig 4.-15: Odd Vee FM law ..... 66
Fig 4.-16: Stepped Linear FM law ..... 67
Fig 4.-17: Block Diagram of Adaptive Mismatched Filter ..... 68
Fig 4.-18: Costas FM Matrix. Frequency Hopping ..... 71
Fig 4.-19: Pulse Formed by Phase Coding ..... 73
Fig 4.-20: Phase Code pulse delayed by $T_n$ ..... 74
Fig 4.-21: Autocorrelation for $= 2T_n$ ..... 74
Fig 4.-22: Autocorrelation for $= 0$ ..... 74
Fig 4.-23: Pulse Compressed by using Phase Coding ..... 75

Fig 5.-24: Burst of pulses ..... 76
Fig 5.-25: Detector used for the simulations ..... 78
Fig 5.-26: Simulation 1, Detected Signal $\Delta fT = 25$ ..... 80
Fig 5.-27: Simulation 1, Detected Signal $\Delta fT = 25$ ..... 80
Fig 5.-28: Simulation 1, Detected Signal $\Delta fT = 50$ ..... 81
Fig 5.-29: Simulation 1, Detected Signal $\Delta fT = 50$ ..... 81
Fig 5.-30: Simulation 1, Detected Signal $\Delta fT = 100$ ..... 82
Fig 5.-31: Simulation 1, Detected Signal $\Delta fT = 100$ ..... 82
Fig 5.-32: Simulation 1, Detected Signal $\Delta fT = 150$ ..... 83
Fig 5.-33: Simulation 1, Spectrum of Transmitted Signal $\Delta fT = 150$ ..... 83
Fig 5.-34: Simulation 1, Secondary Lobe Level and Pulse Width vs $\Delta fT$-product ..... 84
Fig 5.-35: Simulation 2, Detected Signals in presence of Doppler Shift ..... 85
Fig 5.-36: Simulation 2, Ambiguity Function $\Delta fT = 16.6667$ ..... 86
Fig 5.-37: Simulation 2, Ambiguity Function $\Delta fT = 50$ ..... 87
Fig 5.-38: Simulation 2, Ambiguity Function $\Delta fT = 83.3333$ ..... 87
Fig 5.-39: Simulation 2, Ambiguity Function $\Delta fT = 166.6667$ ..... 88
Fig 5.-40: Simulation 2, Ambiguity Function $\Delta fT = 166.6667$ and $f = 1.5\ [Khz]$ ..... 89
Fig 5.-41: Simulation 3, Overshadowing Target by using CHIRP Pulse ..... 90
Fig 5.-42: Simulation 4, Detected Signal $\Delta fT = 25$ ..... 92
Fig 5.-43: Simulation 4, Detected Signal $\Delta fT = 75$ ..... 92
Fig 5.-44: Simulation 4, Detected Signal $\Delta fT = 75$ ..... 93
Fig 5.-45: Simulation 4, Secondary Lobe Level and Pulse Width vs $\Delta fT$-product ..... 93
Fig 5.-46: Simulation 5, Detected Signal $= 4$ ..... 94
Fig 5.-47: Simulation 5, Detected Signal $= 8$ ..... 95

Fig 5.-48: Simulation 5, Detected Signal $= 11$ ..... 95
Fig 5.-49: Simulation 5, Detected Signal $= 15$ ..... 96
Fig 5.-50: Simulation 5, Secondary Lobe Level and Pulse Width vs $n$..... 96
Fig 5.-51: Simulation 6, Detected Signal $F_1 = 0.3$ ..... 97
Fig 5.-52: Simulation 6, Detected Signal $F_1 = 0.5$ ..... 98
Fig 5.-30: Simulation 6, Detected Signal $F_1 = 0.75$ ..... 98
Fig 5.-31: Simulation 6, Secondary Lobe Level and Pulse Width vs $F_1$ ..... 99
Fig 5.-32: Simulation 7, Ambiguity Function by using Truncated Taylor´s Filter ..... 100
Fig 5.-33: Simulation 8, Overshadowing Target by using Truncated Taylor´s Filter ..... 101
Fig 5.-34: Simulation 9, Secondary Lobe Level and Pulse Width vs $\Delta fT$ ..... 102
Fig 5.-35: Simulation 10, Detected Signal $= 2$ ..... 103
Fig 5.-36: Simulation 10, Detected Signal $= 10$ ..... 104
Fig 5.-37: Simulation 10, Detected Signal $= 15$ ..... 104
Fig 5.-38: Simulation 10, Secondary Lobe Level and Pulse Width vs ..... 105
Fig 5.-39: Simulation 11, Detected Signal $= -25\ [dB]$ ..... 106
Fig 5.-40: Simulation 11, Detected Signal $= -37\ [dB]$ ..... 106
Fig 5.-41: Simulation 11, Detected Signal $= -55\ [dB]$ ..... 107
Fig 5.-42: Simulation 10, Secondary Lobe Level and Pulse Width vs ..... 107
Fig 5.-43: Simulation 12, Ambiguity Function by using Taylor´s Filter ..... 108
Fig 5.-44: Simulation 13, Overshadowing Target by using Taylor´s Filter ..... 109
Fig 5.-45: Simulation 14, Detected Signal for $\Delta fT = 150$ (Even quadratic) ..... 111
Fig 5.-46: Simulation 14, Detected Signal for $\Delta fT = 150$ (Odd quadratic) ..... 111
Fig 5.-47: Simulation 14, Detected Signal for $\Delta fT = 150$ (Even vee) ..... 112
Fig 5.-48: Simulation 14, Detected Signal for $\Delta fT = 150$ (Odd vee) ..... 112
Fig 5.-49: Simulation 14, Detected Signal for $\Delta fT = 150$ (Stepped linear FM) ..... 113
Fig 5.-50: Simulation 14, Secondary Lobe Level and Pulse Width vs $\Delta fT$ ..... 113
Fig 5.-51: Simulation 15, Ambiguity Function by using Even quadratic FM law ..... 114
Fig 5.-52: Simulation 15, Ambiguity Function by using Odd quadratic FM law ..... 115
Fig 5.-53: Simulation 15, Ambiguity Function by using Even vee FM law ..... 115
Fig 5.-54: Simulation 15, Ambiguity Function by using Odd vee FM law ..... 116
Fig 5.-55: Simulation 15, Ambiguity Function by using Stepped linear FM law ..... 116
Fig 5.-56: Simulation 16, Overshadowing Target by using Even quadratic FM law ..... 118
Fig 5.-57: Simulation 16, Overshadowing Target by using Odd quadratic FM law ..... 118
Fig 5.-58: Simulation 16, Overshadowing Target by using Even vee FM law ..... 119
Fig 5.-59: Simulation 16, Overshadowing Target by using Odd vee FM law ..... 119
Fig 5.-60: Simulation 16, Overshadowing Target by using Stepped linear FM law ..... 120

Fig 6.-53: Basic Concept. Block Diagram ..... 123
Fig 6.-46: Doppler Shift Identification System. Block Diagram ..... 125

Fig 6.-47: Identification System. Basic idea. $f_{ct} < f_0$ ..... 126
Fig 6.-48: System Identification System. Basic idea. $f_{ct} = f_0$ ..... 126
Fig 6.-49: System Identification System. Basic idea. $f_{ct} > f_0$ ..... 127
Fig 6.-50: Simulation 17, Differential Energy for $f_d = \pm 50, \pm 100\ [KHz]$ ..... 129
Fig 6.-51: Simulation 17, Differential Energy for $f_d = \pm 50, \pm 100\ [KHz]$ ..... 130
Fig 6.-52: Simulation 18, Compensated Ambiguity Function for $\Delta f = 200\ [KHz]$ ..... 131
Fig 6.-53: Simulation 18, Compensated Ambiguity Function for $\Delta f = 300\ [KHz]$ ..... 131
Fig 6.-54: Simulation 18, Compensated Ambiguity Function for $\Delta f = 400\ [KHz]$ ..... 132
Fig 6.-55: Simulation 18, Compensated Ambiguity Function for $\Delta f = 500\ [KHz]$ ..... 132
Fig 6.-56: Simulation 18, Compensated Ambiguity Function for $\Delta f = 600\ [KHz]$ ..... 133
Fig 6.-57: Simulation 18, Compensated Ambiguity Function for $\Delta f = 700\ [KHz]$ ..... 133
Fig 6.-58: Simulation 18, Compensated Ambiguity Function for $\Delta f = 800\ [KHz]$ ..... 134
Fig 6.-59: Simulation 18, Compensated Ambiguity Function for $\Delta f = 900\ [KHz]$ ..... 134
Fig 6.-60: Simulation 18, Compensated Ambiguity Function for $\Delta f = 1000\ [KHz]$ ..... 135
Fig 6.-61: Simulation 18, Cut of compensated Ambiguity Function $t - t_0 = 0$, for $\Delta f = 400\ [KHz]$ ..... 135
Fig 6.-62: Simulation 18, Cut of non-compensated Ambiguity Function $t - t_0 = 0$, for $\Delta f = 400\ [KHz]$ ..... 136
Fig 6.-63: Simulation 18, Error Function for $\Delta f = 100\ [KHz]$ ..... 137
Fig 6.-64: Simulation 18, Error Function for $\Delta f = 200\ [KHz]$ ..... 138
Fig 6.-65 Simulation 18, Error Function for $\Delta f = 300\ [KHz]$ ..... 138
Fig 6.-66: Simulation 18, Error Function for $\Delta f = 400\ [KHz]$ ..... 139
Fig 6.-67: Simulation 18, Error Function for $\Delta f = 500\ [KHz]$ ..... 139
Fig 6.-68: Simulation 18, Error Function for $\Delta f = 600\ [KHz]$ ..... 140
Fig 6.-69: Simulation 18, Error Function for $\Delta f_d = 700\ [KHz]$ ..... 140
Fig 6.-70: Simulation 18, Error Function for $\Delta f = 800\ [KHz]$ ..... 141
Fig 6.-71: Simulation 18, Error Function for $\Delta f = 900\ [KHz]$ ..... 141
Fig 6.-72: Simulation 18, Error Function for $\Delta f = 1000\ [KHz]$ ..... 142
Fig 6.-73: Simulation 19, Compensated Ambiguity Function for $P_n = -40\ [dbW]$ ..... 143
Fig 6.-30: Simulation 19, Compensated Ambiguity Function for $P_n = -30\ [dbW]$ ..... 144
Fig 6.-31: Simulation 19, Compensated Ambiguity Function for $P_n = -20\ [dbW]$ ..... 144
Fig 6.-32: Simulation 19, Compensated Ambiguity Function for $P_n = -10\ [dbW]$ ..... 145
Fig 6.-33: Simulation 19, Compensated Ambiguity Function for $P_n = 0\ [dbW]$ ..... 145
Fig 6.-34: Simulation 19, Error Function for $P_n = -40\ [dbW]$ ..... 146
Fig 6.-35: Simulation 19, Error Function for $P_n = -30\ [dbW]$ ..... 147
Fig 6.-36: Simulation 19, Error Function for $P_n = -20\ [dbW]$ ..... 147
Fig 6.-37: Simulation 19, Error Function for $P_n = -10\ [dbW]$ ..... 148
Fig 6.-38: Simulation 19, Error Function for $P_n = 0\ [dbW]$ ..... 148

Fig A.-1: Example 1. User´s Interface I ..... 153
Fig A.-2: Example 1. Configuration window ..... 154
Fig A.-3: Example 1. User´s Interface II ..... 154

Fig A.-4: Example 1. User´s Interface III ..... 155
Fig A.-5: Example 1. User´s Interface IV ..... 155
Fig A.-6: Example 1. Ambiguity Function configuration ..... 156
Fig A.-7: Example 1. Ambiguity Function Calculation messages ..... 156
Fig A.-8: Example 1. Result of Ambiguity Function Calculation ..... 157
Fig A.-9: Example 2. Setting the Simulation Parameters ..... 157
Fig A.-10: Example 2. Results I ..... 158
Fig A.-11: Example 2. Results II ..... 158
Fig A.-12: Example 3. Setting the Simulation Configuration I ..... 159
Fig A.-13: Example 3. Setting the Simulation Configuration II ..... 159
Fig A.-14: Example 3. Results I ..... 160
Fig A.-15: Example 3. Results II ..... 160
Fig A.-16: Example 4. Setting the Simulation Configuration I ..... 161
Fig A.-17: Example 4. Setting the Simulation Configuration II ..... 161
Fig A.-18: Example 4. Setting the Simulation Configuration III ..... 162
Fig A.-19: Example 4. Stepped Linear FM ..... 162
Fig A.-20: Example 4. Results I ..... 163
Fig A.-21: Example 4. Results II ..... 163

# List of Tables

Table 5.-1: Simulation 1 ..... 79
Table 5.-2: Simulation 2 ..... 85
Table 5.-3: Simulation 3 ..... 89
Table 5.-4: Simulation 4. ..... 91
Table 5.-5: Simulation 5 ..... 94
Table 5.-6: Simulation 6 ..... 97
Table 5.-7: Simulation 7 ..... 100
Table 5.-8: Simulation 8 ..... 101
Table 5.-9: Simulation 9 ..... 102
Table 5.-10: Simulation 10 ..... 103
Table 5.-11: Simulation 11 ..... 105
Table 5.-12: Simulation 12 ..... 108
Table 5.-13: Simulation 13 ..... 109
Table 5.-14: Simulation 14 ..... 110
Table 5.-15: Simulation 15 ..... 114
Table 5.-16: Simulation 16 ..... 117

Table 6.-1: Simulation 17 parameters ..... 128
Table 6.-2: Simulation 18 parameters ..... 129
Table 6.-3: Simulation 19 parameters ..... 143

Table B.-1: chirp_lineal.m ..... 164
Table B.-2: fm_law.m ..... 164
Table B.-3: target.m ..... 164
Table B.-4: hilbert.m ..... 165
Table B.-5: taylor_truncated.m ..... 165
Table B.-6: taylorf.m ..... 165
Table B.-7: detect.m ..... 165
Table B.-8: ran_gate.m ..... 166
Table B.-9: chirp_lineal.m ..... 166
Table B.-10: Other functions ..... 166

# Chapter 1. Introduction

Since the first radar systems were developed during The Second World War, they have experimented a lot of changes. The performances of radars have been improved by using signal processing techniques. Due to the fact that the digital systems are increasing, they offers many possibilities in order to solve the issues which can arise for radar systems.

In the present work, we study one of these techniques. It is known as Pulse Compression, whose usage is widely extended nowadays. Before explaining the pulse compression technique we revise some important concepts, which help us to understand the purpose of the project.

We look, firstly, at the basic concepts of the radar systems; secondly, at basic concepts that are related to signal analysis (Chapter 2) and filtering theory (Chapter 3); thirdly, at the pulse compression theoretic analysis; and to finish, at the results and conclusions obtained.

## 1.1. Radar Systems

Radar means **R**adio **D**etection **A**nd **R**anging. There are many and very different applications based on radar systems, thus the characteristics fulfilled by radars are very wide. However, in general, the basic operation of radars is the same, and it is based on the following principle.

### Basic principle

Let us assume the next scenario, Fig 1.-1, where there are a waveform transmitter, a waveform receiver and an object (target) which possesses electromagnetic properties $(\varepsilon, \mu)$ **[Peyton Z. Peebles Jr, 1998]**.

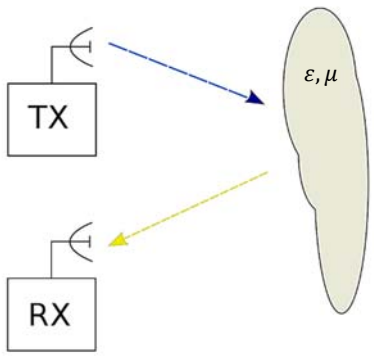


**Fig 1.-1: Basic principle of radar systems.**

Therefore, the emitter illuminates the target by transmitting the following waveform

$$s(t) = A\sin(\omega_0 t + \theta(t)) \qquad \textbf{( 1.-1 )}$$

Where $\theta(t)$ is a possible phase or frequency modulation function.

After reaching the target, the back to receiver signal is

$$r(t) = A'\sin(\omega_0' t + \theta'(t)) \qquad \textbf{( 1.-2 )}$$

Thus, we can extract information about the target by processing **( 1.-2 )**. Once we understand the basic principle of radar, it is interesting to know about the different types of radars.

**Classification of radar systems**

Several criteria to classify the radar systems exist, but the most important criteria are the following **[F. Quesada et al., 2010]**

- According to the **type of target** a radar system can be classified as:

  **Primary.** In this case the target is passive, in other words, the target reflects only the energy transmitted by the radar transponder.

  **Secondary.** The target possesses a receiver and transmitter system, which is able to answer to the request of the radar. This type of radars need less transmission power than the primary radars, since the back to radar signals only go over one-way route.

- Depending on the **relative position between emitter and receiver** the radar systems can be:

  **Monostatics.** The emitter and receiver are placed in the same location.

  **Bistatics.** The emitter are receiver are situated in different places. This fact can have applications in the military area in order to hide the location of the receiver.

- According to its **functionality** a radar can be:

  **Surveillance radar.** These devices are able to detect and identify targets.

**Tracking radar.** These systems are capable of detecting and tracking targets.

**Surveillance-tracking radar.** These devices detect, identify and track targets.

- To finish the classification of radars, there are two different types of radar according to the **transmitted waveform**:

  **Continuous wave radar (CW).** The system is constantly transmitting and receiving a sinusoidal signal. This type of signal is shown in Fig 1.-2.1.

  **Pulsed wave radar.** In this case, the radar takes a time term to transmit, and then, it takes another time interval to receive. The typical signal for this type of radars is illustrated by Fig 1.-2.2.

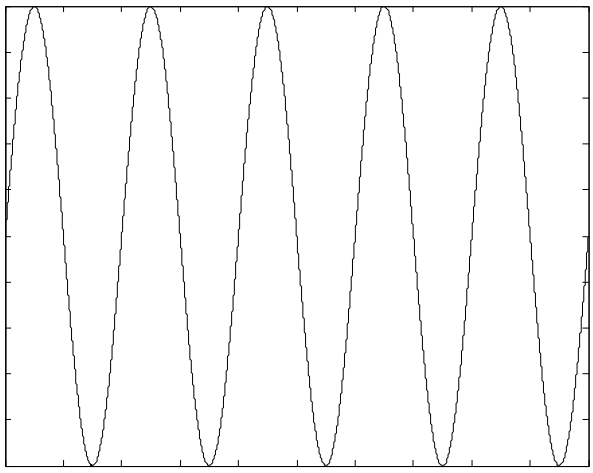

**Fig 1.-2.1: CW-Radar transmitted signal.**

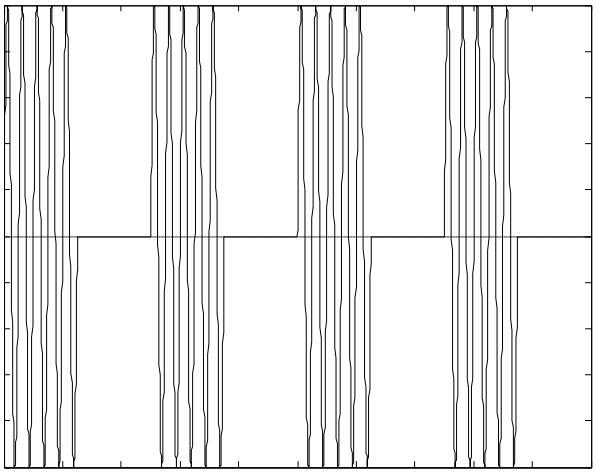

**Fig 1.-2.2: Pulse Radar transmitted signal.**

## 1.2 Energy and power of radar´s signal

As it is described in **[Peyton Z. Peebles Jr, 1998]**, the most general radar´s waveform expression is

$$s(t) = a(t)\sin(\omega_0 t + \phi_0 + \theta(t)) \qquad \textbf{( 1.-3 )}$$

Where $a(t)$ is an arbitrary amplitude modulation function, and, $\theta(t)$ is a phase function due to some form of frequency or phase modulation. **( 1.-3 )** may be defined either $-\infty < t < +\infty$ or in a limited time period. In the second case, the signal can be rewritten as

$$\begin{aligned} s(t) &= a(t)rect\left(\frac{t-\frac{T}{2}}{T}\right)\sin\left(\omega_0 t + \phi_0 + \theta(t)\right) \\ &= \begin{cases} a(t)\sin\left(\omega_0 t + \phi_0 + \theta(t)\right) & 0 \le t \le T \\ 0 & elsewhere \end{cases} \end{aligned} \qquad \textbf{( 1.-4 )}$$

Where $T$ is the time period in which the system is transmitting. The pulse is repeatedly transmitted, thereby **( 1.-4 )** is rewritten as

$$s(t) = a(t)\left\{\sum_{n=1}^{+\infty} rect\left(\frac{t-(n-1)T_R-\frac{T}{2}}{T}\right)\right\}\sin\left(\omega_0 t + \phi_0 + \theta(t)\right) \qquad \textbf{( 1.-5 )}$$

Where $T_R$ is the pulse repetition interval.

### Peak and average powers

It is well-known that any circuit can be simplified by using the Thevenin´s equivalence. Therefore we can model a radar system as the following straightforward circuit (Fig 1.-3)

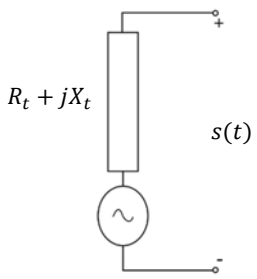


**Fig 1.-3: Thevenin´s equivalent circuit.**

Let us suppose that the system is matched, to fulfill the maximum power transfer theorem; thereby, the available instantaneous power is expressed as

$$P_i(t) = \frac{s(t)^2}{4R_t} = \frac{a(t)^2}{8R_t}[1 + \cos(2\omega_0 t + 2\phi_0 + 2\theta(t))] \quad \textbf{( 1.-6 )}$$

Since $\theta(t)$ varies much slower than $\omega_0 t + \phi_0$, the cosine term can be approximated as a pure cosine, thus, the average instantaneous power is

$$P_t(t) = \frac{a(t)^2}{8R_t} \quad \textbf{( 1.-7 )}$$

Starting from **( 1.-7 )**, we can define the average peak transmitted power as the average transmitted power over one cycle of the carrier when $s(t)$ accomplishes its maximum

$$P_t(t) = \frac{1}{4R_t}[1 - cycle\ average\ s(t)]_{max} \quad \textbf{( 1.-8 )}$$

Where $[\cdot]_{max}$ is the maximum value of the function within brackets.

Also we can calculate the available average transmitted power for a given time interval ($T_R$) as

$$P_{av}(t) = \frac{1}{4R_t T_R}\int_0^{T_R} s(t)^2 dt \quad \textbf{( 1.-9 )}$$

It is often used the next expression for pulsed waveform radars

$$P_{av}(t) = \frac{1}{4R_t T_R}\int_{-\frac{T_R}{2}}^{\frac{T_R}{2}} s(t)^2 dt \quad \textbf{( 1.-10 )}$$

A normalized expression of **( 1.-9 )** or **( 1.-10 )** is usually used, it does not contain the $\frac{1}{4R_t T_R}$ factor.

**Energy**

Also the energy of transmitted signal can be calculated as

$$E_s = \int_0^{T_R} s(t)^2 dt \approx \frac{1}{2}\int_0^{T_R} a(t)^2 dt \qquad \textbf{( 1.-11 )}$$

$T_R$ represents the repetition interval of pulsed signal or the fundamental period of the modulation functions $a(t)$ and $\theta(t)$ in CW radar.

## 1.3 Basic principles of radar systems

Above we studied the basic principle of radar; the purpose of this section is to study another principles of radars used to detect and range the target **[Peyton Z. Peebles Jr, 1998]**.

**Elementary range measurement**

Let us assume a monostatic pulsed system which transmits a square pulse. This pulse strikes a target, therefore a part of the pulse energy is reflected. The reflected energy travels back to the radar system. This fact is illustrated in Fig 1.-4.

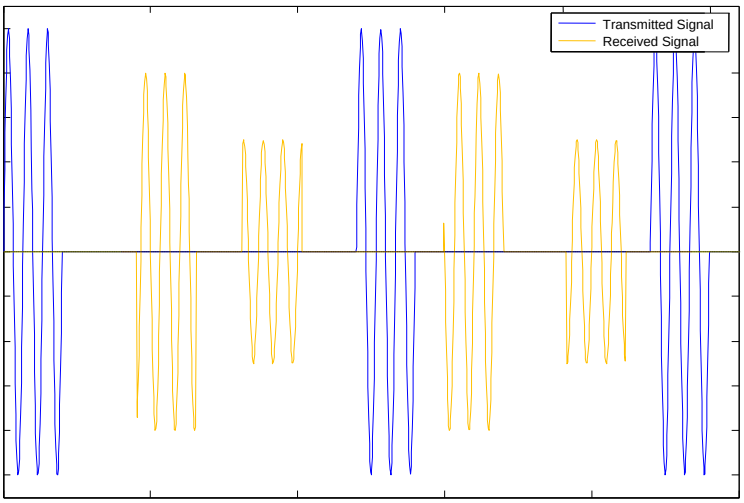


**Fig 1.-4: Pulsed radar. Transmitted signal & Rejected signal from targets.**

The returned pulse to the radar is delayed with respect to the transmitted signal by $T_R$. This fact is due to the path travelled by the signal. As the ligth´s speed is well-known, the radial distance from the radar to the target is

$$R = \frac{CT_R}{2} \qquad \textbf{( 1.-12 )}$$

In this scenario a stationary target was considered. In a real case, the target could be in motion and other effects must be considered. These effects are discussed below.

**Doppler Effect due to target motion**

Let us suppose the scenario shown in Fig 1.-5,

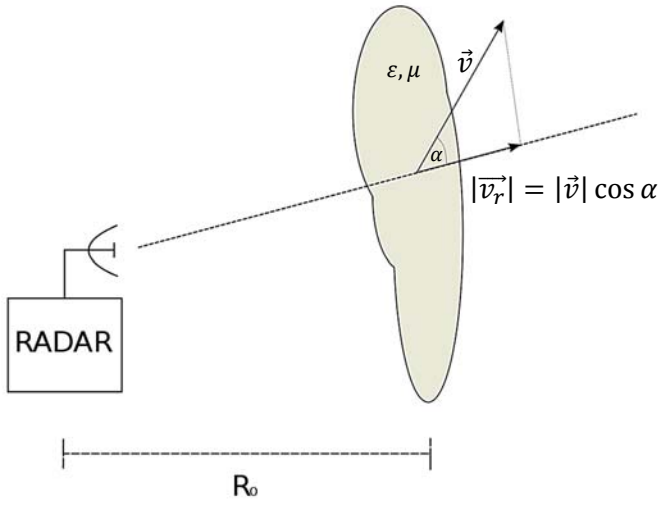


**Fig 1.-5: Scenario with a Target in motion.**

The figure illustrates a radar system which illuminates a target in motion. In order to understand the Doppler Effect concept, we assume the transmitted signal shown in Fig 1.-6.

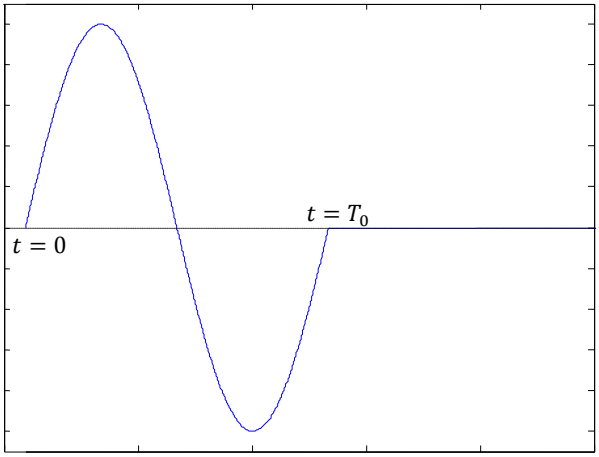


**Fig 1.-6: Transmitted Waveform. Doppler Effect.**

Where $T_0 = \frac{1}{f_0}$. In $t = 0$ the first wave front, $s_t(t = 0)$, leaves from the transmitter, and the target is at a distance $R_0$ **[Peyton Z. Peebles Jr, 1998]**. When the first wave front reaches the target, a $\Delta t_1$ time period has passed, thus the range of target is

$$R_1 = R_0 + |\overrightarrow{v_r}|\Delta t_1 \qquad \textbf{( 1.-13 )}$$

Where $\overrightarrow{v_r}$ is the radial distance as shown in Fig 1.-5. The first wave front takes the next time of travel

$$\Delta t_1 = \frac{R_1}{c} \qquad \textbf{( 1.-14 )}$$

By using the equations **( 1.-13 )** and **( 1.-14 )**, we obtain

$$\Delta t_1 = \frac{R_0}{c + |\overrightarrow{v_r}|} \qquad \textbf{( 1.-15 )}$$

If $t_1$ is the time of arrival to the radar taken by the reflected signal, it must be equal to $2\Delta t_1$

$$t_1 = \frac{2R_0}{c + |\overrightarrow{v_r}|} \qquad \textbf{( 1.-16 )}$$

Then, the second wave front, $s_t(t = T_0)$, is transmitted. When this wave front strikes the target, the new position of the target is

$$R_2 = R_0 + |\overrightarrow{v_r}|T_0 + |\overrightarrow{v_r}|\Delta t_2 \quad \textbf{( 1.-17 )}$$

In the same way as **( 1.-16 )**

$$\Delta t_2 = \frac{\Delta t_2}{C} \quad \textbf{( 1.-18 )}$$

And the time of arrival for the $s_t(t = T_0)$ wave front is

$$t_2 = T + 2\Delta t_2 = \frac{(c + |\overrightarrow{v_r}|)T_0 + 2R_0}{c - |\overrightarrow{v_r}|} \quad \textbf{( 1.-19 )}$$

Therefore, the received waveform is shown in Fig 1.-7

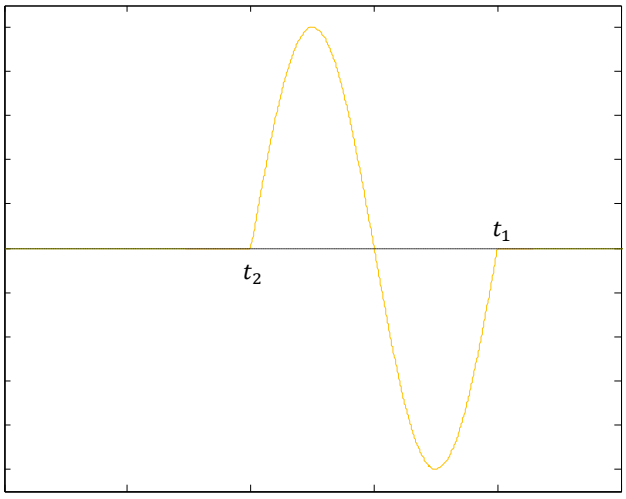


**Fig 1.-7: Back to radar Waveform. Doppler Effect.**

Thereby, the received signal has the next frequency

$$f_r = \frac{1}{t_2 - t_1} = \left(\frac{c - |\overrightarrow{v_r}|}{c + |\overrightarrow{v_r}|}\right) f_0 \quad \textbf{( 1.-20 )}$$

Thus, the frequency increment, $f_d$, is

$$f_d = f_r - f_0 = \frac{-2|\overrightarrow{v_r}|}{c + |\overrightarrow{v_r}|} f \qquad \textbf{( 1.-21 )}$$

Since, $c \gg |\overrightarrow{v_r}|$ often occurs

$$f_d \approx \frac{-2|\overrightarrow{v_r}|}{c} f_0 \qquad \textbf{( 1.-22 )}$$

The frequency change is known as Doppler frequency, and it is one of the most important phenomenon in the radar theory.

**Received waveform**

According to the effects we have studied, if a general radar waveform, equation **( 1.-3 )**, is transmitted, the signal back into the radar is

$$s_r(t) = \alpha a(t - \tau_r) \sin((\omega_0 + \omega_d)(t - \tau_r) + \phi_0 + \theta(t - \tau_r)) \qquad \textbf{( 1.-23 )}$$

Where $\tau_r = \frac{2R_t}{c}$ and $\omega = 2\pi \left(\frac{2|\overrightarrow{v_r}|}{c} f_0\right)$; $R_t$ is the relative range between the radar transponder and the target.

# Chapter 2. Radar signals and networks

The study of general aspects about signals and its passage through networks is needed in order to understand the radar systems. We will revise these concepts in this section.

We start from a real signal and continue to other signal representation forms and their relationships with the real signal **[Peyton Z. Peebles Jr, 1998]**. Then, we will study the networks, which are traversed by the signals, and the optimum filter which maximizes the peak signal power to average noise power ratio.

## 2.1 Real Radar signals

Considering the next radar signal **[Peyton Z. Peebles Jr, 1998]**

$$s(t) = a(t)\cos[\omega_0 t + \phi_0 + \theta(t)] \quad \textbf{( 2.-1 )}$$

Where $a(t)$ is an arbitrary amplitude modulation function and $\theta(t)$ is an arbitrary phase modulation function. Now, we apply the following trigonometric identity to **( 2.-1 )**

$$\cos[x + y] = \cos[x]\cos[y] - \sin[x]\sin[y] \quad \textbf{( 2.-2 )}$$

We obtain

$$\begin{aligned} s(t) &= a(t)\{\cos[\theta(t)]\cos[\omega_0 t + \phi_0] - \sin[\theta(t)]\sin[\omega_0 t + \phi_0]\} \\ &= s_i(t)\cos[\omega_0 t + \phi_0] - s_q(t)\sin[\omega_0 t + \phi_0] \end{aligned} \quad \textbf{( 2.-3 )}$$

Where

$$s_i(t) = a(t)\cos[\theta(t)] \quad \textbf{( 2.-4 )}$$

$$s_q(t) = a(t)\sin[\theta(t)] \quad \textbf{( 2.-5 )}$$

In the expression **( 2.-3 )**, the carrier information is separated from the modulations terms, therefore, this signal form is interesting from a practical point of view.

Another representation of **( 2.-1 )**, by using the expansion of cosine into its exponential form, is

$$s(t) = a(t)\cos[\omega_0 t + \phi_0 + \theta(t)] = \frac{a(t)}{2}\left\{e^{j[\omega_0 t+\phi_0+\theta(t)]} + e^{-j[\omega_0 t+\phi_0+\theta(t)]}\right\} = \frac{1}{2}\left\{g(t)e^{j[\omega_0 t+\phi_0]} + g^*(t)e^{-j[\omega_0 t+\phi_0]}\right\} \quad \textbf{( 2.-6 )}$$

Where

$$g(t) = a(t)e^{j[\theta(t)]} = s_i(t) + js_q(t) \quad \textbf{( 2.-7 )}$$

And its conjugate is

$$g^*(t) = a(t)e^{-j[\theta(t)]} = s_i(t) - js_q(t) \quad \textbf{( 2.-8 )}$$

The function **( 2.-7 )** is called the complex envelope of $s(t)$.

The expression **( 2.-6 )** fulfills the property that it has a complex term, but its sum is a real signal. Now we will interpret **( 2.-6 )** in frequency domain.

### 2.1.1 Spectrum

Applying the Fourier transform to **( 2.-6 )**, we obtain

$$S(\omega) = \frac{1}{2}\left\{G(\omega - \omega_0)e^{j\phi_0} + G^*(-\omega - \omega_0)e^{-j\phi_0}\right\} \quad \textbf{( 2.-9 )}$$

Where $\omega = 2\pi f$ and $\omega_0 = 2\pi f_0$.

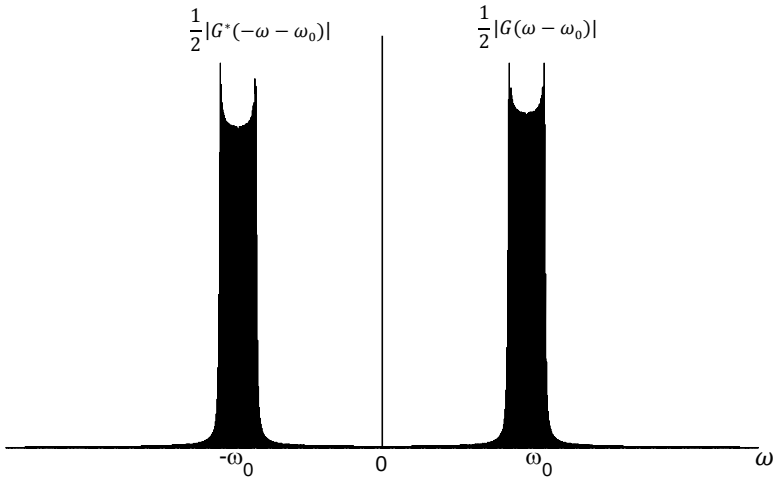


**Fig 2.-1: Real Radar Signal Spectrum.**

Fig 2.-1 shows that the spectrum of $g(t)$ has two principal terms, one in negative $\omega$ region and another one in positive $\omega$ region. This expression assumes that $\omega_0$ is larger than bandwidth of $G(\omega)$, thus, either $G(\omega)$ is bandlimited or the terms do not affect each other (the terms are isolated).

### 2.1.2 Energy

By use of the energy definition to **( 2.-1 )**

$$E_s = \int_{+\infty}^{-\infty} s(t)^2 dt = \int_{+\infty}^{-\infty} a(t)^2 \cos^2[\omega_0 t + \phi_0 + \theta(t)]\, dt$$
$$= \int_{+\infty}^{-\infty} \frac{a(t)^2}{2}\{1 + \cos[2\omega_0 t + 2\phi_0 + 2\theta(t)]\} dt \approx \int_{+\infty}^{-\infty} \frac{a(t)^2}{2} dt \qquad \textbf{( 2.-10 )}$$

According to **( 2.-10 )**, the signal energy depends only on the amplitude $a(t)$, and not on the FM modulation function.

Next, we apply the Parseval´s theorem to calculate the signal energy in the frequency domain

$$E_s = \frac{1}{2\pi}\int_{+\infty}^{-\infty} |s(\omega)|^2 d\omega \qquad \textbf{( 2.-11 )}$$

We can substitute **( 2.-9 )** in **( 2.-11 )**

$$E_s = \frac{1}{2\pi}\int_{+\infty}^{-\infty}\left|\frac{1}{2}\{G(\omega-\omega_0)e^{j\phi_0}+G(-\omega-\omega_0)e^{-j\phi_0}\}\right|^2 d\omega$$
$$= \frac{1}{2\pi}\int_{+\infty}^{-\infty}\frac{1}{4}\left|\{G(\omega-\omega_0)^2e^{2j\phi_0}+2|G(\omega)|^2\right. \quad \textbf{( 2.-12 )}$$
$$\left.+G^*(-\omega-\omega_0)^2e^{-2j\phi_0}\}\right|d\omega = \frac{1}{2}\frac{1}{2\pi}\int_{+\infty}^{-\infty}|G(\omega)|^2 d\omega = \frac{E_g}{2}$$

Where the cross terms have been neglected and $E_g$ is the energy of $g(t)$.

### 2.1.3 Autocorrelation function

By using the autocorrelation definition

$$R_{ss}(\tau) = \begin{cases} \lim_{T\to\mp\infty}\frac{1}{2T}\int_{-T}^{+T} s(t)s(t+\tau)dt & for\ power\ signals \\ \int_{-\infty}^{+\infty} s(t)s(t+\tau)dt & for\ energy\ signals \end{cases} \quad \textbf{( 2.-13 )}$$

The form for the power signals is applied when the signals are continuous (exist in $-\infty < t < +\infty$), for instance, in the CW-radar. Moreover, the form for energy signals is used for pulsed waveforms. $R_{ss}(0)$ gives the average power signal and total energy signal respectively.

## 2.2 Complex Radar signals

In this section, we will study a complex form of $s(t)$. This signal form consists only of the first term of the expression **( 2.-6 )**, **[Peyton Z. Peebles Jr, 1998]**.This signal is denoted by

$$\psi_c(t) = g(t)e^{j[\omega_0 t+\phi_0]} \quad \textbf{( 2.-14 )}$$

Which is related to $s(t)$ by

$$s(t) = Re[\psi_c(t)] \quad \textbf{( 2.-15 )}$$

Now, we demonstrate **( 2.-15 )**

$$\psi_c(t) = g(t)e^{j[\omega_0 t+\phi_0]} = a(t)e^{j[\omega_0 t+\phi_0+\theta(t)]} \\ = a(t)\{\cos[\omega_0 t+\phi_0+\theta(t)] + j\sin[\theta(t)]\sin[\omega_0 t+\phi_0]+\theta(t)\} \quad \textbf{( 2.-16 )}$$

Where it can be observed that the real term is $s(t)$.

The usage of this waveform is useful because its modulus is equal to the amplitude $a(t)$ and its phase is equal to the phase of $s(t)$.

### 2.2.1 Spectrum

By applying a direct Fourier transform to **( 2.-16 )**

$$\Psi_c(\omega) = \int_{+\infty}^{-\infty}\psi_c(t)e^{-j\omega t}dt = \int_{+\infty}^{-\infty} g(t)e^{j[\omega_0 t+\phi_0]}e^{-j\omega t}dt = G(\omega-\omega_0)e^{-j\phi_o} \\ \approx \begin{cases} 2S(\omega) & \omega \geq 0 \\ 0 & \omega < 0 \end{cases} = 2U(\omega)S(\omega) \quad \textbf{( 2.-17 )}$$

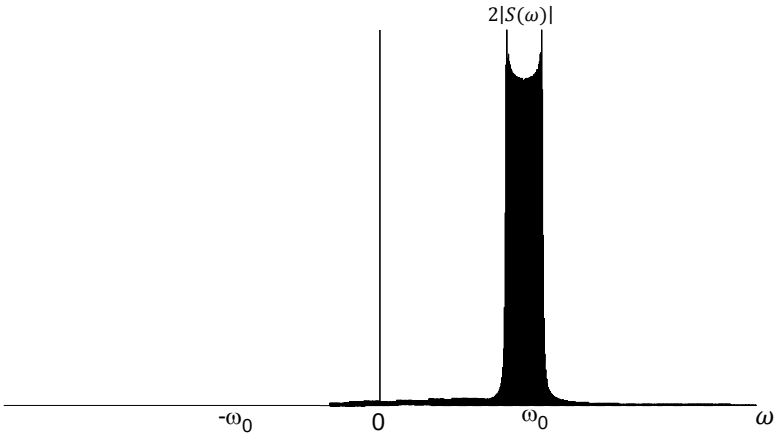


**Fig 2.-2: Complex Radar Signal Spectrum.**

If $\omega_0$ is larger than bandwidth of $g(t)$ and it is bandlimited, zero energy occurs in the $\omega < 0$ region, thereby the approximation used in **( 2.-17 )** is exact. Even in cases where the signal is nonzero in the $\omega < 0$ region, there is a signal transformation that forces the spectral energy in $\omega < 0$ to be zero. The signal resulting from this transformation is called the analytic signal.

### 2.2.2 Autocorrelation function

In same way as in the real signal, the autocorrelation function is defined as

$$R_{\psi_c\psi_c}(\tau) = \begin{cases} \lim_{T\to+\infty} \frac{1}{2T} \int_{-T}^{+T} \psi_c{}^*(t)\psi_c(t+\tau)dt & for\ power\ signals \\ \int_{-\infty}^{+\infty} \psi_c{}^*(t)\psi_c(t+\tau)dt & for\ energy\ signals \end{cases} \quad \textbf{( 2.-18 )}$$

The autocorrelation function is key for pulse compression, since the matched filtering is directly related to this operation as we will study in future sections.

## 2.3 Analytic Radar signals

The analytic signal forces the spectrum in $\omega < 0$ region to be zero **[Peyton Z. Peebles Jr, 1998]**.

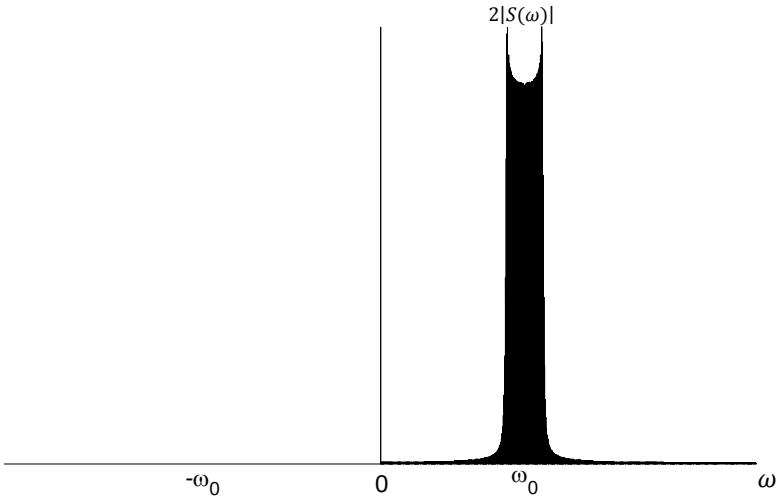


**Fig 2.-3: Analytic Radar Signal Spectrum.**

Note that Fig 2.-3 depicts a spectrum of signal which is completely zero in $\omega < 0$ region. It differs from the spectrum illustrated by Fig 2.-2 that possesses low energy in negative $\omega$ region.

### 2.3.1 Spectrum and waveform

Starting from the assumption that the expression **( 2.-17 )** is exact

$$\Psi(\omega) = 2U(\omega)S(\omega) = [1 + sgn(\omega)]S(\omega) \qquad \textbf{( 2.-19 )}$$

Where $sgn(\omega)$ denotes the sign function in frequency domain.

Now, the signal in the time domain results via applying the inverse Fourier transform. According to the inverse Fourier transform properties

$$X(\omega)Y(\omega) \xrightarrow{TF^{-1}} x(t) * y(t) \qquad \textbf{( 2.-20 )}$$

$$U(\omega) \xrightarrow{TF^{-1}} \frac{1}{2}\delta(t) + \frac{j}{2\pi t} \qquad \textbf{( 2.-21 )}$$

We obtain

$$\psi(t) = 2\int_{-\infty}^{+\infty} s(\xi)\left[\frac{1}{2}\delta(t-\xi) + \frac{j}{2\pi(t-\xi)}\right] d\,\xi = s(t) + j\frac{1}{\pi}\int_{-\infty}^{+\infty} \frac{s(\xi)}{(t-\xi)} d\xi \qquad \textbf{( 2.-22 )}$$
$$= s(t) + j\hat{s}(t)$$

The imaginary part, $\hat{s}(t)$, is known as the Hilbert transform of $s(t)$.

### 2.3.2 Hilbert transform

The real part of **( 2.-22 )** is the real radar signal, and the imaginary part guarantees that the spectrum is zero in the negative $\omega$ region.

If we apply the Hilbert transform to $\hat{s}(t)$, we obtain

$$s(t) = -\frac{1}{\pi}\int_{-\infty}^{+\infty} \frac{\hat{s}(\xi)}{(t-\xi)} d\xi \qquad \textbf{( 2.-23 )}$$

Therefore, $s(t)$ is recovered from $\hat{s}(t)$ by applying a Hilbert transformation. Considering the next fact

$$-\frac{1}{\pi}\int_{-\infty}^{+\infty}\frac{\hat{s}(\xi)}{(t-\xi)}d\xi \overset{TF}{\rightarrow} \hat{S}(\omega)[-jsgn(\omega)] \qquad \textbf{( 2.-24 )}$$

The expression **( 2.-23 )** can be demonstrated by the next graphical sequence in frequency domain

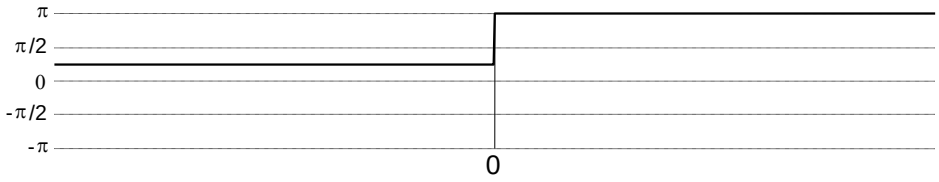


**Fig 2.-4.1: Phase of $s(t)$**

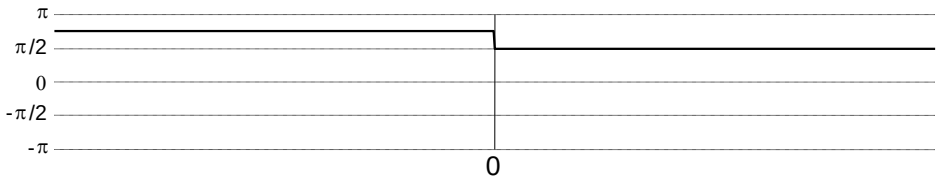


**Fig 2.-4.2: Phase of $TH(s(t))$**

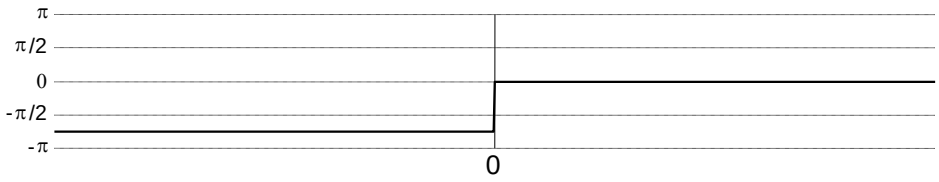


**Fig 2.-4.3: Phase of $TH(\hat{s}(t))$**

The signal phase is shifted in the first step (Fig 2.-4.1 to Fig 2.-4.2), and is once again shifted in the second step (Fig 2.-4.2 to Fig 2.-4.3), resulting a $-\pi$ total shifting. This process is equivalent to filter $s(t)$ by a constant-phase filter, which its response is

$$H(\omega) = -j\ sgn(\omega) = \begin{cases} -j & \omega > 0 \\ 0 & \omega = 0 \\ +j & \omega < 0 \end{cases} \qquad \textbf{( 2.-25 )}$$

This transfer function is not realizable but it can be approximated.

### 2.3.3 Relationship to Complex signal

If $\psi_c(t) = 0$ or $\psi_c(t) \approx 0$ for $\omega < 0$, the complex signal, $\psi_c(t)$, is equal to the analytic signal, $\psi(t)$ ; the most signals used in radars fulfill these conditions. Thus, assuming $s(t)$ bandlimited, it can be easily demonstrated the following relationships.

$$\psi_c(t) = \psi(t) \quad \textbf{( 2.-26 )}$$

$$s(t) = Re[\psi(t)] = a(t)\cos[\omega_0 t + \phi_0 + \theta(t)] \quad \textbf{( 2.- 27 )}$$

$$\hat{s}(t) = Im[\psi(t)] = a(t)\sin[\omega_0 t + \phi_0 + \theta(t)] \quad \textbf{( 2.-28 )}$$

$$|\psi(t)| = a(t) \quad \textbf{( 2.-29 )}$$

$$\arg[\psi(t)] = \tan^{-1}\left[\frac{\hat{s}(t)}{s(t)}\right] = \omega_0 t + \phi_0 + \theta(t) \quad \textbf{( 2.-30 )}$$

### 2.3.4 Energy in Analytic Signal

Now, by using the energy definition and the Parseval´s theorem

$$\begin{aligned} E_\psi = \int_{-\infty}^{+\infty} |\psi(t)|^2 dt = \frac{1}{2\pi}\int_{-\infty}^{+\infty} |\Psi(\omega)|^2 d\omega = \frac{1}{2\pi}\int_{-\infty}^{+\infty} |[1 + sgn(\omega)]S(\omega)|^2 d\omega \\ = \frac{1}{2\pi}\int_{0}^{+\infty} 4|S(\omega)|^2 d\omega = \frac{1}{2\pi}\int_{-\infty}^{+\infty} 2|S(\omega)|^2 d\omega = 2E_s \end{aligned} \quad \textbf{( 2.-31 )}$$

Finally, we can find a relationship between the analytic signal energy and the energies of the other signal forms

$$E_{\psi=}E_{\psi_c} \quad \textbf{( 2.-32 )}$$

$$E_\psi = E_g \quad \textbf{( 2.-33 )}$$

$$E_\psi = 2E_s \quad \textbf{( 2.-34 )}$$

### 2.3.5 Properties of Analytic Signal

Given two analytic signals, $\psi_1(t)$ and $\psi_2(t)$, by application of convolution of the conjugated first signal with the non-conjugated second signal, and via Fourier transform properties

$$\int_{-\infty}^{+\infty} \psi_1^*(t)\psi_2(\tau - t)dt = \Psi_1^*(-\omega)\Psi_2(\omega) = 0 \qquad \textbf{( 2.-35 )}$$

We can show **( 2.-35 )** with a straightforward graphic sequence illustrated in Fig 2.-5.1 and 2.-5.2

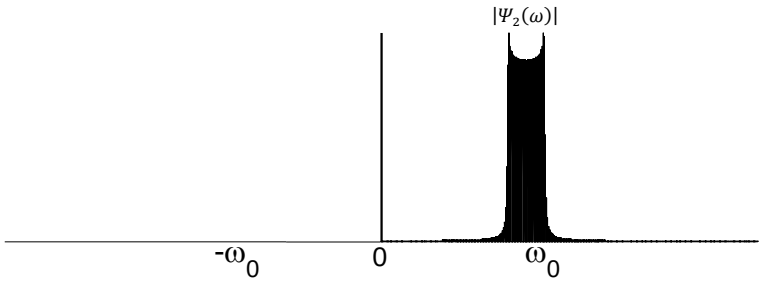


**Fig 2.- 5.1: $\psi_2(t)$ Spectrum**

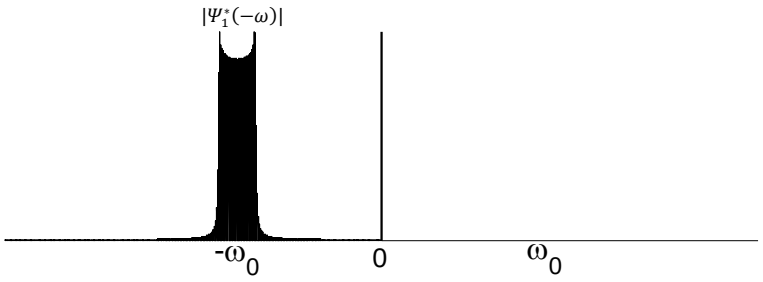


**Fig 2.- 5.2: $\psi_1^*(t)$ Spectrum**

By multiplication of **(Fig 2.-5.1)** and **(Fig 2.-5.2)** a zero spectrum results, thus equation **( 2.-35 )** is demonstrated.

Below we apply the correlation to $\psi_1(t)$ and $\psi_2(t)$

$$\int_{-\infty}^{+\infty} \psi_1(t)\psi_2(\tau + t)d\tau = \psi_1(t) * \psi_2(-t) = \frac{1}{2\pi}\int_{-\infty}^{+\infty} \Psi_1(\omega)[-\Psi_2(-\omega)]e^{-j\omega\tau}d\omega \qquad \textbf{( 2.-36 )}$$
$$= 0$$

In this case the $\psi_2(-t)$ spectrum is reversed $\Psi_2(\omega)$, in the same way as the preceding case. Then by multiplication of $\Psi_1(\omega)$ and $\Psi_2(-\omega)$ zero spectrum is obtained.

However, the following convolution is non-zero

$$\int_{-\infty}^{+\infty} \psi_1(t)\psi_2(\tau - t)dt = \frac{1}{2\pi}\int_{-\infty}^{+\infty} \Psi_1(\omega)\Psi_2(\omega)e^{j\omega\tau}d\omega \neq 0 \qquad \textbf{( 2.-37 )}$$

And the next correlation is also non-zero

$$\int_{-\infty}^{+\infty} \psi_1^*(t)\psi_2(\tau + t)dt = \frac{1}{2\pi}\int_{-\infty}^{+\infty} \Psi_1^*(\omega)\Psi_2(\omega)e^{j\omega\tau}d\omega \neq 0 \qquad \textbf{( 2.-38 )}$$

## 2.4 Interesting parameters: Signal Duration and Frequency

In radar systems, the duration and bandwidth of the signals are often defined differently than in other classical technologies. We will study these concepts in this section, but before, it is necessary revise some properties **[Peyton Z. Peebles Jr, 1998]**.

### 2.4.1 Relationships from Parseval´s theorem

Given a waveform $v(t)$, whose Fourier transform is $V(\omega)$, firstly, we apply the Parseval´s theorem to the following functions $f_1(t) = f_2(t) = (-jt)^m v(t)$ then

$$\begin{aligned}\int_{-\infty}^{+\infty} f_1(t)f_2(t)dt &= \int_{-\infty}^{+\infty} [t^m v(t)]^2 dt = \int_{-\infty}^{+\infty} t^{2m}|v(t)|^2 dt \\ &= \frac{1}{2\pi}\int_{-\infty}^{+\infty} \left|\frac{d^m V(\omega)}{d\omega^m}\right|^2 d\omega \qquad m = 0, 1, 2, 3, \dots\end{aligned} \qquad \textbf{( 2.-39 )}$$

In the same manner, the Parseval´s theorem is applied to the next functions $f_1(t) = f_2(t) = \frac{d^n v(t)}{dt^n}$

$$\begin{aligned}\int_{-\infty}^{+\infty} f_1(t)f_2(t)dt &= \int_{-\infty}^{+\infty} \left[\frac{d^n v(t)}{dt^n}\right]^2 dt = \frac{1}{2\pi}\int_{-\infty}^{+\infty} |(j\omega)^n V(\omega)|^2 d\omega \\ &= \frac{1}{2\pi}\int_{-\infty}^{+\infty} \omega^{2n}|V(\omega)|^2 d\omega \qquad n = 0, 1, 2, 3, \dots\end{aligned} \qquad \textbf{( 2.-40 )}$$

In the last case, we take $f_1(t) = (-jt)^m v(t)$ and $f_2(t) = \frac{d^n v(t)}{dt^n}$

$$\int_{-\infty}^{+\infty} {f_1}^*(t) f_2(t) dt = \int_{-\infty}^{+\infty} (jt)^m v^*(t) \frac{d^n v(t)}{dt^n} dt = j^m \int_{-\infty}^{+\infty} (t)^m v^*(t) \frac{d^n v(t)}{dt^n} dt$$
$$= \frac{j^n}{2\pi} \int_{-\infty}^{+\infty} \left[\frac{d^m V(\omega)}{d\omega^m}\right]^* \omega^n V(\omega) d\omega \quad n = 0, 1, 2, 3, \dots \text{ and } m = 0, 1, 2, 3, \dots \qquad \textbf{( 2.-41 )}$$

### 2.4.2 Mean Time and RMS Duration

In order to measure the radar accuracy, it is necessary to define the Root-Mean-Squared duration of the signal. This parameter gives information about the spread of a signal around a mean time. By use of equation **( 2.-41 )** with m=1 and n=0 and the equation **( 2.-39 )** with m=0 we obtain a mean time expression in the frequency domain.

$$\bar{t}_\psi = \frac{\int_{-\infty}^{+\infty} t|\psi(t)|^2 dt}{\int_{-\infty}^{+\infty} |\psi(t)|^2 dt} = \frac{\frac{-j}{2\pi} \int_0^{+\infty} \Psi(\omega) \left[\frac{d\Psi(\omega)}{d\omega}\right]^* d\omega}{\frac{1}{2\pi} \int_0^{+\infty} |\Psi(\omega)|^2 d\omega} = -j \frac{\int_0^{+\infty} \Psi(\omega) \left[\frac{d\Psi(\omega)^*}{d\omega}\right] d\omega}{\int_0^{+\infty} |\Psi(\omega)|^2 d\omega} \qquad \textbf{( 2.- 42 )}$$

In the same way, this parameter is defined for $s(t)$ and $g(t)$ as

$$\bar{t}_g = \frac{\int_{-\infty}^{+\infty} t|g(t)|^2 dt}{\int_{-\infty}^{+\infty} |g(t)|^2 dt} = -j \frac{\int_{-\infty}^{+\infty} G(\omega) \left[\frac{dG(\omega)^*}{d\omega}\right] d\omega}{\int_{-\infty}^{+\infty} |G(\omega)|^2 d\omega} \qquad \textbf{( 2.-43 )}$$

$$\bar{t}_s = \frac{\int_{-\infty}^{+\infty} t\, s(t)^2 dt}{\int_{-\infty}^{+\infty} s(t)^2 dt} = -j \frac{\int_{-\infty}^{+\infty} S(\omega) \left[\frac{dS(\omega)^*}{d\omega}\right] d\omega}{\int_{-\infty}^{+\infty} |S(\omega)|^2 d\omega} \qquad \textbf{( 2.-44 )}$$

These parameters represent the gravity center of the signals. Once calculated the mean time, now we define the normalized second moment of the three signals (it is called RMS duration)

$${\tau^2}_{\psi,rms} = \frac{\int_{-\infty}^{+\infty} t^2 |\psi(t)|^2 dt}{\int_{-\infty}^{+\infty} |\psi(t)|^2 dt} = \frac{\frac{1}{2\pi} \int_0^{+\infty} \left[\frac{d\Psi(\omega)}{d\omega}\right]^2 d\omega}{\frac{1}{2\pi} \int_0^{+\infty} |\Psi(\omega)|^2 d\omega} = \frac{\int_0^{+\infty} \left[\frac{d\Psi(\omega)}{d\omega}\right]^2 d\omega}{\int_0^{+\infty} |\Psi(\omega)|^2 d\omega} \qquad \textbf{( 2.-45 )}$$

$$\tau^2{}_{g,rms} = \frac{\int_{-\infty}^{+\infty} t|g(t)|^2 dt}{\int_{-\infty}^{+\infty}|g(t)|^2 dt} = \frac{\int_{-\infty}^{+\infty}\left[\frac{dG(\omega)}{d\omega}\right]^2 d\omega}{\int_{-\infty}^{+\infty}|G(\omega)|^2 d\omega} \quad \textbf{( 2.-46 )}$$

$$\tau^2{}_{s,rms} = \frac{\int_{-\infty}^{+\infty} t\, s(t)^2 dt}{\int_{-\infty}^{+\infty} s(t)^2 dt} = \frac{\int_{-\infty}^{+\infty}\left[\frac{dS(\omega)}{d\omega}\right]^2 d\omega}{\int_{-\infty}^{+\infty}|S(\omega)|^2 d\omega} \quad \textbf{( 2.-47 )}$$

It is possible to demonstrate that $\tau^2{}_{\psi,rms} = \tau^2{}_{g,rms} = \tau^2{}_{s,rms}$ by substituting **( 2.-19 )** into **( 2.-45 )** and **( 2.-17 )** into **( 2.- 46 )**

$$\tau^2{}_{\psi,rms} = \frac{\int_0^{+\infty}\left[\frac{d\Psi(\omega)}{d\omega}\right] d\omega}{\int_0^{+\infty}|\Psi(\omega)|^2 d\omega} = \frac{\frac{1}{2}\int_{-\infty}^{+\infty} 4\left[\frac{dS(\omega)}{d\omega}\right]^2 d\omega}{\frac{1}{2}\int_{-\infty}^{+\infty} 4|S(\omega)|^2 d\omega} = \tau^2{}_{s,rms} \quad \textbf{( 2.-48 )}$$

$$\tau^2{}_{g,rms} = \frac{\int_{-\infty}^{+\infty}\left[\frac{dG(\omega)}{d\omega}\right]^2 d\omega}{\int_{-\infty}^{+\infty}|G(\omega)|^2 d\omega} = \frac{\int_0^{+\infty}\left[2\frac{dS(\omega)}{d\omega}\right]^2 d\omega}{\int_0^{+\infty}|2S(\omega)|^2 d\omega} = \frac{\frac{1}{2}\int_{-\infty}^{+\infty} 4\left[\frac{dS(\omega)}{d\omega}\right]^2 d\omega}{\frac{1}{2}\int_{-\infty}^{+\infty} 4|S(\omega)|^2 d\omega} = \tau^2{}_{s,rms} \quad \textbf{( 2.-49 )}$$

For convenience, the zero origin is usually chosen in order to set $\bar{t}_\psi = \bar{t}_g = \bar{t}_s = 0$. Therefore, the RMS duration is related to the energy signal dispersion in the time domain.

### 2.4.3 Mean Frequency and RMS Bandwidth

In the same way as the preceding section, we can define mean frequency and RMS bandwidth. By applying the normalized first central moment in frequency domain, it results

$$\bar{\omega}_\psi = \frac{\int_0^{+\infty}\omega|\Psi(\omega)|^2 d\omega}{\int_0^{+\infty}|\Psi(\omega)|^2 d\omega} \quad \textbf{( 2.-50 )}$$

$$\bar{\omega}_g = \frac{\int_{-\infty}^{+\infty}\omega|G(\omega)|^2 d\omega}{\int_{-\infty}^{+\infty}|G(\omega)|^2 d\omega} \quad \textbf{( 2.-51 )}$$

$$\bar{\omega}_s = \frac{\int_{-\infty}^{+\infty} \omega |S(\omega)|^2 d\omega}{\int_{-\infty}^{+\infty} |S(\omega)|^2 d\omega} \quad \textbf{( 2.-52 )}$$

By replacing **( 2.-19 )** into **( 2.-50 )**

$$\bar{\omega}_\psi = \frac{\frac{1}{2}\int_{-\infty}^{+\infty} 4\omega |S(\omega)|^2 d\omega}{\frac{1}{2}\int_{-\infty}^{+\infty} 4|S(\omega)|^2 d\omega} = \bar{\omega}_g \quad \textbf{( 2.-53 )}$$

By replacing **( 2.-17 )** into **( 2.-50 )** and using the variable change $\lambda = \omega - \omega_0$

- Upper term: $\lambda_u = +\infty$
- Lower term: : $\lambda_l = -\infty$
- Differential term: $d\lambda = d\omega$

$$\bar{\omega}_\psi = \frac{\frac{1}{2}\int_{-\infty}^{+\infty} \omega \left|G(\omega-\omega_0)e^{-j\phi_o}\right|^2 d\omega}{\frac{1}{2}\int_{-\infty}^{+\infty} |G(\omega-\omega_0)e^{-j\phi_o}|^2 d\omega} = \frac{\int_{-\infty}^{+\infty} (\lambda+\omega_0)\left|G(\lambda)e^{-j\phi_o}\right|^2 d\lambda}{\int_{-\infty}^{+\infty} |G(\lambda)e^{-j\phi_o}|^2 d\lambda}$$
$$= \omega_0 \frac{\int_{-\infty}^{+\infty} |G(\lambda)|^2 d\lambda}{\int_{-\infty}^{+\infty} |G(\lambda)|^2 d\lambda} + \frac{\int_{-\infty}^{+\infty} \lambda |G(\lambda)|^2 d\lambda}{\int_{-\infty}^{+\infty} |G(\lambda)|^2 d\lambda} = \omega_0 + \bar{\omega}_g \quad \textbf{( 2.-54 )}$$

Then, we define the RMS bandwidth of the signals in frequency domain

$$\omega_{\psi,rms}^2 = \frac{\int_0^{+\infty} \left[\omega - \bar{\omega}_\psi\right]^2 |\Psi(\omega)|^2 \, d\omega}{\int_0^{+\infty} |\Psi(\omega)|^2 d\omega} = \frac{\int_0^{+\infty} [\omega^2 + \bar{\omega}_\psi{}^2 - 2\omega\bar{\omega}_\psi] |\Psi(\omega)|^2 d\omega}{\int_0^{+\infty} |\Psi(\omega)|^2 d\omega} =$$
$$= \frac{\int_0^{+\infty} \omega^2 |\Psi(\omega)|^2 d\omega + \bar{\omega}_\psi{}^2 \int_0^{+\infty} |\Psi(\omega)|^2 d\omega - 2\bar{\omega}_\psi \int_0^{+\infty} \omega |\Psi(\omega)|^2 d\omega}{\int_0^{+\infty} |\Psi(\omega)|^2 d\omega} \quad \textbf{( 2.-55 )}$$
$$= \frac{\int_0^{+\infty} \omega^2 |\Psi(\omega)|^2 d\omega}{\int_0^{+\infty} |\Psi(\omega)|^2 d\omega} + \bar{\omega}_\psi{}^2 - 2\bar{\omega}_\psi \, \bar{\omega}_\psi = \overline{\omega_\psi^2} - \bar{\omega}_\psi^2$$

$$\omega_{g,rms}^2 = \frac{\int_{-\infty}^{+\infty} \left[\omega - \bar{\omega}_g\right]^2 |G(\omega)|^2 \, d\omega}{\int_{-\infty}^{+\infty} |G(\omega)|^2 d\omega} = \overline{\omega_g^2} - \bar{\omega}_g^2 \quad \textbf{( 2.-56 )}$$

$$\omega_{s,rms}^2 = \frac{\int_{-\infty}^{+\infty} [\omega - \bar{\omega}_s]^2 |S(\omega)|^2 \, d\omega}{\int_{-\infty}^{+\infty} |S(\omega)|^2 d\omega} = \overline{\omega_s^2} - \bar{\omega}_s^2 \quad \textbf{( 2.-57 )}$$

Where $\overline{\omega_\psi^2}$, $\overline{\omega_g^2}$, $\overline{\omega_s^2}$ are normalized second moments. In addition, by using **( 2.-39 )** with m=0, **( 2.-40 )** with n=1 and **( 2.-41 )** with m=0 and n=2, the normalized second moment can have another form

$$\overline{\omega_\psi^2} = \frac{\int_0^{+\infty} \omega^2 |\Psi(\omega)|^2 \, d\omega}{\int_0^{+\infty} |\Psi(\omega)|^2 d\omega} = \frac{\int_{-\infty}^{+\infty} \left|\frac{d\psi(t)}{dt}\right|^2 \, d\omega}{\int_{-\infty}^{+\infty} |\psi(t)|^2 d\omega} \qquad \textbf{( 2.-58 )}$$

$$\overline{\omega_g^2} = \frac{\int_{-\infty}^{+\infty} \omega^2 |G(\omega)|^2 \, d\omega}{\int_{-\infty}^{+\infty} |G(\omega)|^2 d\omega} = \frac{\int_{-\infty}^{+\infty} \left|\frac{dg(t)}{dt}\right|^2 \, d\omega}{\int_{-\infty}^{+\infty} |g(t)|^2 d\omega} \qquad \textbf{( 2.-59 )}$$

$$\overline{\omega_s^2} = \frac{\int_{-\infty}^{+\infty} \omega^2 |S(\omega)|^2 \, d\omega}{\int_{-\infty}^{+\infty} |S(\omega)|^2 d\omega} = \frac{\int_{-\infty}^{+\infty} \left|\frac{ds(t)}{dt}\right|^2 \, d\omega}{\int_{-\infty}^{+\infty} |s(t)|^2 d\omega} \qquad \textbf{( 2.-60 )}$$

The RMS bandwidth gives information about the spectral energy dispersion around $\overline{\omega}_\psi$. A straightforward way to calculate the rms bandwidth is to use **( 2.-56 )** for signals whose $\overline{\omega}_g = 0$. $\overline{\omega}_g = 0$ occurs when $G(\omega)$ has even symmetry, and most of signals used in radar systems fulfil these requirements.

## 2.5 Transmissions of Signals through networks

In this section we are going to study the passage of signals through linear networks. For this purpose, we will study the following situations:

1. Real signal through real networks. This case represents the situation in the real world.
2. Analytic signal through real network.
3. Analytic signal through analytic network. We will revise this case since it is interesting to simplify the signal analysis.

### 2.5.1 Real Signals through Real Networks

This case is a basic application of convolution as shown Fig 2.-6 **[Peyton Z. Peebles Jr, 1998]**

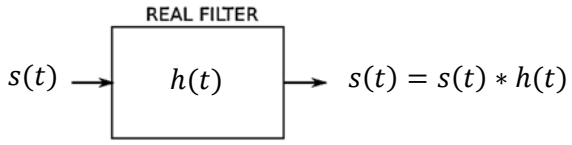


**Fig 2.-6: Real Signal across Real Network.**

Given a real signal $s(t)$ and real impulse response $h(t)$, the output signal, $s_0(t)$, is

$$s_0(t) = \int_{-\infty}^{+\infty} s(\lambda)h(t-\lambda)d\lambda = s(t) * h(t) \qquad \textbf{( 2.-61 )}$$

By Fourier properties the output signal in frequency domain, $S_0(\omega)$, is obtained as

$$S_0(\omega) = S(\omega)H(\omega) \;\; for \;\; -\infty < \omega < +\infty \qquad \textbf{( 2.-62 )}$$

### 2.5.2 Analytic Signal through Real Networks

This situation is depicted by the Fig 2.-7. By using the equation **(2.-22),** $\psi(t) = s(t) + j\hat{s}(t)$, and by applying $\psi(t)$ as input to a real filter, we obtain

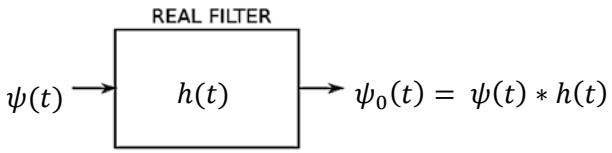


**Fig 2.-7: Analytic Signal across Real Network.**

$$\psi_0(t) = \psi(t) * h(t) = [s(t) + j\hat{s}(t)] * h(t) = s(t) * h(t) + j\hat{s}(t) * h(t) \qquad \textbf{( 2.-63 )}$$

The first term is known as it is **( 2.-61 )**. Now we are interested in the second term, which is expressed as

$$\hat{s}_0(t) = \hat{s}(t) * h(t) = \frac{1}{\pi}\int_{-\infty}^{+\infty} \frac{s_0(\alpha)}{t-\alpha} d\alpha = \frac{1}{\pi}\int_{-\infty}^{+\infty} \frac{\int_{-\infty}^{+\infty} h(\xi)s(\alpha-\xi)d\xi}{t-\alpha} d\alpha \qquad \textbf{( 2.-64 )}$$

Making the variable change $x = \alpha - \xi$

- Upper term: $x_u = +\infty$
- Lower term: : $x_l = -\infty$
- Differential term: $dx = d\alpha$

We can rewrite the integral ( 2.-64 )

$$\hat{s}_0(t) = \frac{1}{\pi}\int_{-\infty}^{+\infty} h(\xi)\int_{-\infty}^{+\infty}\frac{s(x)}{t-\xi-x}dx\,d\xi = \int_{-\infty}^{+\infty} h(\xi)\hat{s}(t-\xi)d\xi \qquad \textbf{( 2.-65 )}$$

According **( 2.-64 )**, we obtain the output signal

$$\psi_0(t) = s_0(t) + j\hat{s}_0(t) \qquad \textbf{( 2.-66 )}$$

Having the Fourier transform

$$\Psi_0(\omega) = \Psi(\omega)H(\omega) = 2U(\omega)S_0(\omega) \qquad \textbf{( 2.-67 )}$$

### 2.5.3 Analytic Signal through Analytic Network

Suppose an Analytic Impulse response

$$z(t) = h(t) + j\hat{h}(t) \qquad \textbf{( 2.-68 )}$$

Its Fourier transform is

$$Z(\omega) = 2U(\omega)H(\omega) \qquad \textbf{( 2.-69 )}$$

If this analytic network is excited by an analytic signal as shown Fig 2.-8

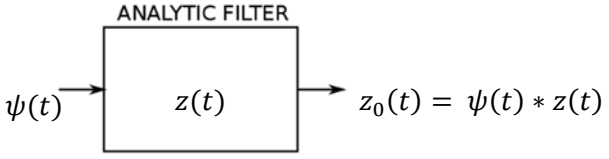


**Fig 2.-8: Analytic Signal across Analytic Network.**

We obtain the next output signal

$$z_0(t) = \psi(t) * z(t) = \psi(t) * \left[h(t) + j\hat{h}(t)\right] = \psi(t) + j\left[\psi(t) * \hat{h}(t)\right] \quad \textbf{( 2.-70 )}$$

We need to calculate the imaginary term

$$\begin{aligned}\psi(t) * \hat{h}(t) = [s(t) + j\hat{s}(t)] * \hat{h}(t) &= \int_{-\infty}^{+\infty} [s(\xi) + j\hat{s}(\xi)]\, h(t-\xi) d\xi \\ &= \int_{-\infty}^{+\infty} [s(\xi) + j\hat{s}(\xi)]\, \frac{1}{\pi} \int_{-\infty}^{+\infty} \frac{h(\alpha)}{t-\xi-\alpha} d\alpha\, d\xi \\ &= \int_{-\infty}^{+\infty} h(\alpha)\, \frac{1}{\pi} \int_{-\infty}^{+\infty} \frac{[s(\xi) + j\hat{s}(\xi)]}{t-\xi-\alpha} d\xi\, d\alpha \\ &= \int_{-\infty}^{+\infty} h(\alpha)\, [\hat{s}(t-\alpha) - js(t-\alpha)] d\alpha = \hat{s}_0(t) - js_0(t) \\ &= -j\psi_0(t)\end{aligned} \quad \textbf{( 2.-71 )}$$

To obtain this last expression we have used the Hilbert transform property **( 2.-22 )**.

Therefore

$$z_0(t) = \psi_0(t) + j[-j\psi_0(t)] = 2\psi_0(t) \quad \textbf{( 2.-72 )}$$

The expression **( 2.-72 )** is exactly twice of **( 2.-66 )**. This result is derived from expression **( 2.-69 )**, in which $Z(\omega)$ is directly related to $2H(\omega)$.

**Conclusions about analytic signals**

We suppose an arbitrary system whose impulse response is $h(t)$ and an arbitrary input $s(t)$. Its analytic forms in frequency domain, by using **( 2.-17 )**, are

$$Z(\omega) = G_f(\omega - \omega_0) e^{j\phi_f} \quad \textbf{( 2.-73 )}$$

$$\Psi(\omega) = G(\omega - \omega_0) e^{j\phi_0} \quad \textbf{( 2.-74 )}$$

Where $G_f(\omega-\omega_0)$ and $G(\omega-\omega_0)$ are the baseband forms shifted to $\omega_0$. If $h(t)$ and $s(t)$ are bandlimited signals, **( 2.-73 )** and **( 2.-74 )** are exact.

Therefore, the output signal is

$$Z(\omega) = G_f(\omega-\omega_0)G(\omega-\omega_0)e^{-j[\phi_f+\phi_0]} \qquad \textbf{( 2.-75 )}$$

Note that the signal analytic analysis let us work with signal baseband forms, and thereby, avoiding to consider the carrier information since it does not affect to the magnitude and the phase terms.

# Chapter 3. Matched Filter and Ambiguity function

In order to interpret and understand pulse compression the study of two important concepts is necessary. These concepts are: the matched filter and the ambiguity function. Both concepts are very useful to know about the performance of pulse compression techniques.

## 3.1. Matched Filter for Nonwhite Noise

For an improvement of the detection of targets, the received signal amplitude larger than average noise signal amplitude is desired. Consequently, we will show a filter which maximizes the signal to noise ratio for a time instant in the case of nonwhite noise **[Peyton Z. Peebles Jr, 1998]**.

Firstly, we start from the sketch depicted by Fig 3.-1 (where $h(t)$ is the impulse response of a real filter, $s_r(t)$ is arbitrary signal and $n_r(t)$ is a noise signal)

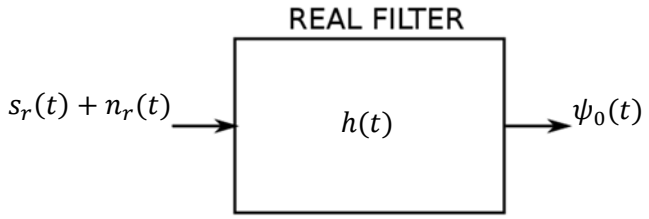


**Fig 3.-1 Received Signal and Noise Signal across Real Filter.**

The output signal can be written, in terms of an analytic signal, as

$$\psi_0(t) = \frac{1}{2}\psi_r(t) * z(t) = \frac{1}{2\pi}\int_{-\infty}^{+\infty} \Psi_0(\omega) e^{j\omega t} d\omega = \frac{1}{2\pi}\int_{-\infty}^{+\infty} \frac{1}{2}\Psi_r(\omega)\, Z(\omega) e^{j\omega t} d\omega \qquad \textbf{( 3.-1 )}$$

$\psi_0(t)$ is the analytic output signal for any time. Here we define $t_0$ as the instant time in which **( 3.-1 )** accomplishes its maximum. Thus

$$\psi_0(t = t_0) = \frac{1}{2\pi}\int_{-\infty}^{+\infty} \frac{1}{2}\Psi_r(\omega)\, Z(\omega) e^{j\omega t_0} d\omega \qquad \textbf{( 3.-2 )}$$

Then, its power is

$$\hat{\psi}_0 = \left| \frac{1}{2\pi} \int_{-\infty}^{+\infty} \frac{1}{2} \Psi_r(\omega)\, Z(\omega) e^{j\omega t_0} d\omega \right|^2 \qquad \textbf{( 3.-3 )}$$

Below, the output noise power will be calculated. The function $n_r(t)$ is a random process, and its power spectral density is $\rho_{NN}(\omega)$. The average output noise power is

$$\begin{aligned} N_0 &= \frac{1}{2\pi} \int_{-\infty}^{+\infty} \rho_{NN}(\omega)\, |H(\omega)|^2 d\omega = \frac{2}{2\pi} \int_{0}^{+\infty} \rho_{NN}(\omega)\, |H(\omega)|^2 d\omega \\ &= \frac{1}{4} \frac{2}{2\pi} \int_{-\infty}^{+\infty} \rho_{NN}(\omega)\, |Z(\omega)|^2 d\omega \end{aligned} \qquad \textbf{( 3.-4 )}$$

Where equation **( 2.-63 )** has been obtained to write **( 3.-4 )** as function of $Z(\omega)$.

According to the preceding result, we define the signal power to average noise power ratio in the filter output as

$$\frac{\hat{\psi}_0}{N_0} = \frac{\frac{1}{4} \left| \frac{1}{2\pi} \int_{-\infty}^{+\infty} \Psi_r(\omega)\, Z(\omega) e^{j\omega t_0} d\omega \right|^2}{\frac{1}{4} \frac{2}{2\pi} \int_{-\infty}^{+\infty} \rho_{NN}(\omega)\, |Z(\omega)|^2 d\omega} = \frac{\left| \frac{1}{2\pi} \int_{-\infty}^{+\infty} \Psi_r(\omega)\, Z(\omega) e^{j\omega t_0} d\omega \right|^2}{\frac{2}{2\pi} \int_{-\infty}^{+\infty} \rho_{NN}(\omega)\, |Z(\omega)|^2 d\omega} \qquad \textbf{( 3.-5 )}$$

The next step is maximize **( 3.-5 )**. We will use the Schwarz´s inequality for this purpose, since the task is more straightforward. Remembering the Schwarz´s inequality

$$\left| \int_{-\infty}^{+\infty} A(\omega) B(\omega)\, d\omega \right|^2 \leq \int_{-\infty}^{+\infty} |A(\omega)|^2 d\omega \int_{-\infty}^{+\infty} |B(\omega)|^2 d\omega \qquad \textbf{( 3.-6 )}$$

Where $A(\omega)$ and $B(\omega)$ are a complex functions of a real variable $\omega$ and $A(\omega)$ is related to $B(\omega)$ as

$$A(\omega) = k\, B^*(\omega) \qquad \textbf{( 3.-7 )}$$

Where $k$ is a nonzero real constant and $\cdot^*$ is the conjugated function, **( 3.-6 )** can be applied if and only if **( 3.-7 )** occurs.

Setting $A(\omega)$ and $B(\omega)$ as

$$A(\omega) = \frac{1}{\sqrt{2\pi}}\sqrt{\rho_{NN}(\omega)}\, Z(\omega) \tag{3.-8}$$

$$B(\omega) = \frac{1}{\sqrt{2\pi}}\frac{\Psi_r(\omega)e^{j\omega t_0}}{\sqrt{\rho_{NN}(\omega)}} \tag{3.-9}$$

The numerator of the expression **( 3.-5 )** can be written in $A(\omega)$ and $B(\omega)$ terms as

$$\begin{aligned}\left|\frac{1}{2\pi}\int_{-\infty}^{+\infty}\Psi_r(\omega)\, Z(\omega)e^{j\omega t_0}d\omega\right|^2 &= \left|\int_{-\infty}^{+\infty}\frac{1}{\sqrt{2\pi}}\frac{\Psi_r(\omega)e^{j\omega t_0}}{\sqrt{\rho_{NN}(\omega)}}\frac{1}{\sqrt{2\pi}}\sqrt{\rho_{NN}(\omega)}\, Z(\omega)d\omega\right|^2 \\ &= \left|\int_{-\infty}^{+\infty}A(\omega)\, B(\omega)d\omega\right|^2\end{aligned} \tag{3.-10}$$

Now, by applying the Schwarz´s inequality, **( 3.-6 )**, thereby we obtain

$$\begin{aligned}\frac{\hat{\psi}_0}{N_0} = \frac{\left|\int_{-\infty}^{+\infty}A(\omega)\, B(\omega)d\omega\right|^2}{\frac{2}{2\pi}\int_{-\infty}^{+\infty}\rho_{NN}(\omega)\,|Z(\omega)|^2d\omega} &\le \frac{\int_{-\infty}^{+\infty}|A(\omega)|^2d\omega\ \int_{-\infty}^{+\infty}|B(\omega)|^2d\omega}{\frac{2}{2\pi}\int_{-\infty}^{+\infty}\rho_{NN}(\omega)\,|Z(\omega)|^2d\omega} \\ &= \frac{\int_{-\infty}^{+\infty}\left|\frac{1}{\sqrt{2\pi}}\sqrt{\rho_{NN}(\omega)}\, Z(\omega)\right|^2 d\omega\ \int_{-\infty}^{+\infty}\left|\frac{1}{\sqrt{2\pi}}\frac{\Psi_r(\omega)e^{j\omega t_0}}{\sqrt{\rho_{NN}(\omega)}}\right|^2 d\omega}{\frac{2}{2\pi}\int_{-\infty}^{+\infty}\rho_{NN}(\omega)\,|Z(\omega)|^2d\omega} \\ &= \frac{\int_{-\infty}^{+\infty}\frac{1}{2\pi}\rho_{NN}(\omega)\,|\, Z(\omega)|^2d\omega\ \int_{-\infty}^{+\infty}\left|\frac{1}{\sqrt{2\pi}}\frac{\Psi_r(\omega)e^{j\omega t_0}}{\sqrt{\rho_{NN}(\omega)}}\right|^2 d\omega}{\frac{2}{2\pi}\int_{-\infty}^{+\infty}\rho_{NN}(\omega)\,|Z(\omega)|^2d\omega} \\ &= \int_{-\infty}^{+\infty}\frac{1}{4\pi}\frac{\left|\Psi_r(\omega)e^{j\omega t_0}\right|^2}{\sqrt{\rho_{NN}(\omega)}}d\omega\end{aligned} \tag{3.-11}$$

Thus, **( 3.-5 )** accomplishes its maximum when

$$\left.\frac{\hat{\psi}_0}{N_0}\right|_{max} = \int_{-\infty}^{+\infty}\frac{1}{4\pi}\frac{\left|\Psi_r(\omega)e^{j\omega t_0}\right|^2}{\sqrt{\rho_{NN}(\omega)}}d\omega \tag{3.-12}$$

To finish, it is necessary to verify the equation **( 3.-7 )**, then by substituting **( 3.-8 )** and **( 3.-9 )** into **( 3.-7 )**

$$\frac{1}{\sqrt{2\pi}}\sqrt{\rho_{NN}(\omega)}\,Z(\omega) = k\frac{1}{\sqrt{2\pi}}\frac{\Psi_r(\omega)^* e^{-j\omega t_0}}{\sqrt{\rho_{NN}(\omega)}} \qquad \textbf{( 3.-13 )}$$

Therefore

$$Z_{opt}(\omega) = k\frac{\Psi_r(\omega)^* e^{-j\omega t_0}}{\rho_{NN}(\omega)} \qquad \textbf{( 3.-14 )}$$

The above expression is the optimum filter, which achieves the maximum signal to noise ratio. It can be rewritten, in real signal terms, as

$$H_{opt}(\omega) = k\frac{S_r(\omega)^* e^{-j\omega t_0}}{\rho_{NN}(\omega)} \qquad \textbf{( 3.-15 )}$$

Note that the optimum filter transfer function is directly related to the conjugated input signal in frequency domain.

## 3.2. Matched Filter for White Noise

In this section we will particularize the preceding Matched filter for white noise perturbations. It is well-known that the white noise power spectral density is **[Peyton Z. Peebles Jr, 1998]**

$$\rho_{NN}(\omega) = \frac{\aleph_0}{2}\ \forall\ \omega \qquad \textbf{( 3.-16 )}$$

By replacing **( 3.-16 )** into **( 3.-12 )** and **( 3.-14 )**

$$\left.\frac{\hat{\psi}_0}{N_0}\right|_{max} = \int_{-\infty}^{+\infty} \frac{1}{4\pi} \frac{\left|\Psi_r(\omega)e^{j\omega t_0}\right|^2}{\frac{\aleph_0}{2}} d\omega = \int_{-\infty}^{+\infty} \frac{1}{2\pi} \frac{\left|\Psi_r(\omega)e^{j\omega t_0}\right|^2}{\aleph_0} d\omega = \frac{E_\psi}{\aleph_0} = \frac{2E_r}{\aleph_0} \quad \textbf{( 3.-17 )}$$

$$Z_{opt}(\omega) = k\frac{\Psi_r(\omega)^* e^{-j\omega t_0}}{\frac{\aleph_0}{2}} = 2k\frac{\Psi_r(\omega)^* e^{-j\omega t_0}}{\aleph_0} \quad \textbf{( 3.-18 )}$$

Where $E_r$ is the energy of the real signal, $s_r(t)$.

Assuming a stationary target, it will provoke a time delay $\tau_r$ in the received signal and the constant $\alpha$ is related to the attenuation which affects the transmitted signal

$$\psi_r(t) = \alpha\psi_t(t-\tau_r) \overset{TF}{\rightarrow} \Psi_r(\omega) = \alpha\Psi_t(\omega)e^{-j\omega\tau_r} \quad \textbf{( 3.-19 )}$$

And from **( 3.-18 )**

$$Z_{opt}(\omega) = \frac{2k\alpha}{\aleph_0}\Psi_t(\omega)^* e^{-j\omega[t_0-\tau_r]} \quad \textbf{( 3.-20 )}$$

Now we are going to analyze the matched filter output. In the frequency domain

$$\Psi_0(\omega) = \frac{1}{2}\alpha\Psi_t(\omega)e^{-j\omega\tau_r}\ Z_{opt}(\omega) = \Psi_t(\omega)\frac{k\alpha^2}{\aleph_0}{\Psi_t}^*(\omega)e^{-j\omega t_0} = \frac{k\alpha^2}{\aleph_0}|\Psi_t(\omega)|^2 e^{-j\omega t_0} \quad \textbf{( 3.-21 )}$$

Focusing on the **( 3.-21 )** second term, we apply the inverse Fourier transform to it

$$\Psi_0(\omega) = \Psi_t(\omega)\frac{k\alpha^2}{\aleph_0}{\Psi_t}^*(\omega)e^{-j\omega t_0} \overset{TF^{-1}}{\longrightarrow} \psi_0(t) = \frac{k\alpha^2}{\aleph_0}R_{\psi_t\psi_t}(t-t_0) \quad \textbf{( 3.-22 )}$$

The output signal is directly related to the transmitted signal autocorrelation. The autocorrelation function maximum occurs in $t = t_0$, same instant in which the maximum peak signal power average noise power ratio is achieved.

**Conclusions**

The matched filter response is directly related to the conjugated transmitted signal. Assuming that the filter is matched to $\psi_r(t)$, we revise the impulse response shaping by using the Fourier transform properties and illustrated by the next graphical sequence

$$S(\omega)e^{-j\omega t_0} \xrightarrow{TF^{-1}} s(t+t_0) \quad \textbf{( 3.-23 )}$$

$$S^*(\omega) \xrightarrow{TF^{-1}} s^*(-t) \quad \textbf{( 3.-24 )}$$

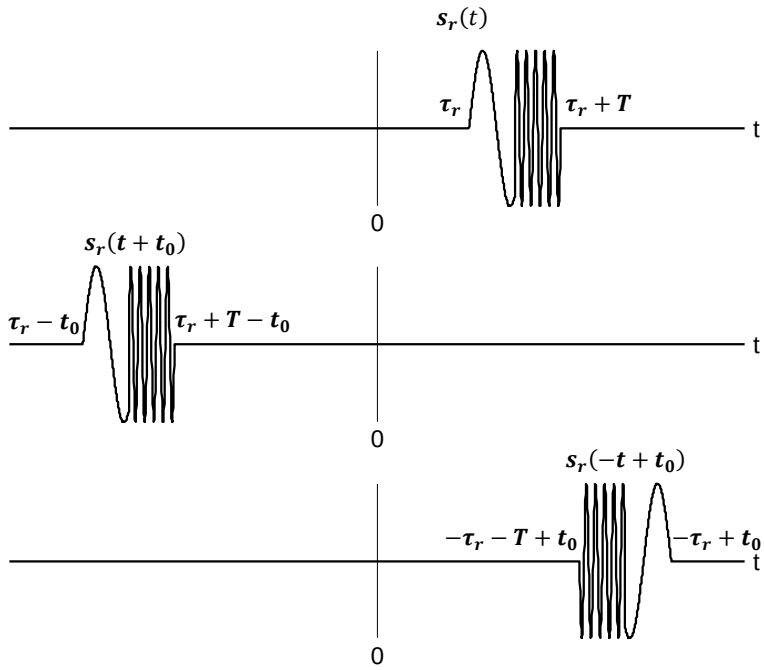


**Fig 3.-2.1 Original received signal.**

**Fig 3.-2.2 -$t_0$ Shifting.**

**Fig 3.-2.3 Folding about the origin.**

This fact is consequence of the instant in which the maximum occurs, $t_0$, that is longer than $\tau_r + T$, where $T$ is the duration of the transmitted pulse.

$$t_0 \geq \tau_r + T \quad \textbf{( 3.-25 )}$$

The preceding condition guarantees that the filter is causal, thus it is realizable.

To continue, we will analyse the filter output signal, which can be written as

$$\psi_0(t) = \frac{1}{2}\psi_r(t) * z_{opt}(t) = \frac{1}{2}\alpha\psi_t(t-\tau_r) * \frac{k\alpha}{\aleph_0}\psi_t{}^*(t_0-\tau_r-t)$$
$$= \frac{1}{2}\int_{-\infty}^{+\infty} \alpha\psi_t(\xi-\tau_r)\,\frac{k\alpha}{\aleph_0}\psi_t{}^*(\xi-\tau_r+t_0-t)\,d\xi \qquad \textbf{( 3.-26 )}$$

Starting from Fig 3.-2.1 and Fig 3.-2.3, we will try to reach conclusions. By convolution definition in time domain; firstly, we replace $t = \xi$; secondly, apply $\xi$ shifting; and finally, we fold the waveform about the origin

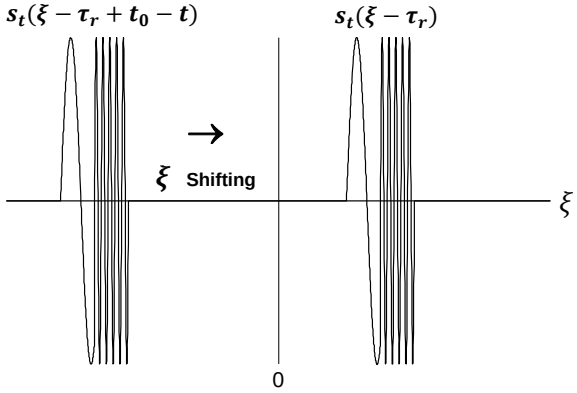


**Fig 3.-3 Graphical convolution.**

The maximum output signal will be achieved when $s_t(\xi-\tau_r+t_0-t)$ matches exactly with $s_t(\xi-\tau_r)$, this will occur when

$$\xi-\tau_r = \xi-\tau_r+t_0-t \;\rightarrow\; t = t_0 \qquad \textbf{( 3.-27 )}$$

The output signal expression in frequency domain is

$$\Psi_0(\omega) = \Psi_t(\omega)\frac{k\alpha^2}{\aleph_0}\Psi_t{}^*(\omega)e^{-j\omega t_0} = \frac{k\alpha^2}{\aleph_0}|\Psi_t(\omega)|^2 e^{-j\omega t_0} \qquad \textbf{(3.- 28 )}$$

Note that the output signal spectrum does not depend on signal phase. It only depends on the modulus of the received signal spectrum, and any phase term is removed.

## 3.3. Ambiguity Function

We have studied the matched filter output when a non-moving target is detected. But in the real applications most of the targets are moving. In this case, the received signal from the target will be **[Peyton Z. Peebles Jr, 1998]**

$$s_r(t) = \alpha\, a(t-\tau_r)\cos[(\omega_0+\omega_D)(t-\tau_r)+\theta(t-\tau_r)+\phi_0] \quad \textbf{( 3.-29 )}$$

Which has its analytic form as

$$\psi_r(t) = \alpha\, a(t-\tau_r)e^{-j[(\omega_0+\omega_d)(t-\tau_r)+\theta(t-\tau_r)+\phi_0]} = \alpha\psi_t(t-\tau_r)e^{-j\omega_d(t-\tau_r)} \quad \textbf{( 3.-30 )}$$

Where $\psi_t(t)$ is the transmitted signal taking its analytic form.

Then, the matched filter output signal is

$$\psi_0(t) = \frac{1}{2}\int_{-\infty}^{+\infty} \alpha\psi_t(\lambda-\tau_r)e^{-j\omega_d(\lambda-\tau_r)}\,\frac{k\alpha}{\aleph_0}\psi_t^*(t_0-\tau_r-t+\lambda)d\lambda \quad \textbf{( 3.-31 )}$$

By using the change of variable $\xi = t_0 - \tau_r - t + \lambda \;\rightarrow\; \lambda - \tau_r = \xi - t_0 + t$

- Upper limit: $\lambda_u = +\infty$
- Lower limit: $\lambda_l = -\infty$
- Differential term: $d\lambda = d\xi$

The integral **(3.-31 )** takes the following form

$$\begin{aligned}\psi_0(t) &= \frac{1}{2}\int_{-\infty}^{+\infty} \alpha\psi_t(\xi-t_0+t)e^{-j\omega_d(\lambda-\tau_r)}\,\frac{2k\alpha}{\aleph_0}\psi_t^*(\xi)d\xi \\ &= \frac{k\alpha^2}{\aleph_0}e^{j\omega_d(t-t_0)}\int_{-\infty}^{+\infty}\psi_t^*(\xi)\,\psi_t(\xi-t_0+t)e^{j\omega_d\tau_r}d\xi\end{aligned} \quad \textbf{( 3.-32 )}$$

This function depends on time, but also it depends on the Doppler shift. That means that the matched filter behavior changes.

Making $\tau = t - t_0$

$$\psi_0(t) = \frac{k\alpha^2}{\aleph_0} e^{j\omega_d\tau} \int_{-\infty}^{+\infty} \psi_t(\xi+\tau) e^{j\omega_d\xi}\, \psi_t^*(\xi) d\xi = \frac{k\alpha^2}{\aleph_0} e^{j(\omega_d+\omega_0)\tau} \left[ e^{-j\omega_0\tau} \int_{-\infty}^{+\infty} \psi_t^*(\xi)\, \psi_t(\xi+\tau) e^{j\omega_d\xi} d\xi \right] \quad \textbf{(3.-33 )}$$

Then, we call the term between brackets $x(\tau, \omega_d)$

$$x(\tau, \omega_d) = e^{-j\omega_0\tau} \int_{-\infty}^{+\infty} \psi_t^*(\xi)\, \psi_t(\xi+\tau) e^{j\omega_d\xi} d\xi \quad \textbf{( 3.-34 )}$$

Thus

$$\psi_0(t) = \frac{k\alpha^2}{\aleph_0} e^{j(\omega_d+\omega_0)\tau} x(\tau, \omega_d) \quad \textbf{( 3.-35 )}$$

Thereby the Doppler shift affects to the matched filter behavior. Note that in **( 3.-31 )** the filter is matched to a non-moving target, but we can redevelop it to match it to a given target moving at a specific speed.

The functions $|x(\tau, \omega_d)|$ and $|x(\tau, \omega_d)|^2$ report about the matched filter performance when a moving target is detected. We can calculate a useful frequency expression from **( 3.-34 )**

$$x(\tau, \omega_d) = e^{-j\omega_0\tau} \int_{-\infty}^{+\infty} \psi_t^*(\xi)\, \psi_t(\xi+\tau) e^{j\omega_d\xi} d\xi = e^{-j\omega_0\tau} \frac{1}{2\pi} \int_{-\infty}^{+\infty} \Psi_t^*(\omega)\, \Psi_t(\omega-\omega_d) e^{j\omega\tau} d\omega \quad \textbf{( 3.-36 )}$$

Where $\Psi_t(\omega)$ is the Fourier transform of $\psi_t(t)$. Other useful form is, by using **( 2.-14 )**

$$\begin{aligned} x(\tau,\omega_d) &= e^{-j\omega_0\tau}\int_{-\infty}^{+\infty}\psi_t^*(\xi)\,\psi_t(\xi+\tau)e^{j\omega_d\xi}d\xi \\ &= e^{-j\omega_0\tau}\int_{-\infty}^{+\infty}g_t^*(\xi)e^{-j[\omega_0\xi+\phi_0]}\,g_t(\xi+\tau)e^{-j[\omega_0(\xi+\tau)+\phi_0]}\,e^{j\omega_d\xi}d\xi \\ &= \int_{-\infty}^{+\infty}g_t^*(\xi)g_t(\xi+\tau)\,e^{j\omega_d\xi}d\xi \\ &= \frac{1}{2\pi}\int_{-\infty}^{+\infty}G_t^*(\omega)G_t(\omega-\omega_d)\,e^{j\omega\tau}d\omega \end{aligned} \quad \textbf{( 3.-37 )}$$

We call $|x(\tau,\omega_d)|$ uncertainty function and $|x(\tau,\omega_d)|^2$ ambiguity function. Below, we will revise the uncertainty function properties and the ambiguity function properties.

### 3.3.1 Properties of Matched Filter Response

- Origin property

$$x(0,0) = \int_{-\infty}^{+\infty}\psi_t^*(\xi)\,\psi_t(\xi)d\xi = \int_{-\infty}^{+\infty}|\psi_t(\xi)|^2d\xi = E_{\psi_t} \quad \textbf{( 3.-38 )}$$

- Folding about $\tau$ and $\omega_d$

$$x(-\tau,-\omega_d) = e^{j\omega_0\tau}\int_{-\infty}^{+\infty}\psi_t^*(\xi)\,\psi_t(\xi-\tau)e^{-j\omega_d\xi}d\xi \quad \textbf{( 3.-39 )}$$

By the change of variables $\xi' = \xi - \tau \;\rightarrow\; \xi = \xi' + \tau$

$$x(-\tau,-\omega_d) = e^{j\omega_0\tau}\int_{-\infty}^{+\infty}\psi_t^*(\xi'+\tau)\,\psi_t(\xi')e^{-j\omega_d(\xi'+\tau)}d\xi' = e^{-j\omega_d\tau}x^*(\tau,\omega_d) \quad \textbf{( 3.-40 )}$$

It indicates that $x(\tau,\omega_d)$ is symmetric in first and third quadrants of the complex plane.

- By the same way, we can show that $x(\tau,\omega_d)$ is symmetric in second and fourth quadrant

$$\begin{aligned} x(-\tau,\omega_d) &= e^{j\omega_0\tau}\int_{-\infty}^{+\infty}\psi_t^*(\xi)\,\psi_t(\xi-\tau)e^{j\omega_d\xi}d\xi \\ &\xrightarrow{\xi'=\xi-\tau} e^{j\omega_0\tau}\int_{-\infty}^{+\infty}\psi_t^*(\xi'+\tau)\,\psi_t(\xi')e^{j\omega_d(\xi'-\tau)}d\xi' \\ &= e^{j\omega_d\tau}x^*(\tau,-\omega_d) \end{aligned} \quad \textbf{( 3.-41 )}$$

- Cut along $\tau$ axe

$$x(\tau,0) = e^{-j\omega_0\tau}\int_{-\infty}^{+\infty}\psi_t^*(\xi)\,\psi_t(\xi+\tau)d\xi = R_{\psi_t\psi_t}(\tau) \quad \textbf{( 3.-42 )}$$

Note that the cut $x(\tau,0)$ is the autocorrelation function of $\psi_t(t)$

- Cut along $\omega_d$ axe

$$x(0,\omega_d) = \frac{1}{2\pi}\int_{-\infty}^{+\infty}\Psi_t^*(\omega)\,\Psi_t(\omega-\omega_d)d\omega = \frac{1}{2\pi}R_{\Psi_t\Psi_t}(-\omega_d) \quad \textbf{( 3.-43 )}$$

Via the equation **( 3.-43 )** we can know how $\omega_d$ affects to the matched filter response when it is maximum.

### 3.3.2 Properties of Ambiguity Function

- According to the definition of ambiguity function

$$\begin{aligned}|x(\tau,\omega_d)|^2 &= \left|e^{-j\omega_0\tau}\int_{-\infty}^{+\infty}\psi_t^*(\xi)\,\psi_t(\xi+\tau)e^{j\omega_d\xi}d\xi\right|^2 \\ &= \left|\int_{-\infty}^{+\infty}\psi_t^*(\xi)\,\psi_t(\xi+\tau)e^{j\omega_d\xi}d\xi\right|^2 \le |x(0,0)|^2 = {E_{\psi_t}}^2 = {E_g}^2 \\ &= 4{E_s}^2\end{aligned} \quad \textbf{( 3.-44 )}$$

Where $E_{\psi_t}$,$E_g$ and $E_s$ are the energies of the analytic signal, complex envelope and real signal respectively It means that the maximum will be accomplished when the filter is fully matched.

- The area of ambiguity function is constant independent of the signal waveform **[D. A. Swick, 1969]**

$$\int_{-\infty}^{+\infty}\int_{-\infty}^{+\infty}|x(\tau,\omega_d)|^2 d\tau\, d\omega_d = 2\pi E_{\psi_t} = 2\pi E_g = 8\pi E_s \quad \textbf{( 3.-45 )}$$

- In the same way as **(3.-39)**, the symmetry in first and third quadrants of $|x(\tau,\omega_d)|^2$ is can be demonstrated in the following way

$$|x(-\tau,-\omega_d)|^2 = \left|\frac{1}{2\pi}\int_{-\infty}^{+\infty}\Psi_t^*(\omega)\,\Psi_t(\omega+\omega_d)e^{-j\omega\tau}d\omega\right|^2 \xrightarrow{\omega'=\omega+\omega_d} \left|\frac{1}{2\pi}\int_{-\infty}^{+\infty}\Psi_t^*(\omega'-\omega_d)\,\Psi_t(\omega')e^{-j\omega\tau}d\omega'\right|^2 = |x^*(\tau,-\omega_d)|^2 = |x(\tau,\omega_d)|^2 \quad \textbf{(3.-46)}$$

- To finish, we demonstrate that the ambiguity is symmetric in second and fourth quadrant by writting

$$|x(-\tau,\omega_d)|^2 = \left|\frac{1}{2\pi}\int_{-\infty}^{+\infty}\Psi_t^*(\omega)\,\Psi_t(\omega-\omega_d)e^{-j\omega\tau}d\omega\right|^2 \xrightarrow{\omega'=\omega-\omega_d} \left|\frac{1}{2\pi}\int_{-\infty}^{+\infty}\Psi_t^*(\omega'+\omega_d)\,\Psi_t(\omega')e^{-j(\omega'+\omega_d)\tau}d\omega'\right|^2 = = |x^*(\tau,-\omega_d)|^2 = |x(\tau,-\omega_d)|^2 \quad \textbf{(3.-47)}$$

### 3.3.3 Examples

- **Square pulse**

Let us assume the following transmitted signal

$$s_t(t) = A\,rect\left(\frac{t}{T}\right)\cos[\omega_0 t+\phi_0] \quad \textbf{(3.-48)}$$

Its complex form is

$$g_t(t) = a(t) = A\,rect\left(\frac{t}{T}\right) \overset{TF}{\rightarrow} G(\omega) = AT\,sinc\left(\frac{\omega T}{2}\right) \quad \textbf{(3.-49)}$$

Thus the matched filter response will result

$$\psi_0(t) = \frac{k\alpha^2}{\aleph_0} e^{j(\omega_d+\omega_0)\tau} x(\tau, \omega_d) \quad \textbf{( 3.-50 )}$$

We focus on the uncertain function, $x(\tau, \omega_d)$,

$$\begin{aligned} x(\tau, \omega_d) &= \int_{-\infty}^{+\infty} g_t^*(\xi) g_t(\xi+\tau)\, e^{j\omega_d \xi} d\xi \\ &= A^2 \int_{-\infty}^{+\infty} rect\left(\frac{\xi}{T}\right) rect\left(\frac{\xi+\tau}{T}\right) e^{j\omega_d \xi} d\xi \end{aligned} \quad \textbf{( 3.-51 )}$$

Note that the integral term seems a Fourier transform between the variables $\xi$ and $\omega_d$. To understand the behavior of the term $rect\left(\frac{\xi}{T}\right) rect\left(\frac{\xi+\tau}{T}\right)$, a graphical analysis is carried out. Let us suppose $\tau = -T + \Delta t$, where $\Delta t$ is an infinitesimal time delay, this case is illustrated by Fig 3.-4.

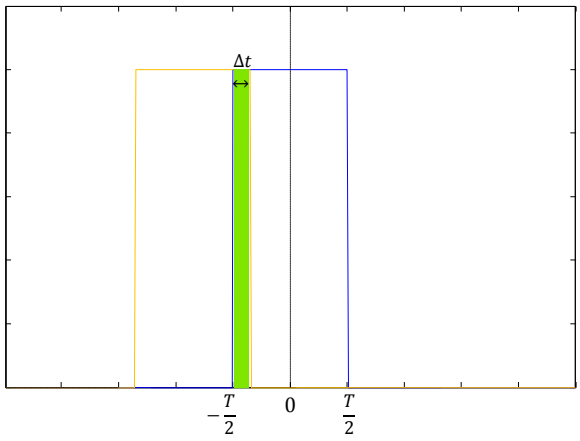


**Fig 3.-4 Ambiguity Function of Square Pulse, $\tau = -T + \Delta t$.**

Thus, the result of the multiplication is a square pulse whose width is $\Delta t$. If $\Delta t$ increases, the width of the pulse too.

Now, let us suppose that the two squares are perfectly centered ($\tau = 0$).

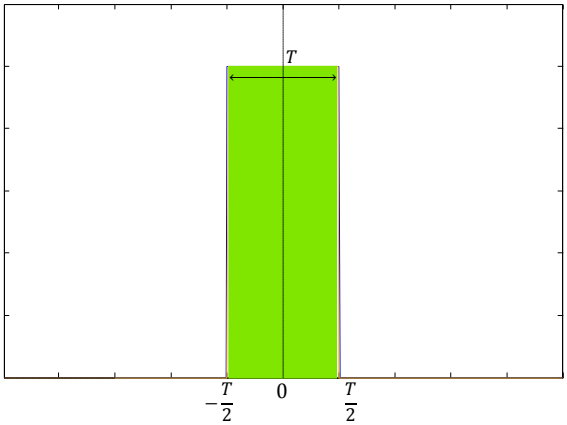


**Fig 3.-5 Ambiguity Function of Square Pulse, $\tau = 0$.**

In the same way as in the preceding case, it results a square pulse, but, whose width is $T$.

Thereby, a $\tau$ shift implies to modify the width of the resulted pulse. By **( 3.-49 )**, we can observe that the width of the pulse affects to the amplitude and scale factor of the spectrum. Furthermore, the central point of the pulse depends also on $\tau$.

Thus,

$$x(\tau, \omega_d) = A^2 T \left(1 - \frac{|\tau|}{T}\right) e^{-j\frac{\omega_d \tau}{2}} sinc\left(\frac{\omega_d T\left(1 - \frac{|\tau|}{T}\right)}{2}\right) \qquad \textbf{( 3.-52 )}$$

Then we focus on the cuts $|x(0, \omega_d)|$ and $|x(\tau, 0)|$. They can be written as

$$|x(0, \omega_d)| = \left|A^2 T\, sinc\left(\frac{\omega_d T}{2}\right)\right| \qquad \textbf{( 3.-53 )}$$

$$|x(\tau, 0)| = \left|A^2 T \left(1 - \frac{|\tau|}{T}\right)\right| = \Lambda\left(\frac{\tau}{T}\right) \qquad \textbf{( 3.-54 )}$$

Where $\Lambda$ is the triangle function.

Fig 3.-6 and 3.-7 illustrate these cuts.

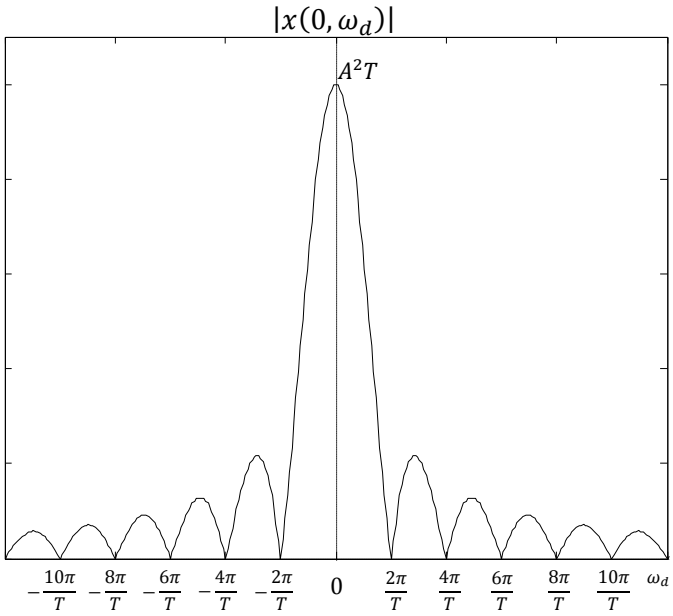


**Fig 3.-6 Ambiguity Function of Square Pulse. Cut $|x(\mathbf{0},\boldsymbol{\omega_d})|$.**

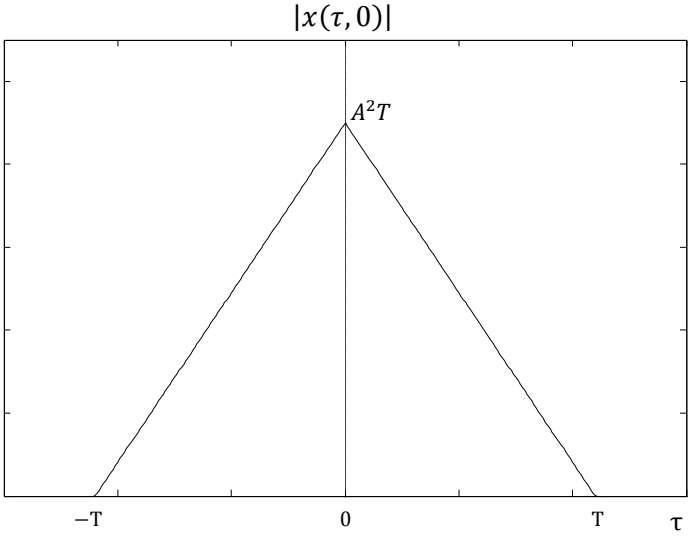


**Fig 3.-7 Ambiguity Function of Square Pulse. Cut $|x(\boldsymbol{\tau},\mathbf{0})|$.**

The cut $|x(0,\omega_d)|$ is the autocorrelation function for a $sinc$ function; it describes the behavior of the matched filter facing moving targets. Note that the output signal fluctuates, this fact supposes a loss of the performance of the matched filter. The cut $|x(\tau,0)|$ is the autocorrelation function for a square signal.

- **Hopping frequency pulse**

Now let is suppose a pulse which has two different frequencies in two different instants. Its it complex envelope is

$$g_t(t) = Arect\left(\frac{t}{T}\right)e^{j(\omega_1+\Delta\omega U(t))t} \quad \textbf{( 3.-55 )}$$

Where $U(t)$ is the step function. Note that when $-\frac{T}{2} < t < 0$ the frequency is $\omega_1$, and when $0 < t < \frac{T}{2}$ the frequency of the signal is $\omega_1 + \Delta\omega$. Thereby, the uncertain function is

$$\begin{aligned} x(\tau,\omega_d) &= \int_{-\infty}^{+\infty} g_t^*(\xi)g_t(\xi+\tau)\,e^{j\omega_d\xi}d\xi \\ &= A^2\int_{-\infty}^{+\infty} rect\left(\frac{\xi}{T}\right)e^{j(\omega_1+\Delta\omega U(\xi))\xi}\,rect\left(\frac{\xi+\tau}{T}\right)e^{-j(\omega_1+\Delta\omega U(\xi+\tau))(\xi+\tau)}e^{j\omega_d\xi}d\xi \\ &= A^2\int_{-\infty}^{+\infty} rect\left(\frac{\xi}{T}\right)\,rect\left(\frac{\xi+\tau}{T}\right)e^{j(\Delta\omega U(\xi)\xi-\omega_1\tau-\Delta\omega U(\xi+\tau)\xi-\Delta\omega U(\xi+\tau)\tau)}e^{j\omega_d\xi}d\xi \\ &= A^2e^{-j\omega_1\tau}\int_{-\infty}^{+\infty} rect\left(\frac{\xi}{T}\right)\,rect\left(\frac{\xi+\tau}{T}\right)e^{j\Delta\omega(U(\xi)\xi-U(\xi+\tau)(\xi+\tau))}e^{j\omega_d\xi}d\xi \end{aligned} \quad \textbf{( 3.-56 )}$$

In the same manner as **( 3.-52 )**, the integral term seems a Fourier transform, and also, it possesses a square function whose width and its central point depend on $\tau$. However, it takes an exponential term, which produces a delay, $\delta(\tau)$, in the signal that depends on $\tau$. This fact provokes that the energy of the signal is concentrated in a time instant as follows.

$$x(\tau,\omega_d) = A^2T\left(1-\frac{|\tau|}{T}\right)e^{-j\frac{\omega_d\tau}{2}}sinc\left(\frac{\omega_dT\left(1-\frac{|\tau|}{T}\right)-\delta(\tau)}{2}\right) \quad \textbf{( 3.-57 )}$$

In the same way as the preceding example, we calculate the cuts of the ambiguity function

$$x(0,\omega_d) = A^2T\,sinc\left(\frac{\omega_dT-\delta(0)}{2}\right) \quad \textbf{( 3.-58 )}$$

$$x(\tau,0) = A^2T\left(1-\frac{|\tau|}{T}\right)sinc\left(\frac{-\delta(\tau)}{2}\right) \quad \textbf{( 3.-59 )}$$

# Chapter 4. Pulse Compression

When a wave propagates through a channel, undesired effects affect to the transmission. One of these effects is the entering of noise in the receiver system. We can diminish some of these effects via applying signal processing techniques in order to improve the detection of the target.

A quality measurement for communications systems is the peak signal power to average noise power ratio, $\frac{S_0}{N_0}$. A good detection is achieved when this ratio is large. We can get a large $\frac{S_0}{N_0}$ by increasing the transmitted energy. This can be done by transmitting along longer time interval. However, in pulsed systems, increase the time transmission produces many blind ranges since the transmitted pulse masks nearby targets; thus the performances of the radar are decreased. Another way to get a good $\frac{S_0}{N_0}$ may be emitting a high peak of energy during a short time instant. This method requires to produce a high stable peak of power during the transmission, and it is quite difficult since it imposes stringent requirements to the design of the transmiter and modulator.

The pulse compression gets a $\frac{S_0}{N_0}$ improvement by transmitting a long pulse and compressing it in the receiver, so that range resolution is not degraded. There are several forms to compress a pulse, and this chapter is focused on compression methods which use frequency modulations.

In the beginning of this chapter, we study the basic concept of pulse compression; next, we focus deeply on usage of FM laws to achieve the compression. Additionally, we study other techniques to carry out the pulse compression.

## 4.1. Basic Concepts

Let us suppose the waveform illustrated in Fig 4.-1, **[F. Quesada et al., 2010]**

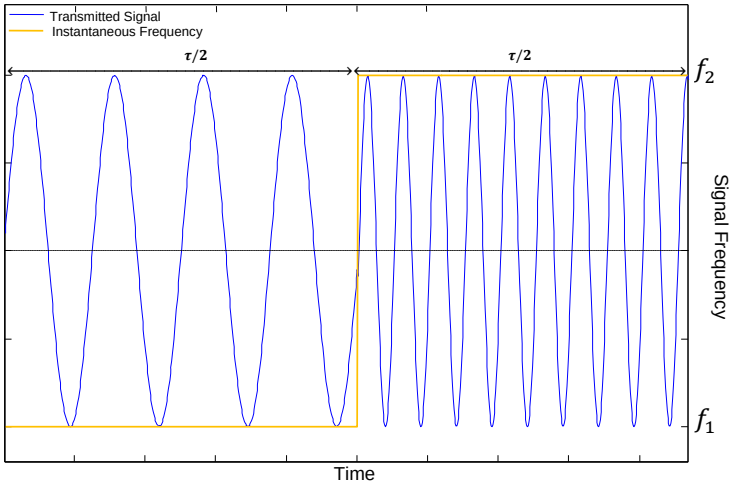


**Fig 4.-1 Transmitted Signal. Pulse Compression Basic Concept.**

The signal is formed by two frequencies, each one being transmitted for $\frac{\tau}{2}$ interval.

Next, we assume the block diagram for the receiver system as Fig 4.-2 shows

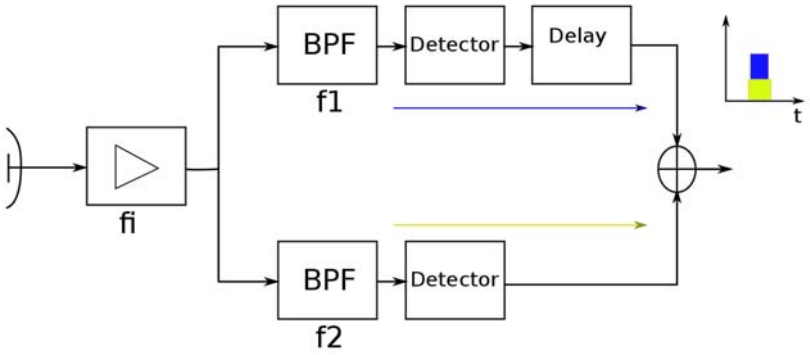


**Fig 4.-2: Block Diagram. Pulse Compression Basic Concept.**

As Fig 4.-2 depicts, $f_1$ and $f_2$ are splitted by the band pass filters, then $f_1$ is delayed $\frac{\tau}{2}$ respect $f_2$. This delay provokes the energy in $f_1$ transmission period is added to the energy signal in $f_2$ transmission period.

Instead of using two just frequencies and the block diagram illustrated in Fig 4.-2, a matched filter and either frequency or phase modulation are used in more practical systems.

## 4.2 Linear FM pulse (CHIRP)

The pulse CHIRP consists of linear frequency modulation, thus it is defined as **[Peyton Z. Peebles Jr, 1998]**

$$s(t) = Arect\left(\frac{t}{T}\right)\cos\left(\omega_0 t + \phi_0 + \frac{\mu}{2}t^2\right) \quad \textbf{( 4.-1 )}$$

Where $A$, $T$, $\omega_0$, and $\mu$ are positive constants and $\phi_0$ is an arbitrary phase angle. The parameter $\mu$ defines the instantaneous frequency slope.

$$\mu = \frac{\Delta\omega}{T}\left(\frac{rad}{s^2}\right) \quad \textbf{( 4.-2 )}$$

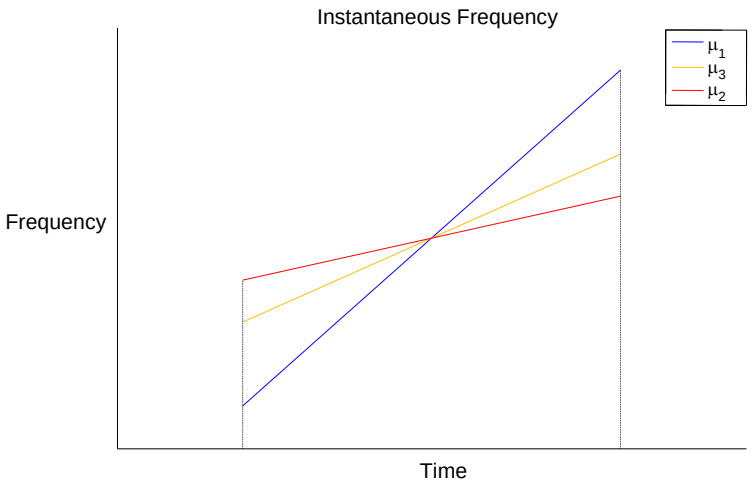


**Fig 4.-3: Instantaneous Frequency for various values of $\mu$. $\mu_1 < \mu_2 < \mu_3$.**

Thus, the instantaneous frequency is calculated as

$$\omega_i = \frac{d\theta(t)}{dt} = \frac{d}{dt}\left[\omega_0 t + \phi_0 + \frac{\mu}{2}t^2\right] = \omega_0 + \mu t \qquad \textbf{( 4.-3 )}$$

In order to study the CHIRP pulse, we do an analytic analysis of **( 4.-1 )**. Therefore, we use the following signal form by using **( 2.-22 )**.

$$\psi_t(t) = Arect\left(\frac{t}{T}\right) e^{j\frac{\mu}{2}t^2} e^{j(\omega_0 t + \phi_0)} \qquad \textbf{( 4.-4 )}$$

Thereby, the reflected back to the receiver signal takes the following form

$$\psi_r(t) = \alpha\psi_t(t - \tau_R) e^{j\omega_d(t-\tau_R)} \qquad \textbf{( 4.-5 )}$$

Where $\alpha$ is a constant related to the amplitude of the received signal.

The signal in equation **( 4.-5 )** is filtered via the following filter response

$$z(t) = \frac{k\alpha}{\aleph_0}\psi_t{}^*(t_0 - \tau_r - t) \qquad \textbf{( 4.-6 )}$$

Therefore, we obtain in the output of the matched filter

$$\psi_0(t) = \frac{k\alpha^2}{\aleph_0} e^{j(\omega_0+\omega_d)(t-t_0)} x(t-t_0, \omega_d) \quad \textbf{( 4.-7 )}$$

Now we focus on the term $x(t-t_0, \omega_d)$, it is the uncertain function (section 3.3).By taking $\tau = t - t_0$

$$x(\tau, \omega_d) = e^{-j\omega_0\tau} \int_{-\infty}^{+\infty} \psi_t^*(\xi)\, \psi_t(\xi+\tau) e^{j\omega_d\xi} d\xi \quad \textbf{( 4.-8 )}$$

And, by replacing **( 4.-4 )** into **( 4.-9 )**

$$\begin{aligned} x(\tau, \omega_d) = e^{-j\omega_0\tau} \int_{-\infty}^{+\infty} & Arect\left(\frac{\xi}{T}\right) e^{-j\frac{\mu}{2}\xi^2} e^{-j(\omega_0\xi+\phi_0)} \\ & Arect\left(\frac{\xi+\tau}{T}\right) e^{j\frac{\mu}{2}(\xi+\tau)^2} e^{j(\omega_0(\xi+\tau)+\phi_0)} e^{j\omega_d\xi} d\xi = \\ A^2 e^{j\frac{\mu}{2}\tau^2} \int_{-\infty}^{+\infty} & rect\left(\frac{\xi}{T}\right) rect\left(\frac{\xi+\tau}{T}\right) e^{j\frac{\mu}{2}(2\tau\xi+\xi^2)} e^{j\omega_d\xi} d\xi \end{aligned} \quad \textbf{( 4.-9 )}$$

Equation **( 4.-9 )** seems a Fourier transform. The function into the integral, $rect\left(\frac{\xi}{T}\right) rect\left(\frac{\xi+\tau}{T}\right) e^{j\omega_d\xi}$, is a square function which has a delay term, and whose width depends on the variable $\tau$. Additionally, there is a quadratic delay term that depends on $\tau$ and $\xi$. Thus it results

$$x(\tau, \omega_d) = \begin{cases} A^2 T\left(1-\frac{|\tau|}{T}\right) e^{-j\omega_d\frac{\tau}{2}} sinc\left[\frac{T}{2}\left(1-\frac{|\tau|}{T}\right)(\mu\tau+\omega_d)\right] & -T \le \tau \le T \\ 0 & elsewhere \end{cases} \quad \textbf{( 4.-10 )}$$

Since **( 4.-10 )** is a complicate function, **( 4.-10 )** cuts are often used to observe its behaviour. The most important and useful cuts are

$$x(\tau, \omega_d = 0) = \begin{cases} AT\left(1-\frac{|\tau|}{T}\right) e^{j\frac{\mu}{2}\tau^2} sinc\left[\frac{\Delta\omega}{2}\left(1-\frac{|\tau|}{T}\right)\right] & -T \le \tau \le T \\ 0 & elsewhere \end{cases} \quad \textbf{( 4.-11 )}$$

And

$$x(\tau = 0, \omega_d) = A^2 T sinc\left[\frac{T}{2}\omega_d\right] \qquad \textbf{( 4.-12 )}$$

We illustrate these cuts in Fig 4.-4

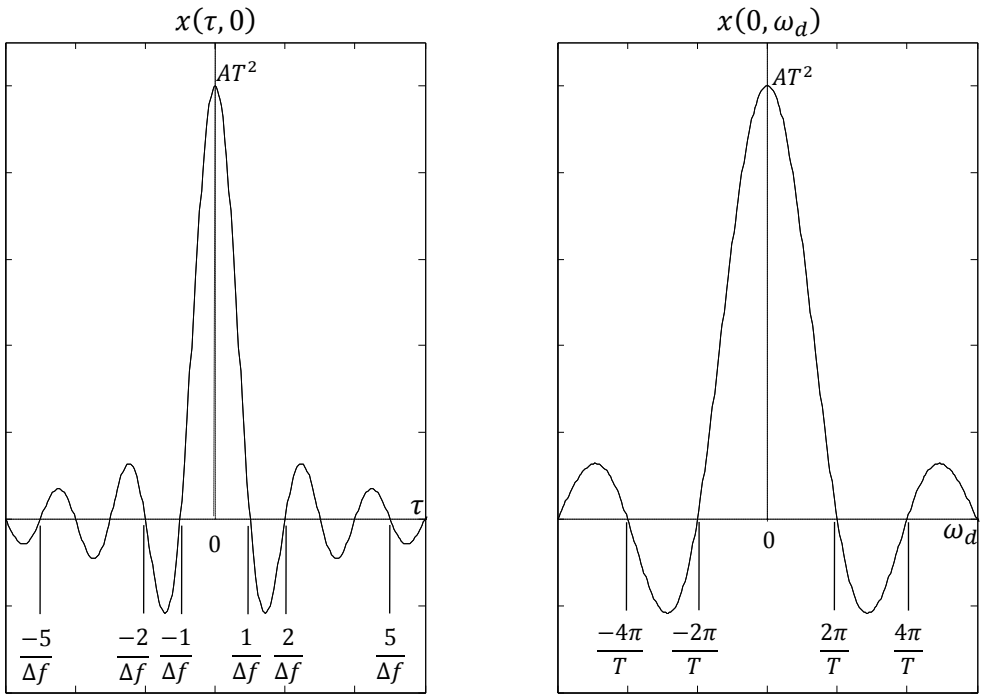


**Fig 4.-4: Cuts of Ambiguity Function of CHIRP Pulse.**

Also it is interesting to observe the contour of **( 4.-10 )** by normalizing and fixing the signal amplitude at $-3.92\ dB$, as

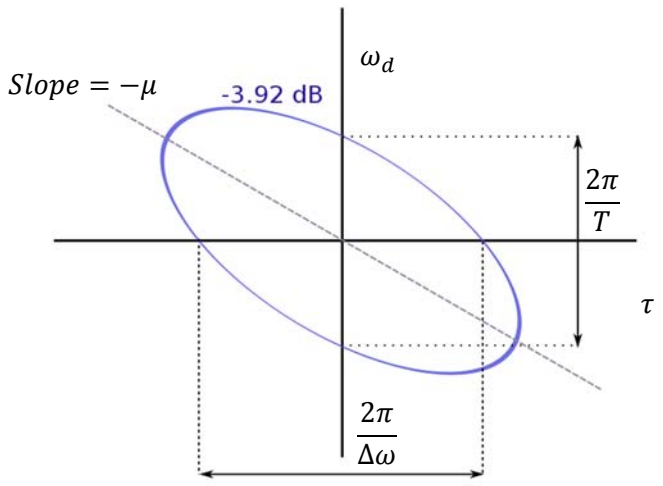


**Fig 4.-5: Contour of Ambiguity Function of CHIRP Pulse.**

**Conclusions:**

As **( 4.-11 )** equation describes, the function $sinc$ depends on $\tau$, $\omega_d$, and $\mu$. The $\mu$ dependency provokes a slope variation in **( 4.-11 )** contour. Therefore, $\mu$ is an important design variable. Note that the maximum of $x(\tau, \omega_d)$ is accomplished in $\tau = 0$ and $\omega_d = 0$, and this situation corresponds with a full matched case. Also the $x(\tau, 0)$ cut shows that the maximum value produced by the matched filter is situated in $\tau = t - t_0 = 0 \rightarrow t = t_0$, as it was explained in section 3.2. If we account for the Doppler effect, a maximum value deviation and attenuation are observed -they are very undesired effects since they will affect the compression capabilities of the algorithm. The following figure depicts a 3-D representation of $x(\tau, \omega_d)$.

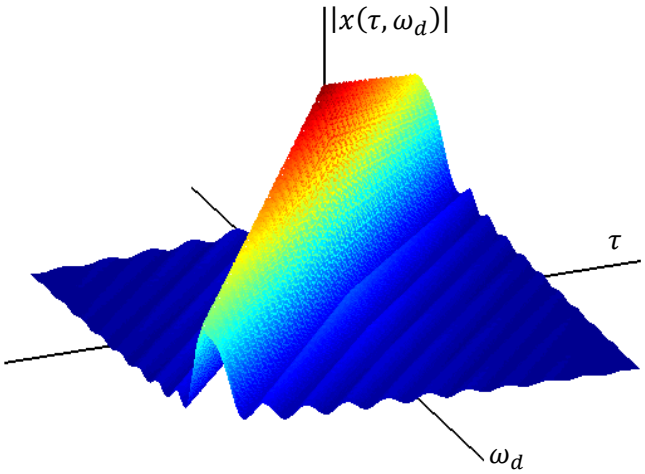


**Fig 4.-6: 3D Ambiguity Function of CHIRP Pulse.**

**Spectrum of CHIRP pulse**

To finish the study of CHIRP pulse, we analyse its spectrum **[Peyton Z. Peebles Jr, 1998]**. By taking the complex envelope of **( 4.-5 )** we write

$$g(t) = Arect\left(\frac{t}{T}\right) e^{j\frac{\mu}{2}t^2} \qquad \textbf{( 4.-13 )}$$

Next, we apply the Fourier transform to it

$$G(\omega) = \int_{-\infty}^{+\infty} Arect\left(\frac{t}{T}\right) e^{j\frac{\mu}{2}t^2} e^{-j\omega t}\, dt = A\int_{-T/2}^{T/2} e^{j\frac{\mu}{2}t^2} e^{-j\omega t}\, dt \qquad \textbf{( 4.-14 )}$$

Next, making the variable change $x = \sqrt{\frac{\mu}{\pi}}\left(t - \frac{\omega}{\mu}\right)$

- Upper limit: $x_u = \sqrt{\frac{\mu}{\pi}}\left(\frac{T}{2} - \frac{\omega}{\mu}\right) = \sqrt{\frac{\Delta f T}{2}}\left(1 - \frac{2f}{\Delta f}\right)$
- Lower limit: $x_l = -\sqrt{\frac{\mu}{\pi}}\left(\frac{T}{2} + \frac{\omega}{\mu}\right) = -\sqrt{\frac{\Delta f T}{2}}\left(1 + \frac{2f}{\Delta f}\right)$
- Differential term: $\mathrm{d}x = \sqrt{\frac{\mu}{\pi}}dt$

Thus

$$G(\omega) = A\sqrt{\frac{\mu}{\pi}}e^{j\frac{\mu}{2}\omega^2}\int_{x_l}^{x_u} e^{j\frac{\pi}{2}x^2}\,dx = A\sqrt{\frac{\mu}{\pi}}e^{j\frac{\mu}{2}\omega^2}\left[\int_0^{x_u} e^{j\frac{\pi}{2}x^2}\,dx - \int_0^{x_l} e^{j\frac{\pi}{2}x^2}\,dx\right] \quad \textbf{( 4.-15 )}$$

The integral terms are related to the Fresnel integrals, $C(x)$ and $S(x)$, and they are defined as

$$C(x) = \int_0^x \cos\left(\frac{\pi}{2}\xi^2\right)d\xi \quad \textbf{( 4.-16 )}$$

$$S(x) = \int_0^x \sin\left(\frac{\pi}{2}\xi^2\right)d\xi \quad \textbf{( 4.-17 )}$$

Note that

$$C(-x) = -C(x) \quad \textbf{( 4.-18 )}$$

$$S(-x) = -S(x) \quad \textbf{( 4.-19 )}$$

Both functions are depicted in Fig 4.-7.

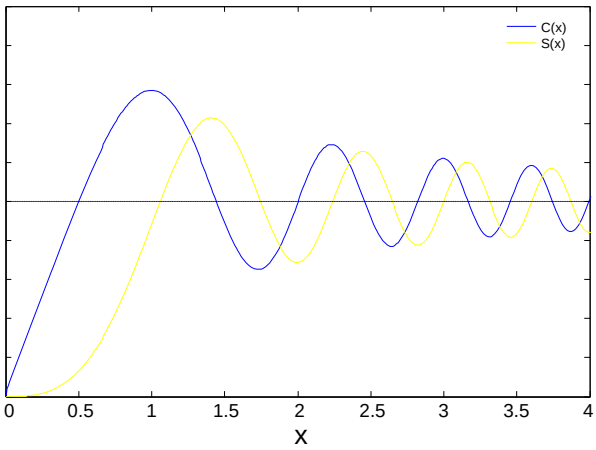


**Fig 4.-7: Fresnell Integral Functions.**

Note that these functions present the next limits

$$\lim_{x\to+\infty} C(x) = \frac{1}{2} \quad \textbf{( 4.-20 )}$$

$$\lim_{x\to+\infty} S(x) = \frac{1}{2} \quad \textbf{( 4.-21 )}$$

Therefore, by using **( 4.-17 )** and **( 4.-18 )**, we obtain

$$G(\omega) = A\sqrt{\frac{\mu}{\pi}}e^{j\frac{\mu}{2}\omega^2}\left[\frac{\big(C(x_u)+C(x_l)\big)+j\big(S(x_u)+S(x_l)\big)}{\sqrt{2}}\right] \quad \textbf{( 4.-22 )}$$

There are two important terms in equation **( 4.-22 )**. The first one is a quadratic shift phase term, $e^{j\frac{\mu}{2}\omega^2}$, and the other one is the complex term inside the brackets. This term (inside the brackets) depends on the values $x_u$ and $x_l$, which are the upper and lower limits, and these variables depend on as much to the variable $f$ as to the product $\Delta fT$. Thereby when $\Delta fT$ increases, the complex term approaches its asymptotic value. According to the fig 4.-7, the amplitude of $C(x)$ and $S(x)$ is reduced it $\Delta fT$ increases. This fact provokes a more stable phase and modulus; Fig 4.-8 and Fig 4.-9 illustrates this behavior. Thus, when $\Delta fT \to +\infty$

$$G(\omega) = A\sqrt{\frac{\mu}{\pi}}e^{j\frac{\mu}{2}\omega^2}\left[\frac{1+j}{\sqrt{2}}\right] = AT\sqrt{\frac{2\pi}{\Delta\omega T}}e^{-j\frac{\omega^2 T}{2\Delta\omega}+j\frac{\pi}{4}} \quad \textbf{( 4.-23 )}$$

The complex term suffers a $\frac{\pi}{4}$ phase shift.

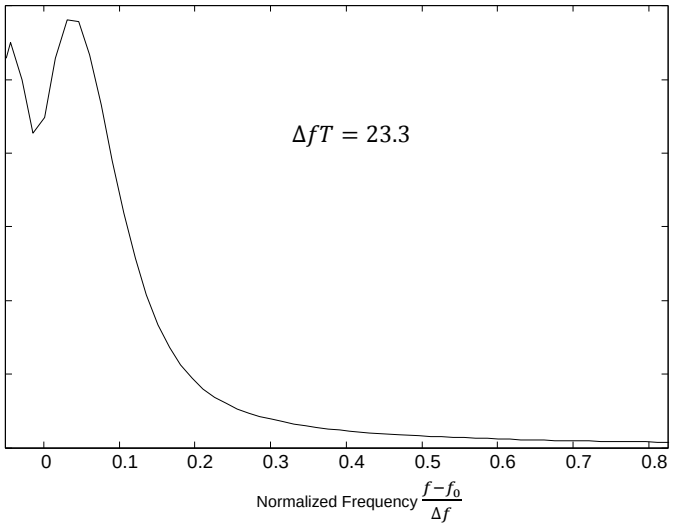


**Fig 4.-8: CHIRP Pulse Spectrum. $\Delta fT = 23.3$.**

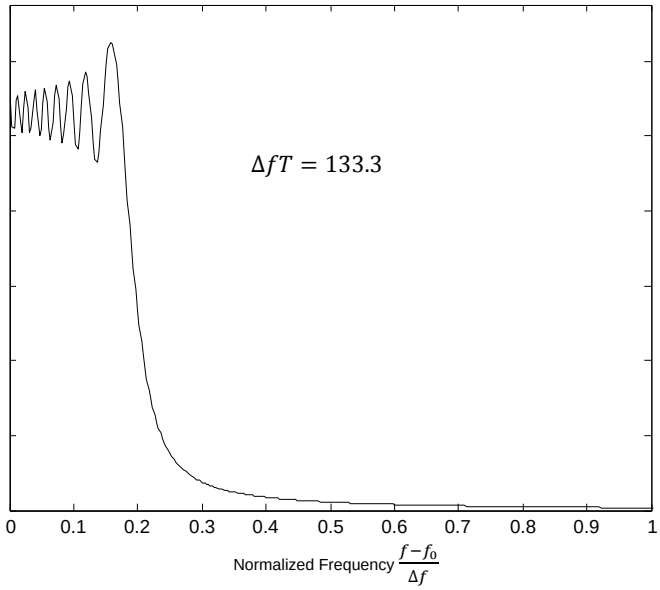


**Fig 4.-9 CHIRP Pulse Spectrum. $\Delta fT = 133.3$.**

## 4.3 Sidelobes suppression

One of the matched filtering issues is the sidelobes presence in the output signal. Thereby, a low scatter target may be masked by a larger scatter target as Fig 4.-10 shows **[S. D. Blunt & K. Gerlach, 2003]**.

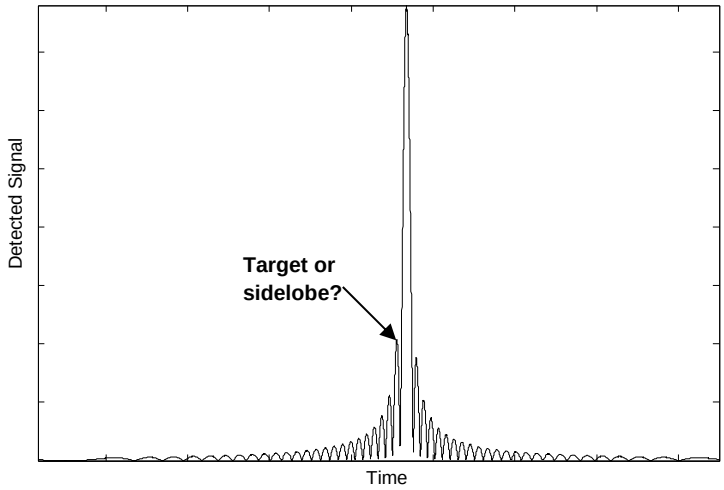


**Fig 4.-10: Small target masked by another bigger one.**

There are several strategies that can be used to decrease the sidelobes level. In this section we study three of them. They are:

- Mismatched filtering.
- Signal design by using FM laws.
- Adaptive pulse compression algorithms.

The last one is discussed less in detail, and more information can be found in **[B. Zrnic et al., 1998]**, **[S. D. Blunt & K. Gerlach, 2003]**, **[S. D. Blunt & K. Gerlach, 2004]** and **[S. D. Blunt et al., 2009]**.

### 4.3.1 Mismatched filtering

As it is depicted in Fig 4.-4, where an ambiguity function cuts are shown, it is possible to observe an undesired effect namely, the sidelobes presence. In order to reduce them, we can place another filter at the output of the matched filter. Because the filters are connected in cascade, the overall system is mismatched, thus the second filter is known as mismatched filter **[Peyton Z. Peebles Jr, 1998]**. We study several filter transfers functions to achieve the sidelobes taper.

#### Dolph-Tchebycheff Filter

The pulse compression sidelobes problem in time domain is analogous to the antennas sidelobes issue in the spatial or angular domain **[Peyton Z. Peebles Jr, 1998]**. Thus equivalent methods can be used in sidelobes reduction. The Dolph-Tchebycheff filter implements an ideal transfer function. This fact means that it is unrealizable, therefore, it is not a practical filter. However, there are methods to approximate this filter transfer function with other similar but more practical transfer functions.

#### Taylor´s Filter

The Taylor´s filter consists of a practical approximation to the Dolph-Tchebycheff distribution **[Peyton Z. Peebles Jr, 1998]**. Taylor´s filter increases the main lobe and decreases the sidelobes a below specified level. Also the main lobe becomes wider in time.

The normalized transfer function is

$$H_T(\omega) = K_T\left\{1 + 2\sum_{m=1}^{\bar{n}-1} F_m \cos\left(\frac{2\pi m\omega}{\Delta\omega}\right)\right\} rect\left(\frac{\omega}{\Delta\omega}\right) \qquad (4.-24)$$

Where $\bar{n}$ is an integer design parameter. Also

$$K_T = \frac{1}{1 + 2\sum_{m=1}^{\bar{n}-1} F_m} \quad \textbf{( 4.-25 )}$$

$$F_m = \begin{cases} (-1)^m \prod_{n=1}^{\bar{n}-1} \left\{ 1 - \left[ \frac{m^2 \sigma_T^{-2}}{A^2 + (n-0.5)^2} \right] \right\} & m = 1,2,3,\ldots \\ 0 & m \geq \bar{n} \end{cases} \quad \textbf{( 4.-26 )}$$

$$A = \frac{1}{\pi} \cosh^{-1}\left(10^{-SLL/20}\right) \quad \textbf{( 4.-27 )}$$

$$\sigma_T^2 = \frac{\bar{n}^2}{A^2 + (\bar{n} - 0.5)^2} \geq 1 \quad \textbf{( 4.-28 )}$$

And $\Delta\omega$ is the FM modulation index used to build the transmitted CHIRP pulse.

After compressing the received CHIRP signal, the mismatched filter output is

$$s(t) = K_T \frac{\Delta\omega}{2\pi} \sum_{m=-(\bar{n}-1)}^{\bar{n}-1} F_m \operatorname{sinc}\left(\frac{\Delta\omega t}{2} + m\pi\right) \quad \textbf{( 4.-29 )}$$

Where $F_{-m} = F_m$ and $F_0 = 1$.

The $-3dB$ pulse width is

$$\tau_T = \sigma_T \tau_D \quad \textbf{( 4.-30 )}$$

Where

$$\tau_D = \frac{4}{\Delta\omega} \left\{ \left[\cosh^{-1}\left(10^{-SLL/20}\right)\right]^2 - \left[\cosh^{-1}\left(\frac{10^{-SLL/20}}{\sqrt{2}}\right)\right]^2 \right\}^{1/2} \quad \textbf{( 4.-31 )}$$

The signal to noise ratio at Taylor´s filter output is related to the matched filter output as

$$\left(\frac{\hat{S}_0}{N_0}\right)_{mf} = \left[1 + 2\sum_{m=1}^{\bar{n}-1} {F_m}^2\right]\left(\frac{\hat{S}_0}{N_0}\right)_{Taylor} \quad \textbf{( 4.-32 )}$$

Where $F_m$ is calculated in equation (4.-26).The bracketed factor represents the signal to noise ratio loss.

**Truncated Taylor´s Filter**

If we observe the $F_m$ values, which are tabulated in **[Peyton Z. Peebles Jr, 1998]**, we find that the largest value is $F_1$. We can get a simpler Taylor´s response by truncating the $\sum_{m=1}^{\bar{n}-1} {F_m}^2$ to $F_1$ **[Peyton Z. Peebles Jr, 1998]**. Therefore the new normalized transfer function is

$$H_T(\omega)|_{truncated} = \frac{1}{1+2F_1}\left\{1 + 2F_1 \cos\left(\frac{2\pi\omega}{\Delta\omega}\right)\right\} rect\left(\frac{\omega}{\Delta\omega}\right) \quad \textbf{( 4.-33 )}$$

Another form of **( 4.-33 )** is

$$H_T(\omega)|_{truncated} = \left\{k + (1-k)\cos^2\left(\frac{2\pi\omega}{\Delta\omega}\right)\right\} rect\left(\frac{\omega}{\Delta\omega}\right) \quad \textbf{( 4.-34 )}$$

Where

$$k = \frac{1-2F_1}{1+2F_1} \quad \textbf{( 4.-35 )}$$

A more generalized form of **( 4.-34 )** is

$$H_T(\omega)|_{truncated} = \left\{k + (1-k)\cos^n\left(\frac{2\pi\omega}{\Delta\omega}\right)\right\} rect\left(\frac{\omega}{\Delta\omega}\right) \quad \textbf{( 4.-36 )}$$

### 4.3.2 Signal Design by using FM laws

Others method to achieve low sidelobes levels exists. One of them is the usage of FM laws. This method do not need mismatched filters **[Peyton Z. Peebles Jr, 1998]**. The analysis of these signals is quiet difficult, but when the $\Delta fT$ product is high, we can use approximations. The FM laws design is based on the Stationary Phase Principle, which is explained below.

**Stationary Phase Principle**

Given the following envelope function $g(t) = a(t)e^{j\theta(t)}$, its Fourier transform is defined as

$$G(\omega) = \int_{-\infty}^{+\infty} a(t)e^{j\theta(t)}e^{-j\omega t}dt = \int_{-\infty}^{+\infty} a(t)e^{j\theta(t)-j\omega t}dt \qquad \textbf{( 4.-37 )}$$

Therefore, the phase term of **( 4.-37 )** is $\theta(t) - \omega t$. Given a $\tau$, using Taylor approximation, it can be written

$$\begin{aligned}\theta(t) - \omega t \approx [\theta(t) - \omega t]|_{t=\tau} + \frac{d[\theta(t) - \omega t]}{dt}|_{t=\tau}(t-\tau) \\ + \frac{d^2[\theta(t) - \omega t]}{dt^2}|_{t=\tau}\frac{(t-\tau)^2}{2} + \cdots \\ = \theta(\tau) - \omega\tau + \left[\dot{\theta}(\tau) - \omega\right](t-\tau) + \frac{\ddot{\theta}(\tau)}{2}(t-\tau)^2\end{aligned} \qquad \textbf{( 4.-38 )}$$

Where the cubic and higher order terms are neglected; and where $\dot{f}(x)$ is the first derivate of $f$ respect $x$ and $\ddot{\theta}(\tau)$ is the second derivate. This approximation is valid in the vicinity around $\tau$: $\tau + \frac{\varepsilon}{2} > t > \tau - \frac{\varepsilon}{2}$.

Given a $\omega = \lambda$, that meets this condition $\dot{\theta}(\tau) - \lambda = 0$ the expression **( 4.-38 )** can be simplified as

$$\theta(t) - \lambda t \approx \theta(\tau) - \lambda\tau + \frac{\ddot{\theta}(\tau)}{2}(t-\tau)^2 \qquad \textbf{( 4.-39 )}$$

Replacing the phase term in the integral expression **( 4.-37 )**

$$G(\lambda) = \int_{\tau-\frac{\varepsilon}{2}}^{\tau+\frac{\varepsilon}{2}} a(t) e^{j\left[\theta(\tau)-\lambda\tau+\frac{\ddot{\theta}(\tau)}{2}(t-\tau)^2\right]} dt = a(t) e^{j[\theta(\tau)-\lambda\tau]} \int_{\tau-\frac{\varepsilon}{2}}^{\tau+\frac{\varepsilon}{2}} e^{\pm j\frac{|\ddot{\theta}(\tau)|}{2}(t-\tau)^2} dt \quad \textbf{( 4.-40 )}$$

Next, making the variable change $x = \sqrt{\frac{|\ddot{\theta}(\tau)|}{\pi}}(t-\tau) \rightarrow (t-\tau)^2 = \frac{\pi}{|\ddot{\theta}(\tau)|}x^2$

- Upper limit: $x_u = \sqrt{\frac{|\ddot{\theta}(\tau)|}{\pi}}\left(\frac{\varepsilon}{2}\right)$
- Lower limit: $x_l = \sqrt{\frac{|\ddot{\theta}(\tau)|}{\pi}}\left(-\frac{\varepsilon}{2}\right) = -x_u$
- Differential term: $\mathrm{d}x = \sqrt{\frac{|\ddot{\theta}(\tau)|}{\pi}} dt \rightarrow \mathrm{d}t = \sqrt{\frac{\pi}{|\ddot{\theta}(\tau)|}} dx$

Thus

$$\begin{aligned} G(\lambda) &= \sqrt{\frac{\pi}{|\ddot{\theta}(\tau)|}} a(\tau) e^{j[\theta(\tau)-\lambda\tau]} \int_{-x_u}^{x_u} e^{\pm j\frac{\pi}{2}x^2} dx \\ &= \sqrt{\frac{\pi}{|\ddot{\theta}(\tau)|}} a(\tau) e^{j[\theta(\tau)-\lambda\tau]} 2[C(x_u) \pm jS(x_u)] \end{aligned} \quad \textbf{( 4.-41 )}$$

Where $x_u = \sqrt{\frac{|\ddot{\theta}(\tau)|}{\pi}}\left(\frac{\varepsilon}{2}\right)$, and $C(x)$ and $S(x)$ are the Fresnel integrals.

If $|\ddot{\theta}(\tau)| \gg 1$ is assumed the Fresnel integrals can be replaced by their asymptotic values. This fact leads to

$$G(\lambda) = \sqrt{\frac{\pi}{|\ddot{\theta}(\tau)|}} a(\tau) e^{j[\theta(\tau)-\lambda\tau]} 2\left[\frac{1}{\sqrt{2}} \pm j\frac{1}{\sqrt{2}}\right] = \sqrt{\frac{2\pi}{|\ddot{\theta}(\tau)|}} a(\tau) e^{j\left[\theta(\tau)-\lambda\tau\pm\frac{\pi}{4}\right]} \quad \textbf{( 4.-42 )}$$

The stationary Phase Principle has been defined in time domain, this procedure is interesting in the frequency domain too. Starting from arbitrary spectrum $G(\omega) = A(w)e^{j\varphi(\omega)}$, applying inverse Fourier transform

$$g(t) = \frac{1}{2\pi}\int_{-\infty}^{+\infty} A(\omega) e^{j\varphi(\omega)} e^{j\omega t} d\omega = \frac{1}{2\pi}\int_{-\infty}^{+\infty} A(\omega) e^{j\varphi(\omega)+j\omega t} d\omega \quad \textbf{( 4.-43 )}$$

Given a fixed frequency $\lambda$ the phase term of **( 4.-43 )** is approximated by Taylor as

$$\begin{aligned}\varphi(\omega)+\omega t &\approx [\varphi(\omega)+\omega t]|_{\omega=\lambda}+\frac{d[\varphi(\omega)+\omega t]}{d\omega}|_{\omega=\lambda}(\omega-\lambda)\\ &+\frac{d^2[\varphi(\omega)+\omega t]}{d\omega^2}|_{\omega=\lambda}\frac{(\omega-\lambda)^2}{2}+\cdots\\ &=\varphi(\lambda)+\lambda t+[\dot{\varphi}(\lambda)+t](\omega-\lambda)+\frac{\ddot{\varphi}(\omega)}{2}(\omega-\lambda)^2\end{aligned} \quad \textbf{( 4.-44 )}$$

Where $\omega$ is evaluated in the vicinity of $\lambda$ $\left(\lambda+\frac{\phi}{2}>\omega>\lambda-\frac{\phi}{2}\right)$ and the terms higher than the second order have been neglected. Given a $\tau$ that fulfils this condition $\dot{\varphi}(\lambda)+\tau=0$, the expression **( 4.-44 )** is simplified as

$$\varphi(\omega)+\omega\tau\approx\varphi(\lambda)+\lambda\tau+\frac{\ddot{\varphi}(\omega)}{2}(\omega-\lambda)^2 \quad \textbf{( 4.-45 )}$$

We can substitute the phase term of the integral in equation **( 4.-43 )**

$$\begin{aligned}g(\tau)&=\frac{1}{2\pi}\int_{\lambda-\frac{\phi}{2}}^{\lambda+\frac{\phi}{2}}A(\lambda)e^{j\left(\varphi(\lambda)+\lambda t+\frac{\ddot{\varphi}(\omega)}{2}(\omega-\lambda)^2\right)}d\omega\\ &=\frac{A(\lambda)}{2\pi}e^{j(\varphi(\lambda)+\lambda\tau)}\int_{\lambda-\frac{\phi}{2}}^{\lambda+\frac{\phi}{2}}e^{\pm j\frac{|\ddot{\varphi}(\omega)|}{2}(\omega-\lambda)^2}d\omega\end{aligned} \quad \textbf{( 4.-46 )}$$

Now, making the change of variables $y=\sqrt{\frac{|\ddot{\varphi}(\omega)|}{\pi}}(\omega-\lambda)\ \rightarrow\ (\omega-\lambda)^2=\frac{\pi}{|\ddot{\varphi}(\omega)|}y^2$

- Upper limit: $y_u=\sqrt{\frac{|\ddot{\varphi}(\omega)|}{\pi}}\left(\frac{\phi}{2}\right)$
- Lower limit: $y_l=\sqrt{\frac{|\ddot{\varphi}(\omega)|}{\pi}}\left(-\frac{\phi}{2}\right)=-y_u$
- Differential term: $\mathrm{d}y=\sqrt{\frac{|\ddot{\varphi}(\omega)|}{\pi}}d\omega\ \rightarrow\ \mathrm{d}\omega=\sqrt{\frac{\pi}{|\ddot{\varphi}(\omega)|}}dy$

Thus the integral **( 4.-46 )** is rewritten as

$$\begin{aligned}g(\tau)&=\sqrt{\frac{\pi}{|\ddot{\varphi}(\omega)|}}\frac{A(\lambda)}{2\pi}e^{j(\varphi(\lambda)+\lambda\tau)}\int_{-y_u}^{y_u}e^{\pm j\frac{pi}{2}y^2}dy\\ &=\sqrt{\frac{1}{\pi|\ddot{\varphi}(\omega)|}}A(\lambda)e^{j(\varphi(\lambda)+\lambda\tau)}\left[C(y_u)\pm jS(y_u)\right]\end{aligned} \quad \textbf{( 4.-47 )}$$

Where $y_u = \sqrt{\frac{|\ddot{\varphi}(\omega)|}{\pi}}\left(\frac{\phi}{2}\right)$.

In same way as in time domain, if $|\ddot{\varphi}(\omega)| \gg 1$ is assumed the Fresnel integrals can be replaced by their asymptotic values. This condition leads to

$$g(\tau) = \sqrt{\frac{1}{|\ddot{\varphi}(\omega)|}} A(\lambda) e^{j(\varphi(\lambda)+\lambda\tau)} \left[\frac{1}{\sqrt{2}} \pm j\frac{1}{\sqrt{2}}\right] = \sqrt{\frac{1}{2\pi|\ddot{\varphi}(\omega)|}} A(\lambda) e^{j\left(\varphi(\lambda)+\lambda\tau\pm\frac{\pi}{4}\right)} \quad \textbf{( 4.-48 )}$$

**Relation between Stationary Phase Principle in time domain and in frequency domain:**

Starting from the preceding expressions and preceding conditions, we can relate the obtained results

$$\dot{\theta}(\tau) = \lambda \rightarrow \theta(\tau) = \int \lambda \, d\tau = \lambda\tau \quad \textbf{( 4.-49 )}$$

$$\dot{\varphi}(\lambda) = -\tau \rightarrow \varphi(\lambda) = \int \tau \, d\lambda = -\lambda\tau \quad \textbf{( 4.-50 )}$$

Equating the amplitudes of **( 4.-39 )** and **( 4.-43 )**, we get

$$|G(\lambda)| = A(\lambda) = \sqrt{\frac{2\pi}{|\ddot{\theta}(\tau)|}} a(\tau) \quad \textbf{( 4.-51 )}$$

$$|g(\tau)| = a(\tau) = \frac{1}{\sqrt{2\pi|\ddot{\varphi}(\omega)|}} A(\lambda) \quad \textbf{( 4.-52 )}$$

We can find a relationship between the Group Delay and the inverse function of the instantaneous frequency. Similar relations can also be established between the instantaneous frequency and the inverse function of the Group Delay too

$$\omega_i(\tau) = \lambda = T_d^{-1}(\tau) \quad \textbf{( 4.-53 )} \qquad T_d(\lambda) = -\tau = w_i^{-1}(\lambda) \quad \textbf{( 4.-54 )}$$

These two couples of equations are the most interesting ones for the signal synthesis problem.

**Signal design using Stationary Phase Principle.**

This technique starts specifying two of the following functions: $a(\tau)$, $A(\lambda)$, $\theta(\tau)$ and $\varphi(\lambda)$; and the preceding results are used to find the other functions. A couple of related options are not interesting to be selected. For example, $\theta(\tau)$ and $\varphi(\lambda)$; since they are directly related through equation **(4.-49)** and **(4.-50)**. The specifications of $a(\tau)$ and $\theta(\tau)$ or $A(\lambda)$ and $\varphi(\lambda)$ are not useful, because we could use the Fourier transform and inverse Fourier transform applied to one pair, respectively, to obtain the other.

The remaining options are $[a(\tau), \varphi(\lambda)]$, $[A(\lambda), \theta(\tau)]$ and $[a(\tau), A(\lambda)]$ . Of these combinations the last one is the most interesting.

Here, we remember that the matched filter output studied or the uncertain function is

$$x(0, \omega_d) = \int_{-\infty}^{+\infty} a(\xi)^2 e^{-j\omega_d \xi} d\xi \qquad \textbf{( 4.-55 )}$$

$$x(\tau, 0) = \int_{-\infty}^{+\infty} A(\xi)^2 e^{-j\xi\tau} d\xi \qquad \textbf{( 4.-56 )}$$

Thus $a(\tau)$ and $A(\lambda)$ are designed to establish desired cuts of ambiguity function in both directions.

As to the signal design, we start from **( 4.-53 )**

$$\dot{\theta}(\tau) = \lambda \xrightarrow{\substack{Taking \\ derivative}} \left|\ddot{\theta}(\tau)\right| = \left|\frac{d\lambda}{d\tau}\right| \qquad \textbf{( 4.-57 )}$$

By applying equation **( 4.-51 )**, we obtain

$$A(\lambda) = \sqrt{\frac{2\pi}{\left|\ddot{\theta}(\tau)\right|}}\, a(\tau) \;\rightarrow a(\tau)^2 d\tau = \frac{A(\lambda)^2}{2\pi} d\lambda \qquad \textbf{( 4.-58 )}$$

In the same way as the preceding case, this following expression is produced by differentiation of **( 4.-54 )** and substitution in **( 4.-52 )**

$$\dot{\varphi}(\lambda) = -\tau \xrightarrow{\substack{Applying \\ differentation}} |\ddot{\varphi}(\lambda)| = \left|\frac{d\tau}{d\lambda}\right| \quad \textbf{( 4.-59 )}$$

$$a(\tau) = \frac{A(\lambda)}{\sqrt{2\pi|\ddot{\varphi}(\lambda)|}} \rightarrow a(\tau)^2 d\tau = \frac{A(\lambda)^2}{2\pi} d\lambda \quad \textbf{( 4.-60 )}$$

By indefinite integration of **( 4.-58 )** or **( 4.-60 )**

$$\int_{-\infty}^{\tau} a(\xi)^2 d\xi = \frac{1}{2\pi}\int_{-\infty}^{\lambda} A(\eta)^2 d\eta \quad \textbf{( 4.-61 )}$$

We call $P(\tau)$ and $Q(\lambda)$ the term on the left of the equal and the term on the right of the equal, respectively. Therefore

$$P(\tau) = \int_{-\infty}^{\tau} a(\xi)^2 d\xi = \frac{1}{2\pi}\int_{-\infty}^{\lambda} A(\eta)^2 d\eta = Q(\lambda) \quad \textbf{( 4.-62 )}$$

If $P(\tau)$ and $Q(\lambda)$ are evaluated in $\tau = \infty$ and $\lambda = \infty$, we obtain the Parseval´s Theorem. From **( 4.-52 )**

$$|\ddot{\varphi}(\omega)| = \frac{1}{2\pi}\frac{A(\lambda)^2}{a(\tau)^2} \quad \textbf{( 4.-63 )}$$

By using double indefinite integration

$$|\dot{\varphi}(\omega)| = \frac{1}{2\pi}\int \frac{A(\lambda)^2}{a(\tau)^2} d\lambda + D_1 \quad \textbf{( 4.-64 )}$$

$$|\varphi(\omega)| = \frac{1}{2\pi}\iint \frac{A(\lambda)^2}{a(\tau)^2} d\lambda^2 + D_1\lambda + D_2 \quad \textbf{( 4.-65 )}$$

In the same way, from **( 4.-51 )**

$$\left|\dot{\theta}(\tau)\right| = 2\pi\int \frac{a(\tau)^2}{A(\lambda)^2} d\tau + C_1 \quad \textbf{( 4.-66 )}$$

$$|\theta(\omega)| = 2\pi \iint \frac{a(\tau)^2}{A(\lambda)^2} d\tau^2 + C_1\tau + C_2 \quad \textbf{( 4.-67 )}$$

According to these results it is possible to design signals that produce low sidelobes in the output matched filter. We are going to review some practical cases in the next section.

**Example of practical signals:**

- Moduli of Same Form

Equating $a(\tau)$ and $A(\lambda)$, by using equation **( 4.-52 )**

$$\frac{a(\tau)}{A(\lambda)} = \sqrt{\frac{1}{2\pi|\ddot{\varphi}(\lambda)|}} \quad \textbf{( 4.-68 )}$$

$$|\ddot{\varphi}(\lambda)| = \frac{1}{2\pi} = K_0 \quad \textbf{( 4.-69 )}$$

We obtain a constant $|\ddot{\varphi}(\lambda)|$, then by double integration of **( 4.-69 )**

$$\varphi(\lambda) = \iint K_0 \, d\lambda = \frac{K_0}{2}\lambda^2 + C_1\lambda + C_2 \quad \textbf{( 4.-70 )}$$

Next, relating $|\ddot{\varphi}(\lambda)|$ with $|\ddot{\theta}(\tau)|$ and using **( 4.-51 )** and **( 4.-52 )**

$$\sqrt{\frac{1}{2\pi|\ddot{\varphi}(\lambda)|}} = \frac{a(\tau)}{A(\lambda)} = \sqrt{\frac{|\ddot{\theta}(\tau)|}{2\pi}} \quad \textbf{( 4.-71 )}$$

$$|\ddot{\theta}(\tau)| = \frac{1}{|\ddot{\varphi}(\lambda)|} = K_1 \quad \textbf{( 4.-72 )}$$

In the same way as **( 4.-71 )**, we obtain

$$\theta(\tau) = \iint K_1 \, d\tau = \frac{K_1}{2}\tau^2 + C_3\tau + C_4 \qquad \textbf{( 4.-73 )}$$

Therefore, we obtain the quadratic functions $\varphi(\lambda)$ and $\theta(\tau)$. According to the preceding results, they agree with the CHIRP pulse. For fulfil the conditions **( 4.-49 )** and **( 4.-50 )**, it is necessary a larger duty cycle and a small frequency excursion. These two conditions are undesired because larger bandwidth is required.

- Constant envelope pulse.

Now we revise an example developed by Key et al. in 1961. Assuming the following signal

$$a(\tau) = Arect\left(\frac{\tau}{T}\right) \qquad \textbf{( 4.-74 )}$$

$$A(\lambda) = \frac{2A\sqrt{\frac{T}{\Delta\omega}}}{\sqrt{1+\left(\frac{\lambda}{\Delta\omega}\right)^2}} \qquad \textbf{( 4.-75 )}$$

Equation **( 4.-74 )** represents a constant pulse of duration $T$ in time domain. By using **( 4.-52 )**, we obtain

$$\left|\ddot{\varphi(\lambda)}\right| = \pm\frac{1}{2\pi}\left(\frac{A(\lambda)}{a(\tau)}\right)^2 = \pm\frac{2T}{\pi\Delta\omega\left(1+\left(\frac{\lambda}{\Delta\omega}\right)^2\right)} \qquad \textbf{( 4.-76 )}$$

By applying integration in **( 4.-76 )** the time delay results as

$$\left|\dot{\varphi(\lambda)}\right| = -T_d = \int \pm\frac{2T}{\pi\Delta\omega\left[1+\left(\frac{\lambda}{\Delta\omega}\right)^2\right]}d\lambda = \pm\frac{T}{\pi}\tan^{-1}\left(\frac{2\lambda}{\Delta\omega}\right) + C_1 \qquad \textbf{( 4.-77 )}$$

Then, setting the constant to be zero (this condition implies $\varphi(0) = 0$) and again applying integration

$$\varphi(\lambda) = \int \pm\frac{T}{\pi}\tan^{-1}\left[\frac{2\lambda}{\Delta\omega}\right]d\lambda = \pm\frac{\Delta\omega T}{2}\left\{\frac{2\lambda}{\pi\Delta\omega}\tan^{-1}\left(\frac{2\lambda}{\Delta\omega}\right) - \frac{1}{2\pi}ln\left(1+\left[\frac{2\lambda}{\Delta\omega}\right]^2\right)\right\} \quad \textbf{( 4.-78 )}$$

Starting from **( 4.-77 )**, the instantaneous frequency is obtained with the inverse function of the group delay

$$-T_d = \pm\frac{T}{\pi}\tan^{-1}\left(\frac{2\lambda}{\Delta\omega}\right) \xrightarrow{inverse\ function} {T_d}^{-1}(\tau) = \omega_i(\tau) = \mp\frac{\Delta\omega}{2}\tan\left(\frac{\pi}{T}\tau\right) \quad \textbf{( 4.-79 )}$$

To finish, we apply integration of **( 4.-79 )**

$$\theta(\tau) = \int \omega_i(\tau)\,d\tau == \mp\frac{\Delta\omega T}{2\pi}\,ln\left(\left|\cos\frac{\pi}{T}\tau\right|\right) + K_1 \quad \textbf{( 4.-80 )}$$

### Other FM laws

Although we have studied waveforms that fulfil the Stationary Phase Principle, other laws that do not meet this principle can be used too. Any FM modulation may be used to compress pulses **[Peyton Z. Peebles Jr, 1998]**. The following figures depict five FM laws which are studied in the section 5.4.

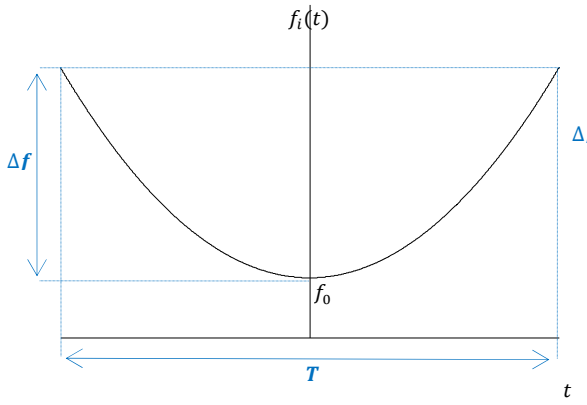


**Fig 4.-12: Even Quadratic FM law.**

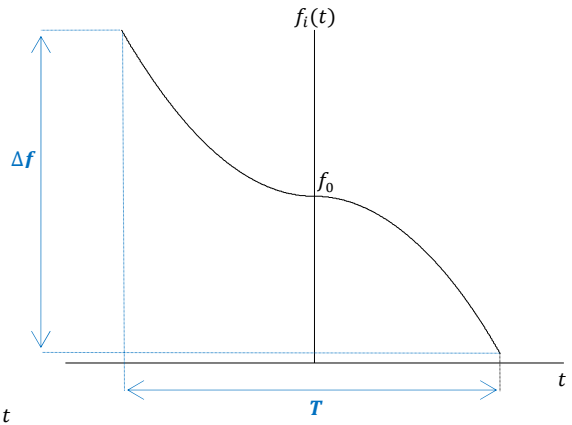


**Fig 4.-11: Odd Quadratic FM law.**

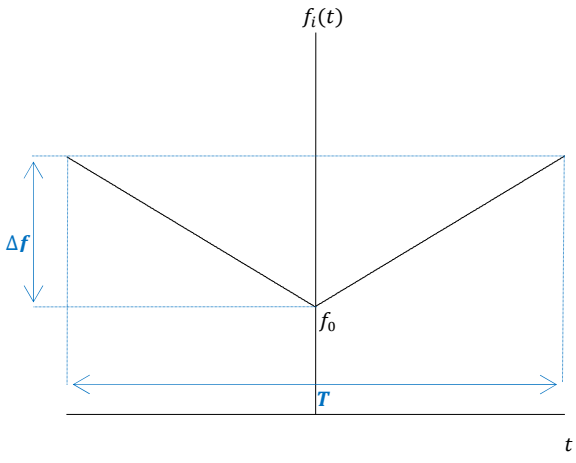


**Fig 4.-14: Even Vee FM law.**

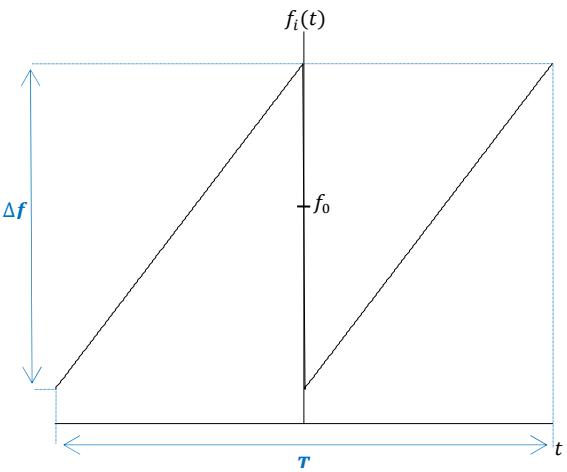


**Fig 4.-13: Odd Vee FM law.**

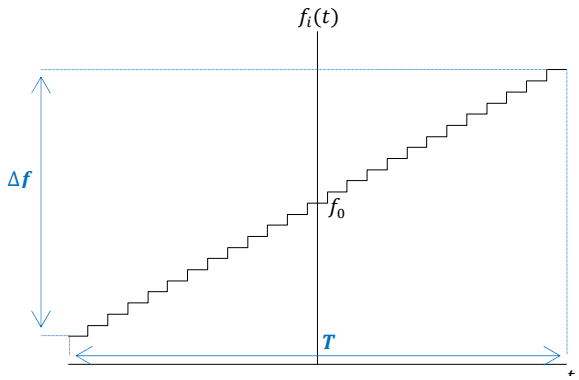


**Fig 4.-15: Stepped Linear FM law.**

### 4.3.3 Adaptive Pulse Compression algorithms

Several authors have studied compression techniques based on adaptive algorithms. They consist of a filter coefficients adjustment. These algorithms are used to evaluate the filter coefficients to their optimum values according to a criterion. Two main criteria are used **[B. Zrnic et al., 1998]**:

- Mean square sidelobe level suppression.
- Peak sidelobe level suppression.

The first approach is useful for uniformly distributed clutter case, and the second one is useful for non-uniformly distributed clutter scenario. Below, we study the **R**ecursive method of **L**east **S**quare (RLS), besides, other iterative approaches exist, such as **I**terative **R**eweighted **L**east **S**quares (IRLS) **[A. J. Zejak et al., 1991]**, **[A. J. Zejak et al., 1994]**; or **M**inimum **M**ean-**S**quare **E**rror **R**eiteration (MMSE) **[S. D. Blunt & K. Gerlach, 2003]**, **[S. D. Blunt & K. Gerlach, 2004]**, **[S. D. Blunt et al., 2009]**.

#### RLS algorithm

Let´s suppose the following transversal filter structure **[B. Zrnic et al., 1998]**

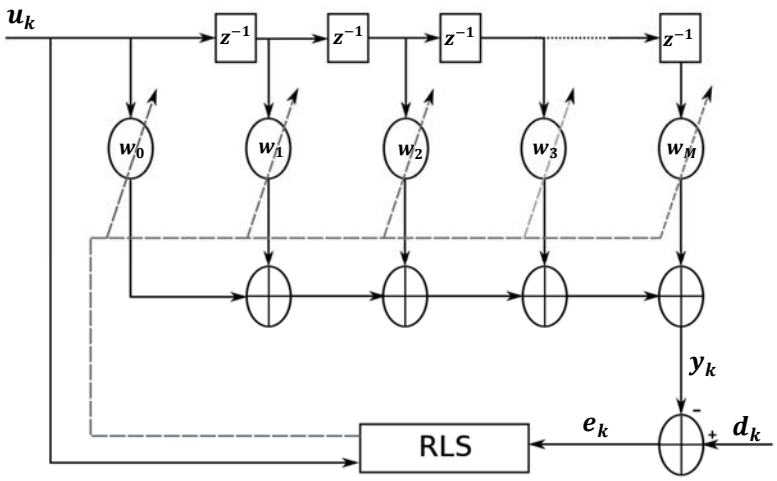


**Fig 4.-16: Block Diagram of Adaptive Mismatched Filter.**

The adaptive criterion is

$$|e_k| \geq TH \qquad \textbf{( 4.-81 )}$$

where TH is the threshold and $e_k = \boldsymbol{d_k} - \boldsymbol{y_k}$. The coefficients are recalculated if the condition **( 4.-82 )** is fulfilled. According to the RLS formulation, a modified procedure is used to calculate the filter coefficients.

Assuming $j = 1,2,3, \dots, L$ as iteration subscript, and $k = 1,2,3, \dots, N + M - 1$ as the values in $k$-th time instant, then we carry out the following steps.

- **Step 1:** Error estimation

$$e_k = d_k - w_k^H u_k \qquad \textbf{( 4.-82 )}$$

- **Step 2:** Gain vector estimation

$$K_k = \begin{cases} \lambda^{-1} P_{k-1} \dfrac{u_k}{(1 + \lambda^{-1} u_k^H P_{k-1} u_k)} & |e_k| \geq TH_{j-1} \\ K_{k-1} & elsewhere \end{cases} \qquad \textbf{( 4.-83 )}$$

Where $\lambda$ is the weigthing factor, $u_k$ is the input vector, which consists of $N$ samples of the input signal, and $P_k$ is a matrix, which carries information about the reliability of the estimation. Moreover $(\cdot)^H$ denotes the Hermitian transpose.

- **Step 3:** Coefficients calculation. We increment $k$. Note that the error function depends on the filter coefficients of the previous stage $(k - 1)$.

$$w_k = \begin{cases} w_{k-1} + K_k e_k & |e_k| \geq TH_{j-1} \\ w_{k-1} & elsewhere \end{cases} \qquad \textbf{( 4.-84 )}$$

- **Step 4:** $P_k$ matrix estimation

$$P_k = \begin{cases} \lambda^{-1} \left( P_{k-1} - K_k u_k^H P_{k-1} \right) & |e_k| \geq TH_{j-1} \\ P_{k-1} & elsewhere \end{cases} \qquad \textbf{( 4.-85 )}$$

- **Step 5:** Threshold setting

$$err_k = |e_k| \quad \text{( 4.-86 )}$$

$$MAX\_ERR_j = \max(err) \quad \text{( 4.-87 )}$$

$$TH_j = \delta \, MAX\_ERR_j \quad \text{( 4.-88 )}$$

Where $\max(\cdot)$ represents the maximum value of the vector, and $\delta$ is a constant related to the convergence rate, which is close or equal to $1$. Note that the threshold is proportional to the maximum error committed in all iterations.

The algorithm need to initialize the vector $w_0$, the matrix $P_0$, and the threshold value $TH$. Note that we perform a new iteration to compute the correction coefficients when the error exceeds or is equal to $TH$ in a time instant. This method attempts to minimize the maximum error value (Minimax criterion). These adaptive filter are known as self-clutter suppression filter.

## 4.4 Other Pulse Compression techniques

The purpose of this section is to review other techniques used in pulse compression. The goal is the same one as with the preceding techniques.

### 4.4.1 Pulse Compression by Costas FM

Varying frequency discretely through the waveform is known as frequency hopping **[Peyton Z. Peebles Jr, 1998]**. It is possible to compress a pulse built by discrete frequencies.

Let us suppose a total waveform duration, $T$, and $N$ fractions of $T$ with the same duration. Therefore

$$T_i = \frac{T}{N} \qquad i = 1,2,3,\dots,N \quad \text{( 4.-89 )}$$

$T_i$ is the time interval in which a discrete frequency is transmitted. Thus, we assume $N$ possible frequencies

$$\omega_i = \omega_0 + 2\pi i \delta f \qquad i = 1,2,3,\dots,N \tag{4.-90}$$

Where $\delta f = \frac{1}{T_i}$. According to **( 4.-91 )** the maximum frequency is

$$\Delta f = N\delta f = \frac{N}{T_i} \tag{4.-91}$$

And the time-bandwidth product of the total pulse is

$$\Delta f T = N^2 \delta f T_i = N^2 \tag{4.-92}$$

Thereby, the duration of the compressed pulse is $\frac{1}{\Delta f} = \frac{T}{N^2}$.

The overall pulse can be viewed as $NxN$ array **[Peyton Z. Peebles Jr, 1998]**, where the columns represent the frequency that is transmitted in a given instant $T_i$, and the rows represent the available frequencies. The next figure, Fig 4.-17, depicts an example

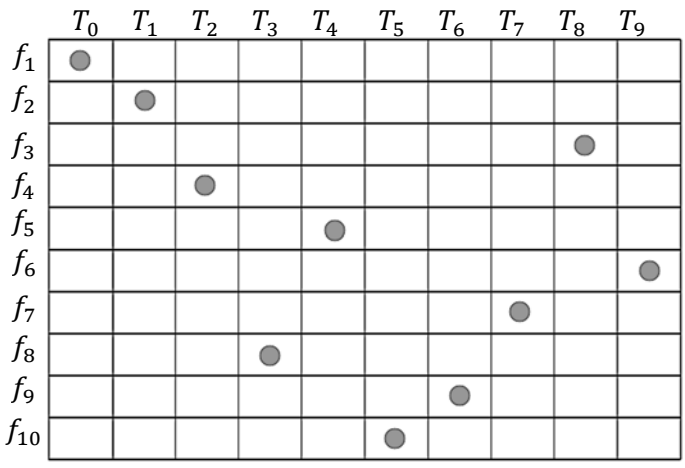


**Fig 4.-17: Costas FM Matrix. Frequency Hopping.**

In this example $f_1$ is the first frequency transmitted, $f_2$ is the second one, then, $\omega_4$ is transmitted, $f_8$ is the fourth one and so on.

Several ways exist to decide what frequency is transmitted in a given time instant, but, the most important is the Costas FM method. This method generates frequency hopping sequences known as Costas sequences.

The Costas FM pulses produce sidelobes down from the main lobe by $\frac{1}{N}$ for all regions of delay-Doppler plane. In other words, the main peak decreases rapidly in the $|x(0,\omega_d)|^2$ and $|x(\tau,0)|^2$ ambiguity function cuts. This fact is desired in applications where small Doppler shifts are expected.

If $N$ increases, the sidelobes and the compressed pulse width decrease. However, the Costas sequences () also decrease, since the Costas sequences must meet the following rule: one frequency per time slot (columns) and one time slot per frequency (rows) **[Peyton Z. Peebles Jr, 1998]**.

Thus, it is more difficult to find a good performance sequences (there are $N_c = 4$ Costas sequences for $N = 3$, thus $\frac{N_c}{N!} = \frac{2}{3} = 0.667$, in other words, the probability of finding a Costas sequence is $66{,}7\%$ when the code length is $3$; there are $N_c = 12$ Costas sequences for $N = 4$, thus $\frac{N_c}{N!} = \frac{1}{2} = 0.5$; and, there are $N_c = 7852$ Costas sequences for $N = 12$, thus $\frac{N_c}{N!} = \frac{1963}{119750400} = 1.639\ 10^{-5}$).

## 4.4.2 Pulse Compression by Phase Coding

A pulse can be compressed by using phase modulation **[Peyton Z. Peebles Jr, 1998]**. There are two approaches namely, use either binary codes or M-phase codes to perform the phase modulation. We discuss the basic concept for the binary codes case.

### Basic concept

In the same way as Costas FM, the pulse is divided in $N$ fractions (subpulses), whose duration is $T_n = \frac{T}{N}$, where $T$ is the total pulse duration **[Peyton Z. Peebles Jr, 1998]**. Each subpulse maintains the same carrier frequency, but the phase changes between subpulses. It results a waveform with constant modulus and variable phase over $T$; codes sequences of discrete values can describe these phase changes. The basic idea consists of designing a code in order to achieve low sidelobes.

Let us suppose a binary phase coding; the possible phase values are $0$ and $\pi$ (since they are the values most separated, in terms of the phase signal). The complex envelope of the pulse is

$$g(t) = \sum_{n=1}^{N} A\, rect\left(\frac{t + \left(\frac{N+1}{2} - n\right)T_n}{T_n}\right) e^{j\theta_n} = A\sum_{n=1}^{N} d_n\, rect\left(\frac{t + \left(\frac{N+1}{2} - n\right)T_n}{T_n}\right) \quad \textbf{( 4.-93 )}$$

Where $A$ is a nonzero constant and $d_n = \begin{cases} +1\ for\ \theta_n = 0 \\ -1\ for\ \theta_n = \pi \end{cases}$.

From **( 3.-42 )**, and in complex envelope terms, the matched filter output for $\omega_d = 0$ is

$$x(\tau, 0) = \int_{-\infty}^{+\infty} g^*(\xi)\, g(\xi + \tau) d\xi \quad \textbf{( 4.-94 )}$$

The preceding expression is the autocorrelation function of $g(t)$. By supposing the following pulse, with $N = 6$, as shown in Fig 4.-18

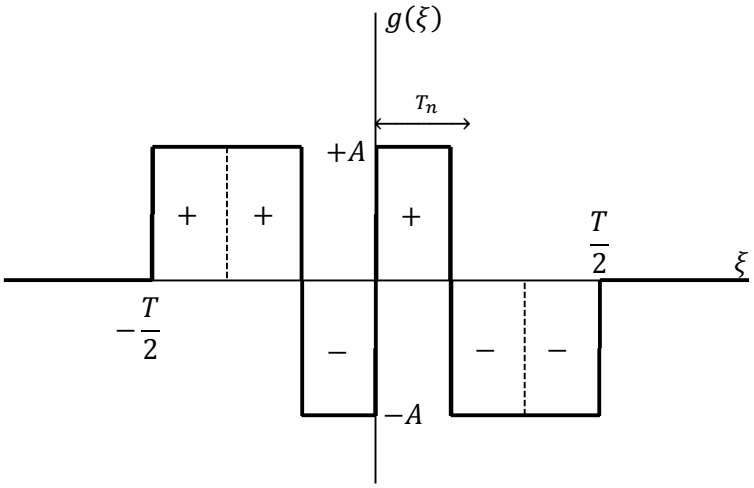


**Fig 4.-18: Pulse Formed by Phase Coding.**

According to the expression **( 4.-94 )**, for $\tau = 2T_n$ we obtained the signal shown in Fig 4.-19.

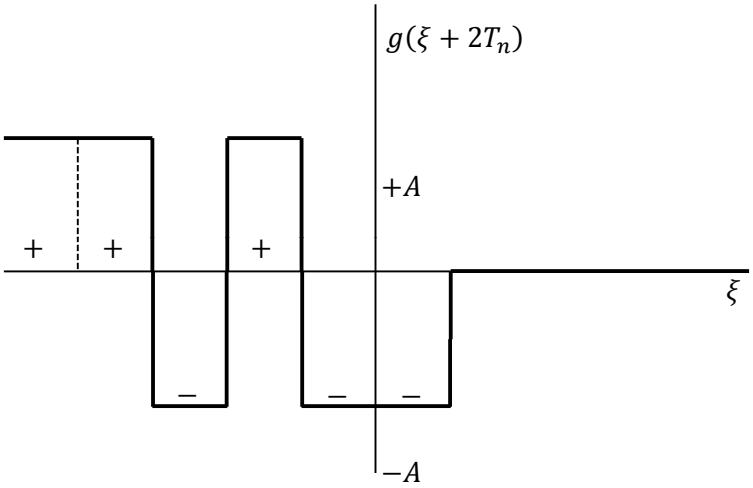


**Fig 4.-19: Phase Code pulse delayed by $2T_n$.**

Thereby, by the product $g(\xi)g(\xi + 2T_n)$, it results into the signal shown in Fig 4.-20.

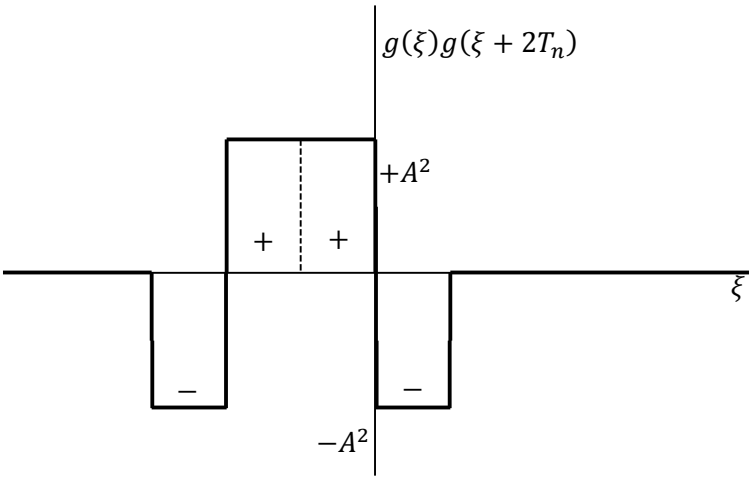


**Fig 4.-20: Autocorrelation for $\tau = 2T_n$.**

The area of this function is $0$. Next, when $\tau = 0$ the signal shown in Fig 4.-21 is obtained.

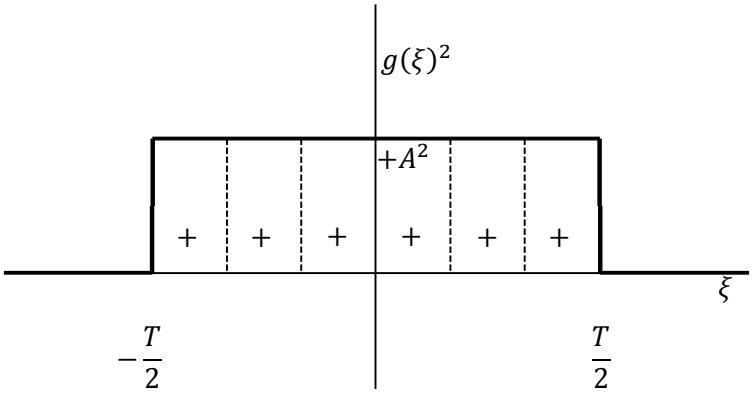


**Fig 4.-21: Autocorrelation for $\tau = 0$.**

In this case, the area is $+6A^2T_n$. According to the process described above, the matched filter output is shown in Fig 4.-22.

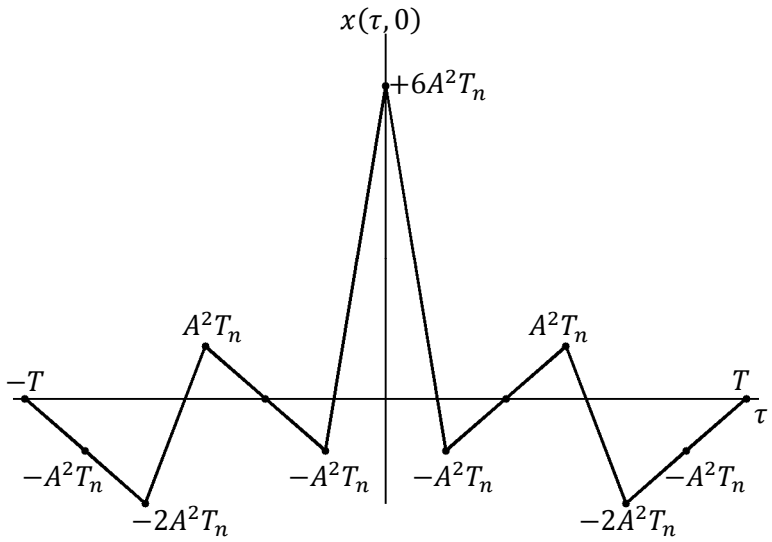


**Fig 4.-22: Pulse Compressed by using Phase Coding.**

Notice that we achieve the goal of compressing the pulse with rather low side lobe levels.

# Chapter 5. Simulation Results

This section provides the results and conclusions obtained in this work. We got these results by using Matlab Tool. We implemented the necessary functions whose information are available in the Appendix B. Before discussing the results it is necessary to clarify some aspects of the simulations carried out.

## 5.1. Considerations

**Burst of Pulses**

In preceding sections we studied the matched filter output for either continuous or a single pulse. The results presented in this chapter were obtained by using various pulse replications. Below we revise a multiple pulses case to interpret better the results.

Let us suppose that the transmitted signal is composed of various replications of a given pulse, whose complex envelope is $g_1(t)$. Thus we can write complex envelope of the complete signal as **[Peyton Z. Peebles Jr, 1998]**

$$g(t) = \sum_{n=0}^{N-1} g_1(t - nT_r) \qquad \textbf{( 5.-1 )}$$

Where $T_r$ is the separation between adjacent pairs of pulses; condition $T_r > 2T_1$ (where $T_1$ is the duration of a single pulse) is fulfilled in order to avoid overlap replicas as Fig 5.-1 shows.

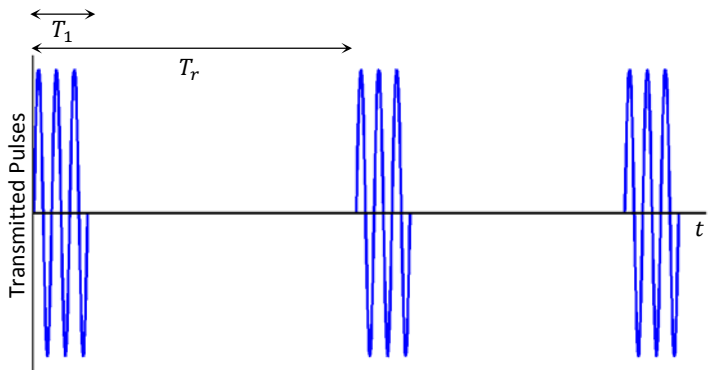


**Fig 5.-1: Burst of pulses.**

Thus, from equation **( 3.-34 )** , we can write the uncertain function of the complete signal as

$$x(\tau,\omega_d)=\sum_{n=0}^{N-1}\sum_{m=0}^{N-1}e^{jn\omega_d T_r}x_1(\tau-(m-n)T_r,\omega_d) \qquad \textbf{( 5.-2 )}$$

Note that **( 5.-2 )** is the sum of shifted replicas of $x_1(t)$ by $(m-n)T_r$, and weighted by a phase factor.

By taking $k=m-n$

$$\begin{aligned}x(\tau,\omega_d)=&\sum_{k=-(N-1)}^{0}\sum_{m=0}^{N-1+k}e^{j(m-k)\omega_d T_r}x_1(\tau-kT_r,\omega_d)\\&+\sum_{k=1}^{N-1}\sum_{n=0}^{N-1-k}e^{j(m-k)\omega_d T_r}x_1(\tau-kT_r,\omega_d)\end{aligned} \qquad \textbf{( 5.-3 )}$$

Considering the following mathematical identity

$$\sum_{n=0}^{M}e^{jn\beta}=e^{jM\frac{\beta}{2}}\frac{\sin\left(\frac{(M+1)\beta}{2}\right)}{\sin\left(\frac{\beta}{2}\right)} \qquad \textbf{( 5.-4 )}$$

We can rewrite **( 5.-3 )** as

$$\begin{aligned}x(\tau,\omega_d)=e^{j(N-1)\omega_d\frac{T_r}{2}}&\sum_{k=-(N-1)}^{N-1}(N-|k|)x_1(\tau\\&-kT_r,\omega_d)\;e^{-jk\omega_d\frac{T_r}{2}}\left[\frac{\sin\big((N-|k|)T_r\omega_d/2\big)}{(N-|k|)\sin(T_r\omega_d/2)}\right]\end{aligned} \qquad \textbf{( 5.-5 )}$$

Note that the replicas of $x_1(t)$ are centered in $kT_r$-delays for $k=\pm1,\pm2,\dots,\pm(N-1)$, with amplitudes $N-|k|$. Finally

$$|x(\tau,\omega_d)|=\sum_{k=-(N-1)}^{N-1}(N-|k|)|x_1(\tau-kT_r,\omega_d)|\left|\frac{\sin\big((N-|k|)T_r\omega_d/2\big)}{(N-|k|)\sin(T_r\omega_d/2)}\right| \qquad \textbf{( 5.-6 )}$$

Therefore, the term $\frac{\sin\left((N-|k|)T_r\omega_d/2\right)}{(N-|k|)\sin(T_r\omega_d/2)}$ accomplishes it maximum in $\omega_d = \frac{q2\pi}{T_r}$ (where $q$ is an integer), and then it decreases rapidly. This fact provokes that the signal level increases and decreases repeatedly.

**Doppler sign**

The criterion used to fix the Doppler sign varies between authors. We assumed that the Doppler sign is positive when target is moving away, and negative when the target is approaching the radar.

**Pulse detection**

All the simulations have been carried out by using a non-coherent detection system to get the baseband information of the received signal. Thus, there is not negative level of signal of the detected signals. We used the detection diagram block depicted in Fig 5.-2.

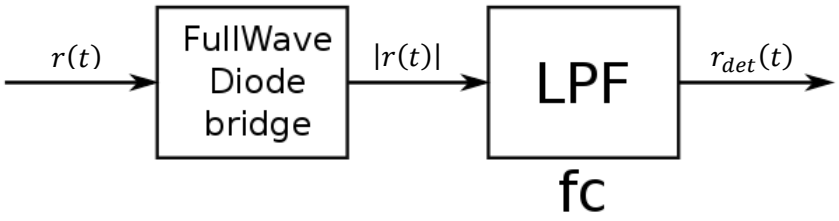


**Fig 5.-2: Detector used for the simulations.**

## 5.2. Linear FM pulse (CHIRP)

The first set of results were carried out for understanding the compression process. For this purpose we simulated the compression of a CHIRP pulse in different situations. First, we started from varying the pulse parameters in the presence of nonmoving target to observe the spectrum and the compressed pulse behavior. Next, we simulated the CHIRP pulse compression for moving targets and calculated the ambiguity functions. Finally, we simulated a pulse compression in the presence of two nearby targets, namely a big scatter target and a small scatter target.

### 5.2.1 $\Delta fT$-product dependency for CHIRP pulse

As it was studied in section 4.2, the $\Delta fT$-product affects to the quality of the spectrum of a CHIRP pulse. Thereby it also affects to the compressed pulse. The parameters used to probe the $\Delta fT$ dependency are shown in Table 5.-1.

| ***Table 5.-1: Simulation 1.*** |
|---|
| $f_0 = 10\ [MHz]$ |
| $prf = 3\ [KHz]$ |
| $T = 166.667\ [\mu s]$ |
| $Number\ of\ pulse = 5$ |

We performed a $\Delta f$ variable sweep for values included between $100KHz$ and $1MHz$ with a $50KHz$ step. The figures included in this section are the most important ones.

Fig 5.-3 and Fig 5.-4 have been obtained for $\Delta f = 150\ [KHz]$, and the $\Delta fT$-product is equal to $25$. Note that a peak amplitude appears in $t = 166.667\ [\mu s]$ approximately. This time instant corresponds to the end of the transmitted pulse (it means that the target is at zero distance), and the surrounding level of the signal is much lower that the main lobe. Fig 5.-3 confirms the functionality of the pulse compression by using CHIRP pulses. By focusing on the spectrum of compressed signal (Fig 5.-4), we note that the width of the spectrum is equal to $2\Delta f$ because of the fact that the instantaneous frequency is defined between $f_0$ and $f_0 + \Delta f$ (Carson bandwidth rule), besides the spectrum is symmetric with respect to $f_0 + {}^{\Delta f}/_{2}$.

If the $\Delta fT$-product increases, the width of the compressed pulse decreases. We can note this fact by observing Fig 5.-5, Fig 5.-6 (for $\Delta f = 300\ [KHz]$); Fig 5.-7, Fig 5.-8 (for $\Delta f = 600\ [KHz]$) ; and Fig 5.-9, Fig 5.-10 (for $\Delta f = 900\ [KHz]$). Note that the wider the spectrum of the CHIRP pulse, the narrower the compressed pulse and the lower the level of the second lobes. Besides, the spectrum quality increases if $\Delta fT$-product increases due to the Fresnell integrals terms (see equation **(4.-22)** in section 4.2).

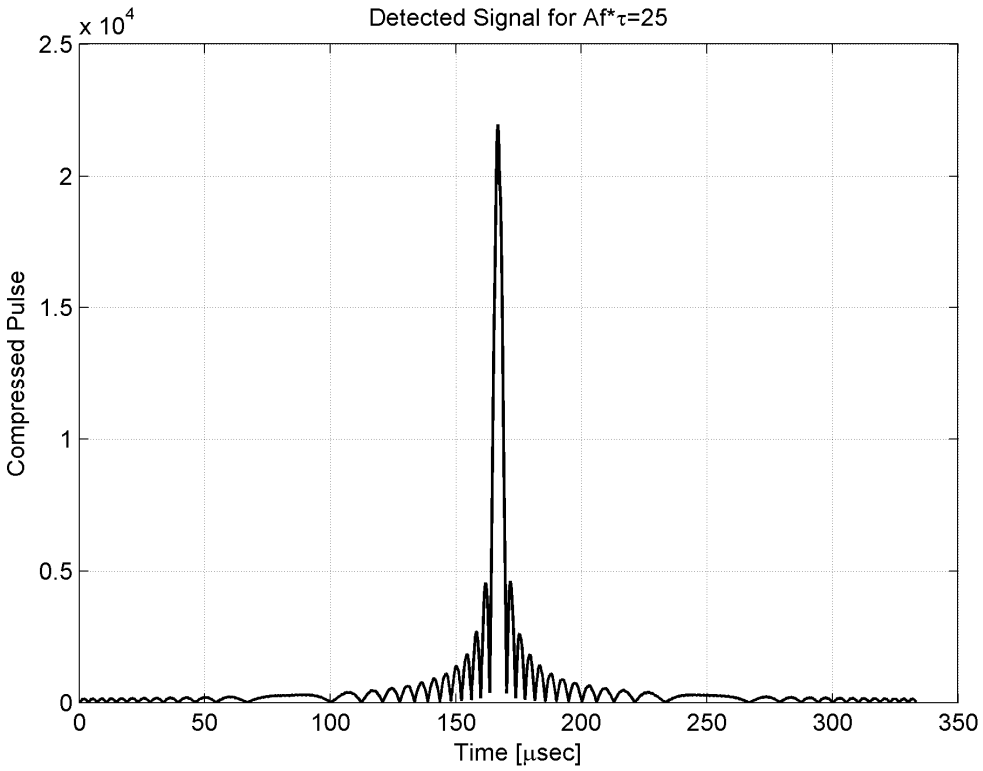


**Fig 5.-3: Simulation 1, Detected Signal $\Delta fT = 25$.**

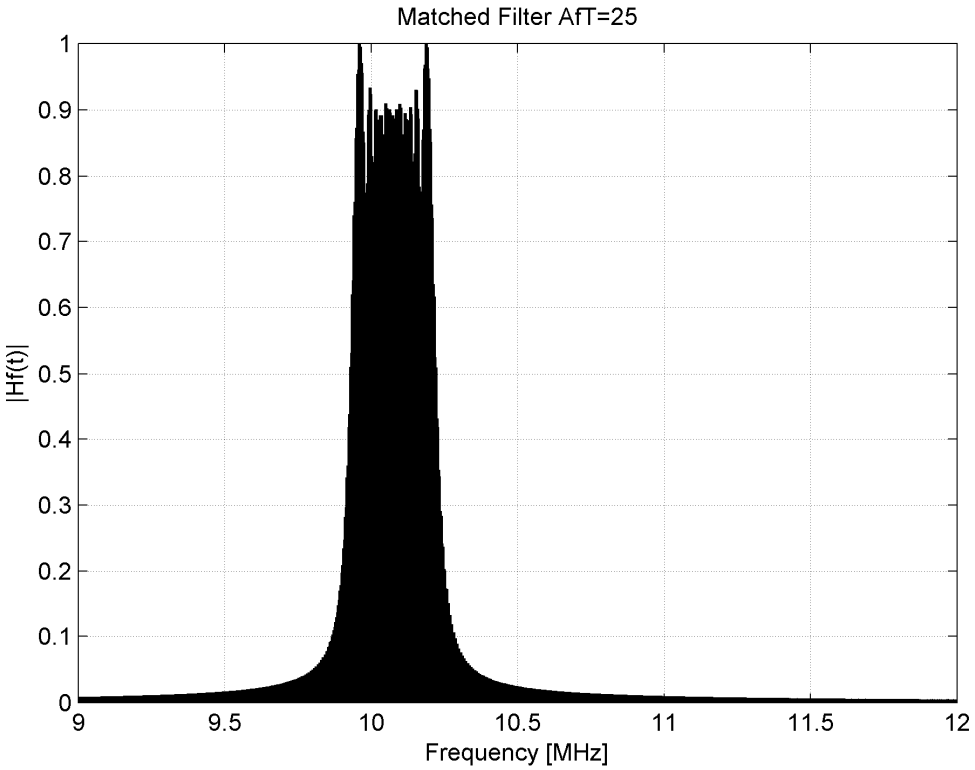


**Fig 5.-4: Simulation 1, Detected Signal $\Delta fT = 25$.**

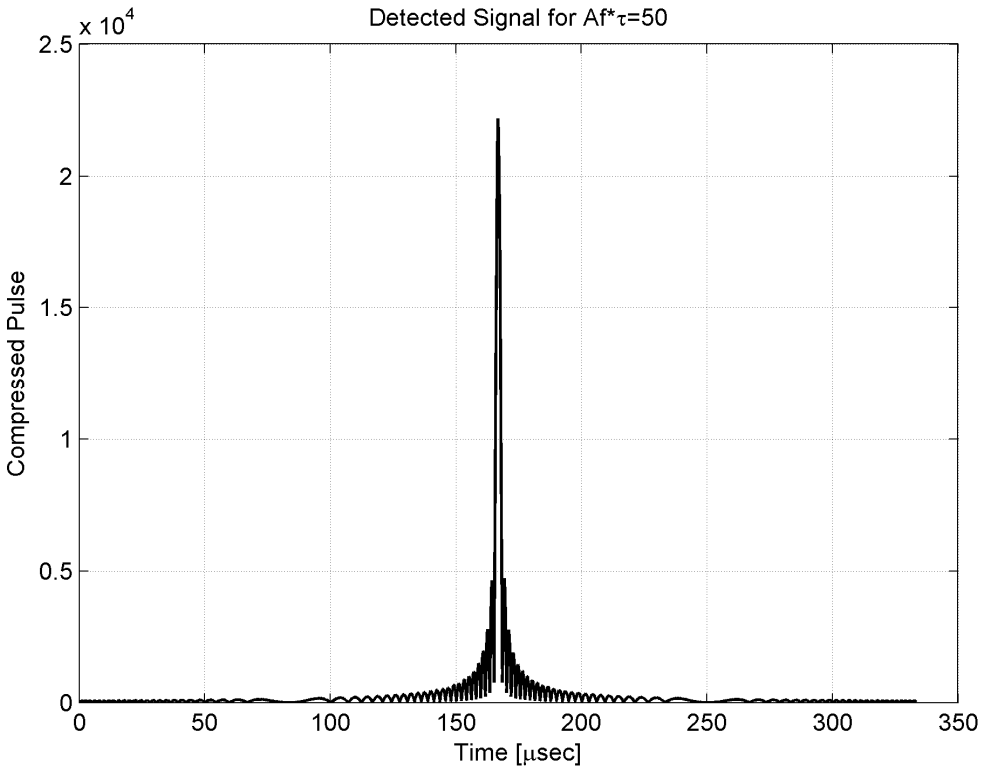


**Fig 5.-5: Simulation 1, Detected Signal $\Delta fT = 50$.**

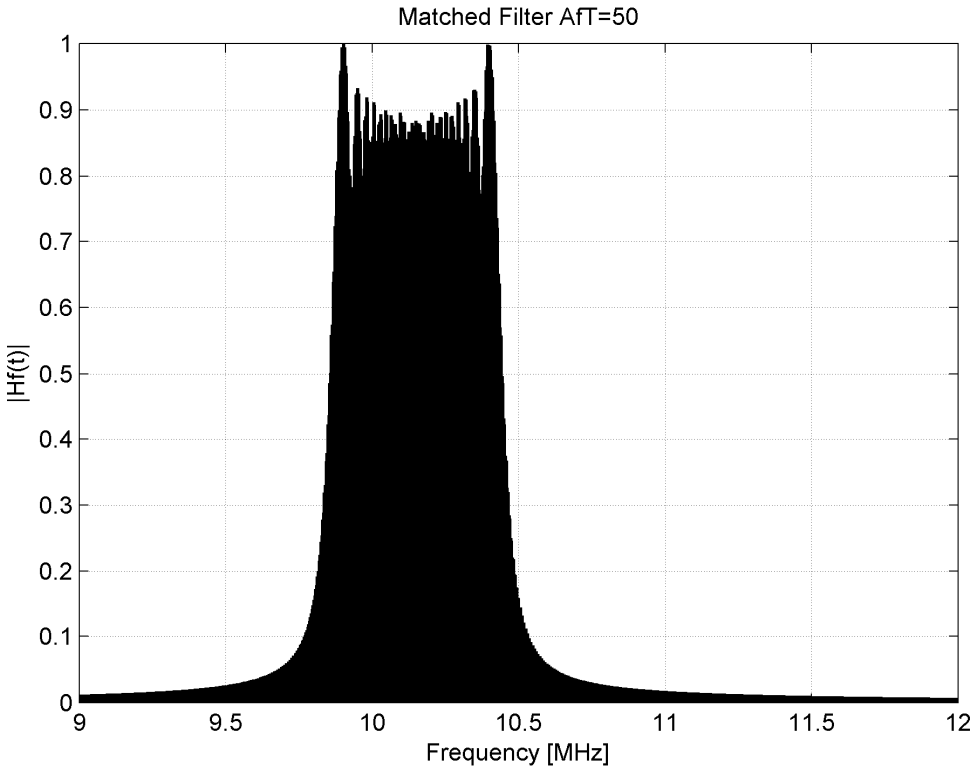


**Fig 5.-6: Simulation 1, Detected Signal $\Delta fT = 50$.**

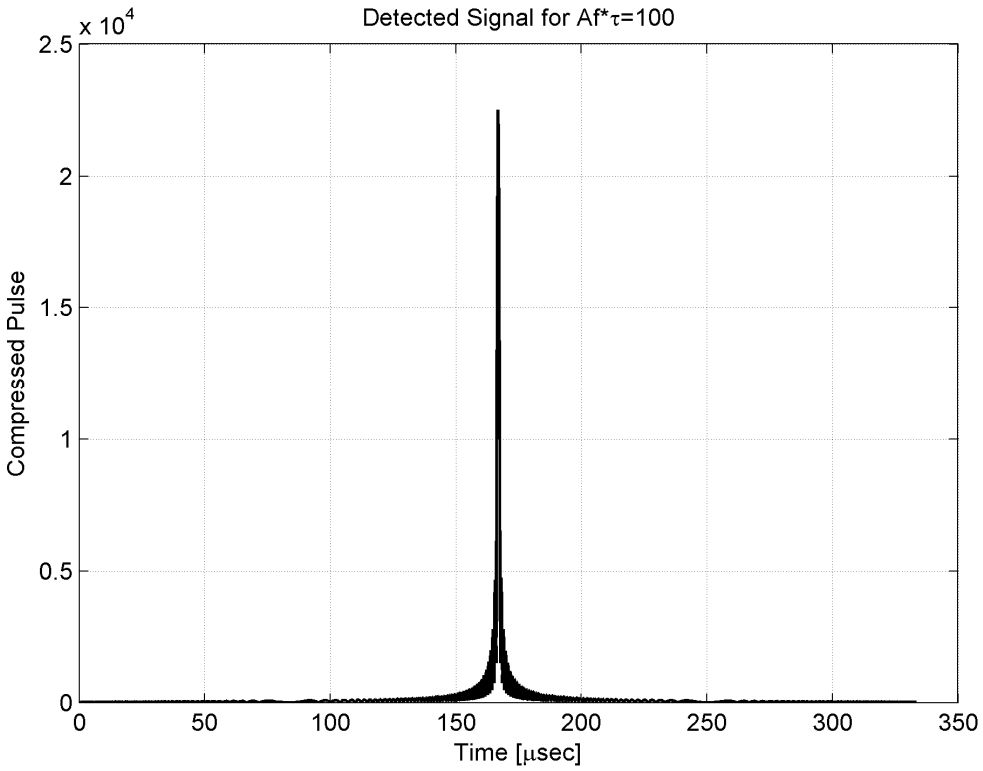


**Fig 5.-7: Simulation 1, Detected Signal $\Delta fT = 100$.**

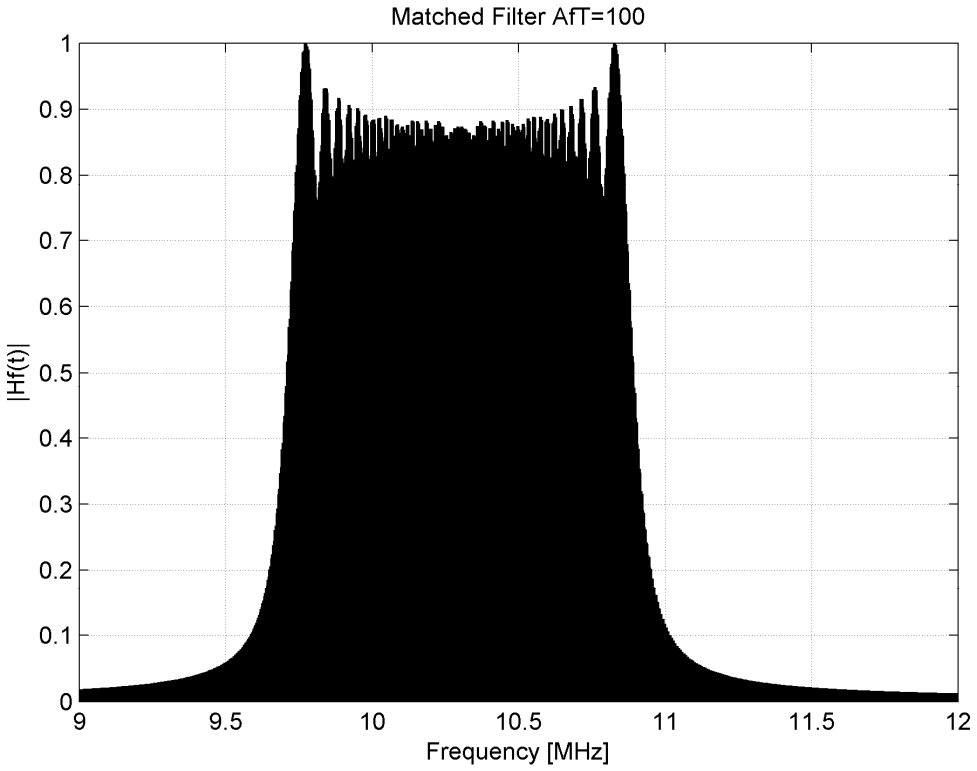


**Fig 5.-8: Simulation 1, Detected Signal $\Delta fT = 100$.**

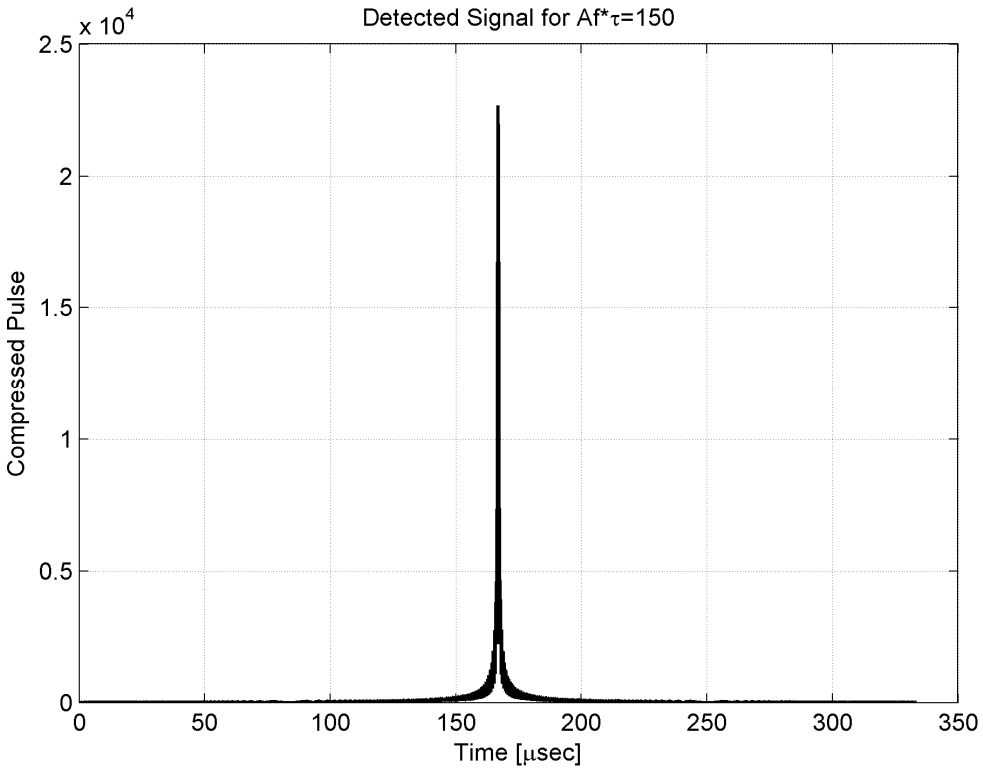


**Fig 5.-9: Simulation 1, Detected Signal $\Delta fT = 150$.**

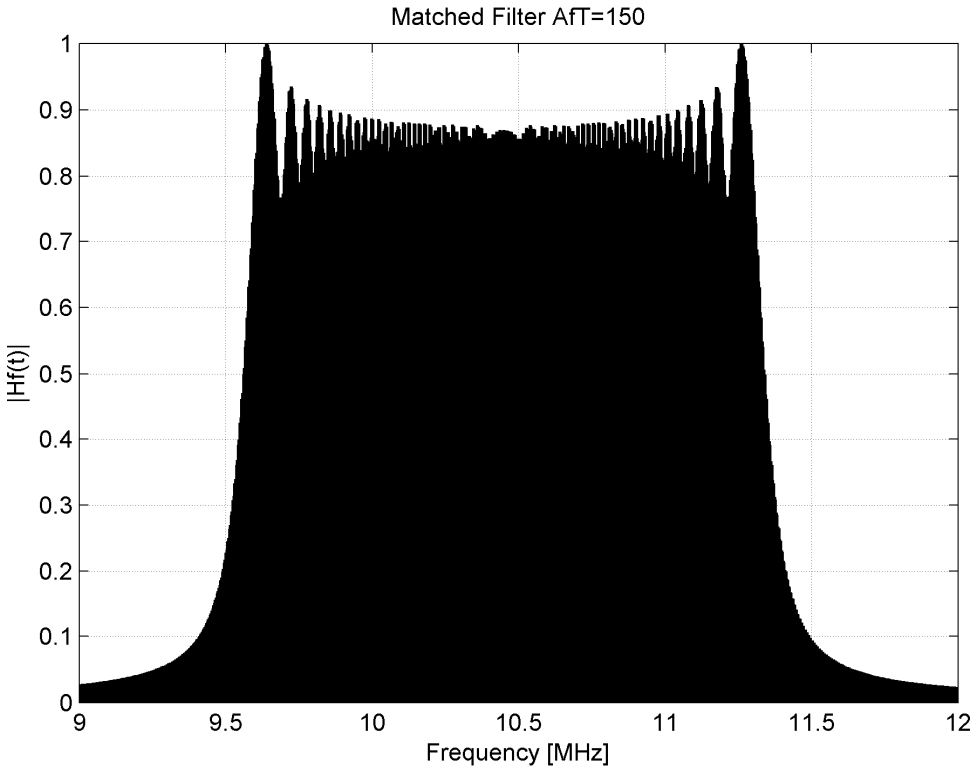


**Fig 5.-10: Simulation 1, Spectrum of Transmitted Signal $\Delta fT = 150$.**

In order to summarize the behavior described above, Fig 5.-11 depicts the secondary lobe level and evolution of pulse width for all values of $\Delta fT$ used in this experiment. Fig 5.-11 confirms that the pulse width decreases if the $\Delta fT$-product increases. Besides when the $\Delta fT$ product is very large the reduction of the width of the compressed pulse is smoother (it has an asymptotic behavior). Also the secondary lobes are smoothly decreased by increasing the $\Delta fT$ product over $50$.

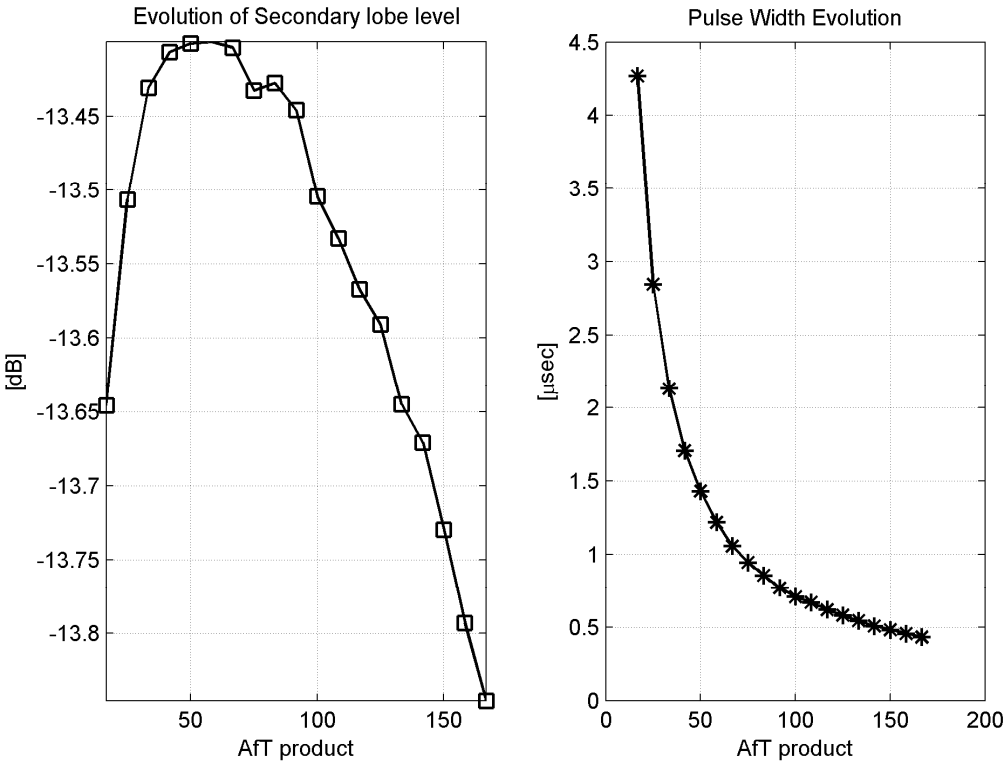


**Fig 5.-11: Simulation 1, Secondary Lobe Level and Pulse Width vs $\Delta fT$-product.**

### 5.2.2 CHIRP pulse compression for moving targets

We continued with moving target simulations. For these simulations we fixed the parameters as is shown in Table 5.-2.

| ***Table 5.-2: Simulation 2.*** |
|---|
| $f_0 = 10\ [MHz]$ |
| $\Delta f = 400\ [KHz]$ |
| $prf = 3\ [KHz]$ |
| $T = 166.667\ [\mu s]$ |
| $Number\ of\ pulse = 5$ |

We performed five simulations setting the distance to the target to zero and the next values of Doppler Effect: $f_d = -15, 5, 0, 5$ and $15[KHz]$. The compressed pulses are shown in Fig 5.-12. Note that the maximum of the compressed pulse appears in different time instants despite the fact that the range to the target does not change. Besides the amplitude of the compressed signal varies if the Doppler Shift varies.

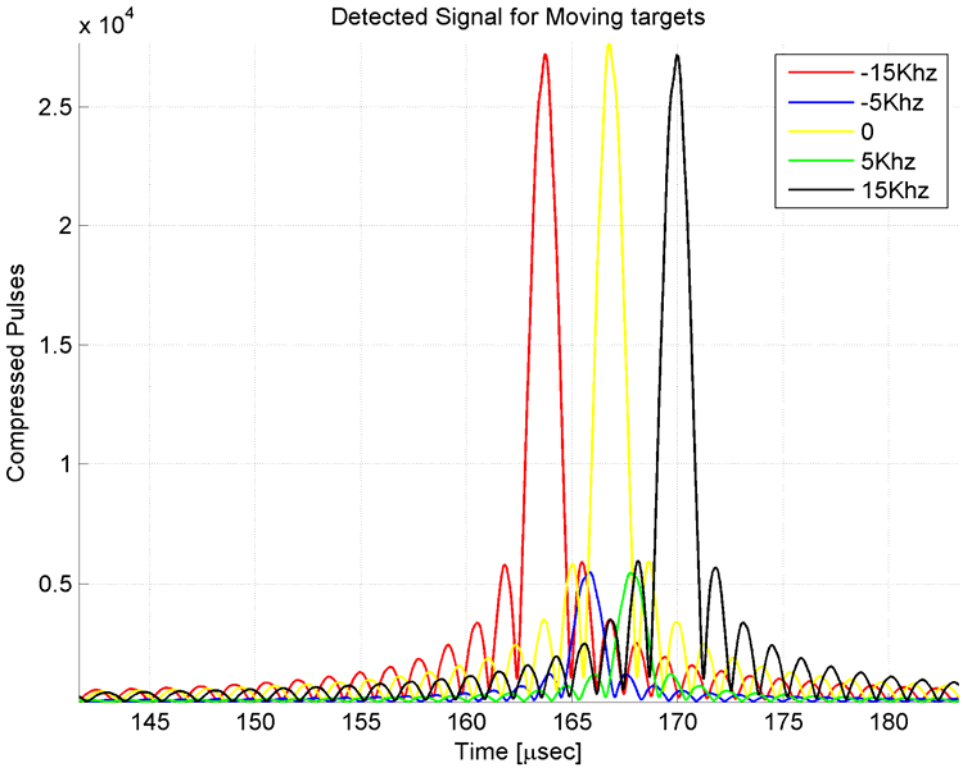


**Fig 5.-12: Simulation 2, Detected Signals in presence of Doppler Shift.**

The ambiguity function provides information to observe better the Doppler Effect in the pulse compression. Thus, we calculated the ambiguity functions for different values of $\Delta f$ and fixing the other parameters as in the preceding simulation (Table 5.-2). Fig 5.-13, Fig 5.-14, Fig 5.-15 and Fig 5.-16 illustrate the more representative ambiguity functions obtained for different values of $\Delta f$ $(100, 300, 500$ and $1000\ [KHz]$ respectively).

By observing from Fig 5.-13 to Fig 5.-16, we note that the maximum values of the filter output are shifted along the time axis, if the Doppler frequency varies. This fact produces an error in the range measurement when a target is moving. The straight lines obtained by connecting two maximums have different slopes in the different cases. This slope depends on the modulation index $\mu$ (see Fig 4.-3 in section 4.2). If $\mu$ increases, the slope tends to the vertical axis. In a full matching case (ideal case) the slope is $\infty$. Furthermore, the filter output fluctuates, thus it complicates the detection of the target. As it was commented in section 5.2.1, the larger $\Delta fT$-product, the wider the pulse.

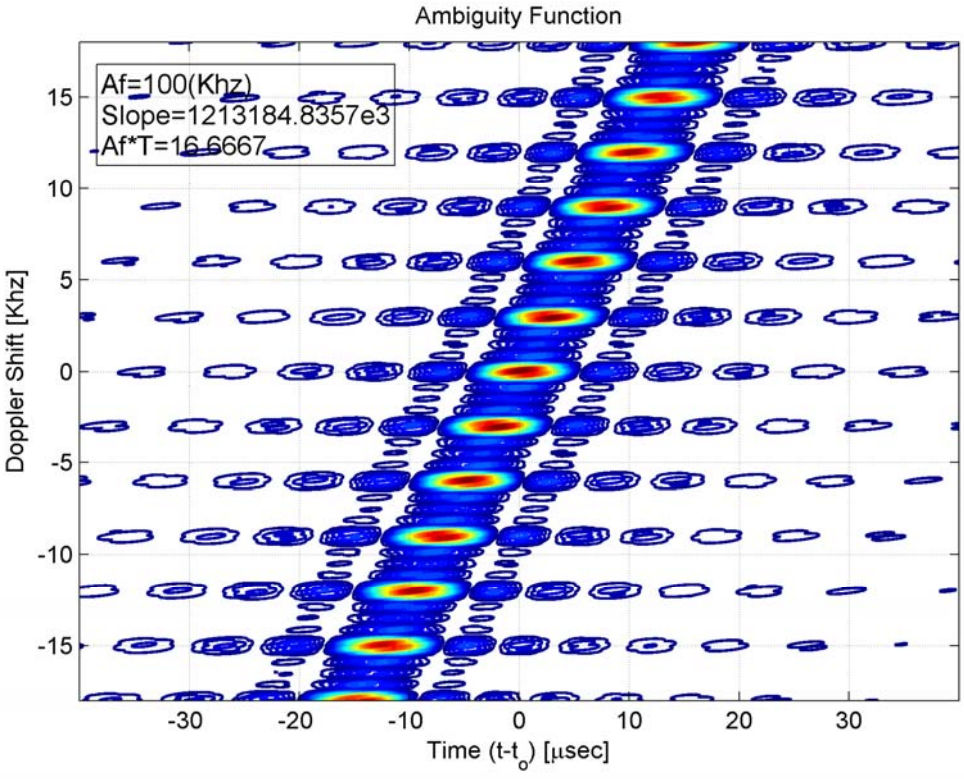


**Fig 5.-13: Simulation 2, Ambiguity Function $\Delta fT = 16.6667$.**

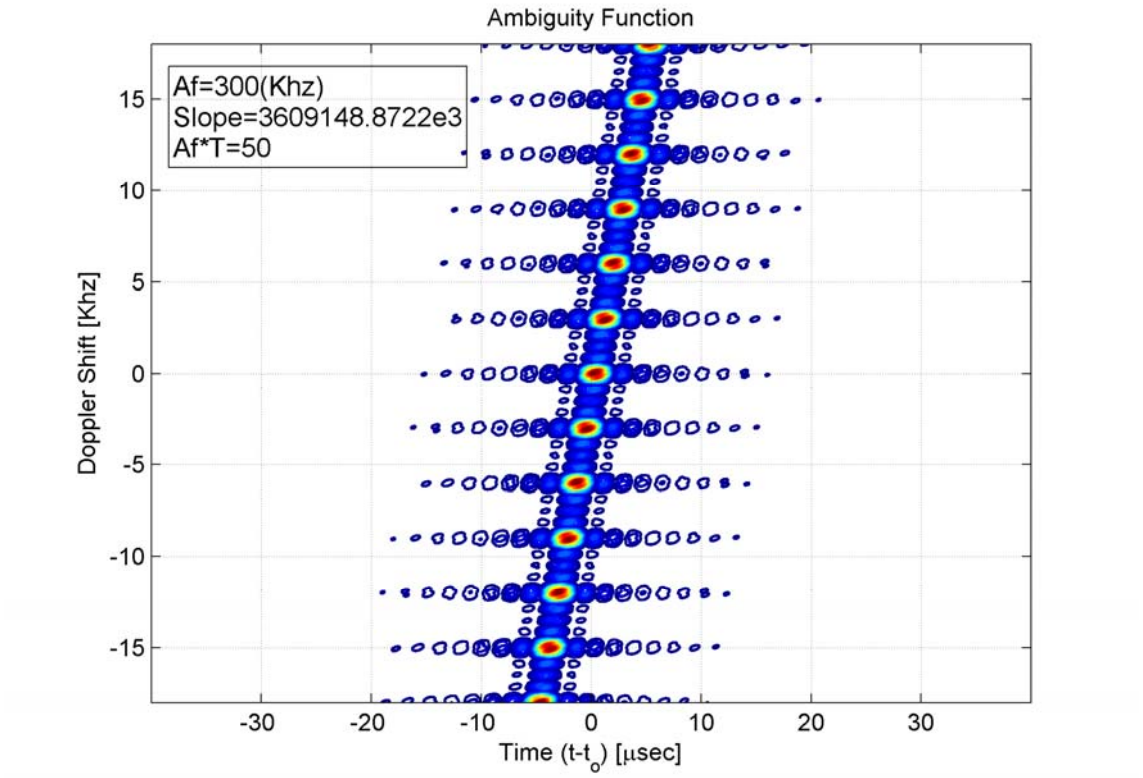


**Fig 5.-14: Simulation 2, Ambiguity Function $\Delta fT = 50$.**

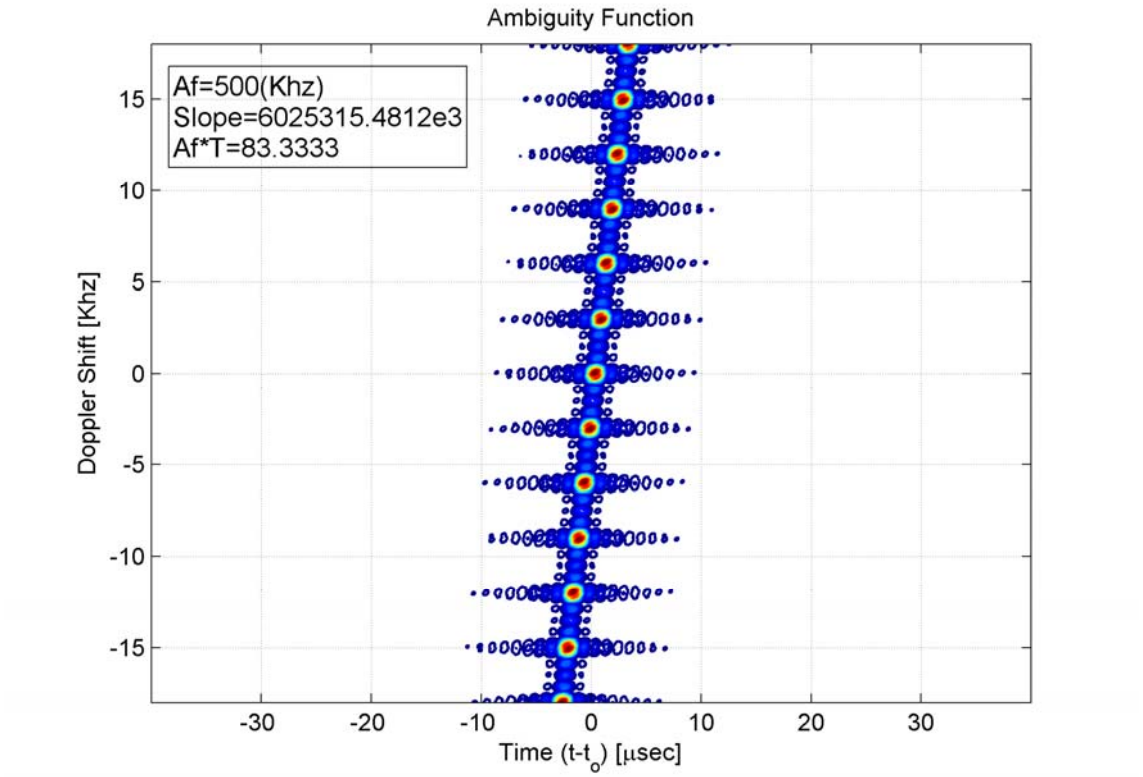


**Fig 5.-15: Simulation 2, Ambiguity Function $\Delta fT = 83.3333$.**

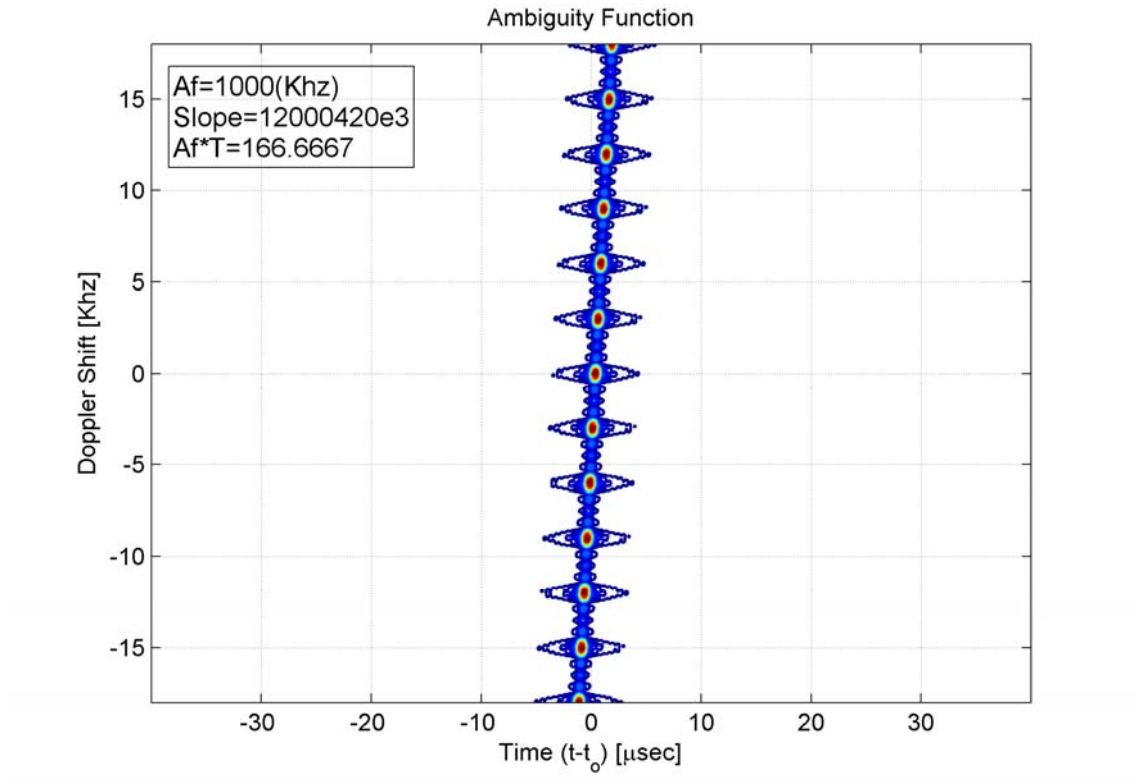


**Fig 5.-16: Simulation 2, Ambiguity Function $\Delta fT = 166.6667$.**

By analyzing the maximum positions in the preceding results, we notice that the distance between maximums do not differ for different values of $\Delta f$; the separation between maximums depends directly on the transmission instant, in which the transmitted pulse is active. In the preceding simulations the duty cycle was $Tprf = 0.5$. Thus for a lesser value of $prf$ (maintaining the same duty cycle), the maximums are nearer, as it is shown in Fig 5.-17. This ambiguity function were obtained via fixing the $prf$ to $1.5\ [KHz]$. However if we reduce the $prf$ of the transmitted pulse, the blind ranges increase.

The Chapter 6 provides information about a novel method to solve the issues commented above (maximum values deviation and output signal fluctuations). It consists of identify and compensate the Doppler shift by using tunable filters.

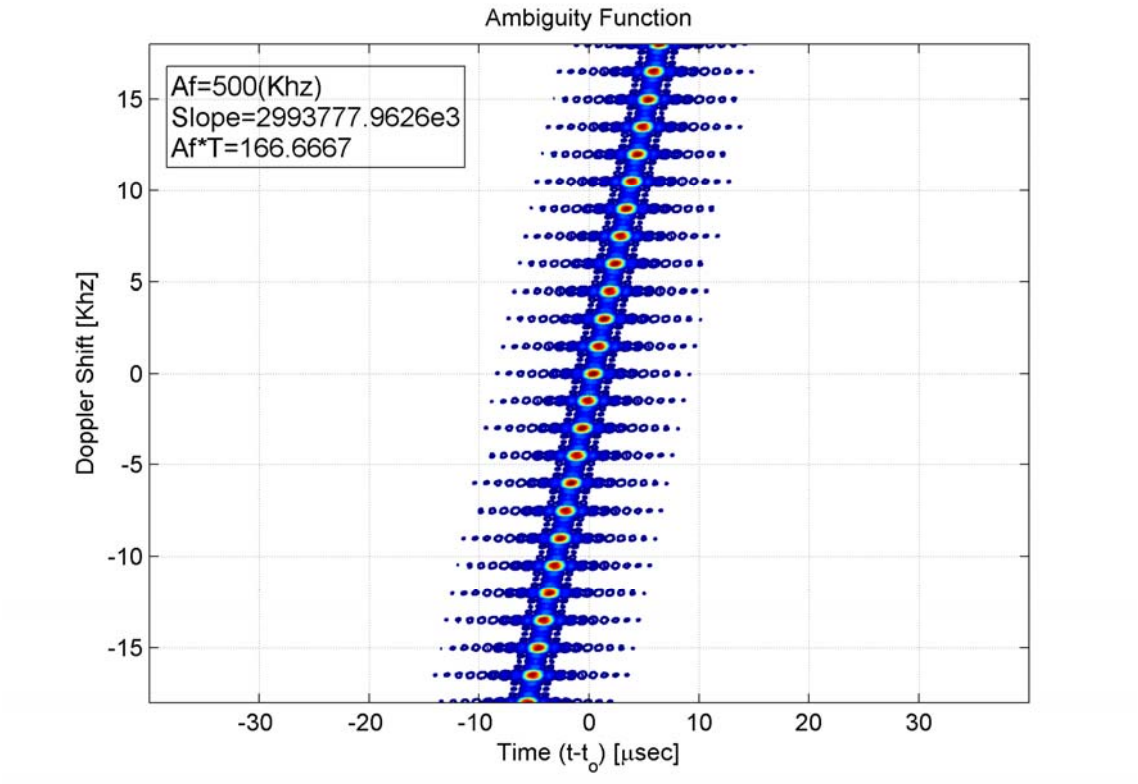


**Fig 5.-17: Simulation 2, Ambiguity Function $\Delta fT = 166.6667$ and $prf = 1.5\ [Khz]$.**

### 5.2.3 Small Target hidden by a larger target

As we commented in preceding sections, a small scattered target may be masked by a larger target, this effect is known as overshadowing (the large one overshadows the small one). This fact is due to the sidelobes presence. We simulated an overshadowing case. For this simulation the values were fixed as shown in Table 5.-3.

| ***Table 5.-3: Simulation 3.*** |
|---|
| $f_0 = 10\ [MHz]$ |
| $\Delta f = 800\ [KHz]$ |
| $prf = 3\ [KHz]$ |
| $T = 166.667\ [\mu s]$ |
| $Number\ of\ pulse = 5$ |

Fig 5.-18 displays a target overshadowed by another bigger target due to the sidelobes. This fact causes a bad detection of the smaller target. Thus, it is necessary to reduce the sidelobes to improve the target detection. Additionally, a large level of sidelobes could cause false alarms.

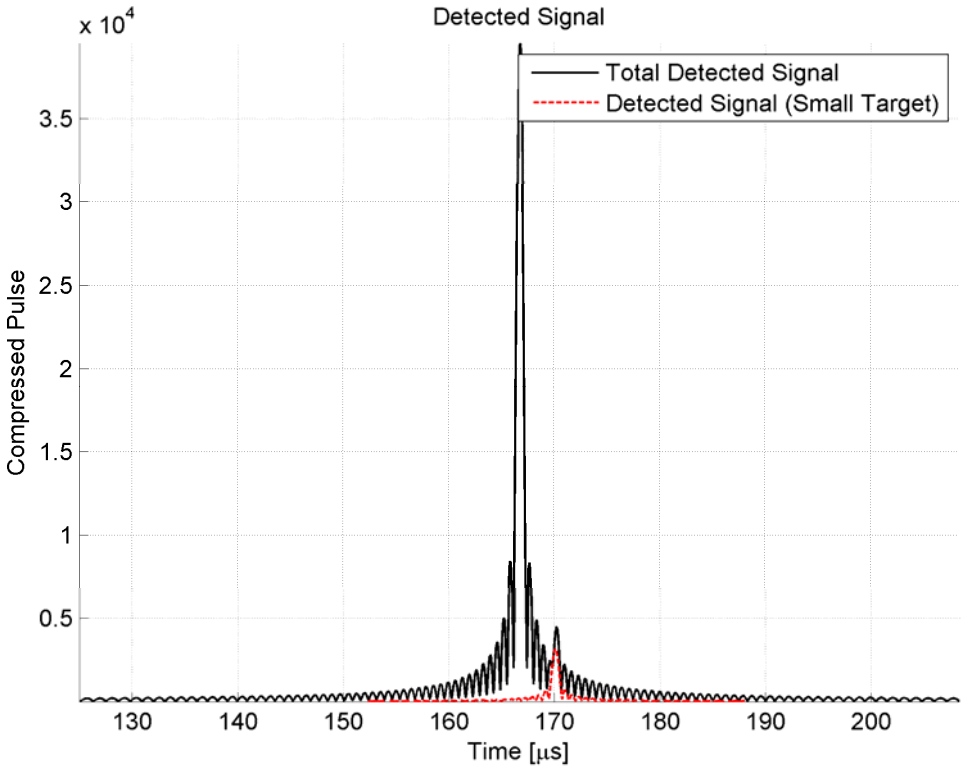


**Fig 5.-18: Simulation 3, Overshadowing Target by using CHIRP Pulse.**

## 5.3. Sidelobes suppression. Mismatching Filtering

This section provides information about the sidelobes suppression by using mismatched filters. We have implemented two filters, the Taylor Filter and its truncated version. We start the study with the second one.

### 5.3.1 Truncated Taylor´s Filter

In this section we observe the result of pulse compression by using a truncated Taylor Filter. We start from assessing the compression performance varying the $\Delta fT$-product by entering a truncated Taylor Filter. Next, we discuss the results obtained by performing a sweep varying the filter parameters to assess how to they affect to the sidelobes suppression. Also we observed the filter transfer function. Before, it is necessary to remember the truncated Taylor´s Filter Transfer Function (see equation **( 4.-36 )** in section 4.3.1):

$$H_T(\omega)|_{truncated} = \left\{k + (1-k)\cos^n\left(\frac{2\pi\omega}{\Delta\omega}\right)\right\} rect\left(\frac{\omega}{\Delta\omega}\right) \qquad \textbf{( 5.-7 )}$$

Where $k = \frac{1-2F_1}{1+2F_1}$.

**Influence of $\Delta fT$-product**

For this simulation we fixed the parameters as Table 5.-4 shows.

| ***Table 5.-4: Simulation 4.*** |
|---|
| $f_0 = 10\ [MHz]$ |
| $prf = 3\ [KHz]$ |
| $T = 166.667\ [\mu s]$ |
| $Number\ of\ pulse = 5$ |
| $n = 4$ |
| $F_1 = 0.4235$ |

The Fig 5.-19, Fig 5.-20, Fig 5.-21 depict the most important results obtained. Notice that, as shown in Fig 5.-6, the final filtered compressed pulses are wider than the compressed pulses without using the mismatched filter. We obtained lower a secondary sidelobe level for some values of the $\Delta fT$-product. However, for other values of the $\Delta fT$-product, we lose the

performances of the mismatched filtering, because the compressed signal deteriorated. These facts summarized in Fig 5.-22.

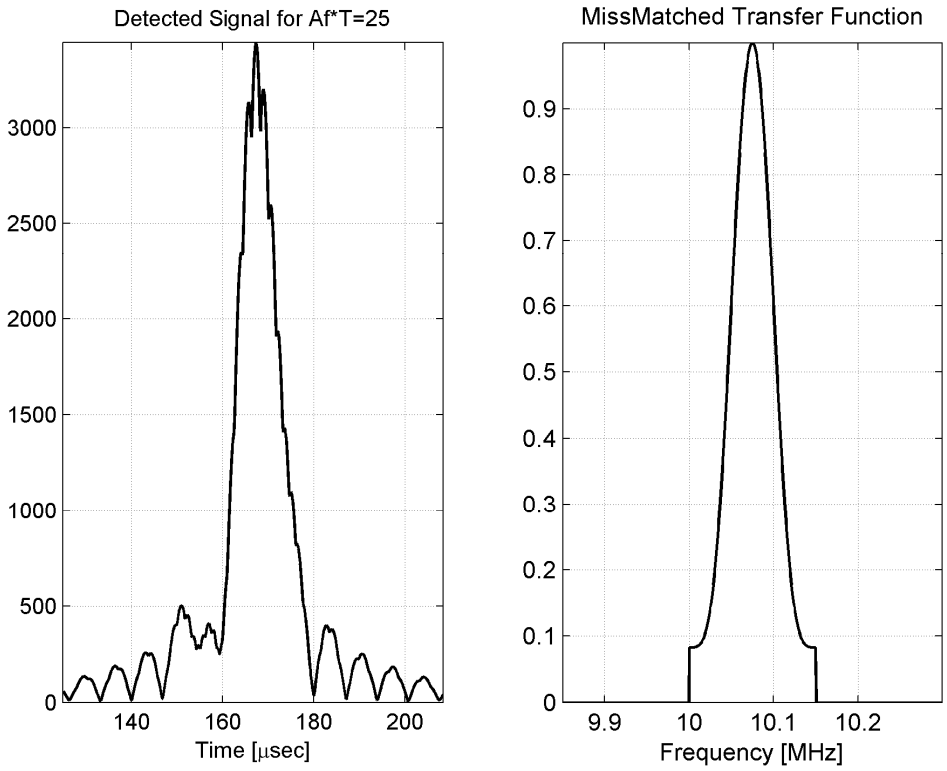


**Fig 5.-19: Simulation 4, Detected Signal $\Delta fT = 25$.**

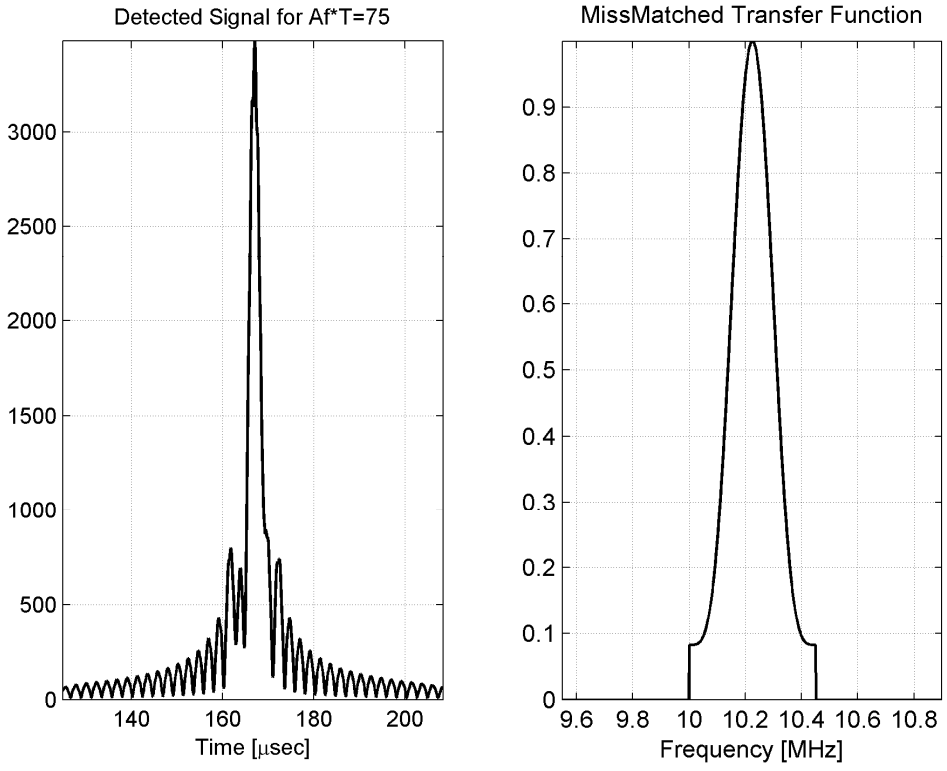


**Fig 5.-20: Simulation 4, Detected Signal $\Delta fT = 75$.**

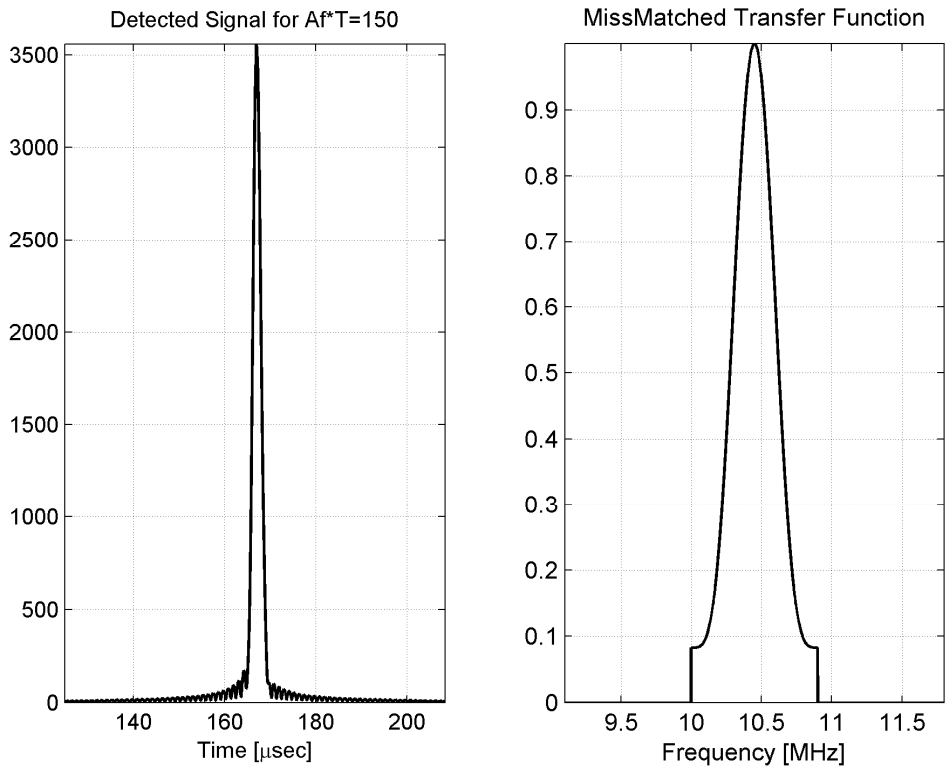


**Fig 5.-21: Simulation 4, Detected Signal $\Delta fT = 75$.**

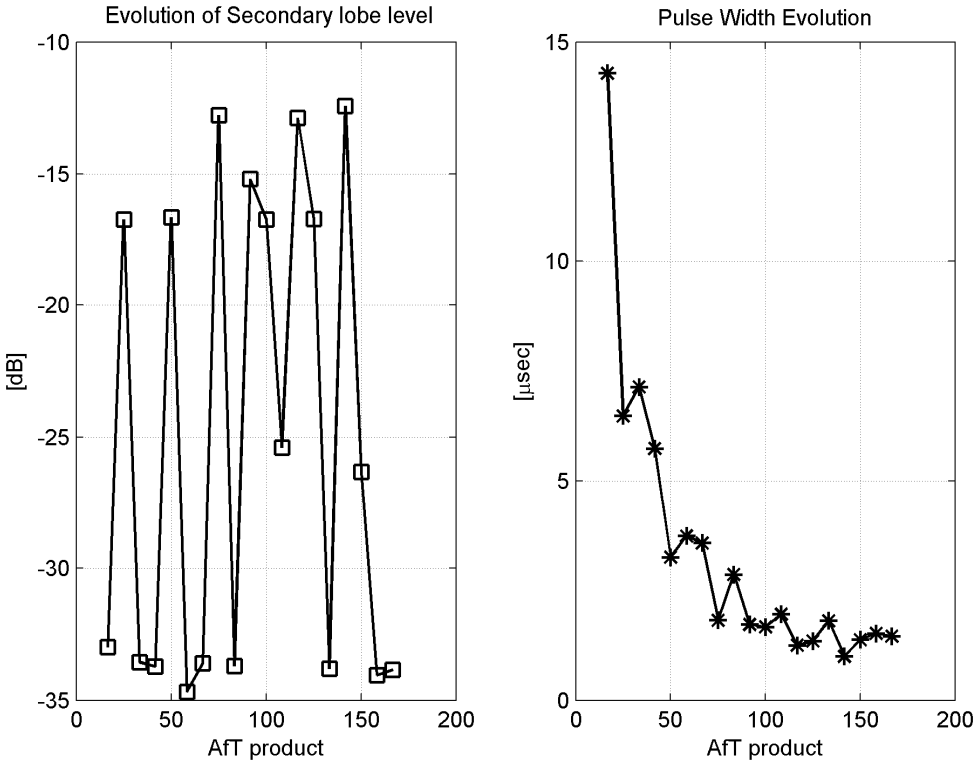


**Fig 5.-22: Simulation 4, Secondary Lobe Level and Pulse Width vs $\Delta fT$-product.**

**Influence of $n$ parameter**

In this section the goal is to assess the influence of the $n$ parameter over the final filtered compressed pulse (see equation **( 5.-7 )**). Table 5.-5 shows the parameters used in these simulations.

| ***Table 5.-5: Simulation 5.*** |
|---|
| $f_0 = 10\ [MHz]$ |
| $\Delta f = 900\ [KHz]$ |
| $prf = 3\ [KHz]$ |
| $T = 166.667\ [\mu s]$ |
| $Number\ of\ pulse = 5$ |
| $F_1 = 0.4235$ |

We have performed a $n$ variable sweeping from $n = 2$ to $n = 15$. The most important results obtained in this set of simulation are depicted in Fig 5.-23, Fig 5.-24, Fig 5.-25 and Fig 5.-26. And Fig 5.-27 summarizes all results obtained.

By observing Fig 5.-27, we conclude that: the minimum value for secondary lobe level is accomplished for $n = 4$, and for some values of $n$ the signal deteriorates, therefore, some performance loss is obtained. Also the pulse width tends to increase (with oscillations), if $n$ increases. Finally, the filter transfer function takes more slope if $n$ increases, due to $\cos^n\left(\frac{2\pi\omega}{\Delta\omega}\right)$ factor (see equation **( 5.-7 )**). Note that the filter transfer function is narrower in Fig 5.-26 than in Fig 5.-23.

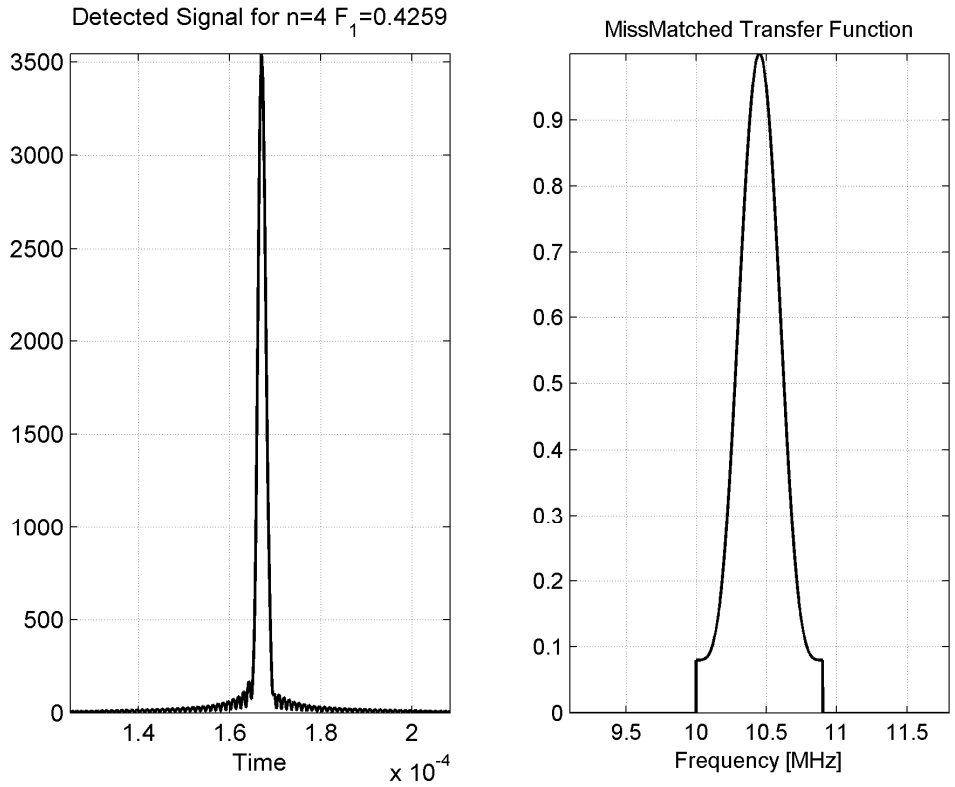


**Fig 5.-23: Simulation 5, Detected Signal $n = 4$.**

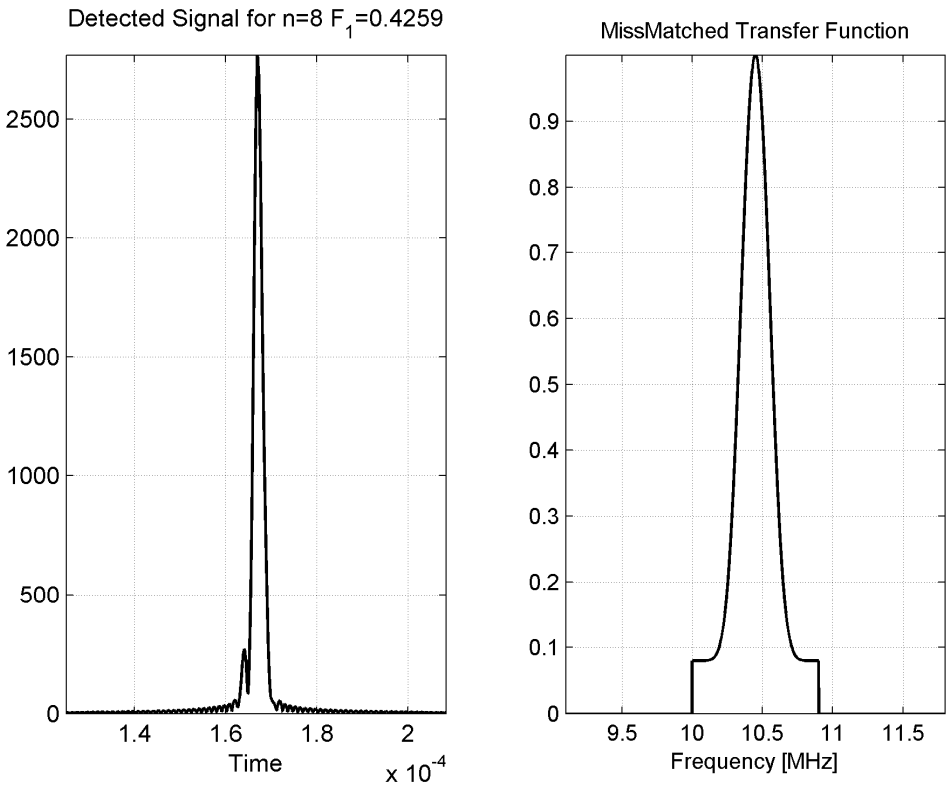


**Fig 5.-24: Simulation 5, Detected Signal $n = 8$.**

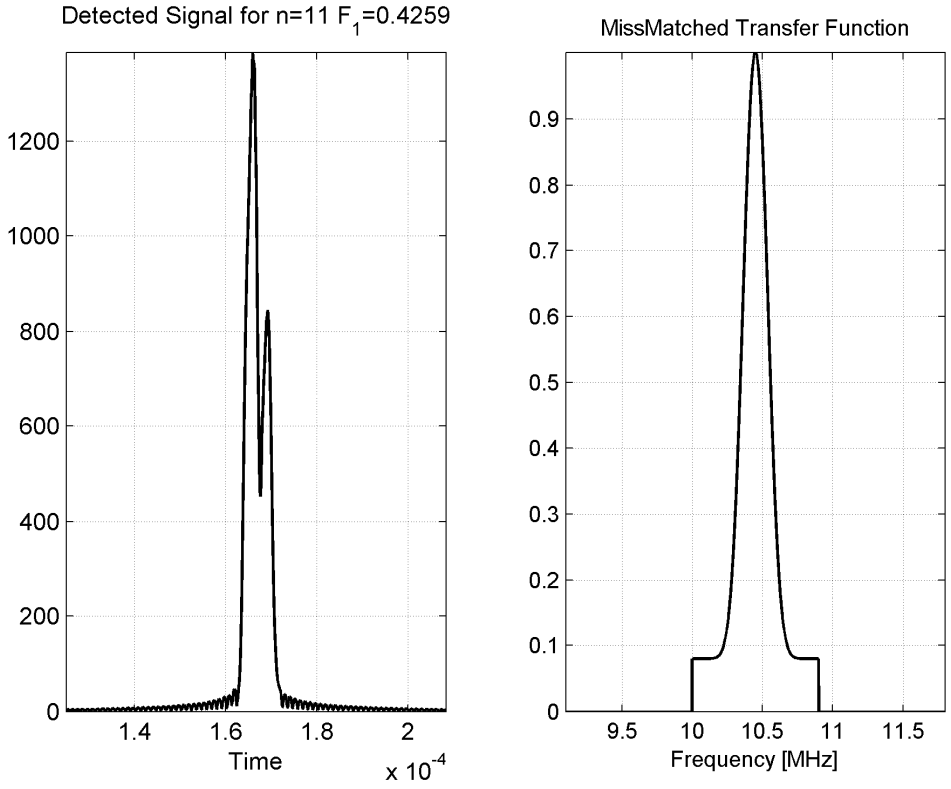


**Fig 5.-25: Simulation 5, Detected Signal $n = 11$.**

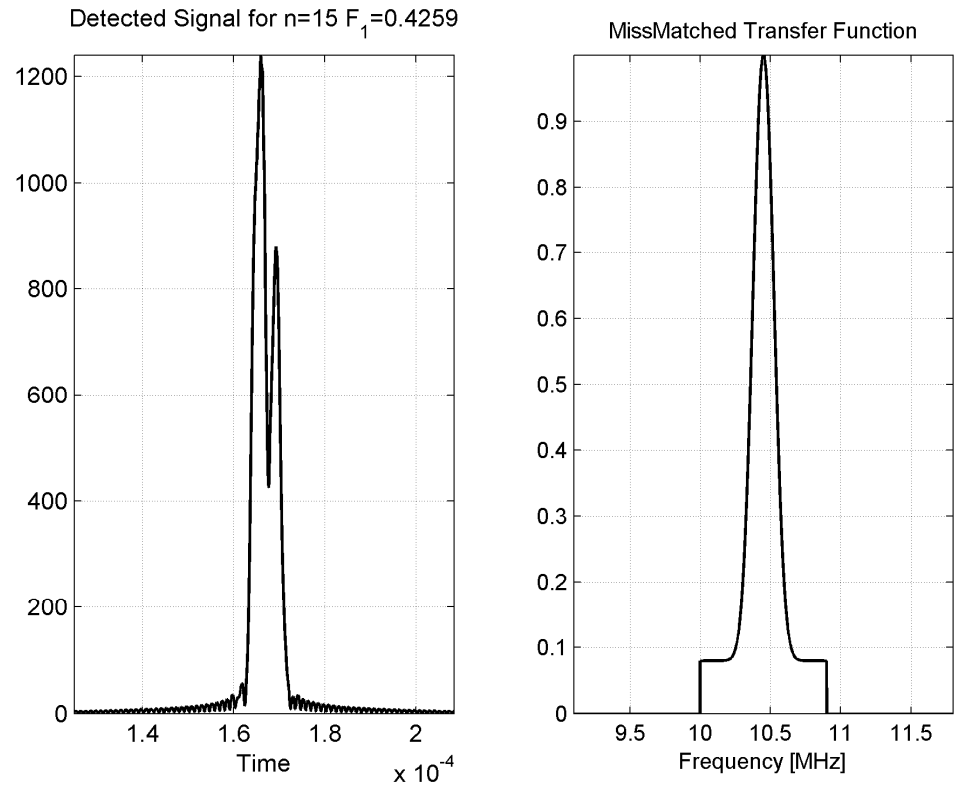


**Fig 5.-26: Simulation 5, Detected Signal $n = 15$.**

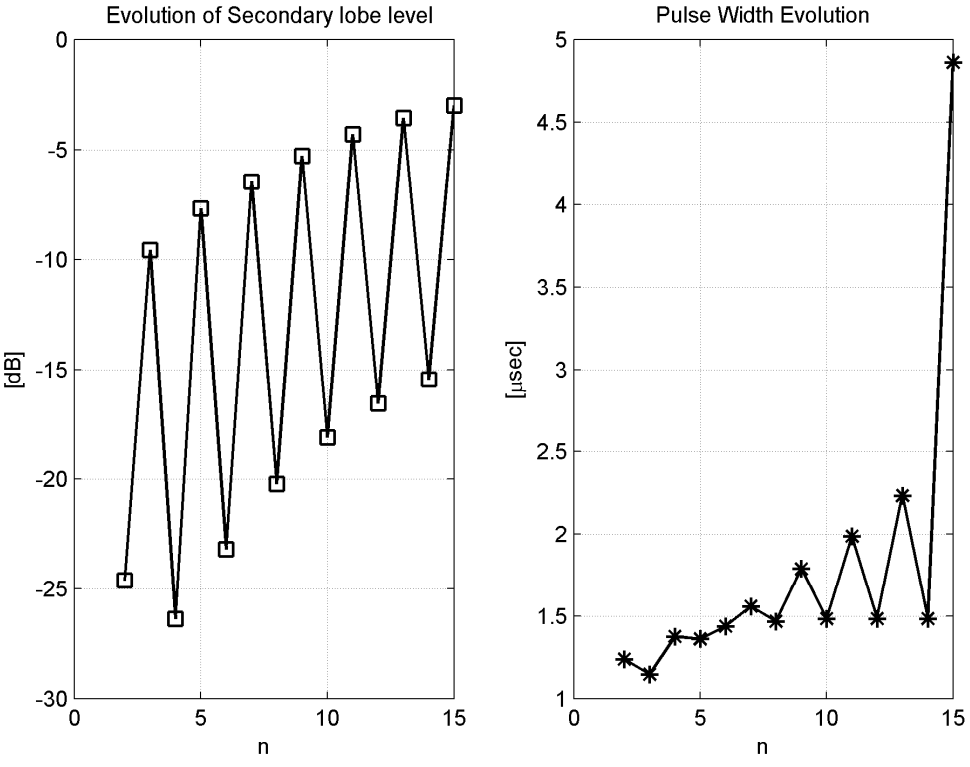


**Fig 5.-27: Simulation 5, Secondary Lobe Level and Pulse Width vs $n$.**

### Influence of $F_1$ parameter

Now we examine the results obtained by sweeping the $F_1$ parameter between $0.3$ and $0.8$ (see equation **( 5.-7 )**). The parameters for this simulation were fixed as Table 5.-6 shows.

| ***Table 5.-6: Simulation 6.*** |
|---|
| $f_0 = 10\ [MHz]$ |
| $\Delta f = 900\ [KHz]$ |
| $prf = 3\ [KHz]$ |
| $T = 166.667\ [\mu s]$ |
| $Number\ of\ pulse = 5$ |
| $n = 4$ |

The most important results are shown in Fig 5.-28, Fig 5.-29 and Fig 5.-30. Fig 5.-31 summarizes the results obtained in terms of secondary lobe level and width of the final filtered pulse.

Notice that the parameter $F_1$ affects to the filter transfer function amplitude, due to the $k$ dependency in the expression **( 5.-7 )**. Also, by observing Fig 5.-31, we notice that the minimum value of $-3dB$ secondary lobe level is accomplished for a value close to $F_1 = 0.5$ value. Also, the pulse width increases, if $F_1$ increases when $F_1$ takes values less than $0.75$; for $F_1 > 0.75$ the pulse width decreases.

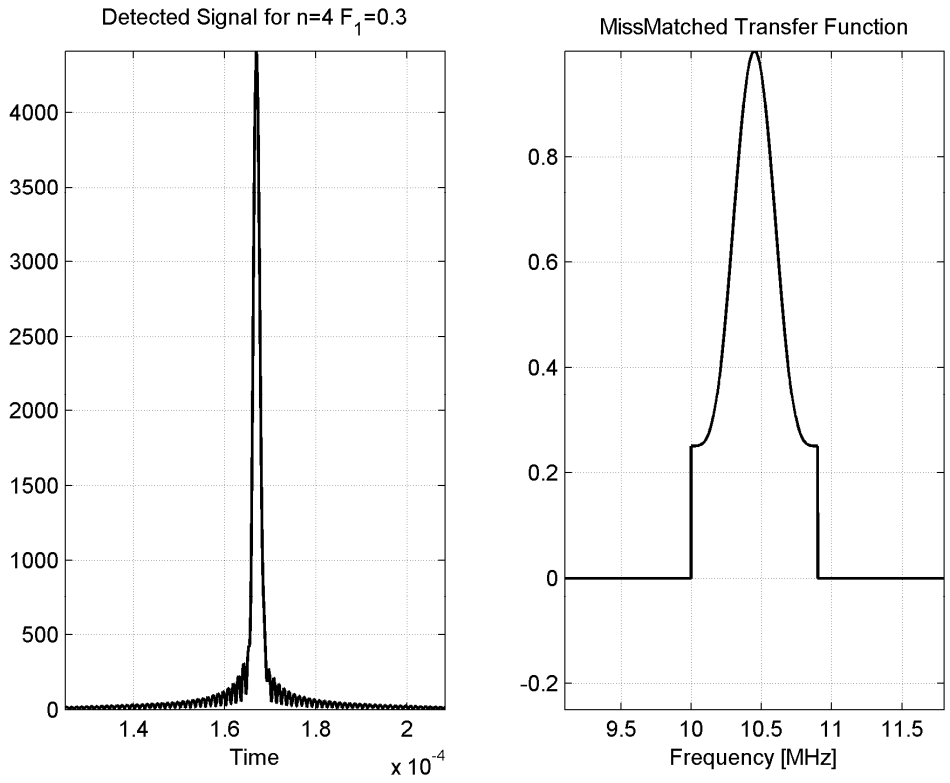


**Fig 5.-28: Simulation 6, Detected Signal $F_1 = 0.3$.**

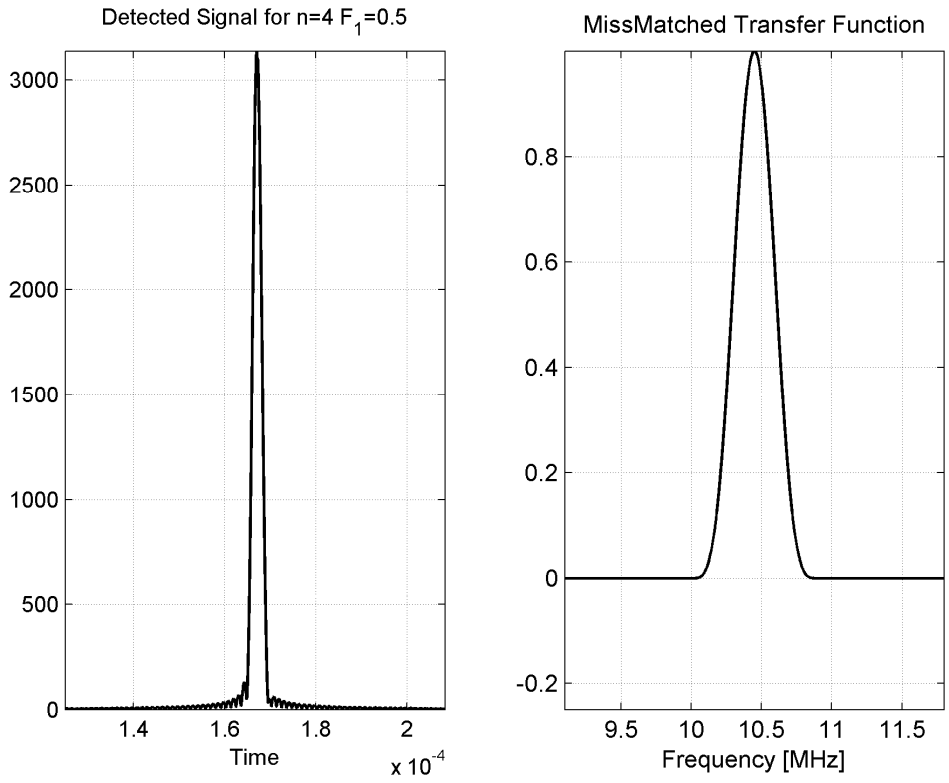


**Fig 5.-29: Simulation 6, Detected Signal $F_1 = 0.5$.**

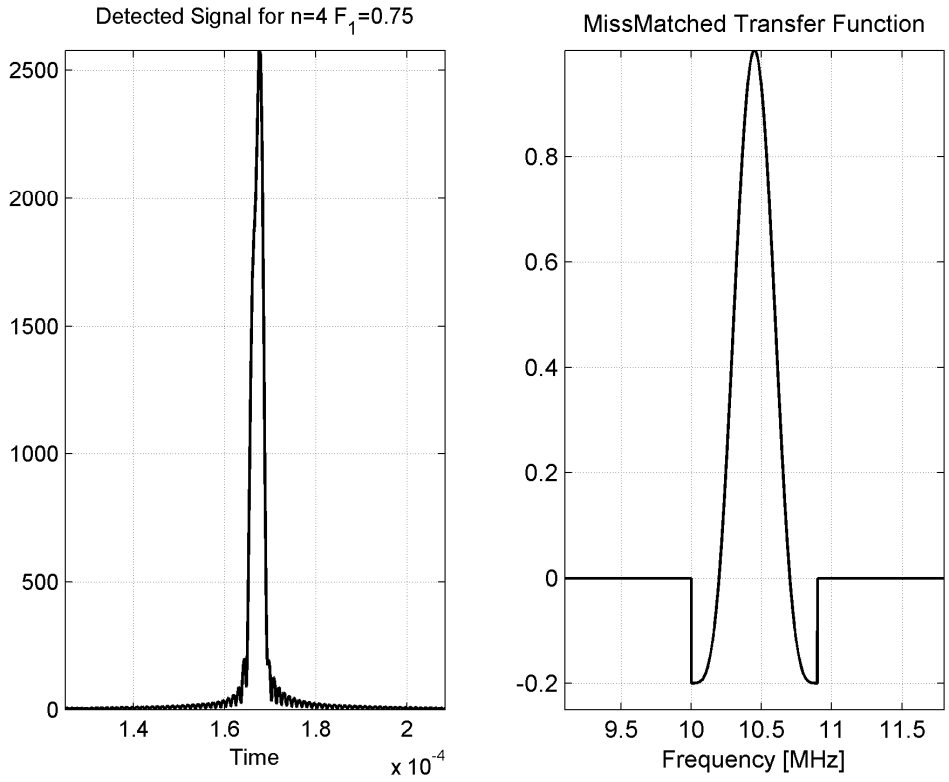


**Fig 5.-30: Simulation 6, Detected Signal $F_1 = 0.75$.**

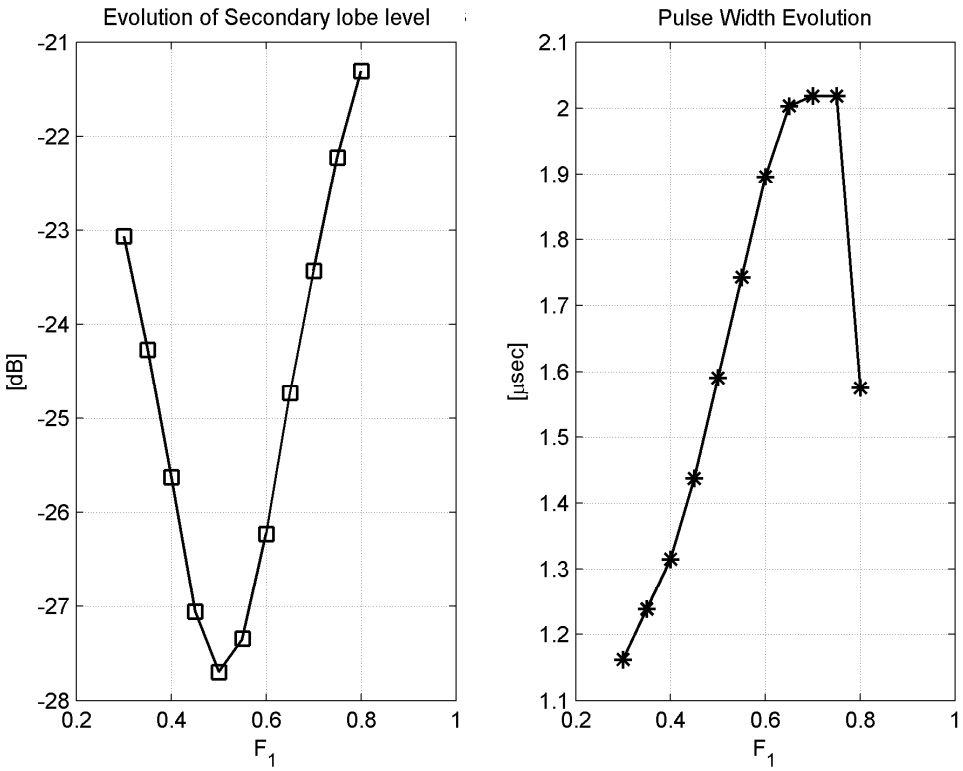


**Fig 5.-31: Simulation 6, Secondary Lobe Level and Pulse Width vs $F_1$.**

**Influence of Doppler shift**

In order to evaluate how the Doppler Effect influences the sidelobes suppression, we calculate the ambiguity function of the detected pulse by entering a truncated Taylor filter. The simulations parameters were fixed as Table 5.-7 shows.

| ***Table 5.-7: Simulation 7.*** |
|---|
| $f_0 = 10\ [MHz]$ |
| $\Delta f = 1000\ [KHz]$ |
| $prf = 3\ [KHz]$ |
| $T = 166.667\ [\mu s]$ |
| $Number\ of\ pulse = 5$ |
| $n = 4$ |
| $F_1 = 0.45$ |

We obtained the following ambiguity function:

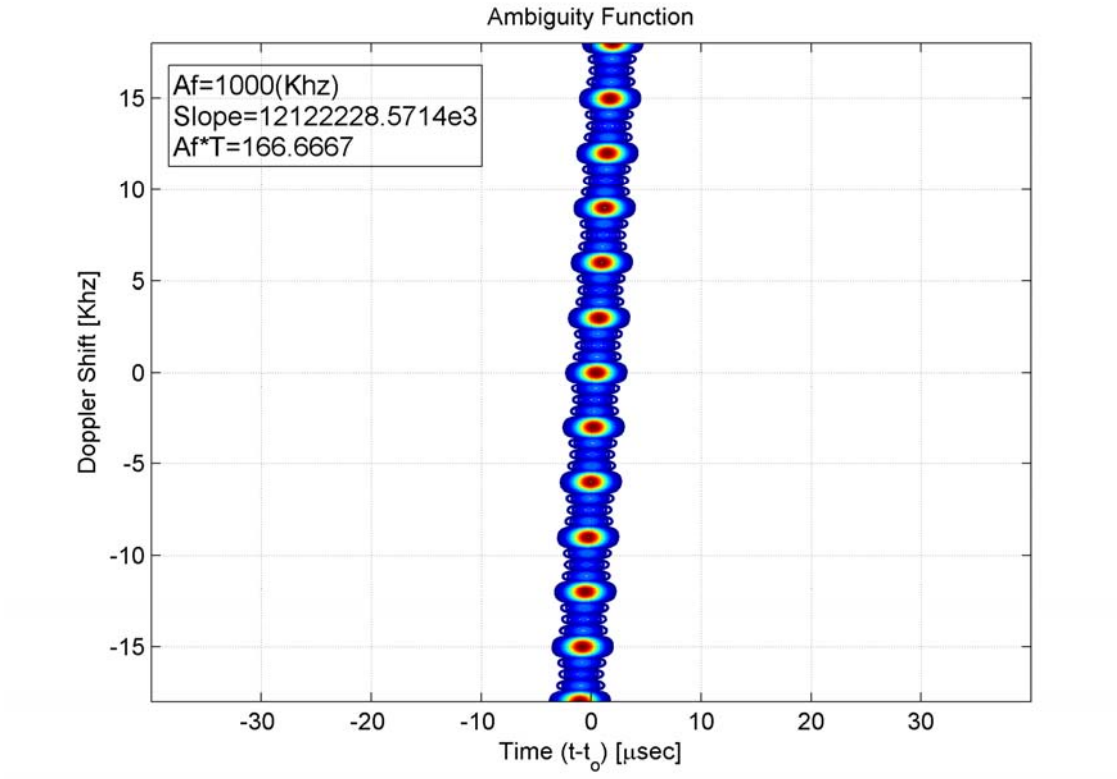


**Fig 5.-32: Simulation 7, Ambiguity Function by using Truncated Taylor´s Filter.**

Notice that the preceding ambiguity function has smaller sidelobe levels than the one depicted by Fig 5.-16 (result obtained without mismatched filter). However, the pulse is significantly wider.

**Discovering a hidden target by using truncated Taylor´s Filter**

In section 5.2.3 we evaluated the issue of overshadowing of a small target. We now perform the same experiment, but including a mismatched filter. The purpose is to verify how a mismatched filter can help in the detection of overshadowing targets. The signal and filter parameters were fixed as Table 5.-8 shows.

| ***Table 5.-8: Simulation 8.*** |
|---|
| $f_0 = 10\ [MHz]$ |
| $\Delta f = 800\ [KHz]$ |
| $prf = 3\ [KHz]$ |
| $T = 166.667\ [\mu s]$ |
| $Number\ of\ pulse = 5$ |
| $n = 4$ |
| $F_1 = 0.45$ |

Fig 5.-33 illustrates the compressed pulses obtained. We can observe that the hidden target is not discovered, since the pulses are wider than without using the truncated Taylor´s Filter. This fact provokes target overshadowing risks. Thus this fact is a drawback.

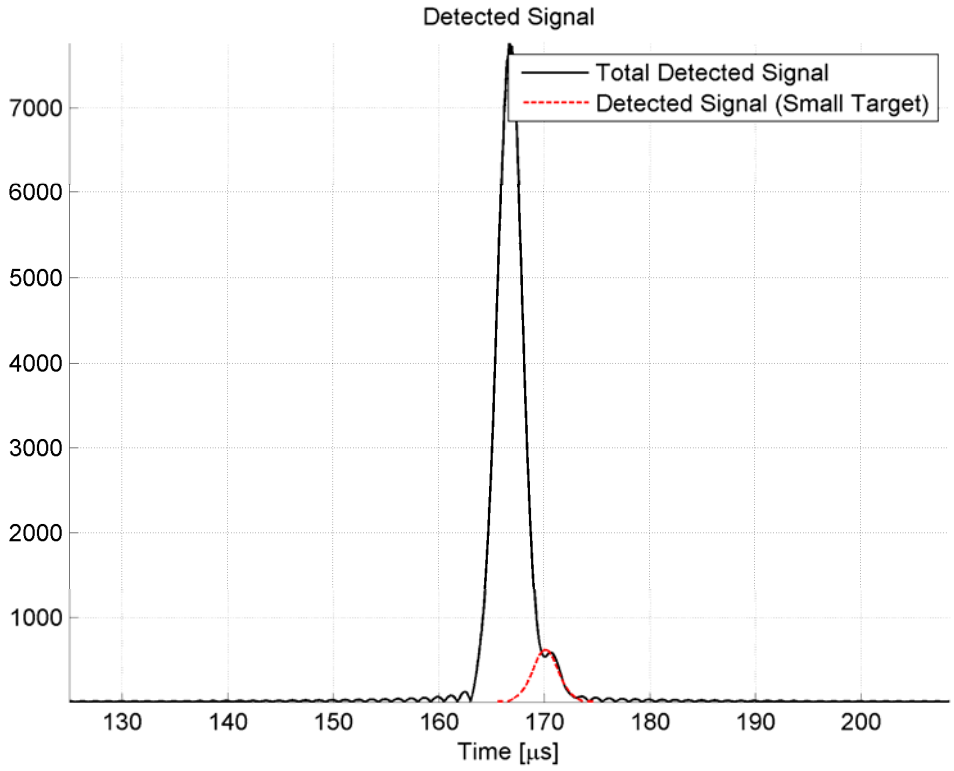


**Fig 5.-33: Simulation 8, Overshadowing Target by using Truncated Taylor´s Filter.**

### 5.3.2 Taylor Filter

In this section we report about the results obtained by using the Taylor Filter to suppress the sidelobes. The transfer function of the Taylor Filter was presented in section 4.3.1.

#### Influence of $\Delta fT$-product

The tendency of the compressed pulse is the same as truncated Taylor Filter case. The parameters used for this simulation are shown by Table 5.-9.

| ***Table 5.-9: Simulation 9*** |
|---|
| $f_0 = 10\ [MHz]$ |
| $prf = 3\ [KHz]$ |
| $T = 166.667\ [\mu s]$ |
| $Number\ of\ pulse = 5$ |
| $n = 4$ |
| $SLL = -32\ [dB]$ |

The pulse width and the secondary sidelobe level are illustrated in Fig 5.-34 to summarize this behavior. Note that for some values of the $\Delta fT$-product the sidelobes decrease, but for other values the final filtered signal deteriorates. Furthermore, the larger the $\Delta fT$-product, the narrower the pulse. We concluded that the Taylor Filter performances are better than its truncated version, since the first one produces narrower filtered pulses for the same secondary lobe level (Fig 5.-22).

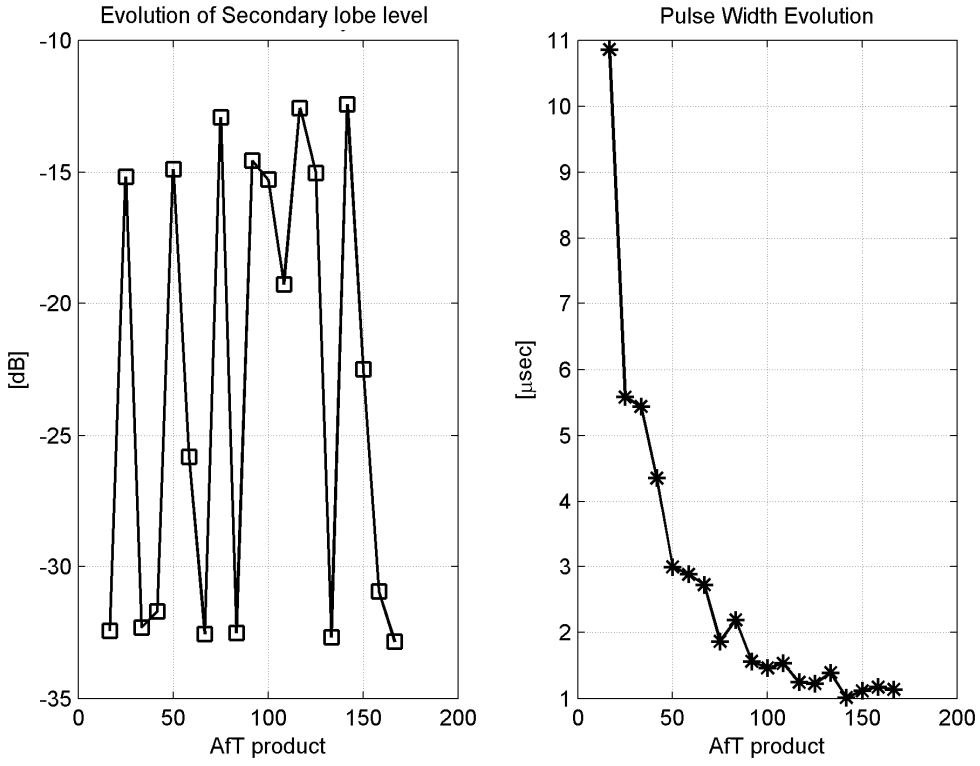


**Fig 5.-34: Simulation 9, Secondary Lobe Level and Pulse Width vs $\Delta fT$.**

**Influence of $n$ parameter**

For this experiment we perform a sweep on the variable $n$ (see equation **( 4.-24 )** in section 4.3.1), and the other parameters were fixed as Table 5.-10 shows.

| ***Table 5.-10: Simulation 10.*** |
|---|
| $f_0 = 10\ [MHz]$ |
| $\Delta f = 900\ [KHz]$ |
| $prf = 3\ [KHz]$ |
| $T = 166.667\ [\mu s]$ |
| $Number\ of\ pulse = 5$ |
| $SLL = -32\ [dB]$ |

Next, we show some detected signals obtained from this experiment in Fig 5.-35, Fig 5.-36 and Fig 5.-37. Also the secondary lobe level and pulse width evolution is depicted by Fig 5.-38.

By observing from Fig 5.-35 to Fig 5.-37, we note that the Filter Transfer function varies, if $n$ varies; namely, the larger the variable $n$, the narrower the transfer function of the Taylor Filter. According to Fig 5.-38, the second lobe level tends to decrease slowly, if $n$ increases. However, this tendency saturates for $n > 3$. Also, notice that the pulse width varies slightly, although it remains relatively constant for all the values selected for "n".

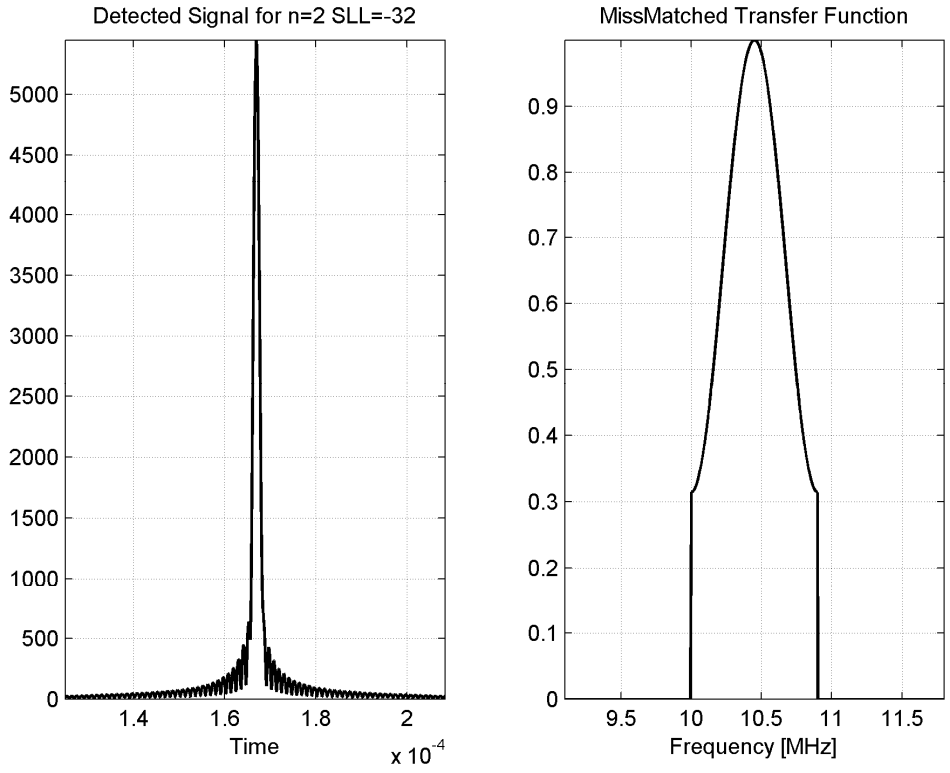


**Fig 5.-35: Simulation 10, Detected Signal $n = 2$.**

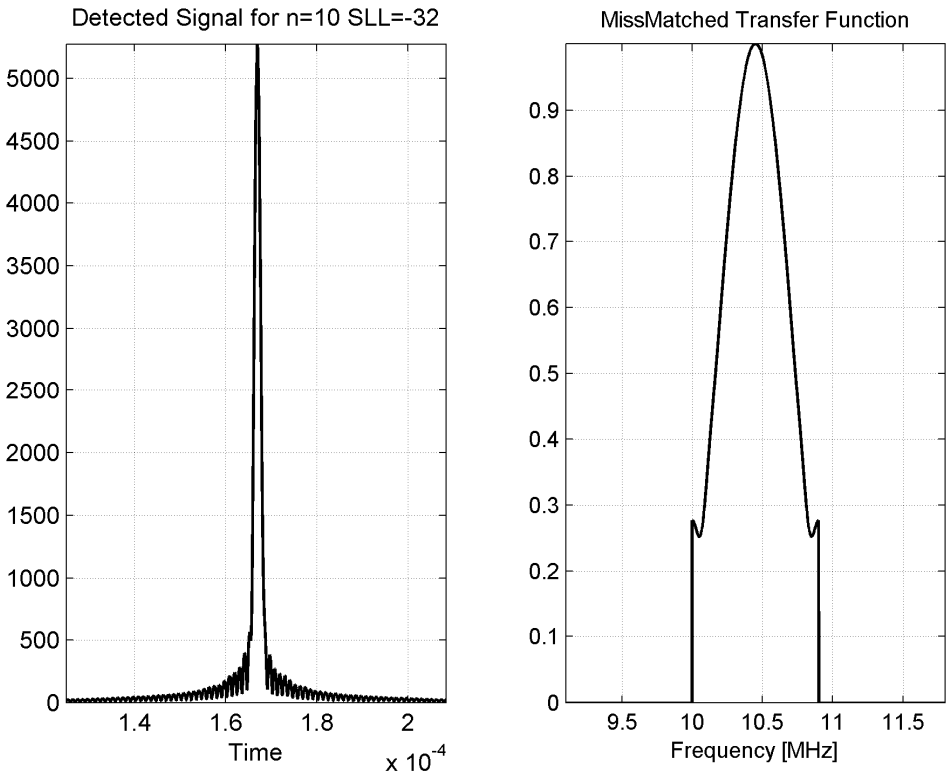


**Fig 5.-36: Simulation 10, Detected Signal $n = 10$.**

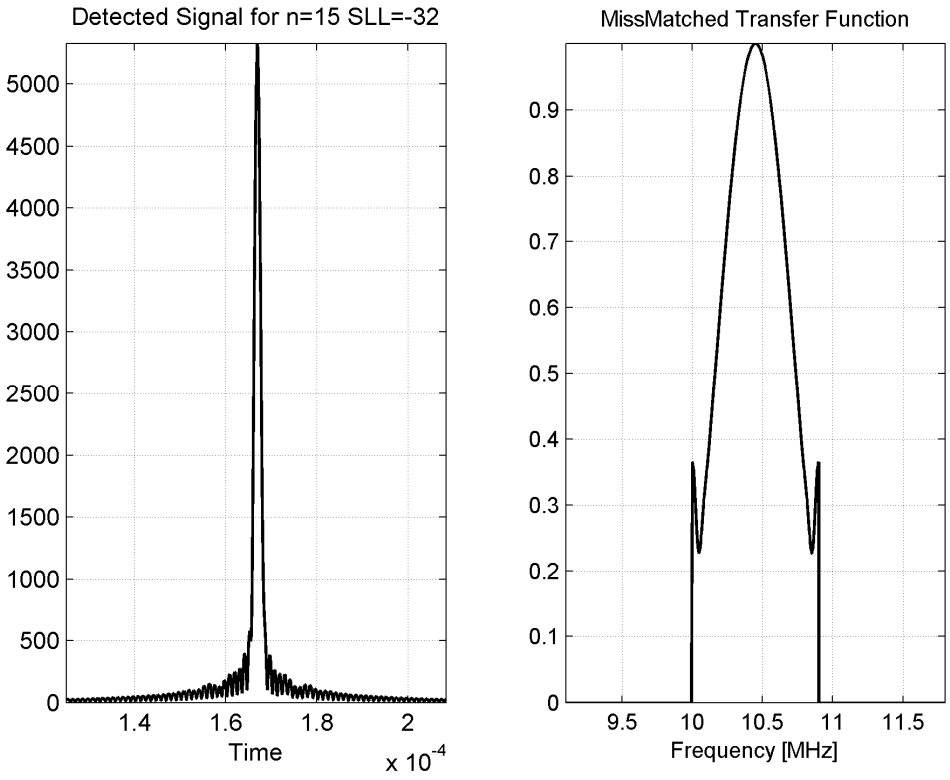


**Fig 5.-37: Simulation 10, Detected Signal $n = 15$.**

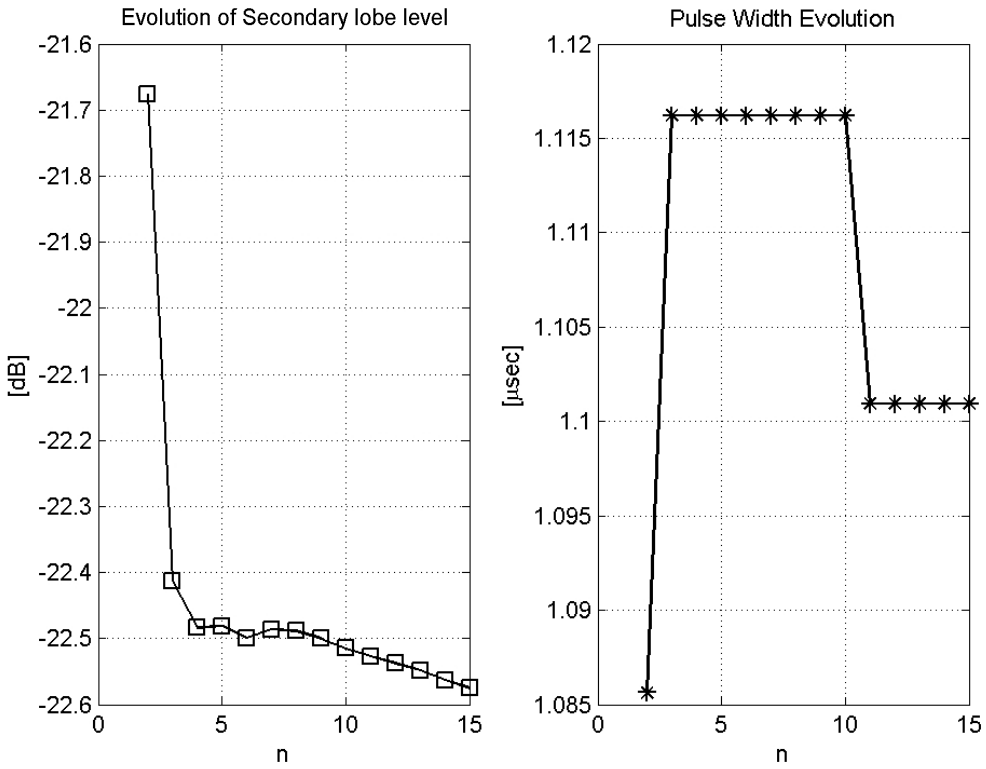


**Fig 5.-38: Simulation 10, Secondary Lobe Level and Pulse Width vs $n$.**

### Influence of $SLL$ parameter

To continue the Taylor Filter study, we performed an $SLL$ parameter sweep, from $-22\ to\ -50\ [dB]$ with $-3\ [dB]$ step size. This parameters represents the desired secondary lobe level (see equations from **( 4.-24 )** to **( 4.-32 )** in section 4.3.1). The signal parameters were fixed as Table 5.-11 shows.

| ***Table 5.-11: Simulation 11.*** |
|---|
| $f_0 = 10\ [MHz]$ |
| $\Delta f = 900\ [KHz]$ |
| $prf = 3\ [KHz]$ |
| $T = 166.667\ [\mu s]$ |
| $Number\ of\ pulse = 5$ |
| $n = 4$ |

The more relevant results are illustrated in Fig 5.-39, Fig 5.-40 and Fig 5.-41. Additionally, Fig 5.-42 summarizes all results obtained in this simulation. The results depicted above shown that the secondary lobe level decreases if the $SLL$ parameter decreases. As can be seen in Figure Fig 5.-42, the compressed pulse width increases if $SLL$ parameter decreases.

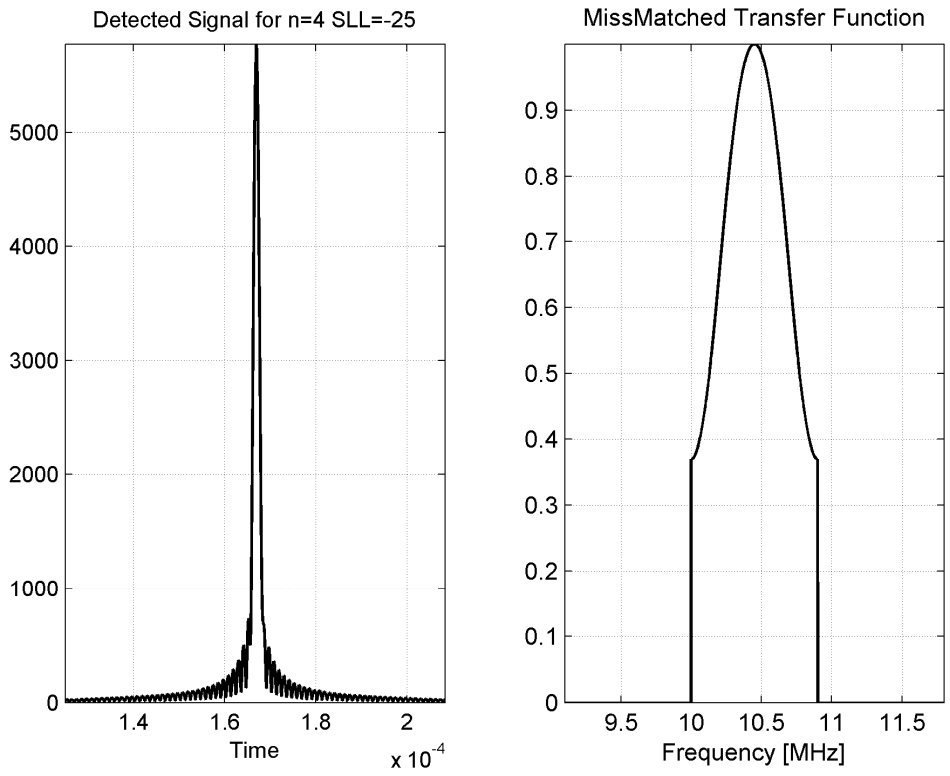


**Fig 5.-39: Simulation 11, Detected Signal $SLL = -25\ [dB]$.**

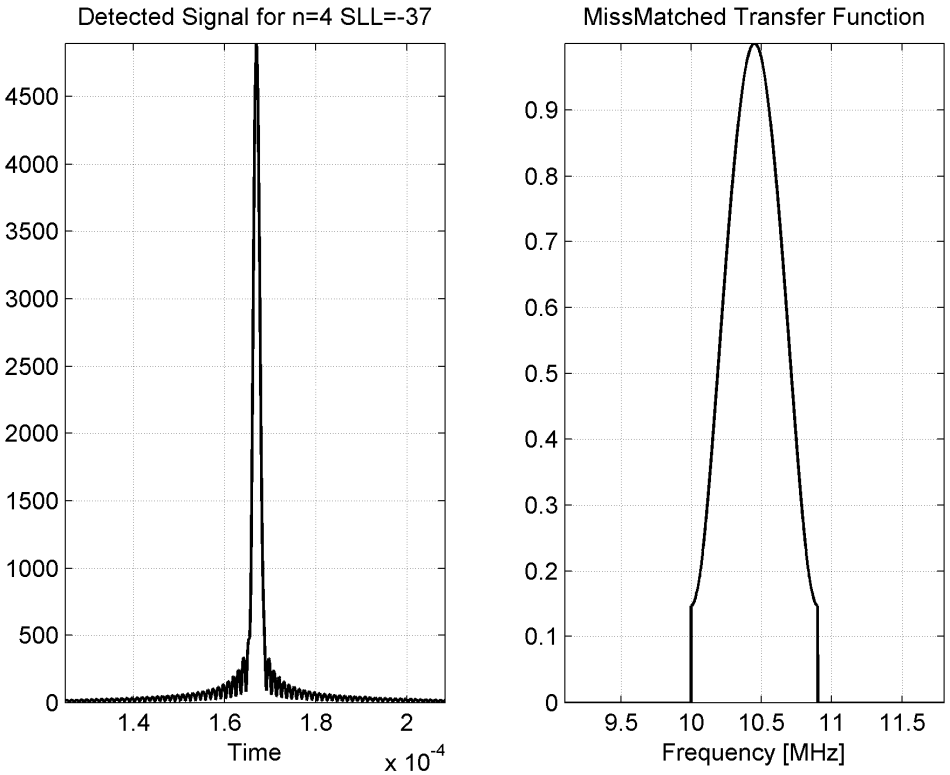


**Fig 5.-40: Simulation 11, Detected Signal $SLL = -37\ [dB]$.**

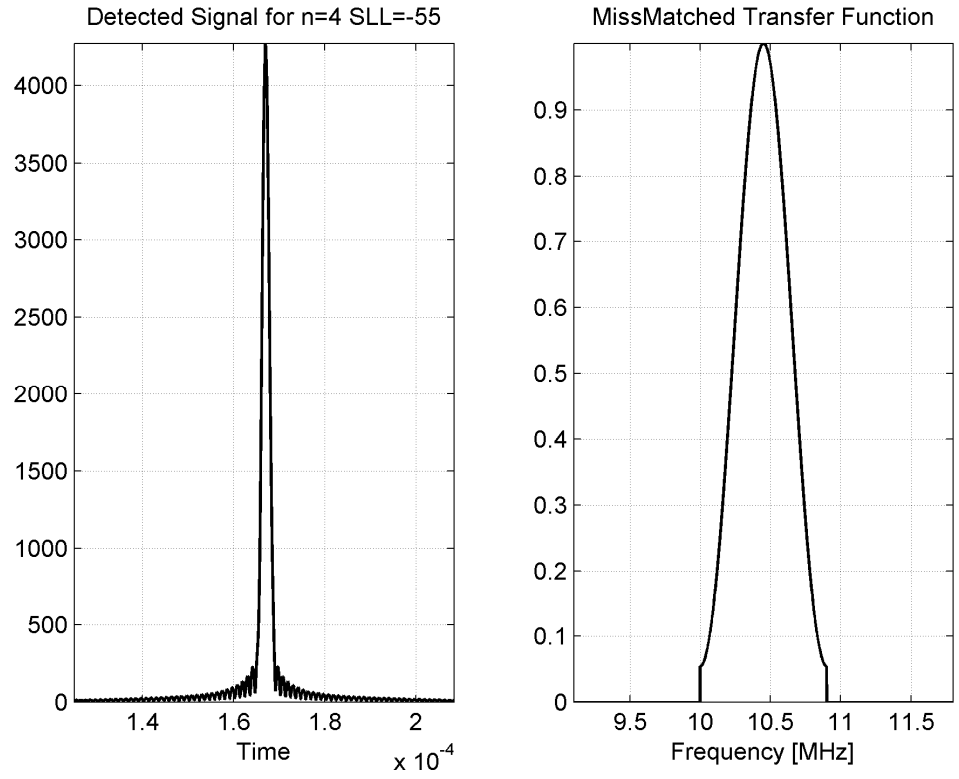


**Fig 5.-41: Simulation 11, Detected Signal $SLL = -55\ [dB]$.**

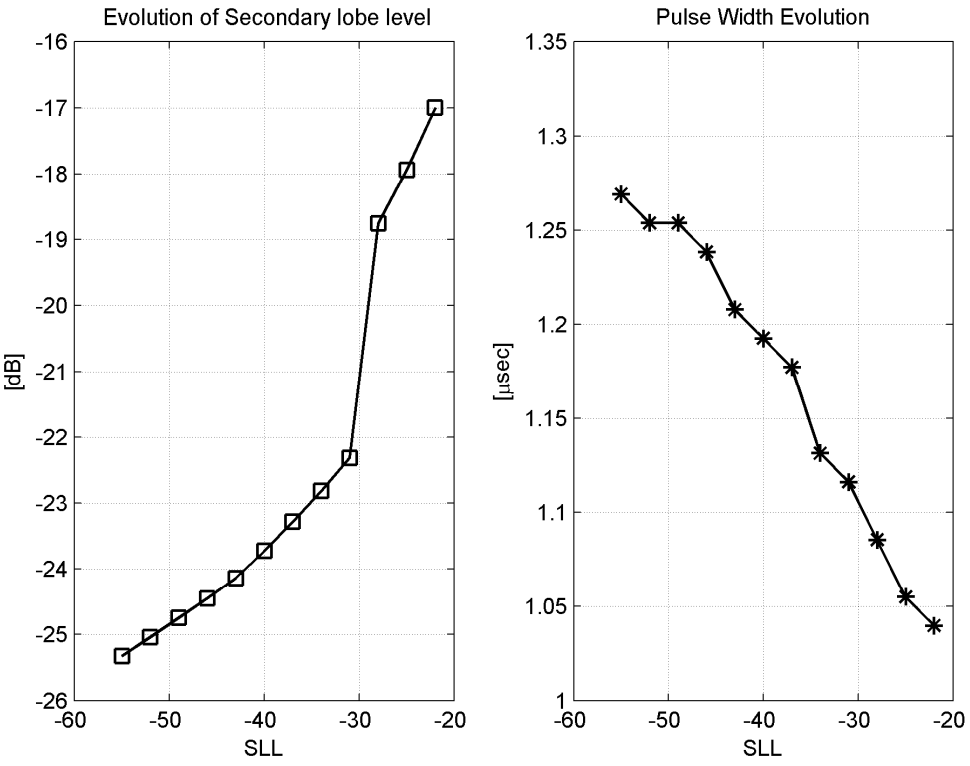


**Fig 5.-42: Simulation 10, Secondary Lobe Level and Pulse Width vs $SLL$.**

**Influence of Doppler shift**

Next, we observe the ambiguity function (Fig 5.-43) calculated by using the Taylor mismatched filter with the parameters shown if Table 5.-12.

| ***Table 5.-12: Simulation 12.*** |
|---|
| $f_0 = 10\ [MHz]$ |
| $\Delta f = 1000\ [KHz]$ |
| $prf = 3\ [KHz]$ |
| $T = 166.667\ [\mu s]$ |
| $Number\ of\ pulse = 5$ |
| $n = 4$ |
| $SLL = -32\ [dB]$ |

Notice that the ambiguity function shown in Fig 5.-43 is narrower than the ambiguity function obtained by using the truncated Taylor´s Filter (Fig 5.-27). Furthermore, the maximums deviation due to Doppler shift is the same as the preceding simulations, Fig 5.-27 and Fig 5.-12. Also the separation between maximums is the same. This fact confirms that the distance between maximums depends only on the $PRF$, and not on the mismatched filter applied to reduce sidelobe levels.

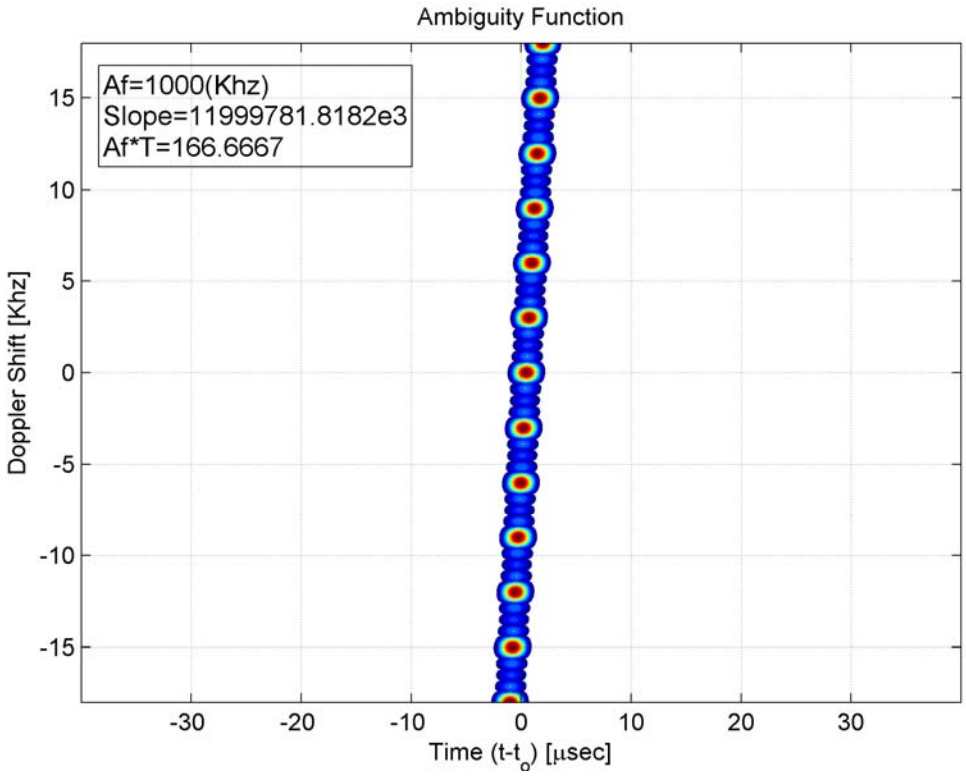


**Fig 5.-43: Simulation 12, Ambiguity Function by using Taylor´s Filter.**

**Discovering a hidden target by using Taylor´s Filter**

To characterize completely this mismatched filter, we repeated the experiment of a small target masked by another bigger one. The parameters used are shown in Table 5.-13.

| ***Table 5.-13: Simulation 13.*** |
|---|
| $f_0 = 10\ [MHz]$ |
| $\Delta f = 800\ [KHz]$ |
| $prf = 3\ [KHz]$ |
| $T = 166.667\ [\mu s]$ |
| $Number\ of\ pulse = 5$ |
| $n = 4$ |
| $SLL = -32\ [dB]$ |

According to Fig 5.-44, the Fig 5.-33 and Fig 5.-18, we conclude that the Taylor´s Filter is better than its truncated version to unmask a small target. Besides, this last result presents narrower pulses than in Fig 5.-13. However, the suppression sidelobes is worse than in Fig 5.-28, due to the parameters selected for the simulation.

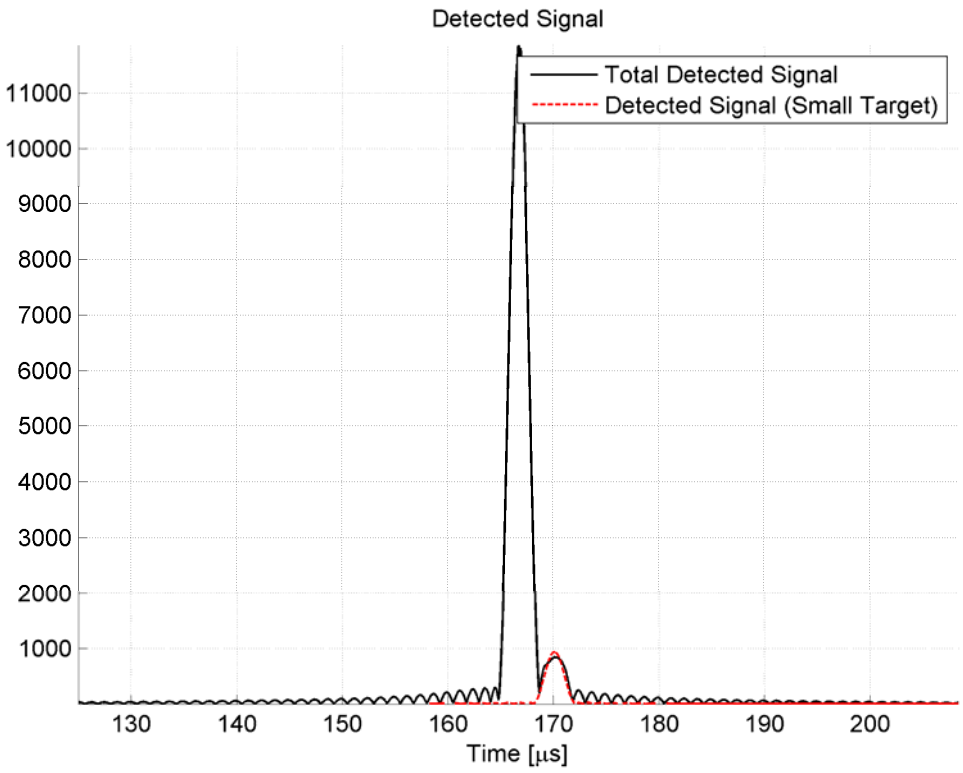


**Fig 5.-44: Simulation 13, Overshadowing Target by using Taylor´s Filter.**

## 5.4. Sidelobes suppression. FM laws

This section provides information about the simulations of pulse compression by using FM laws. We have used the five FM laws described in section 4.3.2. To summarize the results, we review the more relevant graphs. Furthermore, the Appendix B provides more information about these experiments. All FM laws were analyzed jointly. The FM laws used below are depicted in the figures from Fig 4.-11 to Fig 4.-15.

### 5.4.1 $\Delta fT$-product dependency for FM laws

Firstly, we evaluated the performances of the compressed pulse for several values of $\Delta fT$-product by using the different FM laws. The parameters for this experiment were fixed as shown in Table 5.-14.

| ***Table 5.-14: Simulation 14.*** |
|---|
| $f_0 = 10\ [MHz]$ |
| $prf = 3\ [KHz]$ |
| $T = 166.667\ [\mu s]$ |
| $Number\ of\ pulse = 5$ |

The $\Delta f$ sweep was set from $100\ to\ 1000\ [KHz]$. Since for the most of these compressed waveforms it is quite difficult to measure their secondary lobe level, we changed the measuring criterion. To measure the performance, in terms of sidelobes suppression, we calculated the mean level of signal when the amplitude of signal is under $-3dB$ with respect to its maximum. Thus we can express this criterion with the following mathematical relation

$$MSL\ (Mean\ Sidelobes\ Level) = \frac{1}{n}\sum s_c(t)|_{s_c<-3dB} \qquad \textbf{(5.-8)}$$

Where $s_c(t)$ is the normalized compressed signal in logarithmic scale, and $n$ is the length of the summation operator (number of samples that fulfill $s_c < -3dB$).

The figures Fig 5.-45, Fig 5.-46, Fig 5.-47, Fig 5.-48 and Fig 5.-49 illustrate the results obtained for $\Delta fT = 900\ [KHz]$ by using the FM Laws studied in section 4.3.2. In addition, Fig 5.-50 summarizes the results obtained for all values of $\Delta f$ and for all FM laws.

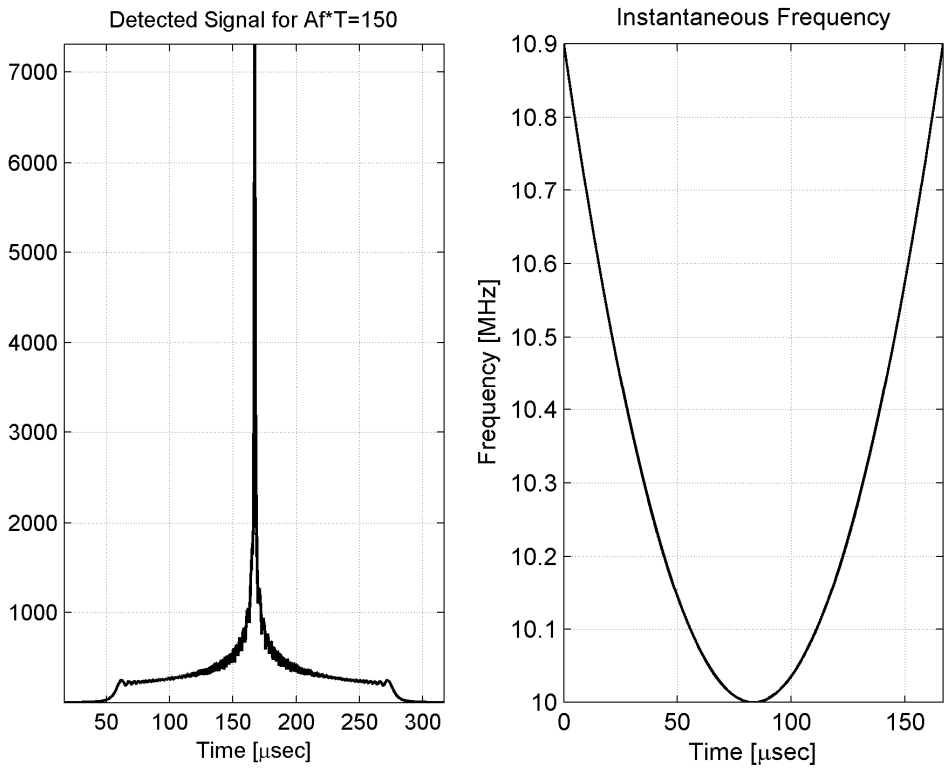


**Fig 5.-45: Simulation 14, Detected Signal for $\Delta fT = 150$ (Even quadratic).**

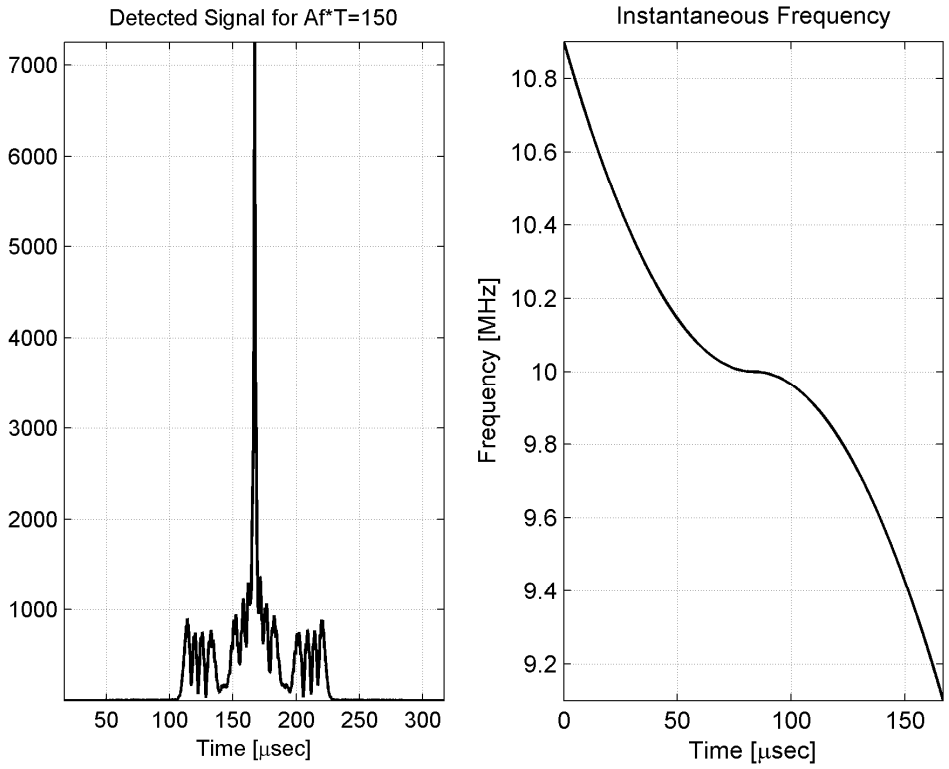


**Fig 5.-46: Simulation 14, Detected Signal for $\Delta fT = 150$ (Odd quadratic).**

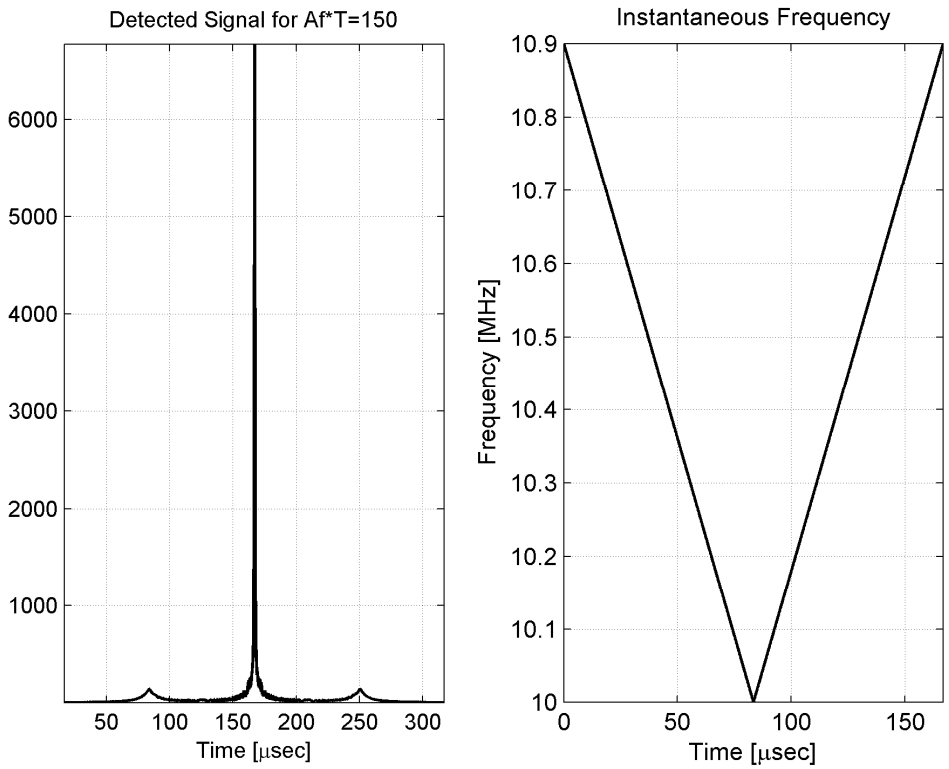


**Fig 5.-47: Simulation 14, Detected Signal for $\Delta fT = 150$ (Even vee).**

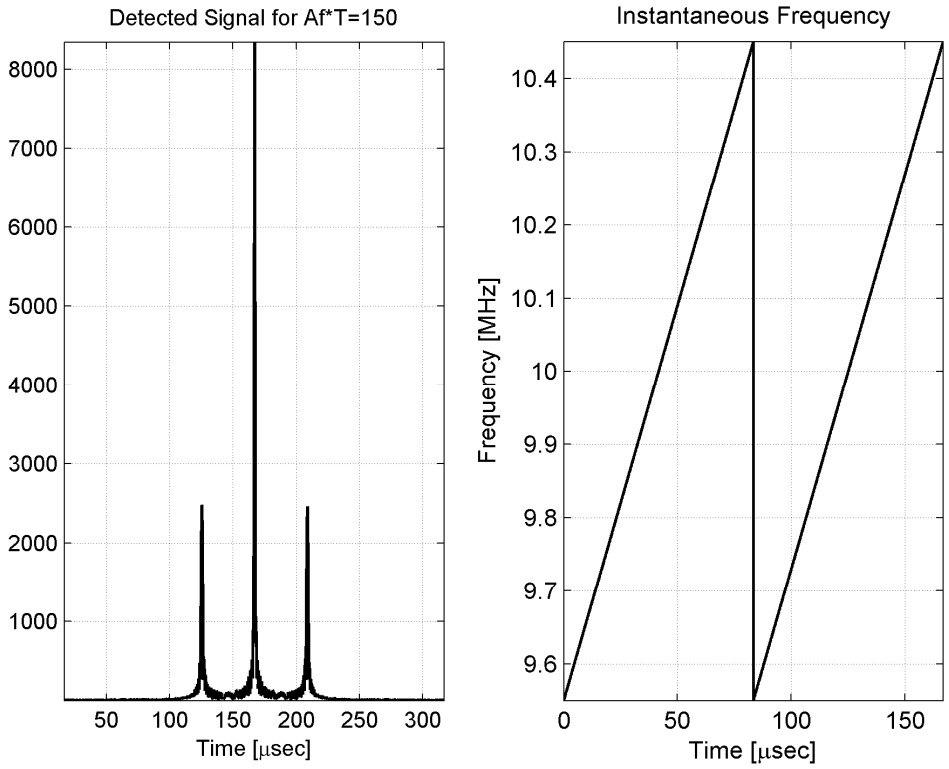


**Fig 5.-48: Simulation 14, Detected Signal for $\Delta fT = 150$ (Odd vee).**

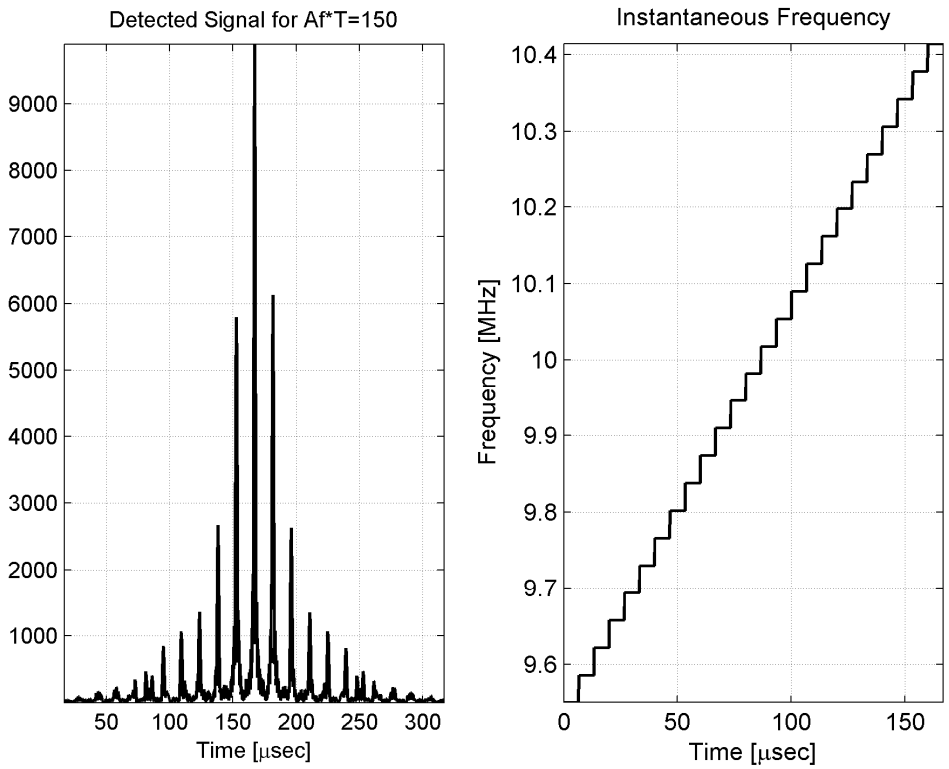


**Fig 5.-49: Simulation 14, Detected Signal for $\Delta fT = 150$ (Stepped linear FM).**

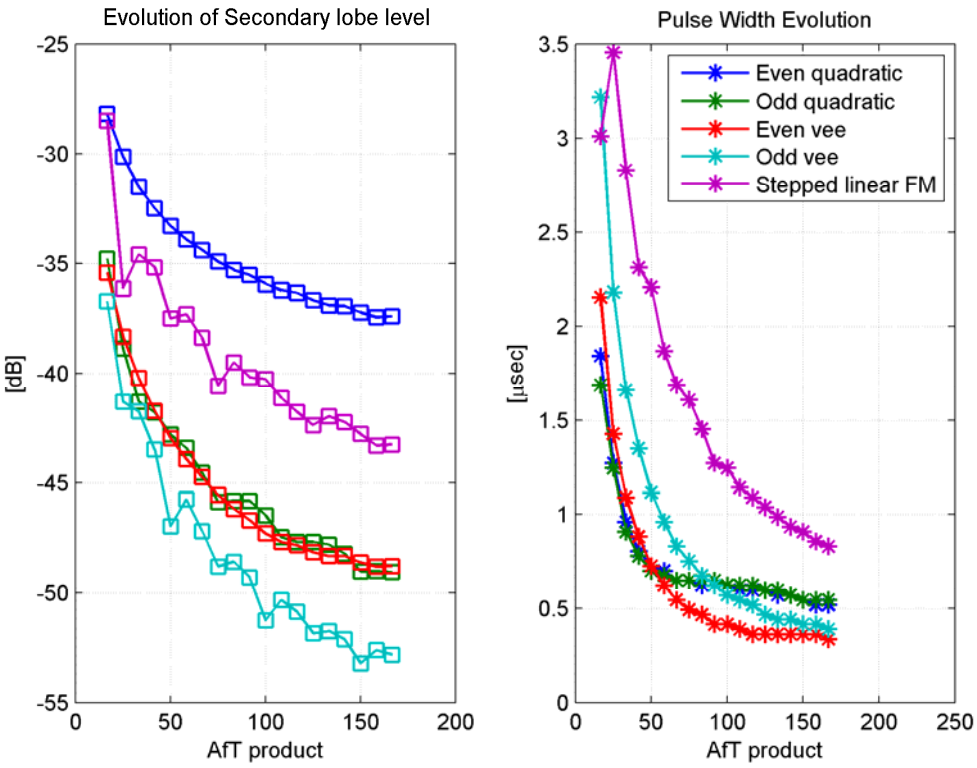


**Fig 5.-50: Simulation 14, Secondary Lobe Level and Pulse Width vs $\Delta fT$.**

According to Fig 5.-50, which shows the secondary lobe level at $-3dB$ and pulse width evolution, the **Odd vee** FM law presents, in terms of suppression of sidelobes, the best performances for all considered values of $\Delta fT$-product. Additionally, it also presents a good pulse width. The **Even vee** FM law is the best option in terms of pulse width if $\Delta fT > 50$, however it presents a same behavior, in terms of suppression sidelobes, as the **Odd quadratic** FM law (worse than **Odd vee**). **Odd quadratic** FM law has very similar pulse width evolution than the **Even quadratic** FM law, which presents the worst performances in sidelobes suppression terms. Finally, the **Stepped linear FM** presents the widest compressed pulse, but in secondary lobe reduction is better than the **Even quadratic** FM law.

### 5.4.2 FM laws pulse compression for moving targets

To evaluate the Doppler Effect when we use FM laws, we have computed the ambiguity functions for the preceding FM laws. For this purpose, the simulation parameters were fixed as shown in Table 5.-15.

| ***Table 5.-15: Simulation 15.*** |
|---|
| $f_0 = 10\ [MHz]$ |
| $\Delta f = 1000\ [KHz]$ |
| $prf = 3\ [KHz]$ |
| $T = 166.667\ [\mu s]$ |
| $Number\ of\ pulse = 5$ |

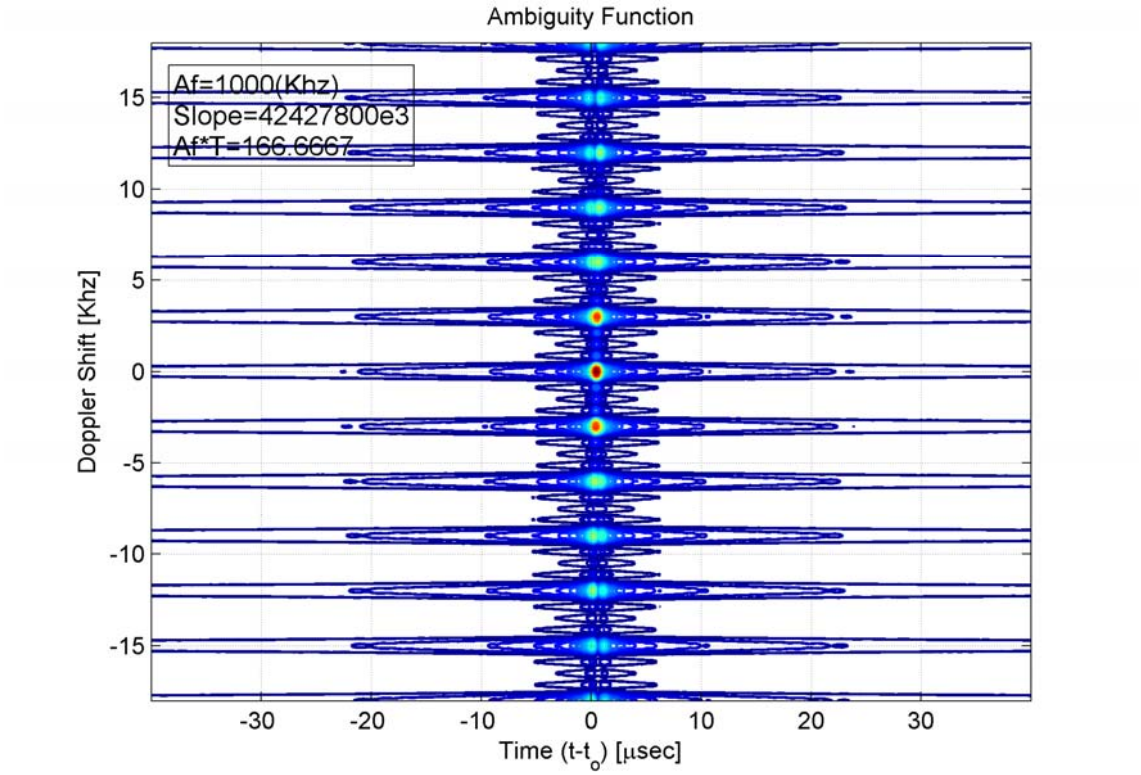


**Fig 5.-51: Simulation 15, Ambiguity Function by using Even quadratic FM law.**

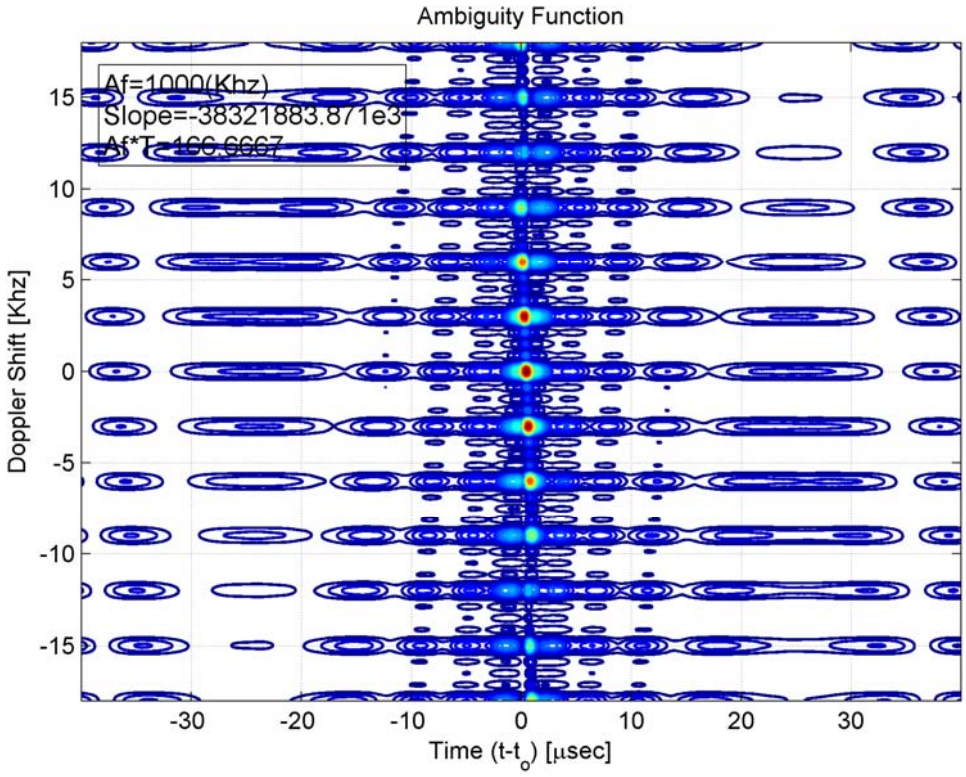


**Fig 5.-52: Simulation 15, Ambiguity Function by using Odd quadratic FM law.**

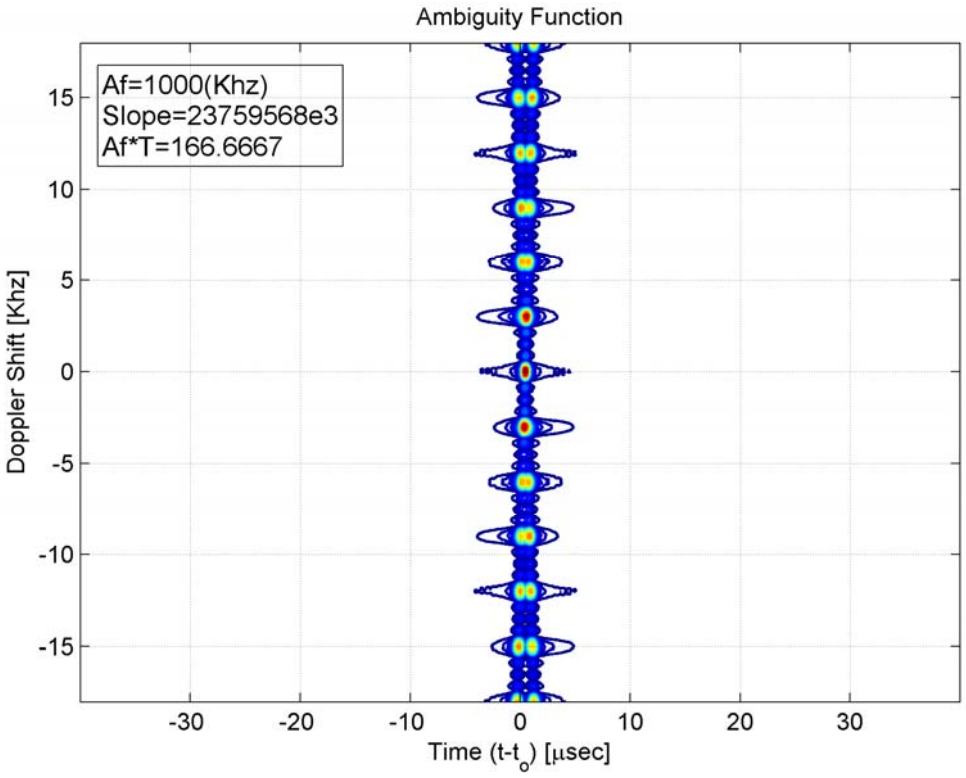


**Fig 5.-53: Simulation 15, Ambiguity Function by using Even vee FM law.**

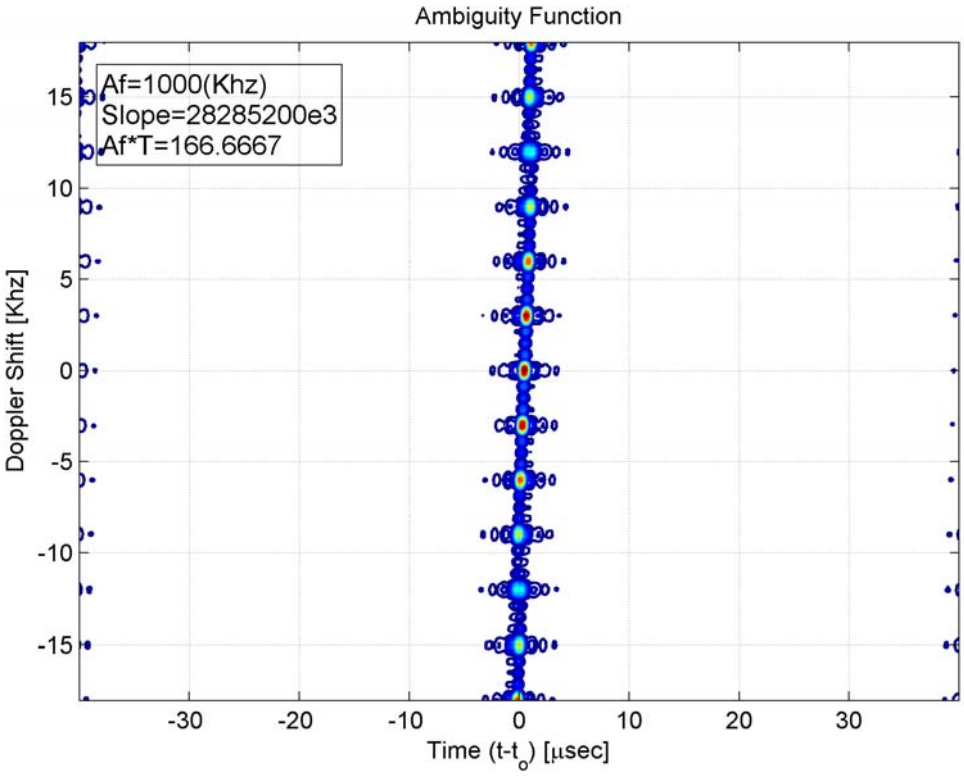


**Fig 5.-54: Simulation 15, Ambiguity Function by using Odd vee FM law.**

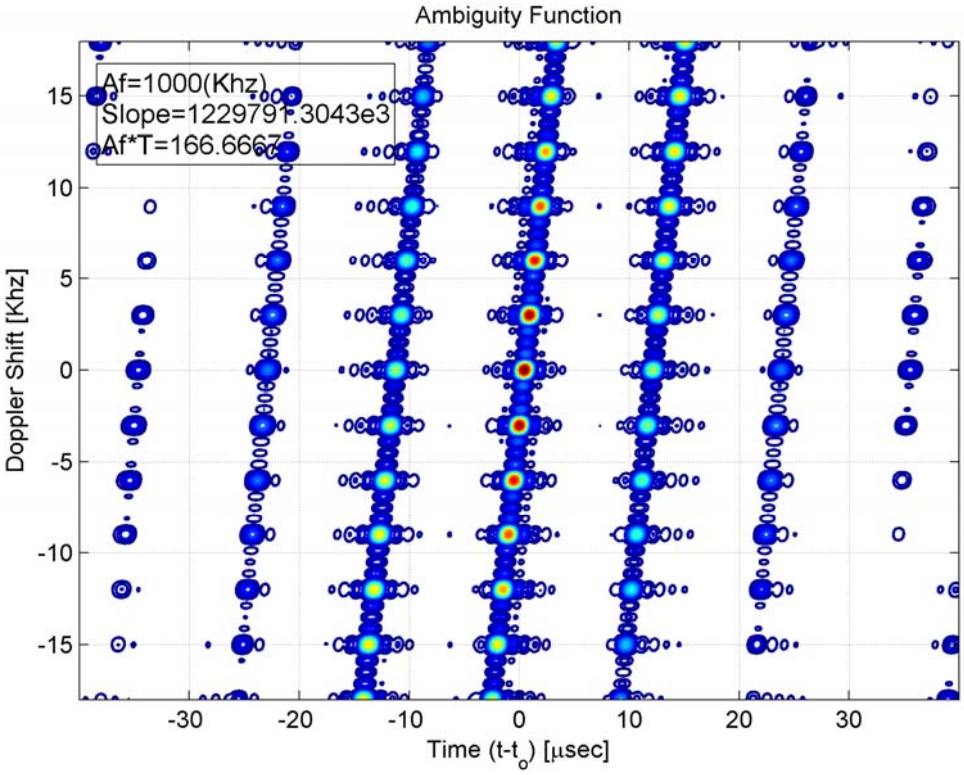


**Fig 5.-55: Simulation 15, Ambiguity Function by using Stepped linear FM law.**

First we start analysing the Even quadratic law shown in Fig 5.-51. It can be observed that the slope (formed by connecting maximums of the Ambiguity Function) is larger than the slope obtained by using CHIRP pulses. This fact means that the Even quadratic FM law presents lower sensitivity to Doppler shift. However, for large Doppler Effect ($|f_d| > 5\ [Khz]$) the pulse is wider. In this situation, the pulse is duplicated, and the sidelobes are not totally suppressed.

According to Fig 5.-52 (Odd quadratic law), we can notice that the slope is also stepper than the slope presented in Fig 5.-16 (CHIRP pulse). Furthermore, its behavior is similar to the Even quadratic FM law, in terms of sensitivity to Doppler. Also, it can be noticed that its sidelobes fluctuates more than in the preceding case.

By observing Fig 5.-53 (Even vee law), we conclude that the ambiguity function slope is less step than the preceding ambiguity functions. Therefore, its sensitivity to Doppler is greater. Also, it presents the duplicity problem for large Doppler shifts. However, its sidelobes suppression is more effective.

In the case of Fig 5.-54 (Odd vee law), we notice that it presents a worse sensitivity to Doppler Effect than the preceding FM laws (slope fewer). Additionally, the signal level fluctuates if Doppler shift varies, but it does not present the duplicity issue. Finally, we observe a good sidelobes suppression, but it presents peaks in other time instants.

To finish this study, we present Fig. 5.-55 with the results obtained for the Stepped linear FM law. Note that the ambiguity function slope is similar to the slope achieved by using pulse CHIRP. Therefore, this FM law presents the highest sensitivity to Doppler shift of all FM laws studied. However, it does not present the duplicity problem, although the signal level fluctuates. Also, it presents the worst sidelobes suppression.

### 5.4.3 Discovering a hidden target by using FM laws

To finish this set of experiments, we probed to unmask a small target overshadowed by another bigger one. For this purpose, we set the simulation parameters as it is shown in Table 5.-16.

| ***Table 5.-16: Simulation 16.*** |
|---|
| $f_0 = 10\ [MHz]$ |
| $\Delta f = 800\ [KHz]$ |
| $prf = 3\ [KHz]$ |
| $T = 166.667\ [\mu s]$ |
| $Number\ of\ pulse = 5$ |

The results obtained in this experiment are shown in Fig 5.-56, Fig 5.-57, Fig 5.-58, Fig 5.-59 and Fig 5.-60.

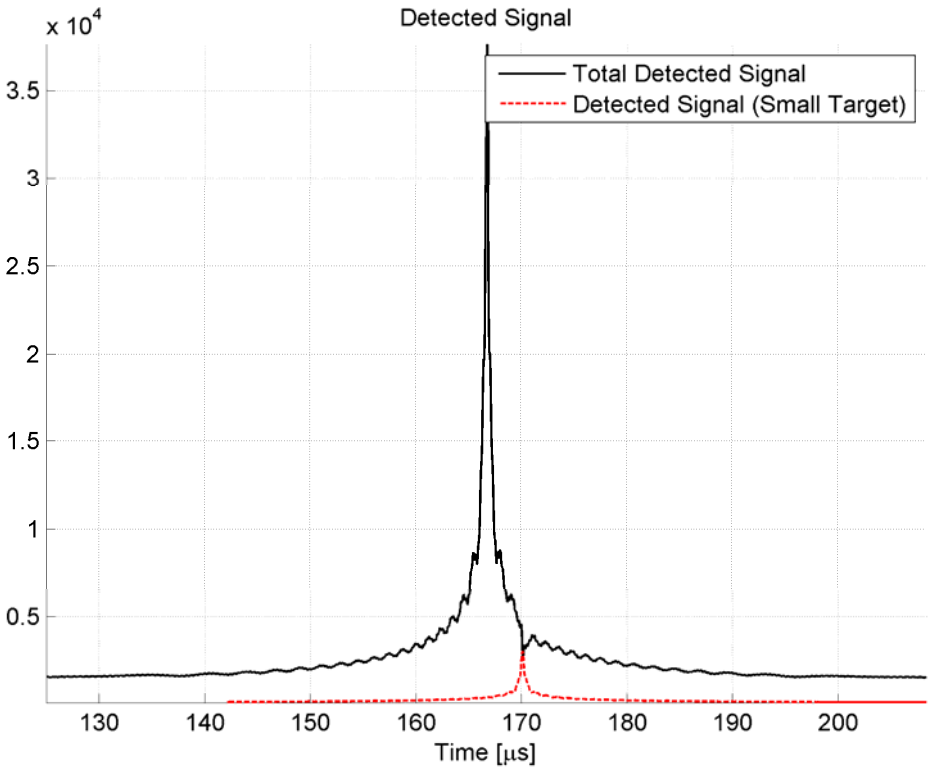


**Fig 5.-56: Simulation 16, Overshadowing Target by using Even quadratic FM law.**

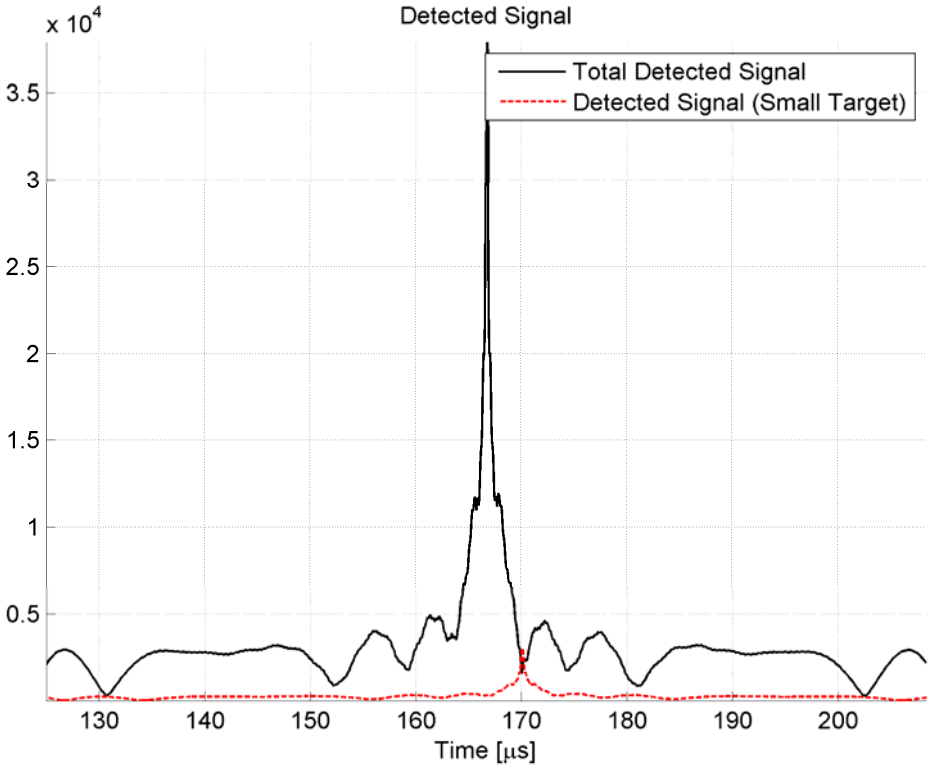


**Fig 5.-57: Simulation 16, Overshadowing Target by using Odd quadratic FM law.**

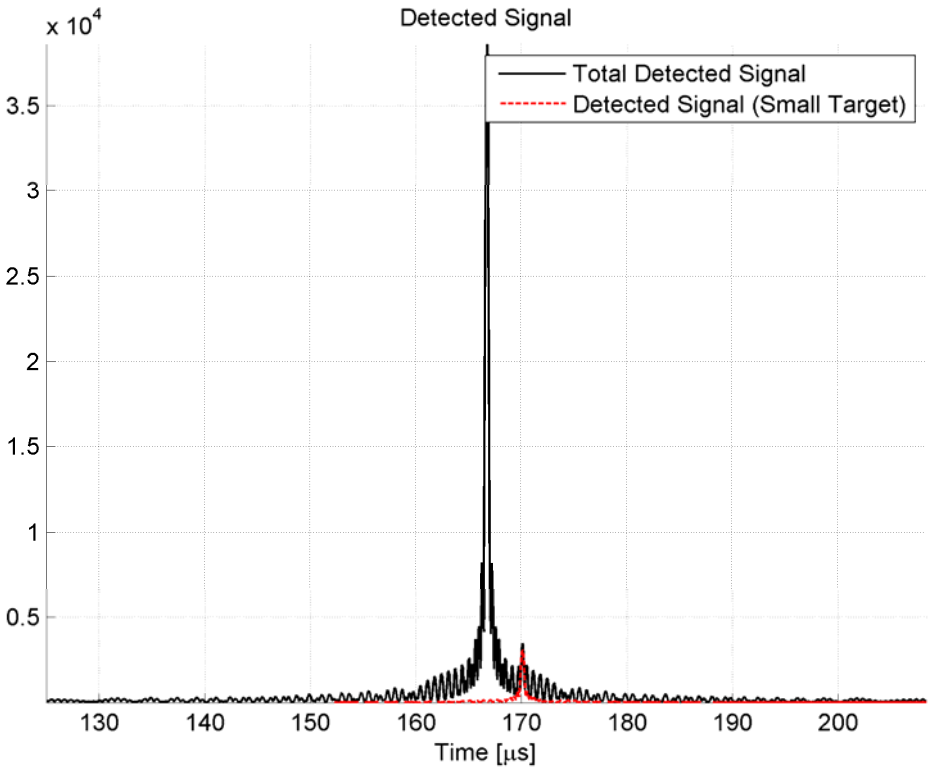


**Fig 5.-58: Simulation 16, Overshadowing Target by using Even vee FM law.**

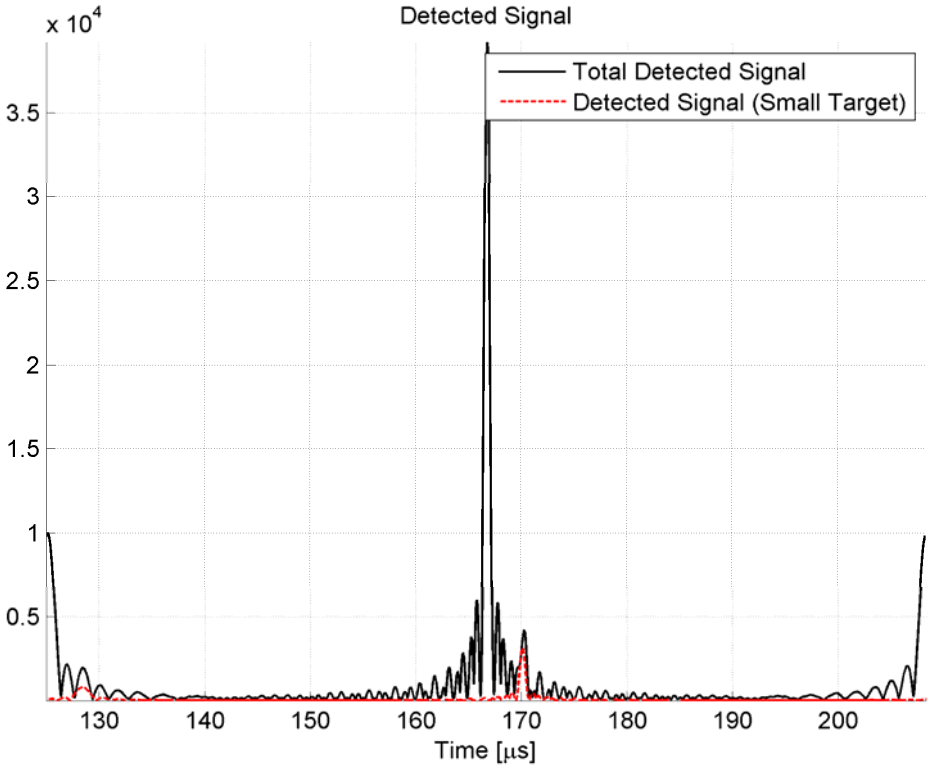


**Fig 5.-59: Simulation 16, Overshadowing Target by using Odd vee FM law.**

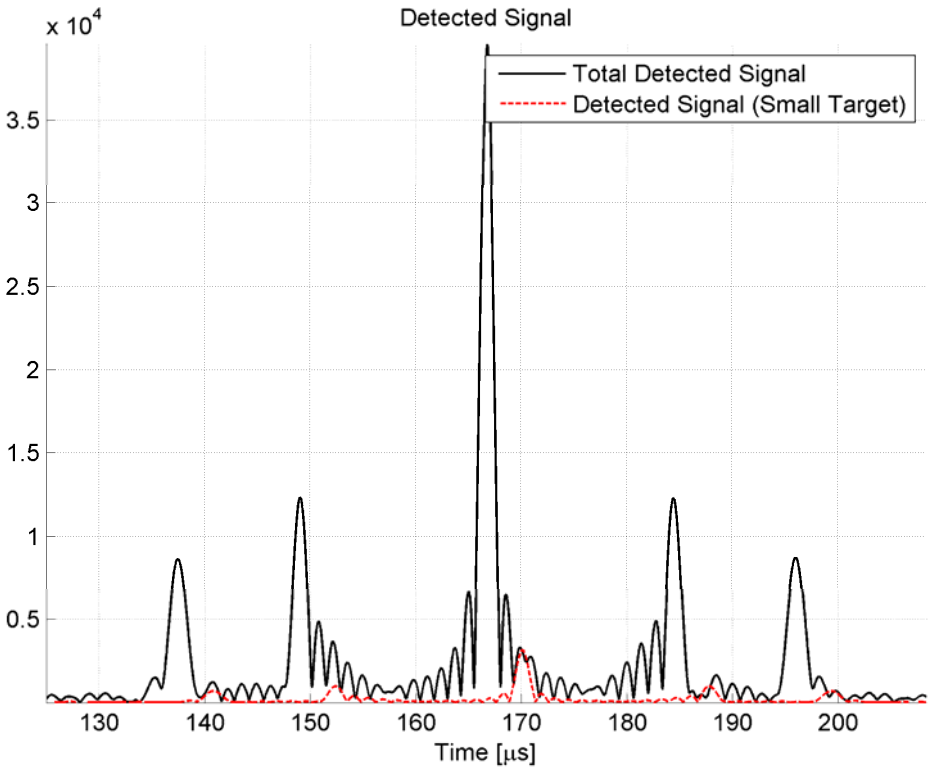


**Fig 5.-60: Simulation 16, Overshadowing Target by using Stepped linear FM law.**

Notice that in the cases of Even quadratic FM law (Fig 5.-56) and Odd quadratic FM law (Fig 5.-57), the unmasking of the small target was not achieved. In the other three cases (from Fig 5.-58 to Fig 5.-60), the hidden target was unmasked. However, note that, in the case of Even vee FM law (Fig 5.-58), Odd vee FM law (Fig 5.-59) and Stepped linear FM law (Fig 5.-60), overshadowing risk exists due to their sidelobes level. The Even vee FM law (Fig 5.-58) offers the best performances for unmasking a hidden target.

## 5.5. Conclusions

**Pulse Compression using CHIRP pulses:**

The **benefits of pulse compression techniques using CHIRP pulses**, as well as their **limitations**, have been assessed in section 5.2. According to the results obtained, we conclude that:

- The **signal to noise ratio improves without range resolution loss** by using CHIRP pulse compression.
- The Spectrum purity of a CHIRP pulse improves if the $\Delta fT$-product increases (section 5.2.1). This fact influences the width of the **compressed pulse: the larger the $\Delta f\tau$-product the narrower the compressed pulse**. Also if $\Delta fT$ increases over $50$, the sidelobes reduce smoothly (see Fig 5.-11).
- When the target is moving (section 5.2.2), the compressed signal suffers **undesired effects**: compressed signal attenuation and the compressed signal shifted in time (wrong range measurements). We confirmed that if $\mu = \Delta f/T$ increases, the second undesired effect decreases, but it is never mitigated.
- **Overshadowing risk exists** due to the sidelobes of the compressed signal (section 5.2.3).

**Sidelobes supression by using Mismatched Filtering:**

In section 5.3 we assessed the **functionality of two types of mismatched filters in order to suppress the sidelobes obtained with plain CHIRP Pulses**. According to the results obtained, the main conclusions are:

- In general, the **width of the final filtered pulse is wider** by using mismatched filtering (Truncated Taylor Filter in section 5.3.1; and Taylor Filter 5.3.2). Also, both filters achieve the goal of **decreasing the sidelobes level**.
- Comparing the **Taylor Filter** and the Truncated Taylor Filter, the first one **achieves compressed pulses narrower** than the second one.
- The **optimal parameters**, in terms of sidelobes suppression, of the Truncated Taylor Filter (see equation 4.) are $\boldsymbol{n = 4}$ and $\boldsymbol{F_1 \approx 0.5}$. Besides, we found values of $n$ for which the filtered signal deteriorates.
- For the Taylor Filter (see equation 4.), **if $\boldsymbol{n}$ increases, the sidelobes decreases** and the width of the pulse does no change significantly. Also, **if $\boldsymbol{SSL}$ decreases the sidelobes decreases**, but the width of the pulse increases.
- **The undesired effects due to a moving target are found** in the two types of filters (Truncated Taylor Filter and Taylor Filter).
- Finally, we can conclude that the **Taylor Filter offers better performances for unmasking targets than its truncated version**. Although they are not a great solutions since the masking risks increases due to the increase of the width of the pulse.

**Pulse compression by using FM laws:**

In section 5.4 we reviewed the use of FM laws for pulse compression. According to the results obtained, we conclude that:

- **The Odd vee FM law offers the best performances in terms of sidelobes suppression**. Moreover, **the Even vee FM law is the best option in terms of the width of compressed pulse** if $\Delta fT > 50$.
- We conclude that **the Linear Stepped FM law offers the worst performances**.
- In general, the **undesired effects due to moving target are found** in the ambiguity functions computed. However, some FM laws mitigates the maximum deviations for low Doppler shifts. However for larger Doppler shifts, the pulse duplicates. Therefore, **some FM laws are a great solution for low Doppler applications**.
- **The Even vee FM law is the best option for unmasking a target**. However, no FM laws provide a great solution for the overshadowing issue.

# Chapter 6. Doppler Compensation in CHIRP Pulse Compression

This chapter provides information about a novel method which allows to compensate the mismatching provoked by moving targets in pulse compression systems.

If we observe the ambiguity functions obtained in section 5.2.2, we note that the filter output presents two undesired effects when the Doppler Effect is nonzero: the filtered signal amplitude fluctuates and the maximum peak of the output signal is shifted in timer with respect to its desired position. Note also that the use of some FM Laws mitigates the maximums deviation (section 5.4.2), but only for small range of Doppler frequencies. Therefore very fast targets could be undetectable or provoke wrong range measurements.

Below we study a solution for these issues. We look, firstly, at the basic concept which this method is based on. Finally, at the results obtained, in terms of ambiguity function and the error introduced by the proposed Doppler compensation mechanism.

## 6.1. Basic concept

The basic idea for achieving the Doppler compensation is depicted in Fig 6.-1.

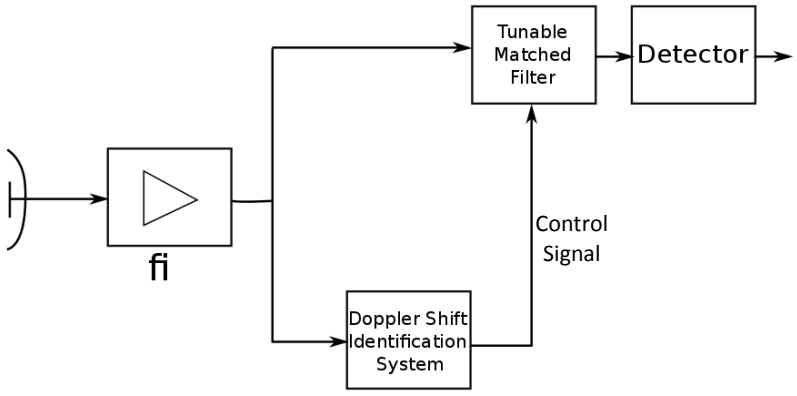


**Fig 6.-1: Basic Concept. Block Diagram.**

Note that the matched filter is connected to a Shift Doppler Identification System in parallel. This block is able to acquire the received signal, detect the frequency in which the received

spectrum is centered and tune the matched filter in order to remove the mismatching due to target motion. The challenge is how to detect the center frequency.

**CHIRP pulse spectrum symmetry**

In section 4.2 we studied the CHIRP pulse deeply. Note that the spectrum of a pulse CHIRP, in complex envelope terms, is

$$G(\omega) = A\sqrt{\frac{\mu}{\pi}}e^{j\frac{\mu}{2}\omega^2}\left[\frac{\big(C(x_u)+C(x_l)\big)+j\big(S(x_u)+S(x_l)\big)}{\sqrt{2}}\right] \quad \textbf{( 6.-1 )}$$

Where $x_u = \sqrt{\frac{\Delta f T}{2}}\left(1-\frac{2f}{\Delta f}\right)$ and $x_l = -\sqrt{\frac{\Delta f T}{2}}\left(1+\frac{2f}{\Delta f}\right)$. By observing Fig 4.-8 and Fig 4.-9, we notice that the CHIRP pulse spectrum is symmetric with respect to $f_0$ (carrier frequency). This fact can be exploited to detect the center frequency and compensate the Doppler Shift.

**Doppler Shift Identification System**

In order to detect the center frequency of a symmetric spectrum, we could use the block diagram shown in Fig 6.-2.

As Fig 6.-2 depicts, the system consists of a bank of two tunable bandpass filters, which are used for sweeping the received spectrum in the frequency domain. Thus, by observing the differential energy between the energies of the signals which cross the filters, we can determine the frequency shift due to the target speed.

The center frequency of the bandpass filters are

$$f_{c1} = f_0 + \Delta f/2 + \delta \boldsymbol{X} \quad \textbf{( 6.-2 )}$$

$$f_{c2} = f_0 + 3\,\Delta f/2 + \delta \boldsymbol{X} \quad \textbf{( 6.-3 )}$$

The bandwidth of the filters are

$$AB_1 = AB_2 = \Delta f \quad \textbf{( 6.-4 )}$$

And $\boldsymbol{X}$ is a control signal used to perform a frequency sweep. Finally, $\delta$ is the step used for the sweep. Note that the transfer functions of the filters are overlapped, in other words, for $\boldsymbol{X} =$

**0** the spectrum of the first filter starts at $f_0$ and ends at $f_0 + \Delta f$; whereas the spectrum of the second Filter stars at $f_0 + \Delta f$ and ends at $f_0 + 2\Delta f$). Thus the frequency, in which the transfer functions of the filters are overlapped, is

$$f_{ct} = \frac{f_{c1} + f_{c2}}{2} = f_0 + \Delta f + \delta \boldsymbol{X} \qquad \textbf{( 6.-5 )}$$

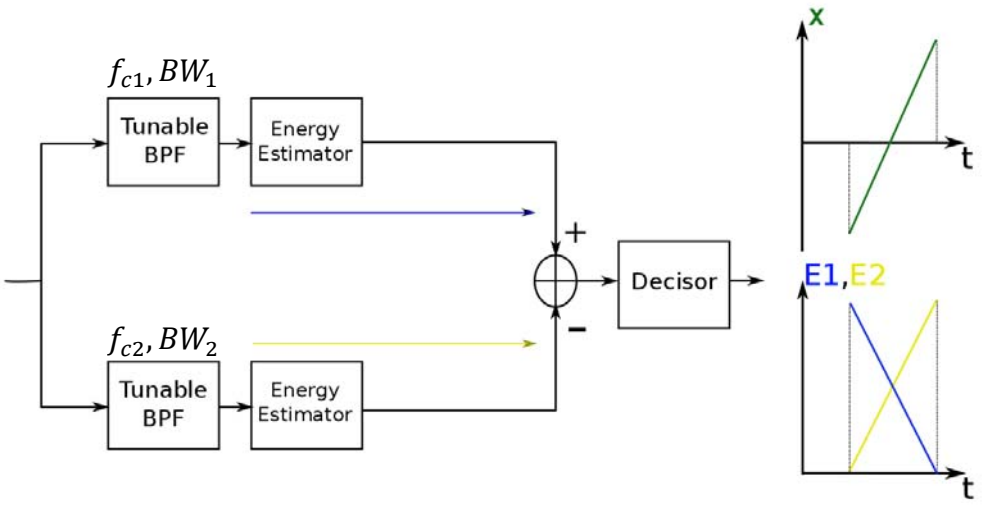


**Fig 6.-2: Doppler Shift Identification System. Block Diagram.**

To understand the Doppler Shift Identification System operation, we illustrate it by supposing a nonmoving target ($f_d = 0\ Hz$). According to the center frequency of the tunable filters ($f_{ct}$) we find three situations:

1. Filters are centered in $f_{ct} < f_0$. For the case illustrated in Fig 6.-3, the energy that goes through the bandwidth of the first filter ($BW_1$) is much larger than the energy that goes through the bandwidth of the first filter ($BW_2$). Hence the differential energy is positive.

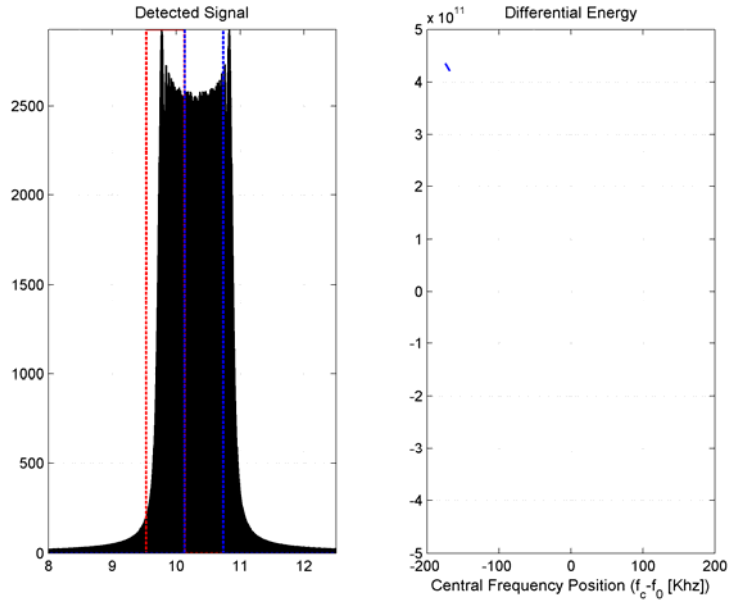


**Fig 6.-3: Identification System. Basic idea. $f_{ct} < f_0$.**

2. Filters are centered in $f_{ct} = f_0$. In this situation the energy that goes through $BW_1$ is similar to the energy that goes through $BW_2$. Now the differential energy is close to zero, as Fig 6.-4 shows.

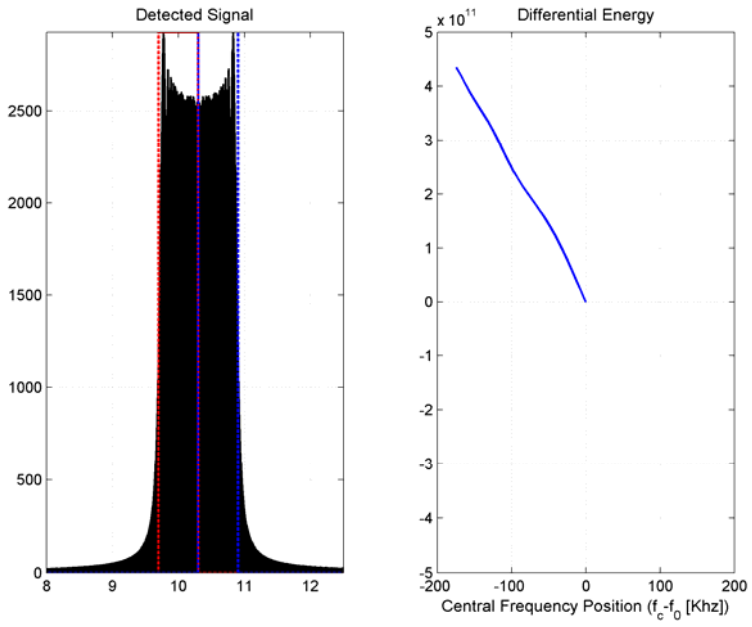


**Fig 6.-4: System Identification System. Basic idea. $f_{ct} = f_0$.**

3. Filters are centered in $f_{ct} > f_0$. This case is the opposite to the situation described before. Thus the amount of energy that goes through $BW_2$ is larger than the energy that does through $BW_1$. Thereby, the differential energy takes negative values as cam be seen in Fig 6.-5.

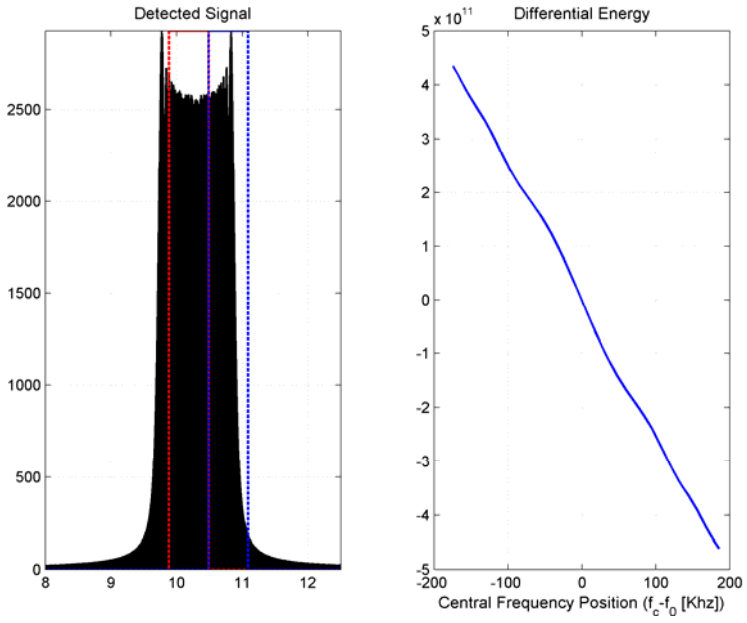


**Fig 6.-5: System Identification System. Basic idea. $f_{ct} > f_0$.**

If we are able to identify the crossing through zero energy, we can measure and compensate the spectrum deviation due to the Doppler Effect by tuning the matched filter. This concept has been proved in numerical simulations by using ideal filters (with square transfer functions). The results obtained are shown in the following section.

## 6.2. Results

To evaluate the performance of the Doppler Compensation System, we have performed various simulations, in which the influence of some parameters are tested. We have focused on the ambiguity functions resulted and on the error function of the estimation of the Doppler shift. Before these verifications, we have carried out simple simulations to confirm the system functionality.

### 6.2.1 Verification of the Compensation System functionality

For this initial experiment, we observed the Differential Energy curve obtained at the end of the frequency sweep performed by the tunable bandpass filters. The parameters were fixed as shown Table 6.-1.

| ***Table 6.-1: Simulation 17 parameters.*** |
|---|
| $f_0 = 10\ [MHz]$ |
| $\Delta f = 600\ [KHz]$ |
| $prf = 3\ [KHz]$ |
| $T = 166.667\ [\mu s]$ |
| $Number\ of\ pulse = 5$ |

We simulated four situations according to the Doppler Effect produced by the moving target: $f_d = \pm 50\ KHz$ and $f_d = \pm 100\ KHz$. After simulating these situations we obtained the graph shown in Fig 6.-6.

Notice that, in Fig 6.-6, the zero energy point occurs in different values of $f_{ct}$. This point is centered near to $f_0 + f_d$ frequencies, or in other words, $f_{ct} - f_0 \cong f_d$. Therefore, it confirms that this idea is valid for identifying the Doppler Shift. In the same way, the Fig 6.-5 depicts the zero Doppler case.

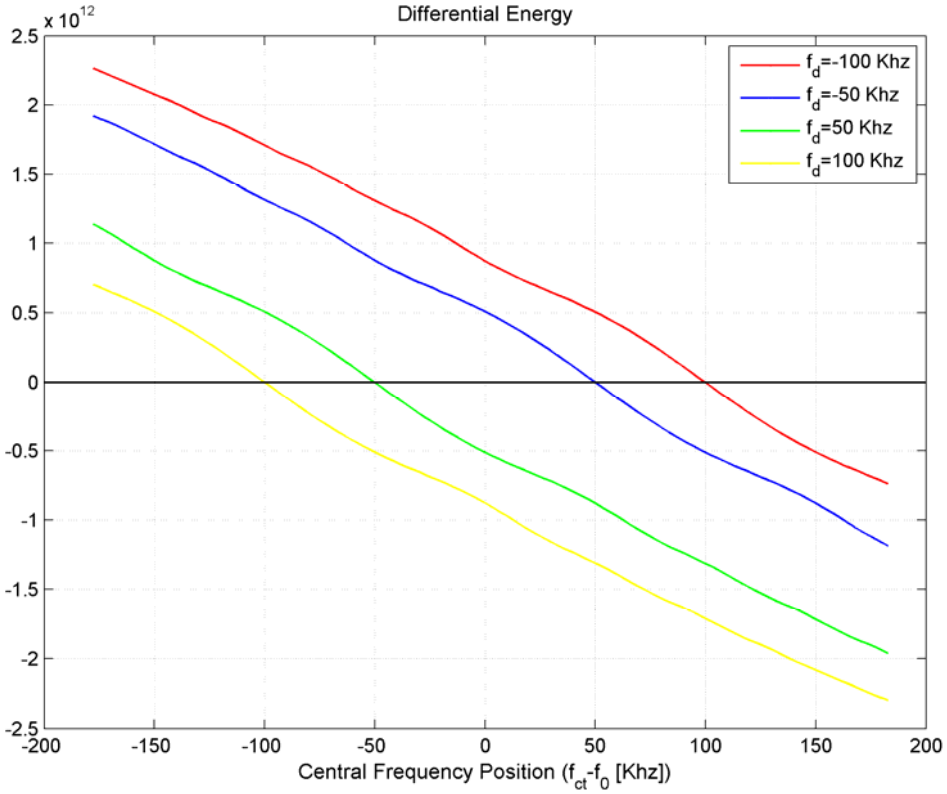


**Fig 6.-6: Simulation 17, Differential Energy for $f_d = \pm 50, \pm 100\ [KHz]$.**

### 6.2.2 Compensated Ambiguity Function

In this set of simulations we have evaluated the performance of the purposed system by calculating the ambiguity function for several values of $\Delta f$ (the frequency index of the linear FM modulation). We used the parameters shown in Table 6.-2 for numerical tests.

| ***Table 6.-2: Simulation 18 parameters.*** |
|---|
| $f_0 = 10\ [MHz]$ |
| $prf = 3\ [KHz]$ |
| $T = 166.667\ [\mu s]$ |
| $Number\ of\ pulse = 5$ |

The results are illustrated in Fig 6.-7, Fig 6.-8, Fig 6.-9, Fig 6.-10, Fig 6.-11, Fig 6.-12, Fig 6.-13, Fig 6.-14, Fig 6.-15 and Fig 6.-16 for values of $\Delta f$ from $100$ to $1000\ [KHz]$ by taking a $100\ [KHz]$ step.

Note that in all of these simulations the maximum deviations due to Doppler Shifts have been mitigated. Thereby, the slope formed by connecting the maximums of the output signal tends to infinite (it tends to the vertical axis). Also the output signal fluctuations have been decreased, thus, targets that were undetectable in the preceding Chapter (section 5.2.2) become visible to the radar system. This fact is easy to observe by analyzing the Ambiguity Function cut $|x(\tau = 0, f_d)|^2$. We compare this cut for a compensated case (Fig 6.-17) to the non-compensated case (Fig 6.-18) for $\Delta f = 400\ [KHz]$.

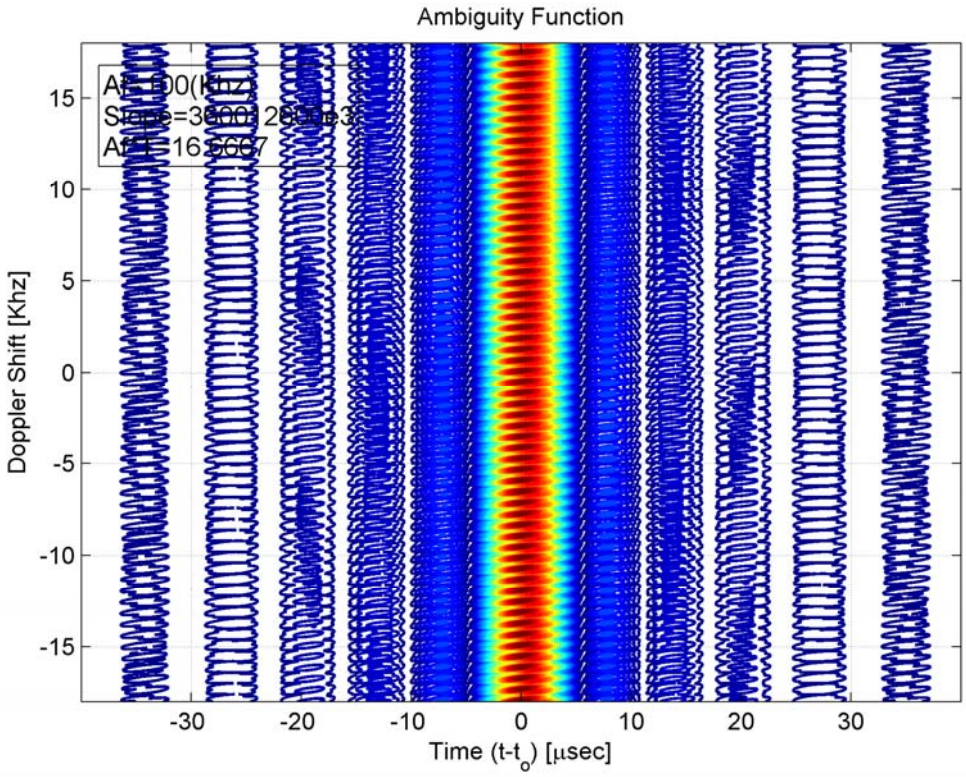


**Fig 6.-7: Simulation 18, Compensated Ambiguity Function for $\Delta f = 100\ [KHz]$.**

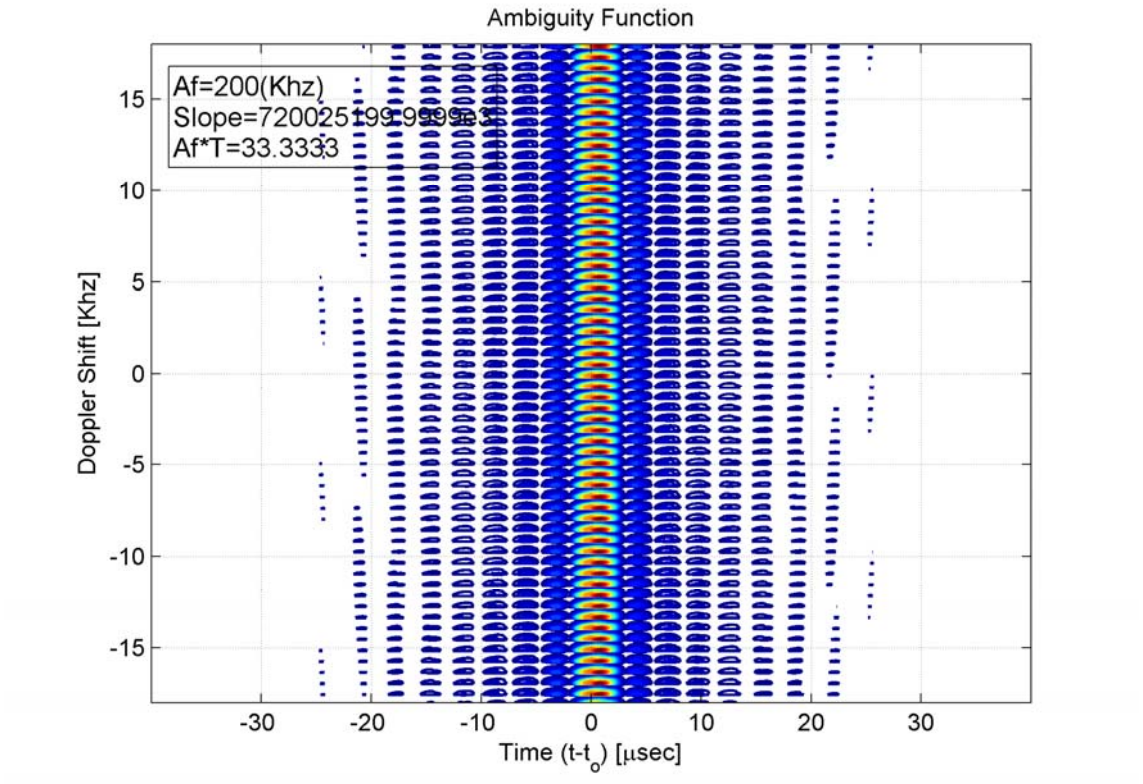


**Fig 6.-8: Simulation 18, Compensated Ambiguity Function for $\Delta f = 200\ [KHz]$.**

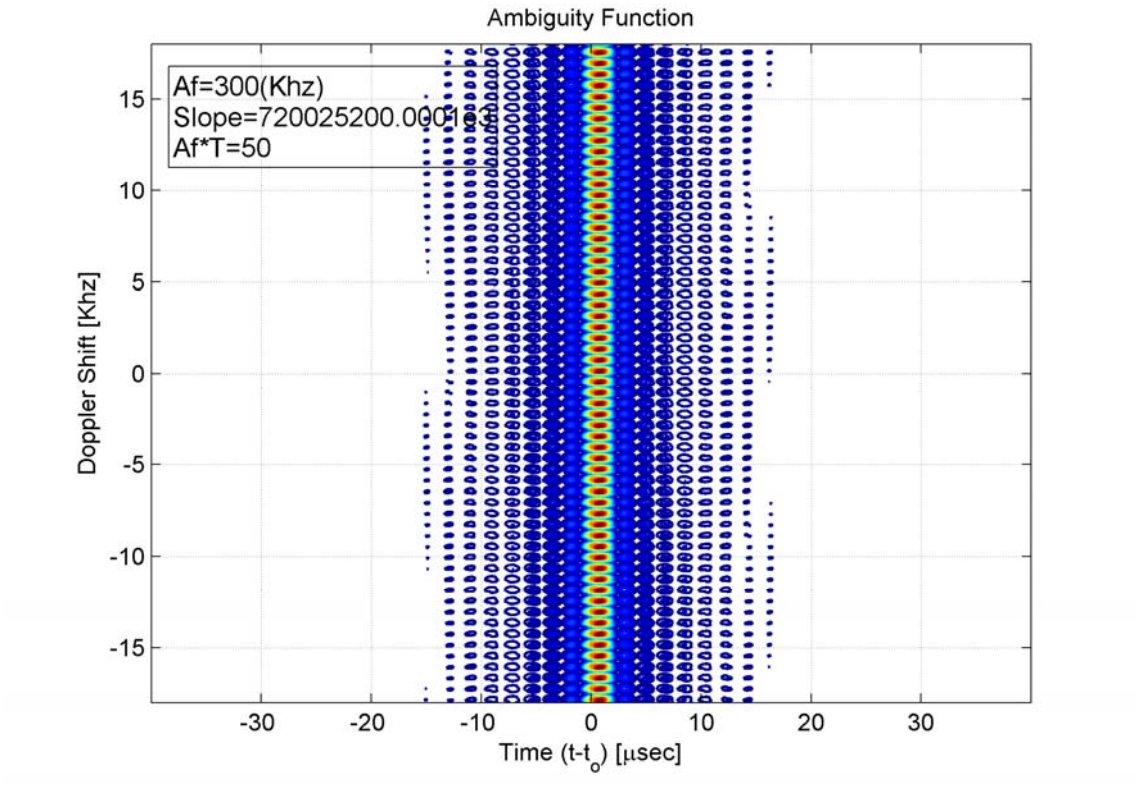


**Fig 6.-9: Simulation 18, Compensated Ambiguity Function for $\Delta f = 300\ [KHz]$.**

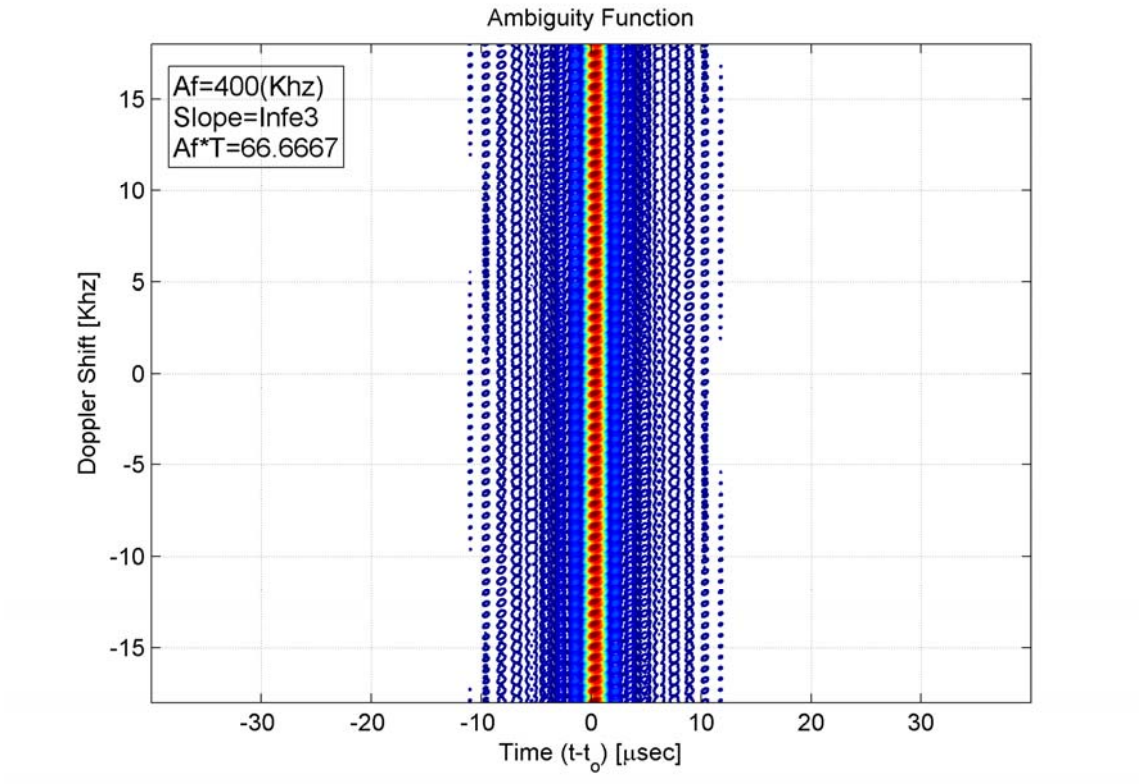


**Fig 6.-10: Simulation 18, Compensated Ambiguity Function for $\Delta f = 400\ [KHz]$.**

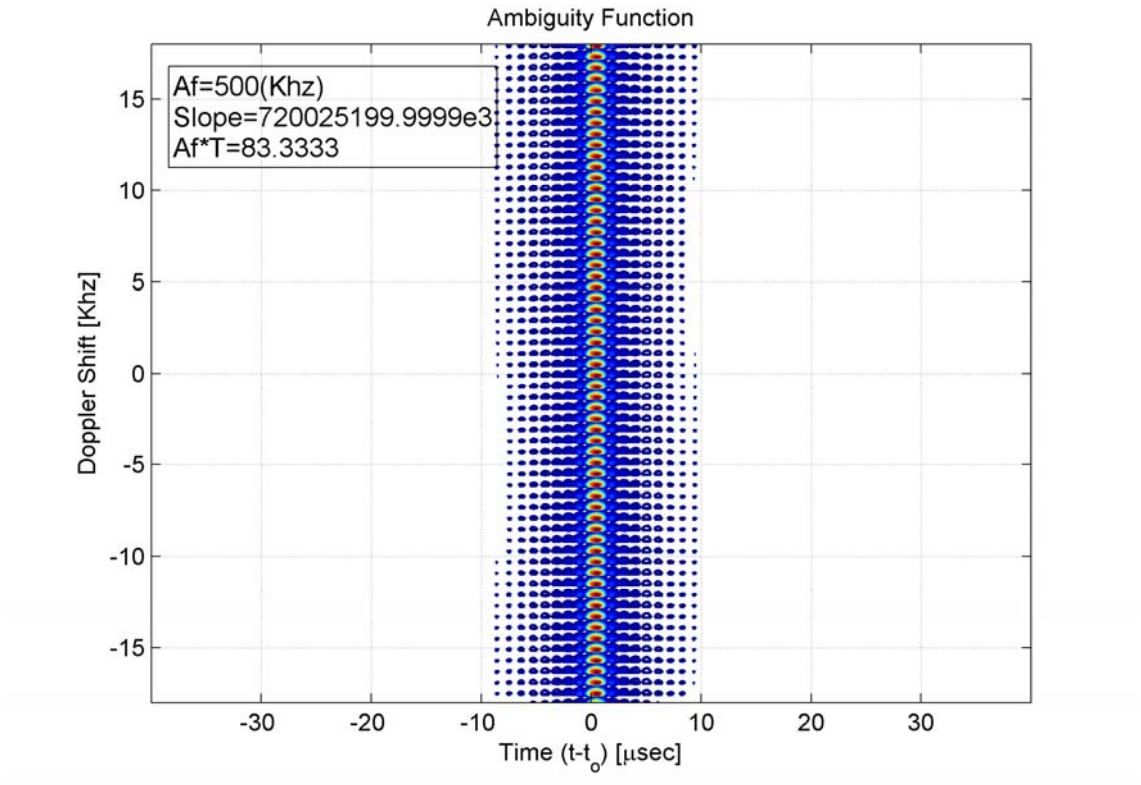


**Fig 6.-11: Simulation 18, Compensated Ambiguity Function for $\Delta f = 500\ [KHz]$.**

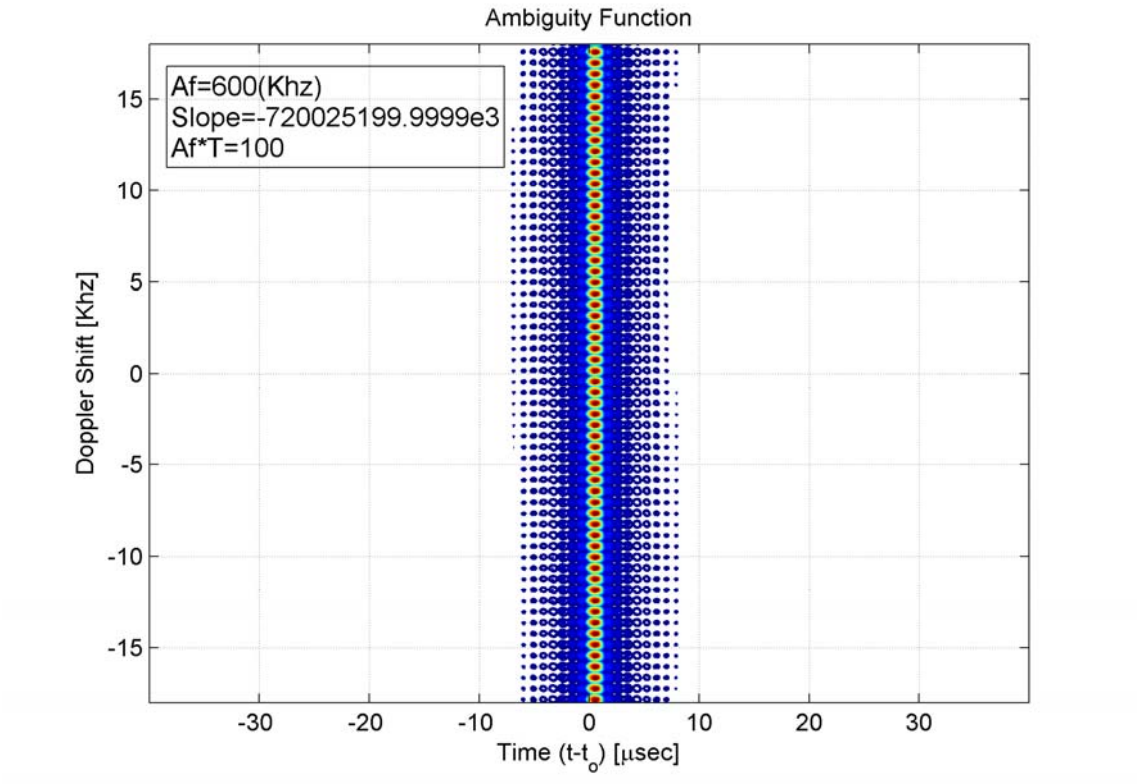


**Fig 6.-12: Simulation 18, Compensated Ambiguity Function for $\Delta f = 600\ [KHz]$.**

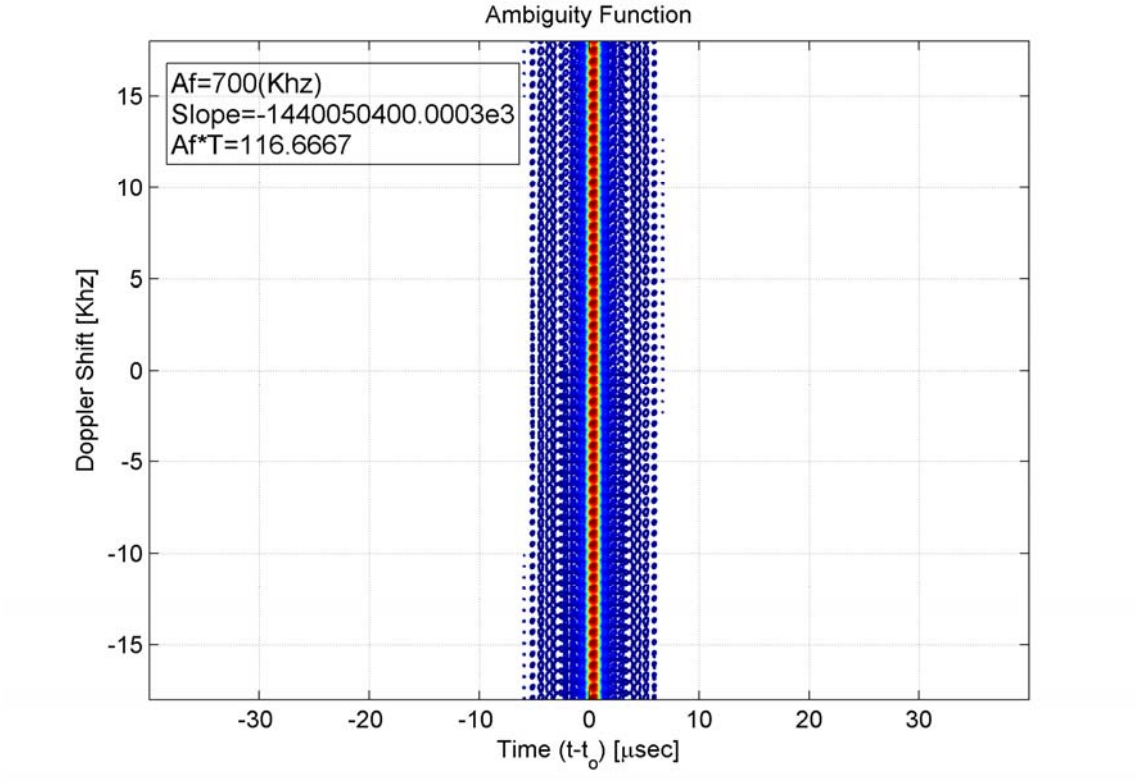


**Fig 6.-13: Simulation 18, Compensated Ambiguity Function for $\Delta f = 700\ [KHz]$.**

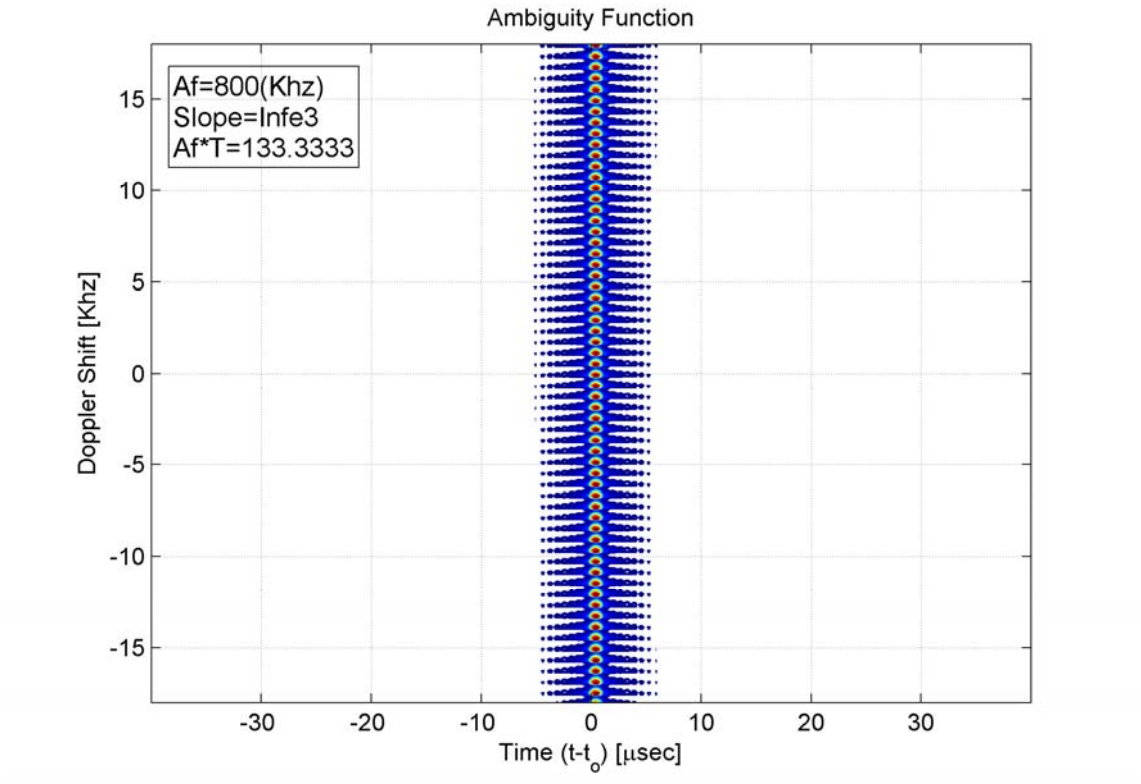


**Fig 6.-14: Simulation 18, Compensated Ambiguity Function for $\Delta f = 800\ [KHz]$.**

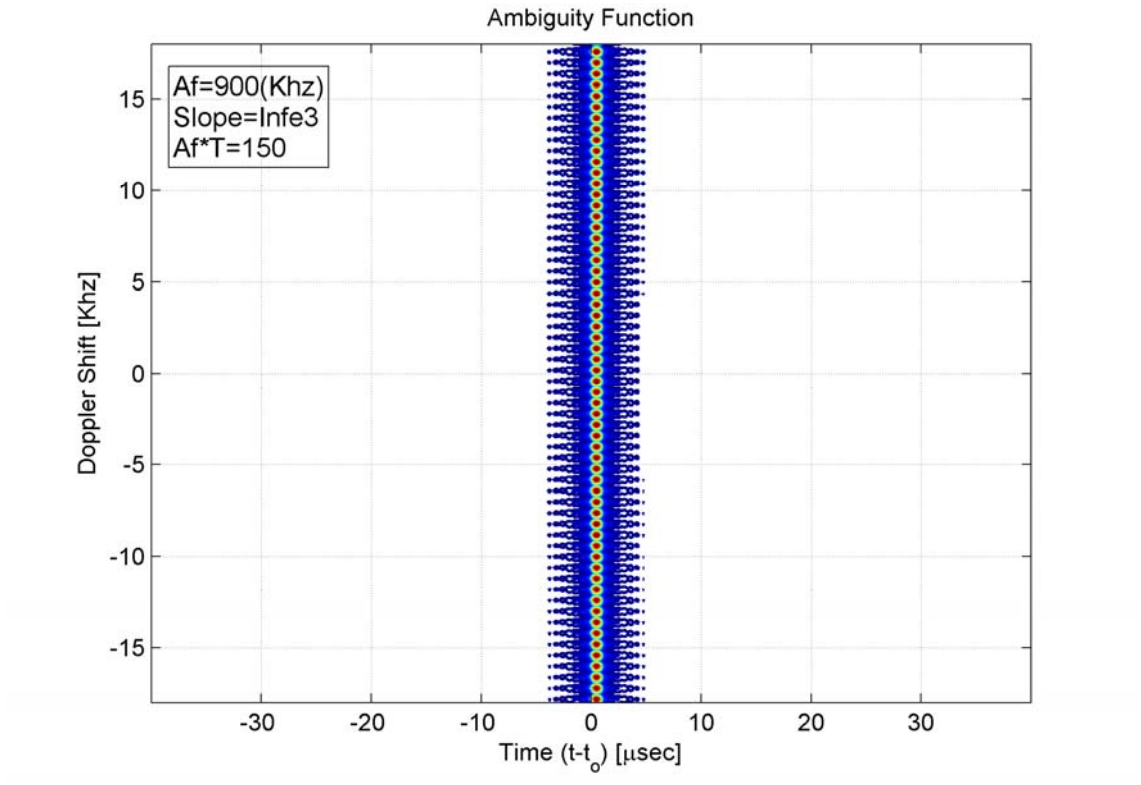


**Fig 6.-15: Simulation 18, Compensated Ambiguity Function for $\Delta f = 900\ [KHz]$.**

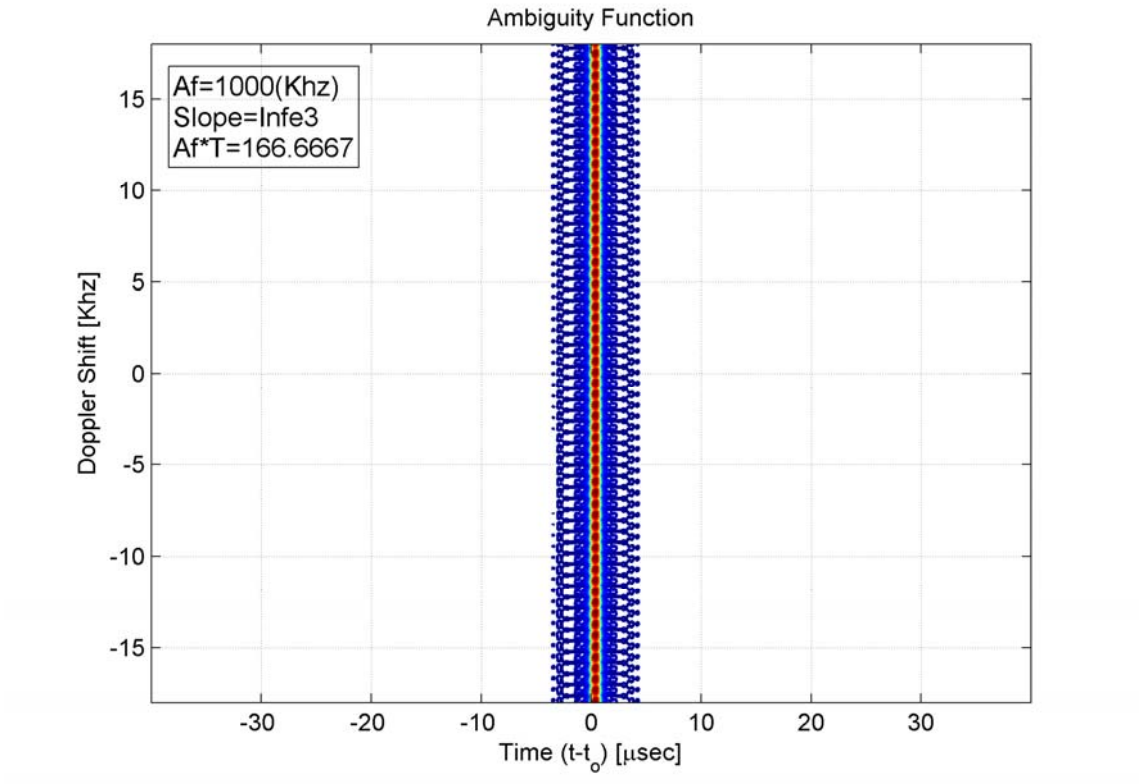


**Fig 6.-16: Simulation 18, Compensated Ambiguity Function for $\Delta f = 1000\ [KHz]$.**

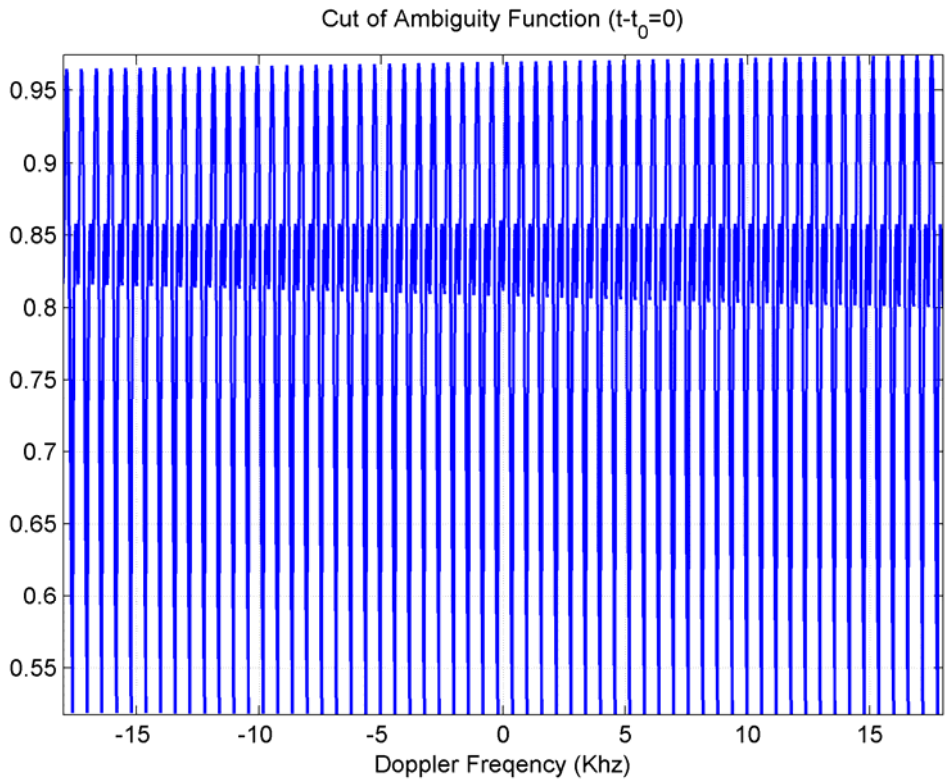


**Fig 6.-17: Simulation 18, Cut of compensated Ambiguity Function $t - t_0 = 0$, for $\Delta f = 400\ [KHz]$.**

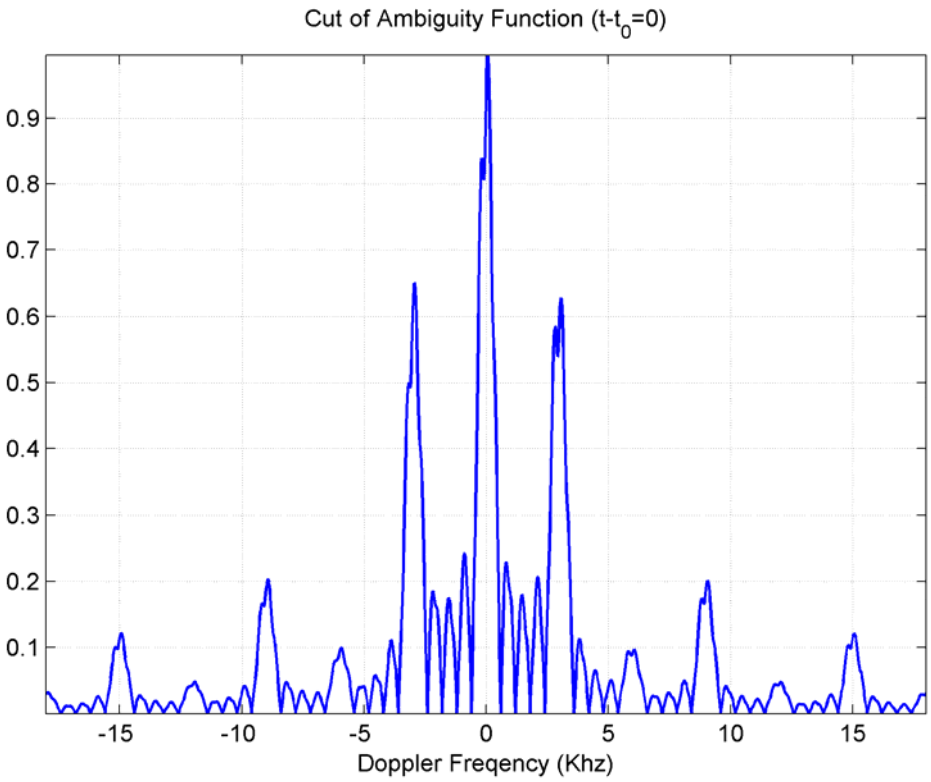


**Fig 6.-18: Simulation 18, Cut of non-compensated Ambiguity Function $t - t_0 = 0$, for $\Delta f = 400\ [KHz]$.**

Note that the output signal depicted by Fig 6.-17 never reaches zero value (specifically it oscillates between $0.55$ and $0.95$), whereas the output signal illustrated in Fig 6.-18 reaches null values for several values of $f_d$. The output signal fluctuates because of the error in the Doppler Shift estimation. Therefore, it is important to observe the error committed. Next we analyse the error function.

**Error function**

The error functions were calculated as

$$e(f_{ds}) = f_d - f_{ds} \qquad \textbf{( 6.-6 )}$$

Where $f_d$ is the real Doppler Shift due to target motion and $f_{ds}$ is the Doppler Shift estimation calculated by the proposed mismatching compensation system. These simulations were carried out by using the parameters shown in Table 6.-4. The results are depicted from Fig 6.-19 to Fig 6.-28. These errors could be due to numerical limitations of the simulations. Note that all error functions calculated exhibit the same repetitive behavior due to the spectrum

sampling. Notice also that the error function for $\Delta f = 700\ [KHz]$ (Fig 6.-25) has a strange behavior when $f_d > 0\ [KHz]$. No explication have been found to understand this fact at this moment. Besides, the error functions do not seem to have a clear relation with $\Delta f$. Nonetheless, the error committed is acceptable since the ambiguity functions improved with respect to the ambiguity functions obtained in the preceding chapter.

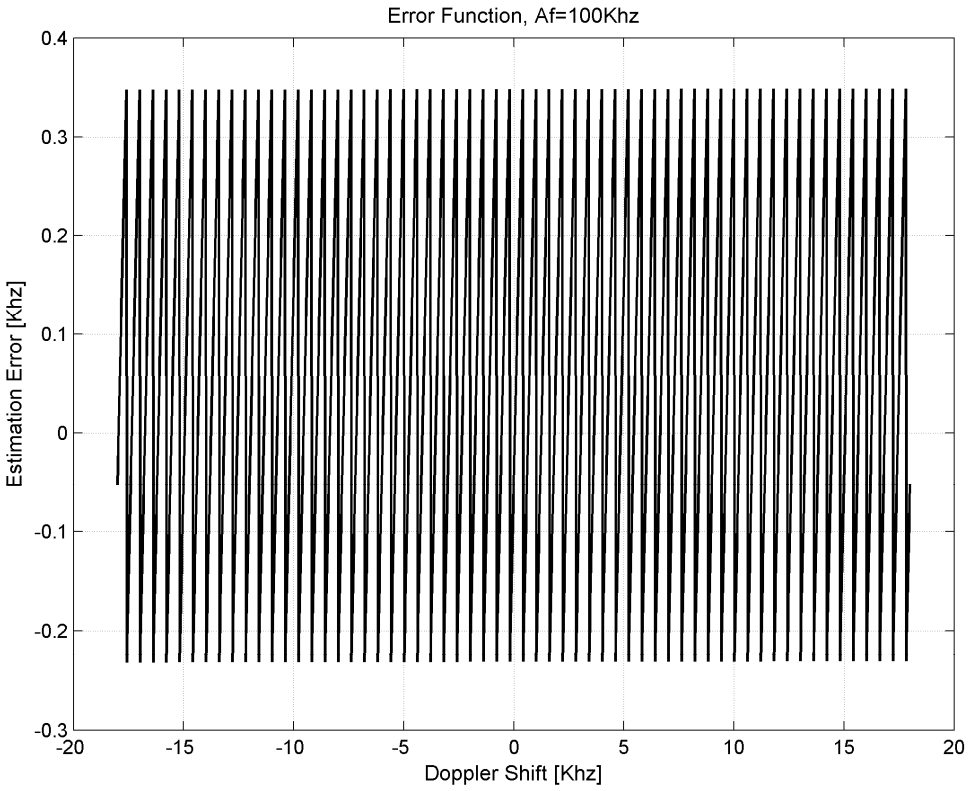


**Fig 6.-19: Simulation 18, Error Function for $\Delta f = 100\ [KHz]$.**

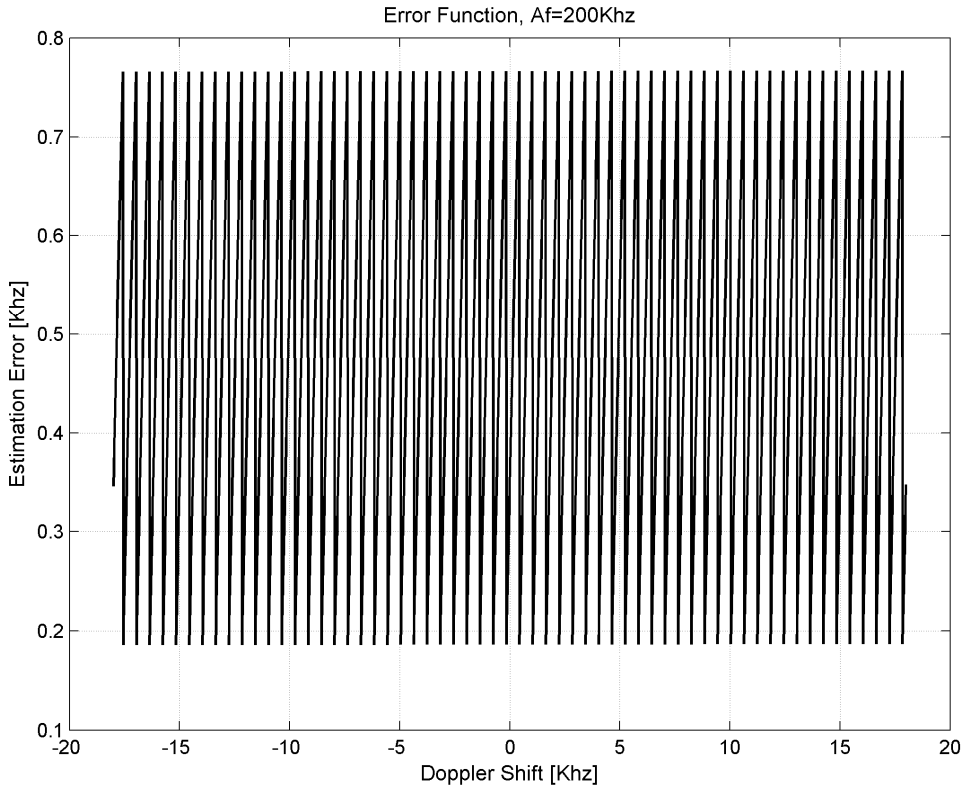


**Fig 6.-20: Simulation 18, Error Function for $\Delta f = 200\ [KHz]$.**

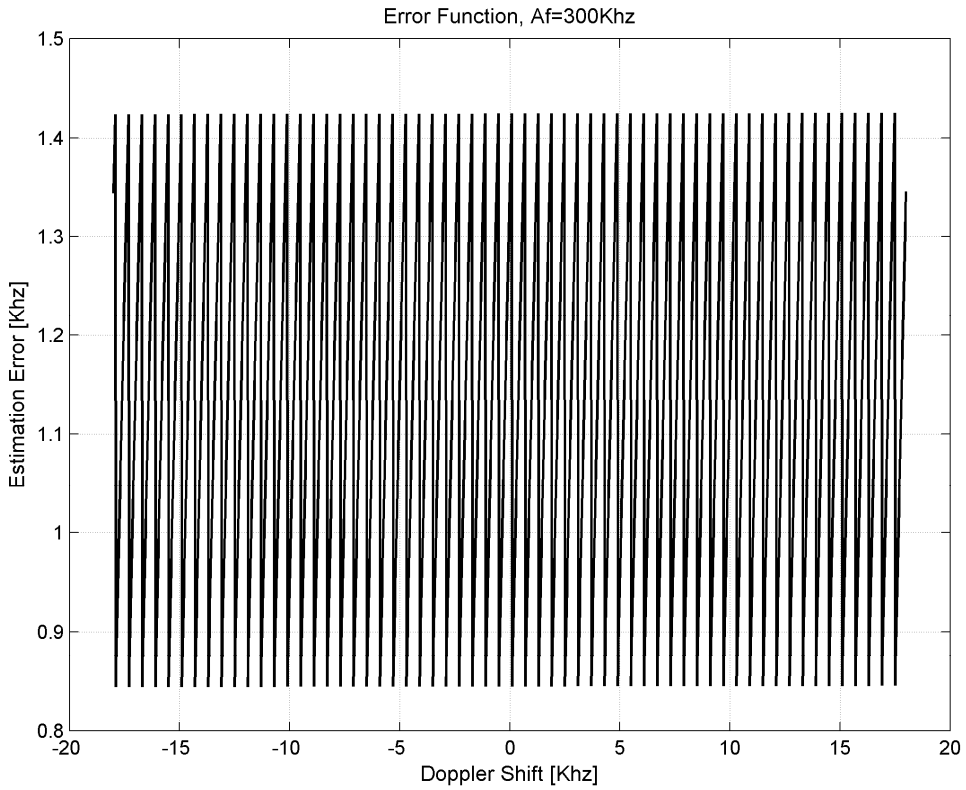


**Fig 6.-21: Simulation 18, Error Function for $\Delta f = 300\ [KHz]$.**

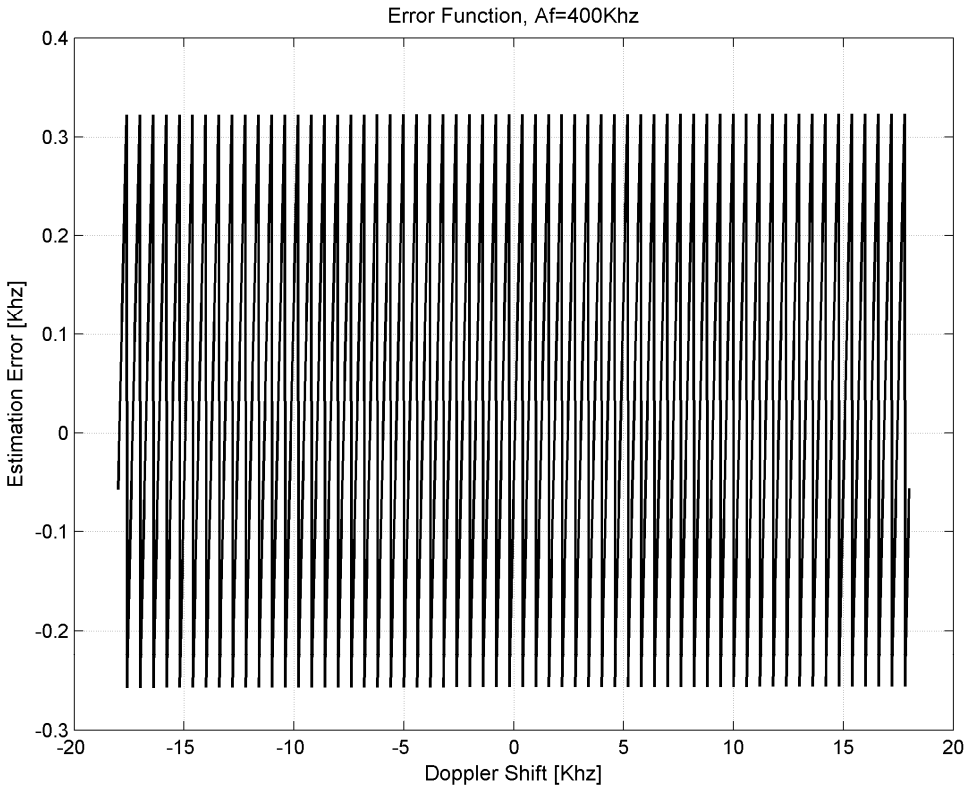


**Fig 6.-22: Simulation 18, Error Function for $\Delta f = 400\ [KHz]$.**

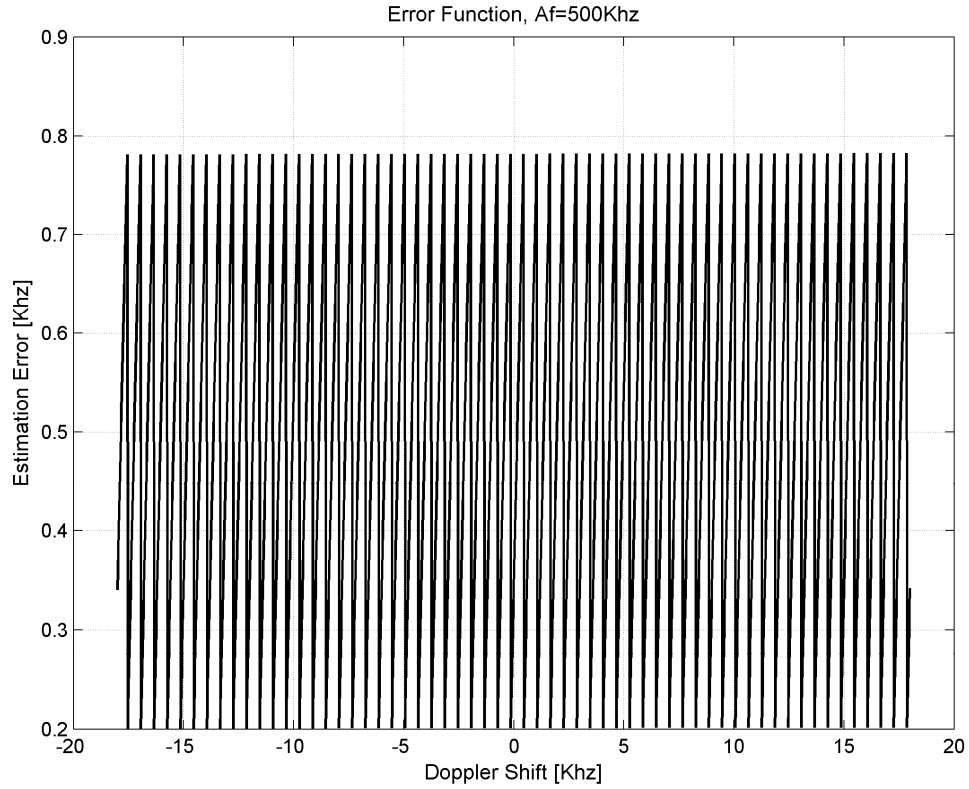


**Fig 6.-23: Simulation 18, Error Function for $\Delta f = 500\ [KHz]$.**

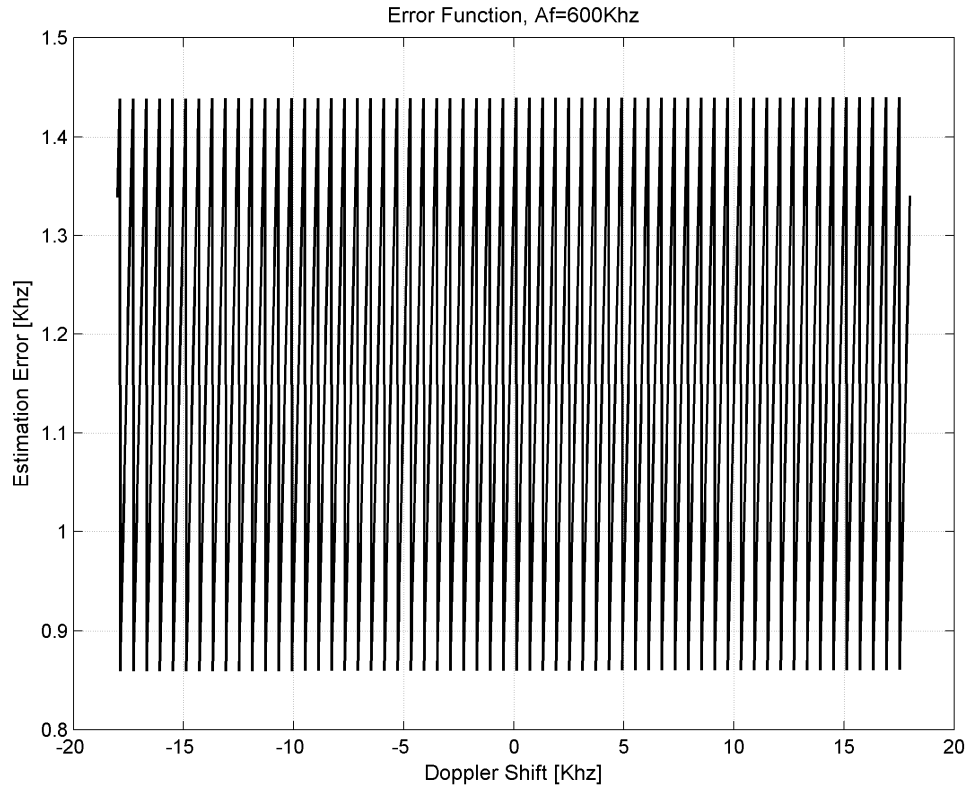


**Fig 6.-24: Simulation 18, Error Function for $\Delta f = 600\ [KHz]$.**

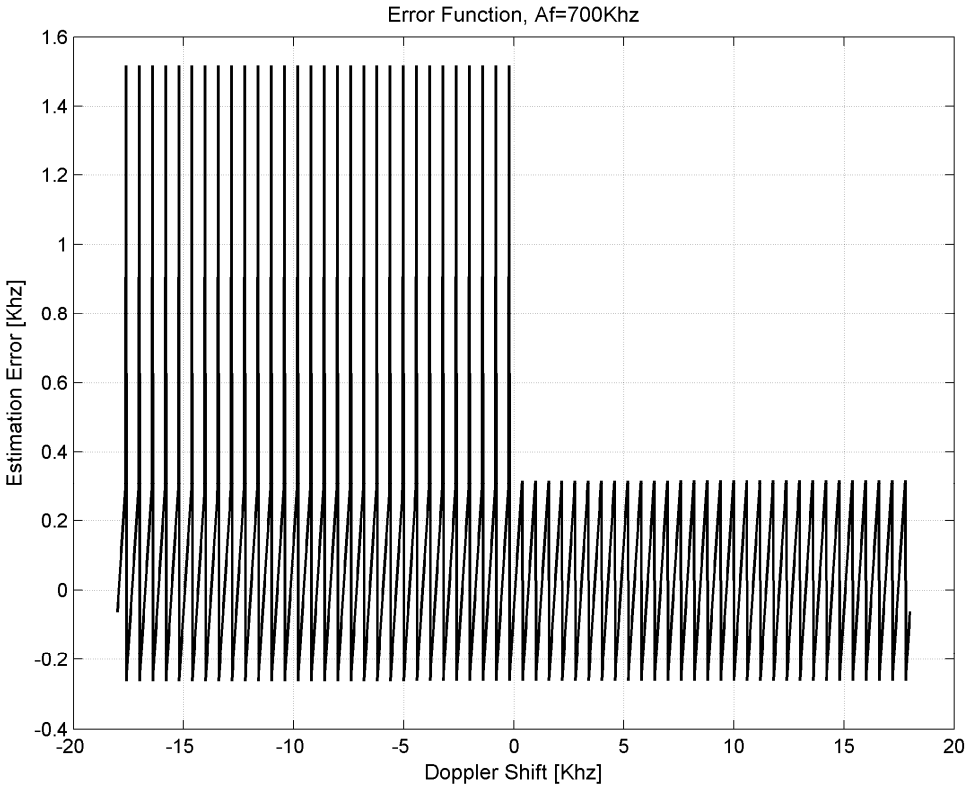


**Fig 6.-25: Simulation 18, Error Function for $\Delta f_d = 700\ [KHz]$.**

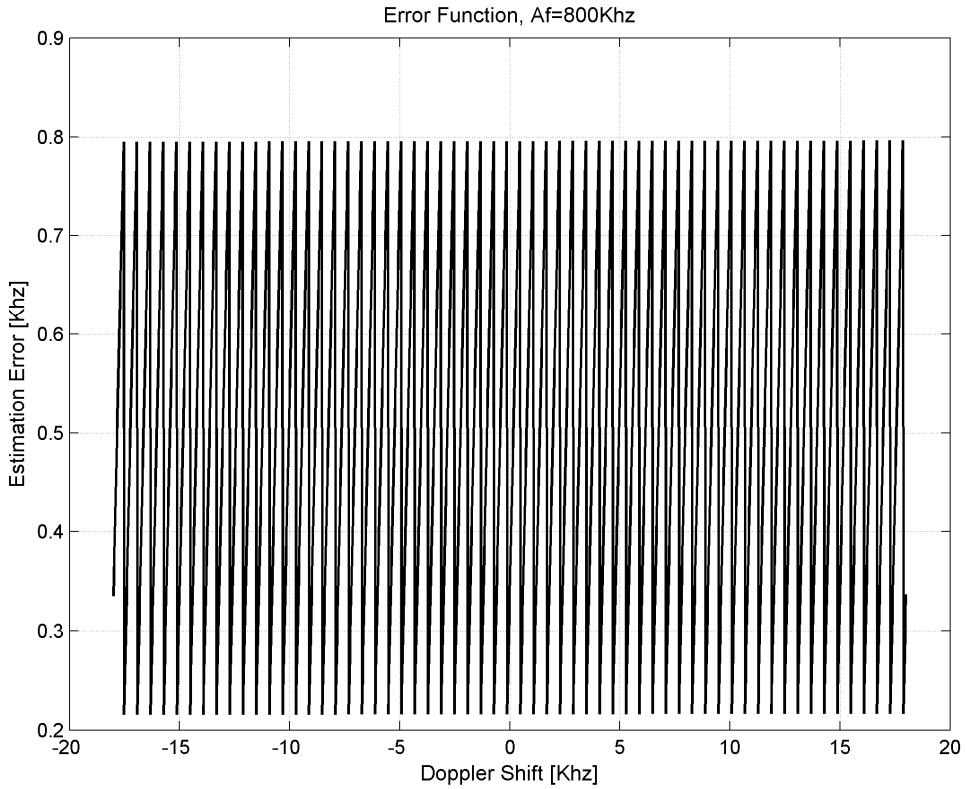


**Fig 6.-26: Simulation 18, Error Function for $\Delta f = 800\ [KHz]$.**

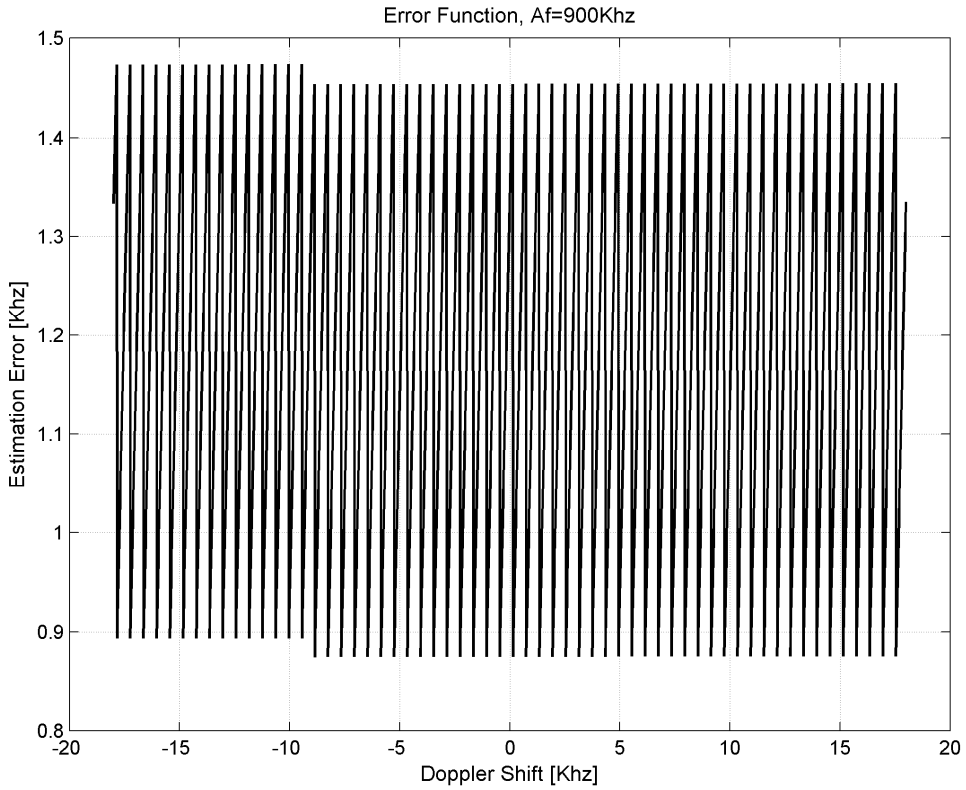


**Fig 6.-27: Simulation 18, Error Function for $\Delta f = 900\ [KHz]$.**

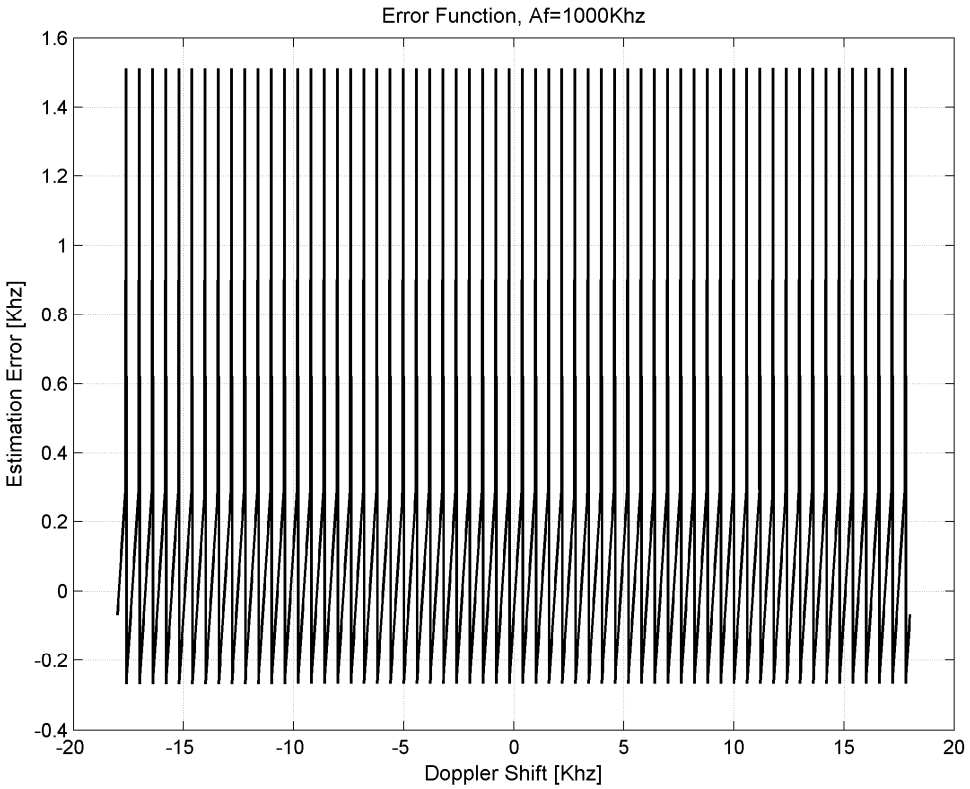


**Fig 6.-28: Simulation 18, Error Function for $\Delta f = 1000\ [KHz]$.**

Additionally, other error sources exist in a real case, such as undesired noise signal. This fact is assessed in the following section.

### 6.2.3 Doppler Compensation in presence of noise

This section provides the results obtained by including a white Gaussian noise source in Doppler compensation system. The simulations were carried out by varying the power of noise, and the other parameters were fixed as Table 6.-3 shows.

| ***Table 6.-3: Simulation 19 parameters.*** |
|---|
| $f_0 = 10\ [MHz]$ |
| $\Delta f = 900\ [KHz]$ |
| $prf = 3\ [KHz]$ |
| $T = 166.667\ [\mu s]$ |
| $Number\ of\ pulse = 5$ |

We observed different situations with various values of noise power, $-40, -30, -20, -10$ and $0\ [dbW]$. The transmitted power is $0.25\ [W]$, which corresponds with $-6\ [dbW]$. The Ambiguity Functions resulted are depicted from Fig 6.-29 to Fig 6.-33. Note that when the power noise increases, the result is worse. Fig 6.-29, Fig 6.-30 and Fig 6.-31 illustrate a acceptable compensated ambiguity function.

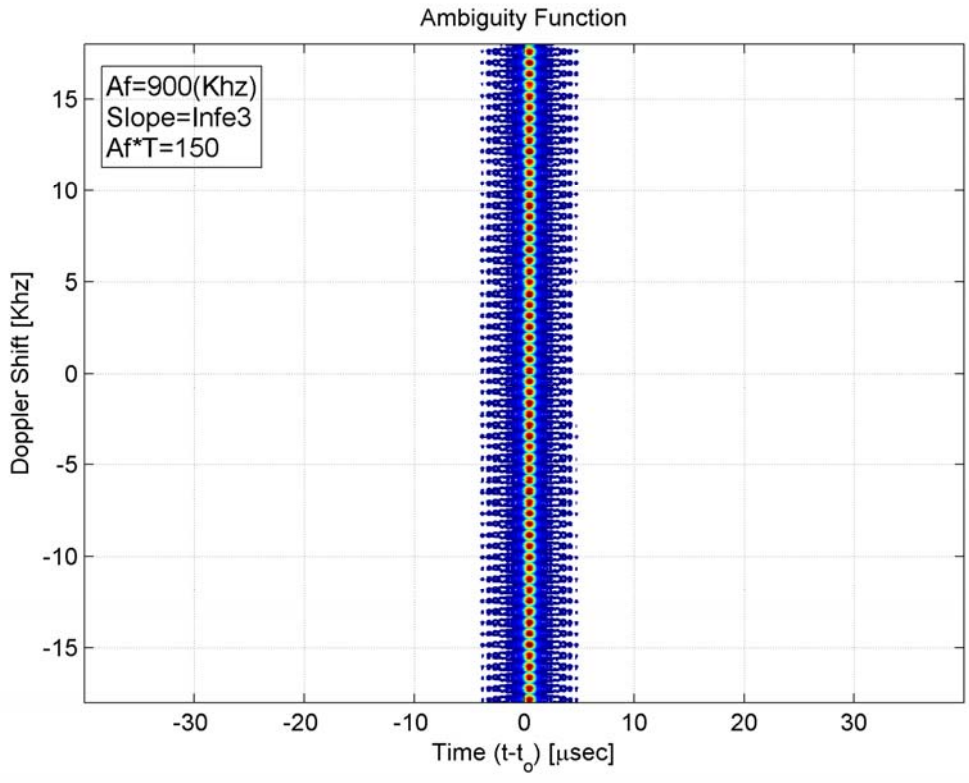


**Fig 6.-29: Simulation 19, Compensated Ambiguity Function for $P_n = -40\ [dbW]$.**

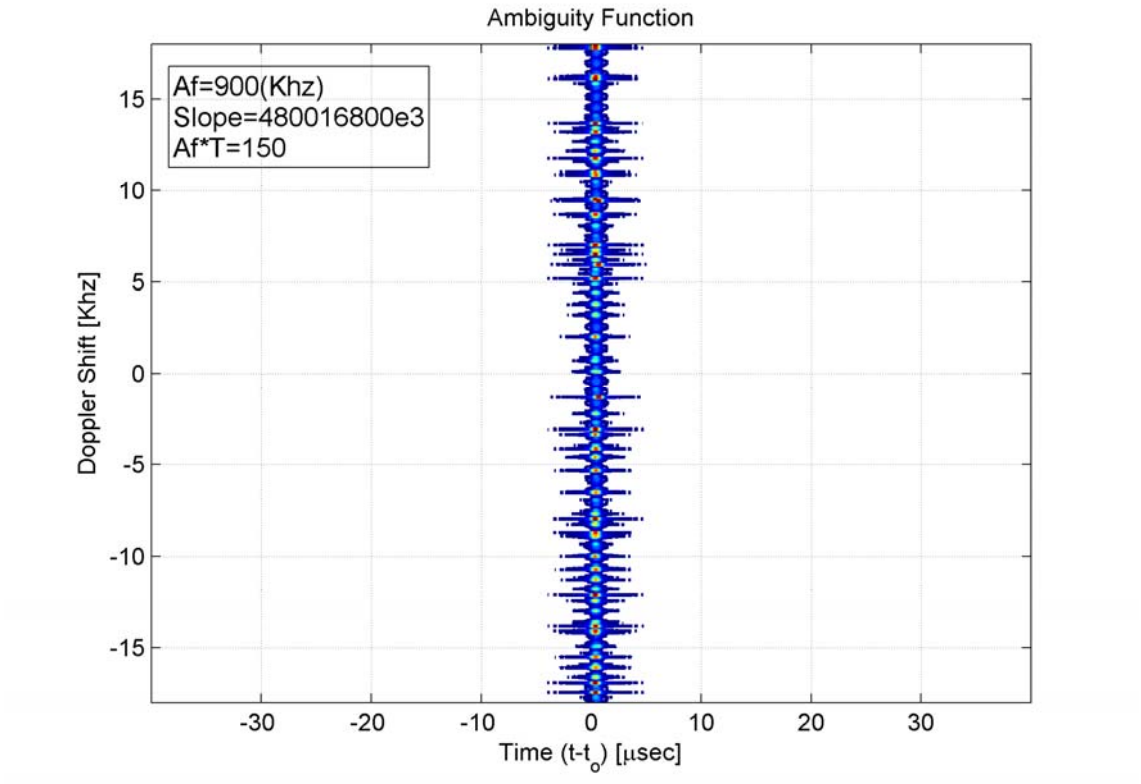


**Fig 6.-30: Simulation 19, Compensated Ambiguity Function for $P_n = -30\ [dbW]$.**

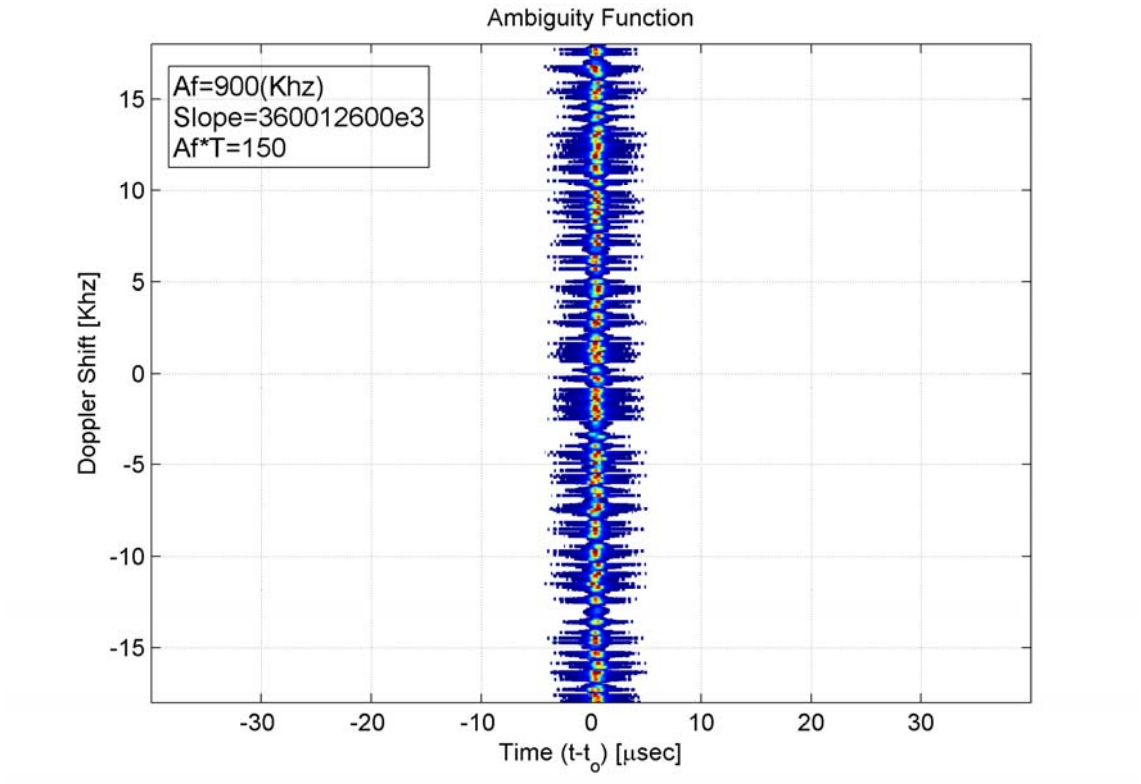


**Fig 6.-31: Simulation 19, Compensated Ambiguity Function for $P_n = -20\ [dbW]$.**

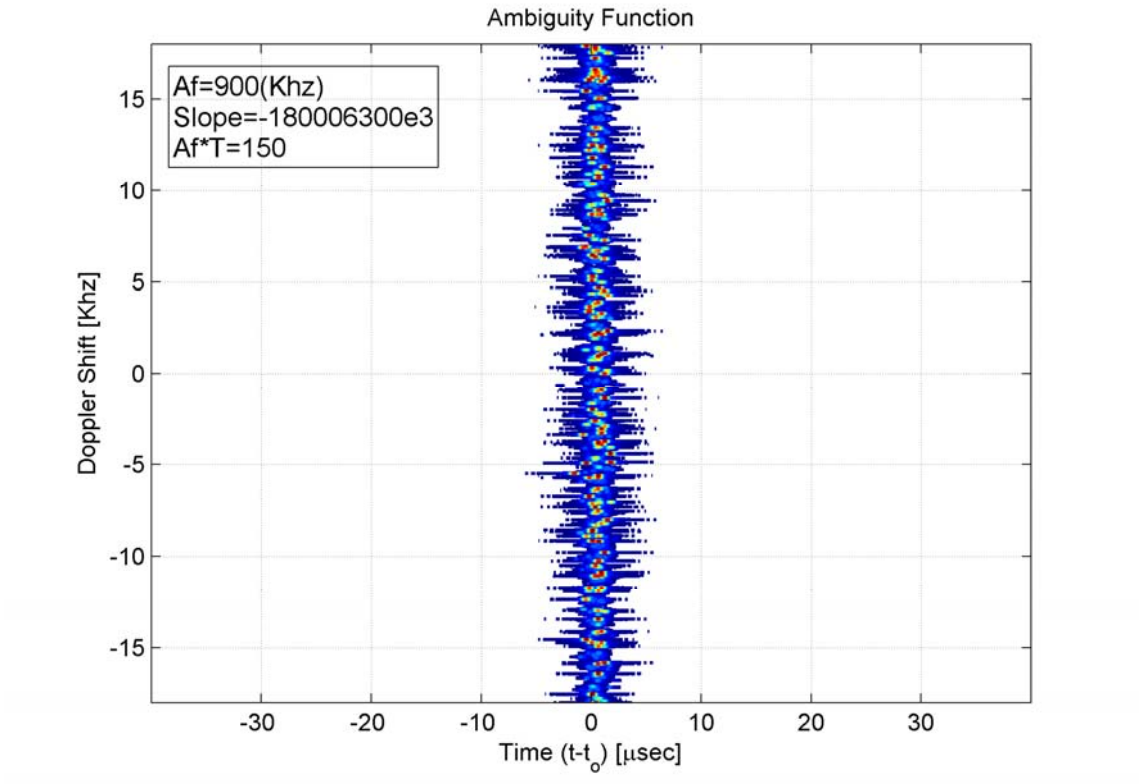


**Fig 6.-32: Simulation 19, Compensated Ambiguity Function for $P_n = -10\ [dbW]$.**

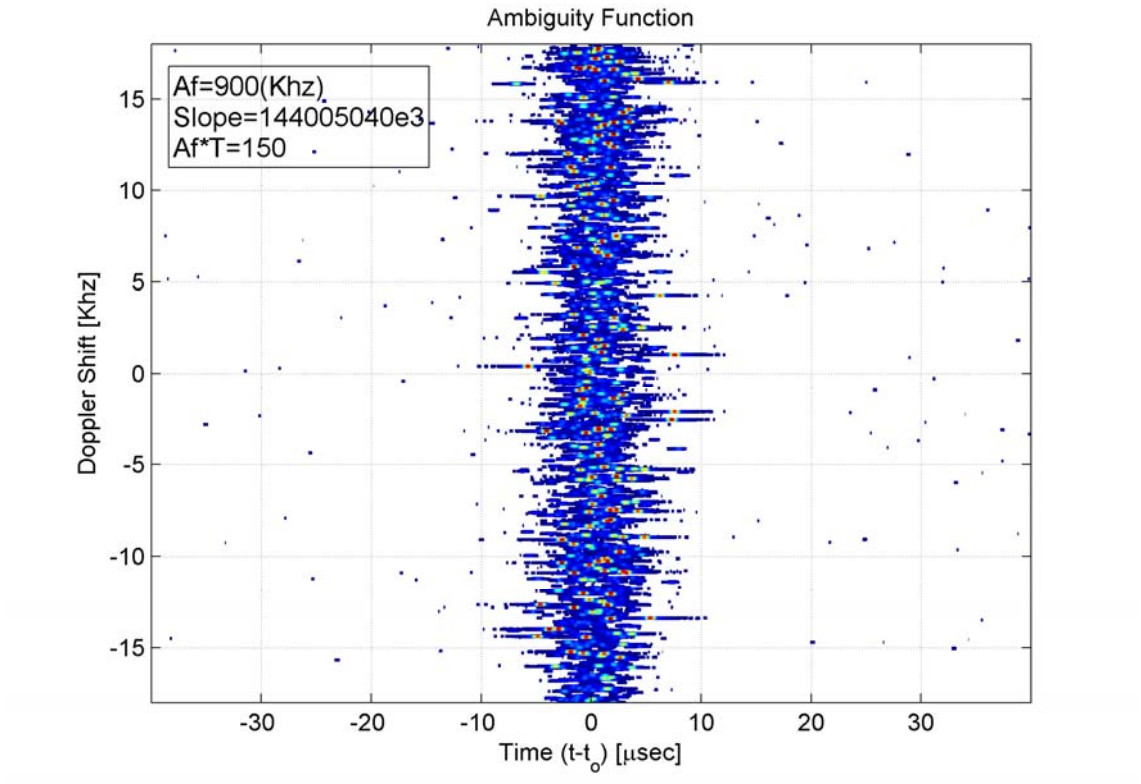


**Fig 6.-33: Simulation 19, Compensated Ambiguity Function for $P_n = 0\ [dbW]$.**

**Error function**

The parameters of the simulation were fixed as Table 6.-3 shows. The figures from Fig 6.-34 to 6.-38 illustrate the error committed by considering in the system a noise signal. These figures show the function error when the power of noise is $-40$, $-30$, $-20$, $-10$ and $0\ [dbW]$ respectively. Note that if the power of noise increases the error also increases, since the random power of noise, which enters in the tunable filters, affects to the estimation. This fact is a limitation of the approach studied in this chapter. For power noise of $-20\ [dbW]$ (it is corresponds with $SNR = 14\ [db]$), the error is acceptable.

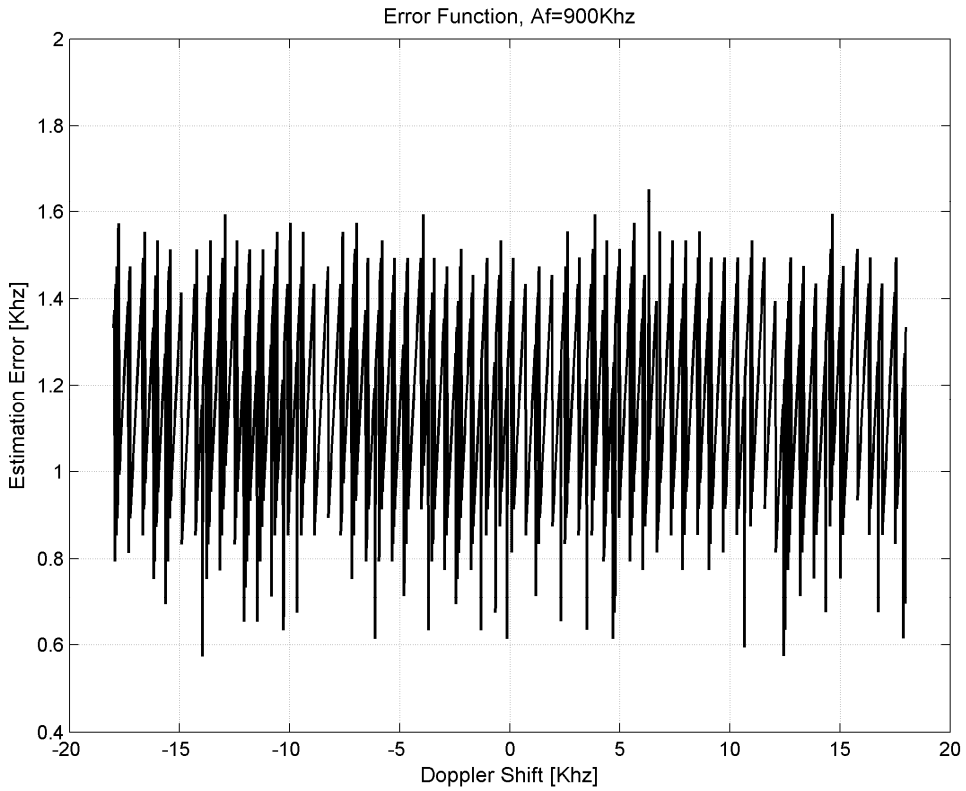


**Fig 6.-34: Simulation 19, Error Function for $P_n = -40\ [dbW]$.**

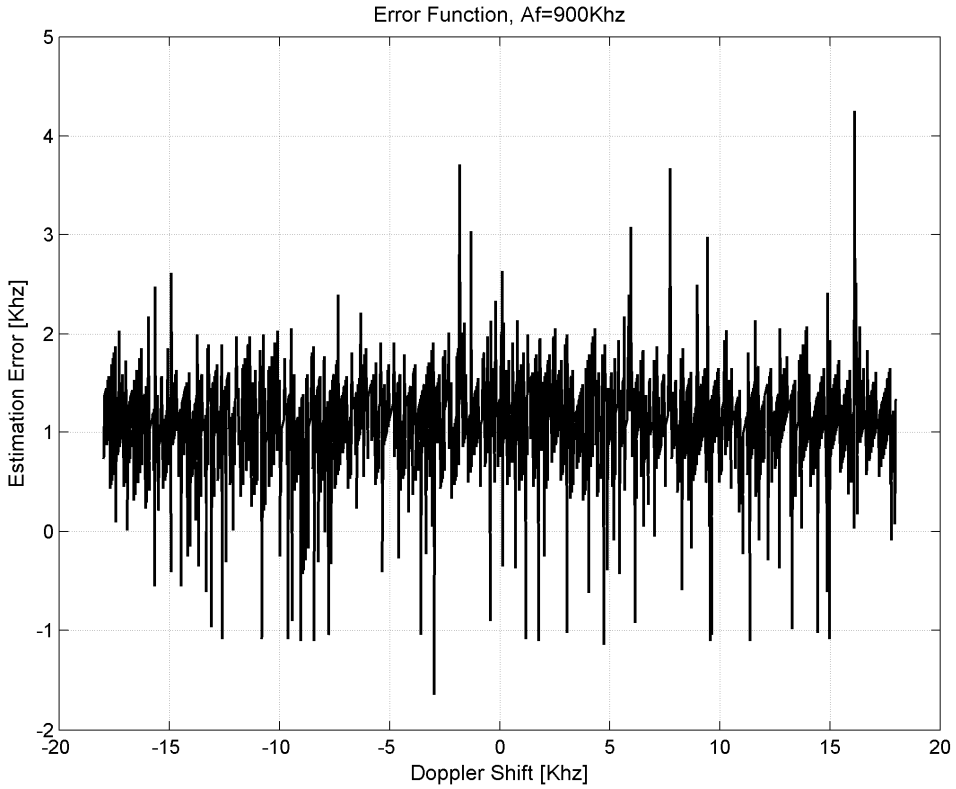


**Fig 6.-35: Simulation 19, Error Function for $P_n = -30\ [dbW]$.**

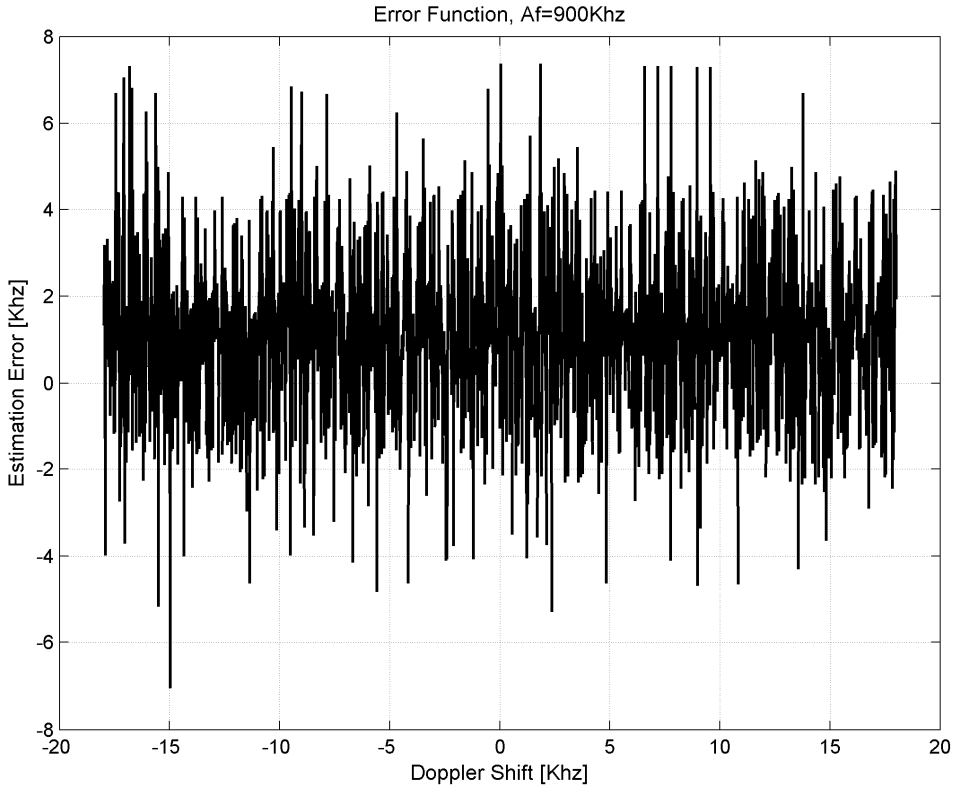


**Fig 6.-36: Simulation 19, Error Function for $P_n = -20\ [dbW]$.**

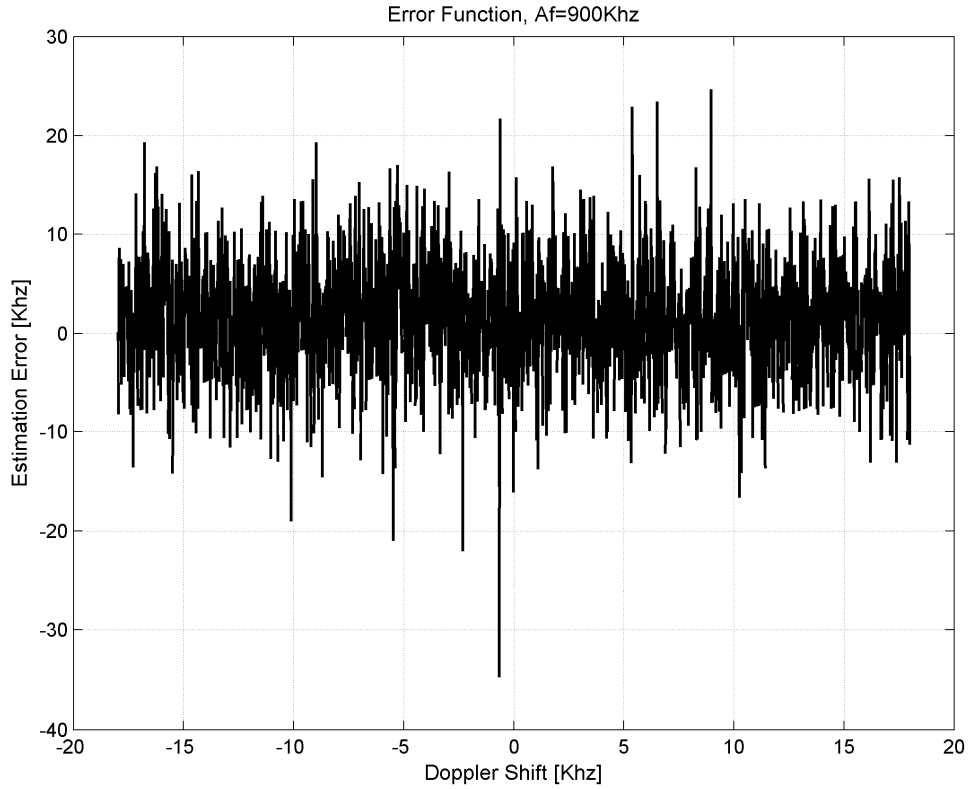


**Fig 6.-37: Simulation 19, Error Function for $P_n = -10$ $[dbW]$.**

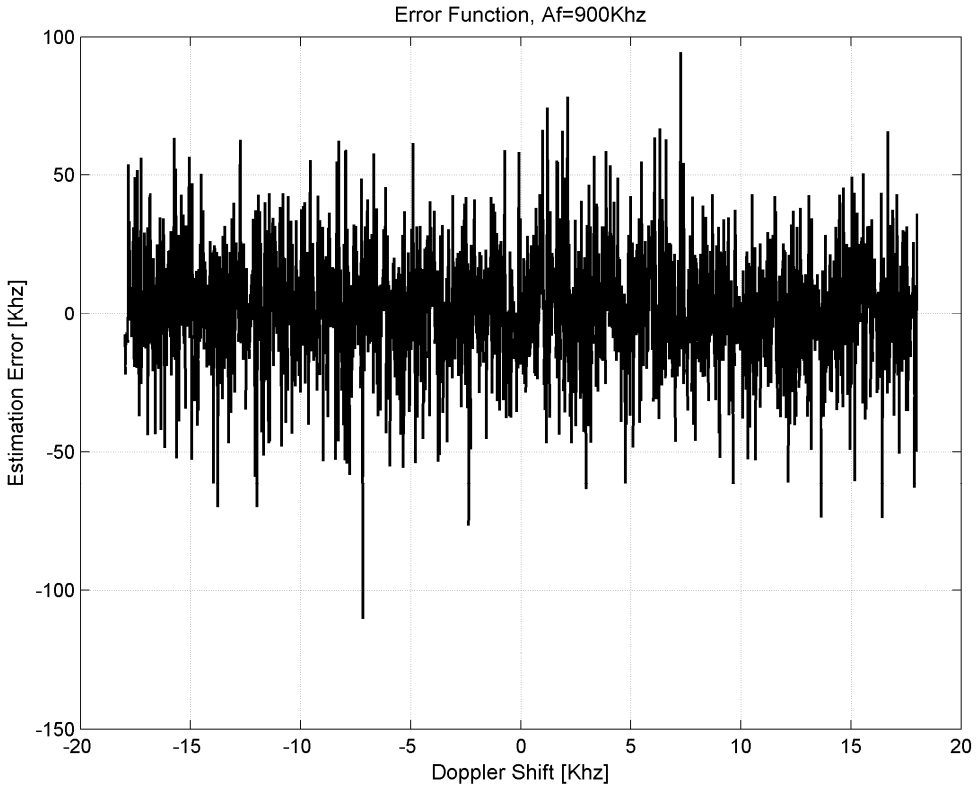


**Fig 6.-388: Simulation 19, Error Function for $P_n = 0$ $[dbW]$.**

## 6.3 Conclusions

In this 6 we have proposed a new approach solution to the undesired effects provoked by the Doppler Effect in pulse compression. After assessing the novel system, we can conclude that:

- **The novel approach is valid for identifying and compensating the Doppler Shift** due to a moving target.
- This technique achieves the goal of **mitigating the maximum deviations and decreasing the fluctuations of the final filtered signal due to the Doppler effect of moving targets**.
- If we use proposed system, we commit an **error in the estimation** of the Doppler Shift. **When a noise signal enters in the system, the error increases considerably**. Thus, this fact is a **limitation** for the proposed system.

# Chapter 7. Conclusions and Future Work

This chapter provides the main conclusions of the work and lays the foundations for future work.

## 7.1. Conclusions

In this work we have studied several techniques of pulse compression. We started studying some important concepts theoretically in the first three chapters. Then, we reviewed the theory associated to pulse compression techniques by using frequency modulation in Chapter 4.

Once we understood the principles of the pulse compression, we assessed these principles via numerical simulations using Matlab. We started from applying compression CHIRP pulses, observing their limitations and best trade-off for the different parameters of the system. One of the drawbacks of this technique is that compressed pulses exhibit rather large sidelobe levels. In order to improve the situation, I reviewed techniques to reduce sidelobe levels. These techniques included the use of mismatched filters and also the introduction of alternative FM modulation signals different from the CHIRP signal.

With respect to the use of mismatched filters it was found that the sidelobes were significantly reduced. However the final filtered signal exhibited a larger width than without using mismatched filters.

With respect to the use of FM laws it was found that the compressed pulse differed from the compressed CHIRP pulse. Depending on the specifications of the application, it is interesting to use some of the waveforms studied.

For performing theses simulations we developed our own code in Matlab. This code has been used to implement a learning-purpose application, which is able to simulate the scenarios covered in Chapter 5 (Appendix A provides a brief guide of its usage, including examples).

The preceding studied techniques have similar drawbacks when a moving target is detected: the temporal shift of the compressed pulse and the fluctuations of the output signal. In order to reduce these effects we proposed a novel technique in Chapter 6. We tested this technique to know about its performances and basic operation. We found that the maximum deviation is mitigated and the fluctuations of the filtered signal are reduced. Also we found that when noise enters in the system, its performances decrease.

## 7.2. Future Work

The future work can be approached in two different lines. The first one is to extend the theoretical and numerical analysis of the techniques of pulse compression. The second one is to extend the study of the Doppler compensation technique in order to get more insight about its performances and its viability. Thus the main future steps to follow are:

**Pulse compression techniques:**

- The analysis could be extended, including and comparing other pulse compression techniques described in section 4 (Pulse compression by Costas FM and by Phase Coding, for example Barker Codes).
- In the same way as the pulse compression techniques, the analysis could be extended for observing adaptive pulse compression techniques (section 4.3.3).
- Also the preceding techniques could be included in the Pulse Compression Matlab´s application.
- Finally, it is interesting to implement the methods of pulse compression over hardware architecture (such as FPGA) to assess their performances in real environments.

**Doppler Compensation Technique:**

- We could extend the study of the proposed novel approach via replacing the ideal function transfer of the tunable band pass filters to real filters, such as those found in FIR filter architecture.
- The analysis of the error functions could be extended to understand better their behavior.
- We could also test more complex combinations of filters (for example, try using three filters) and introduce other changes in the compensation algorithm (for example, establishing stop criteria for the frequency sweep).
- We could check the proposed system in more stressful scenarios, i.e. considering several target with different speeds.

# APPENDIX

# Appendix A. Guide: Pulse Compression Matlab´s Gui

This appendix provides a description of the application designed, whose purpose is to simulate the pulse compression mainly by using FM modulation. The tool used to carry out this application was Matlab R2013a. First, we perform a simple example as introduction to user´s interface, next, we carry out three more complex examples to prove the functionality of the developed tool.

## A.1. Example 1: The user´s interface & A Simple Simulation

First, change the current directory to the directory where the .m files and .fig files are placeA. Next, tip “guide” in the Matlab´s Command Window and open the “gui.fig” file. Then, you will view the user´s interface illustrated in Fig A.-1.

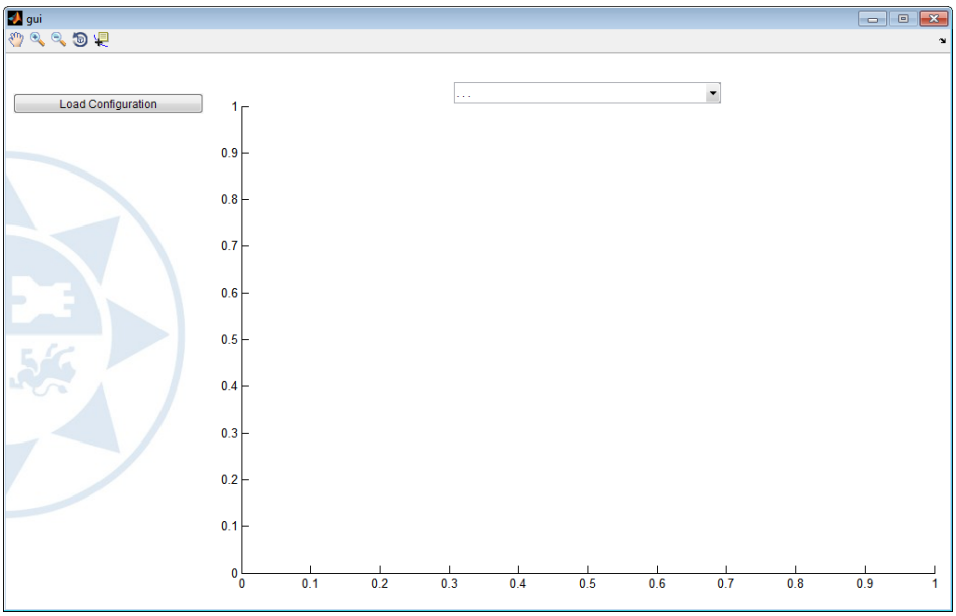


**Fig A.-1: Example 1. User´s Interface I.**

Note that there is only a button (“Load Configuration”), push it.

The configuration window shown in Fig A.-2 will appear.

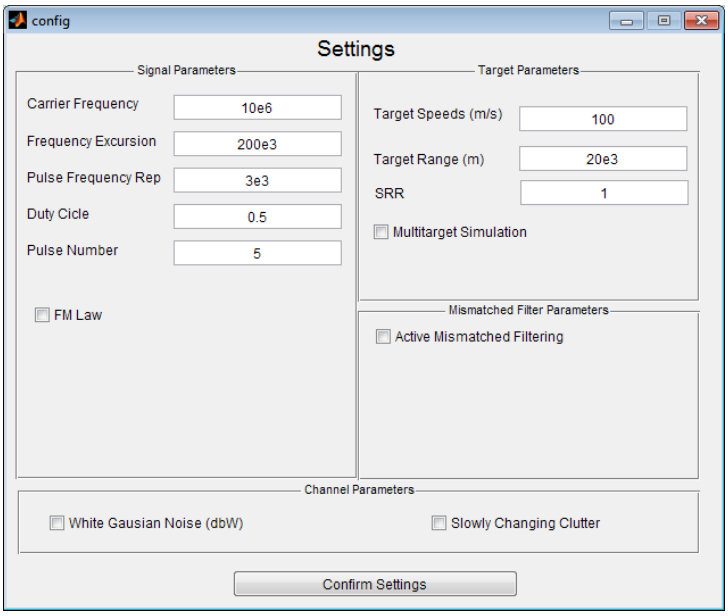


**Fig A.-2: Example 1. Configuration window.**

This window allows to configure the simulation parameters. Note that there are a button and four panels: Signal Parameters; Target Parameters; Mismatched Filter Parameters and Channel Parameters. We will use the default parameters for this first simulation, therefore, push "Confirm Settings". Next, note that a new button ("Simulate") is visible below the "Load Configuration" button (Fig A.-3).

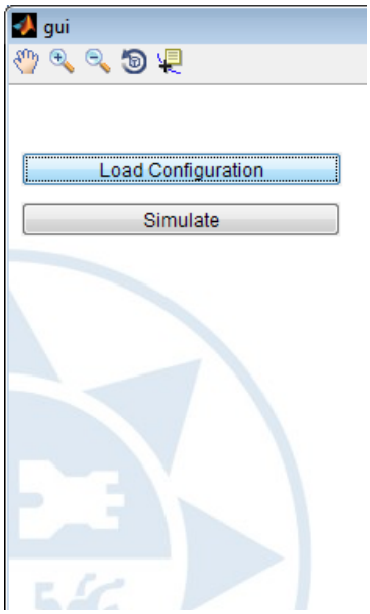


**Fig A.-3: Example 1. User´s Interface II.**

To start the simulation push “Simulate”. Now we are able to observe the results as shown Fig A.-4.

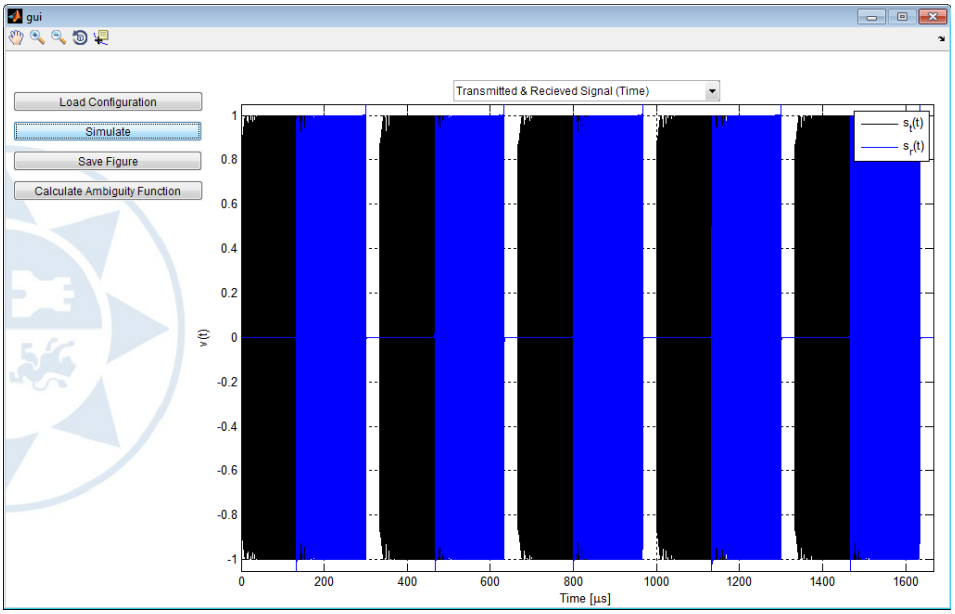


**Fig A.-4: Example 1. User´s Interface III.**

Note that, there is a popup menu, which allows to select the observed graph. Also, two new buttons appear, “Save Figure” and “Calculate Ambiguity Function”. After switching to “Range Gates (Detection of target)”, we will view the graph shown in A.-5.

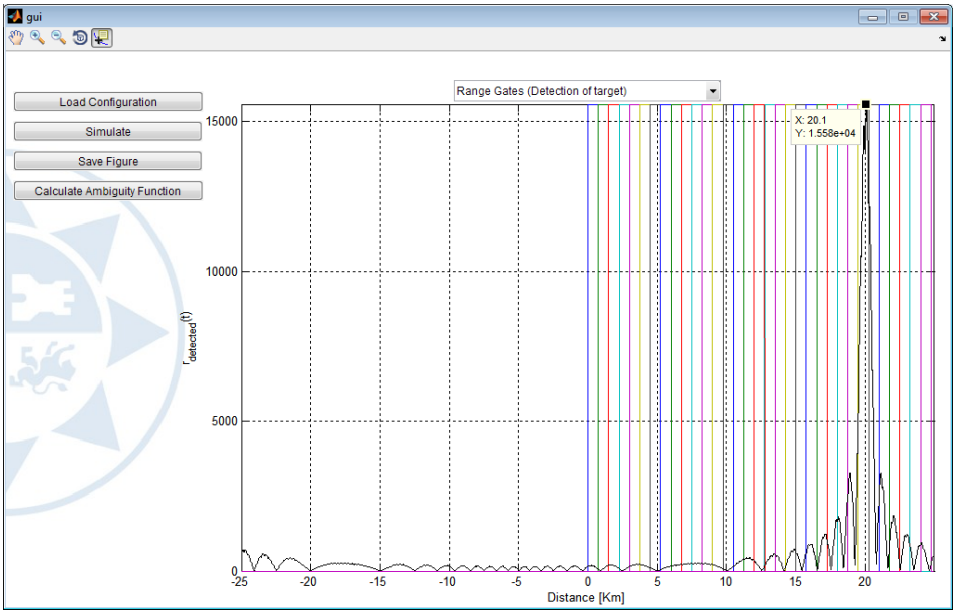


**Fig A.-5: Example 1. User´s Interface IV.**

Other window emerges by pushing the “Calculate Ambiguity Function” button. This window allows to fix the sweeping parameters in order to calculate the contour of ambiguity function. We will use the default settings shown in Fig A.-6.

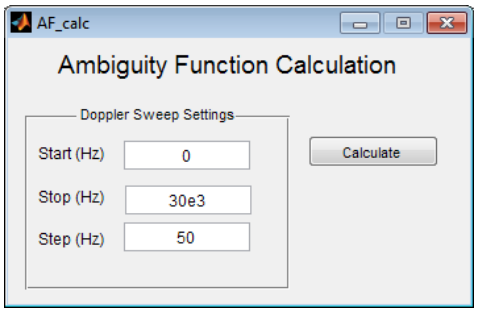


**Fig A.-6: Example 1. Ambiguity Function configuration.**

Next, push “Calculate”. Note that, after pushing “Calculate”, the Matlab´s Command Window shows messages, which give information about the Doppler Shift and Delay applied to the transmitted signal.

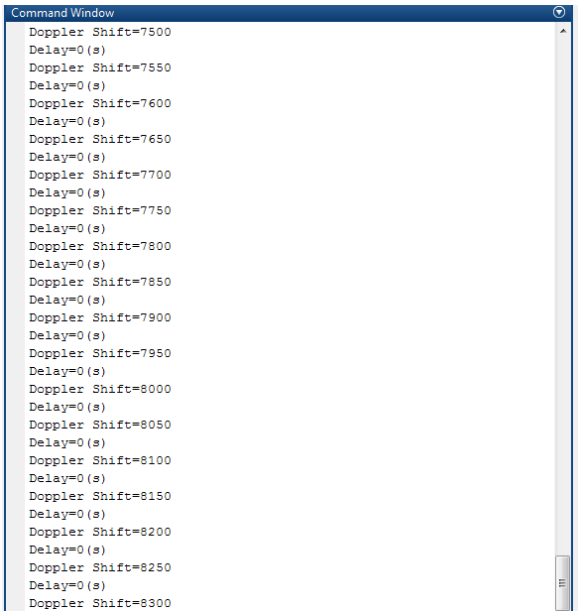


**Fig A.-7: Example 1. Ambiguity Function Calculation messages.**

After stopping appearing messages, a figure appears where it depicts the Ambiguity Function contour (Fig A.-8).

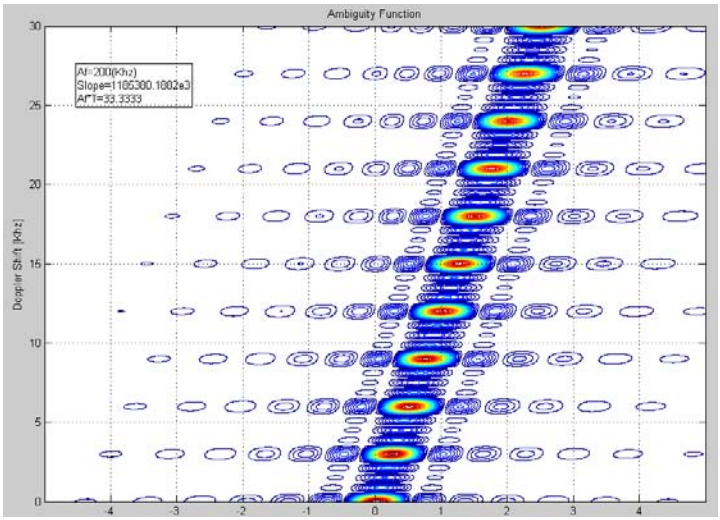


**Fig A.-8: Example 1. Result of Ambiguity Function Calculation.**

## A.2. Example 2: Pulse Compression in presence of two moving targets

In this example we try simulating a detection of two targets. For this purpose, we will use the configuration shown in Fig A.-9:

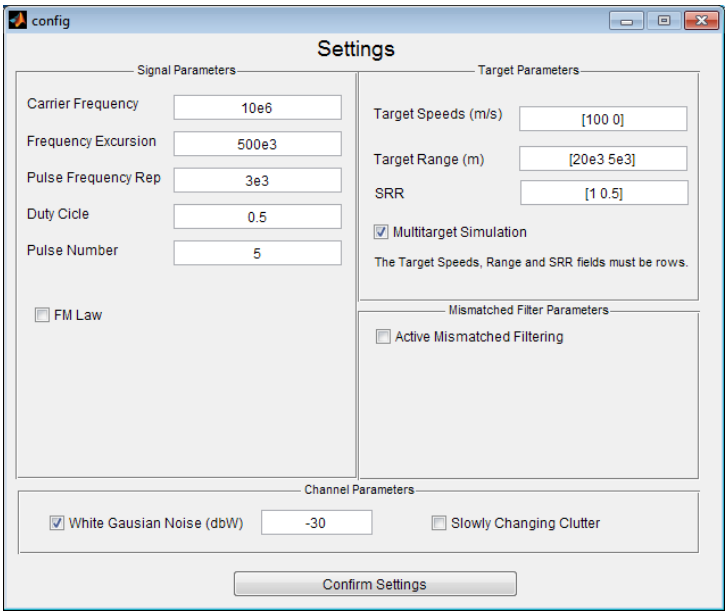


**Fig A.-9: Example 2. Setting the Simulation Parameters.**

Note that the paremeters are entered as vectors of two elements in the fields “Target Speeds (m/s)”, “Target Range (m)” and SRR; in addition, the “Multitarget Simulation” and “White Gaussian Noise (dbW)” boxes are on.

Then, after pushing “Simulate”, we obtain the graphs illustrated in Fig A.-10 and Fig A.-11.

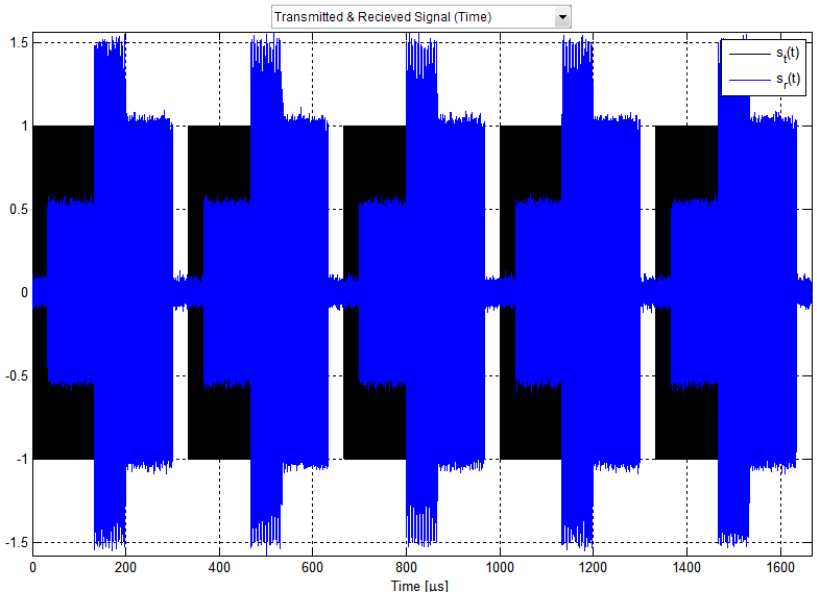


**Fig A.-10: Example 2. Results I.**

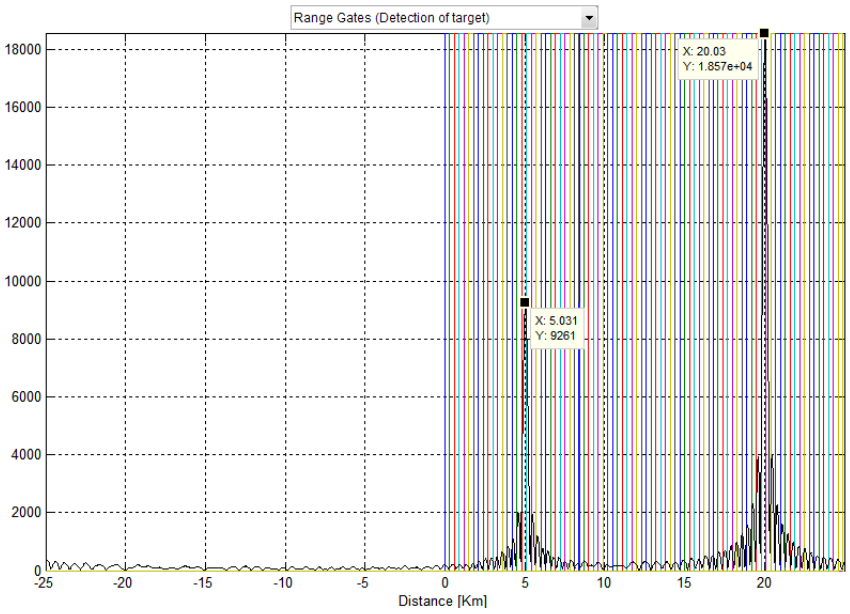


**Fig A.-11: Example 2. Results II.**

Note that the received signal shown in Fig A.-10 is very hazy, since it is very difficult to differ the pair of targets. But once the pulse is compressed, we can distinguish the two target perfectly, as Fig A.-11 shows. Furthermore, the noise signal is suppressed in the pulse compression process.

## A.3. Example 3: Pulse Compression by using Mismatching Filtering in presence of Slowly Changing Clutter

In this example we demonstrate how to simulate the pulse compression by using mismatched filtering. Firstly, we have to fix the simulation parameters; thus, push "Load Configuration", and mark the "Active Mismatched Filtering" as Fig A.-12 shows.

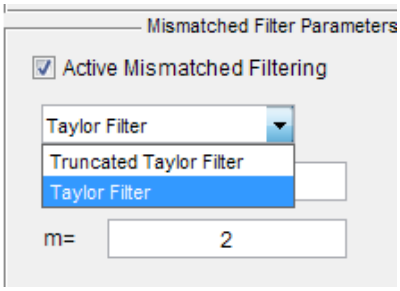


**Fig A.-12: Example 3. Setting the Simulation Configuration I.**

The rest of parameters are fixed as Fig A.-13 shows; note that the "Slowly Change Clutter" box is on.

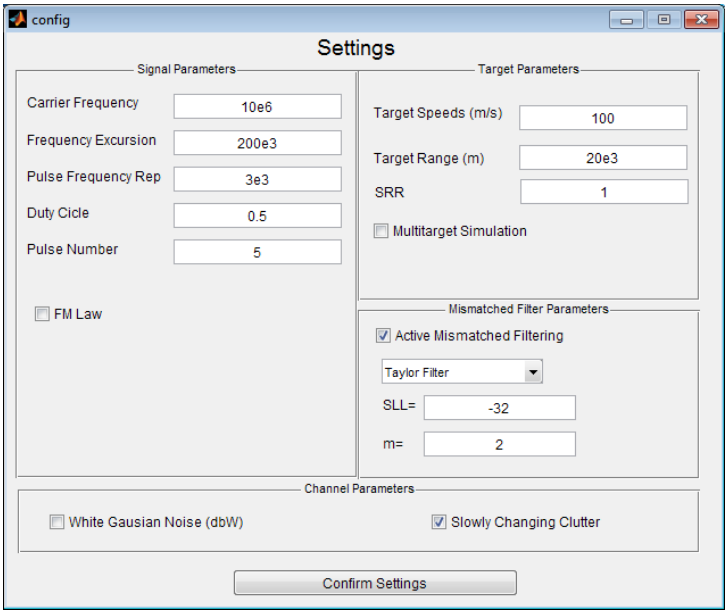


**Fig A.-13: Example 3. Setting the Simulation Configuration II.**

Next, push “Confirm Settings” and later push “Simulate”. We will focus on the results shown in Fig A.-14 and A.-15.

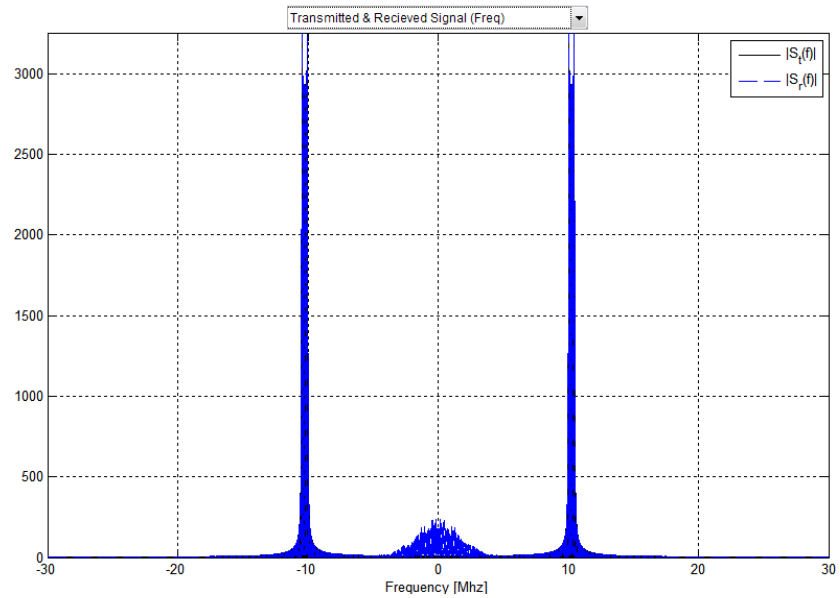


**Fig A.-14: Example 3. Results I.**

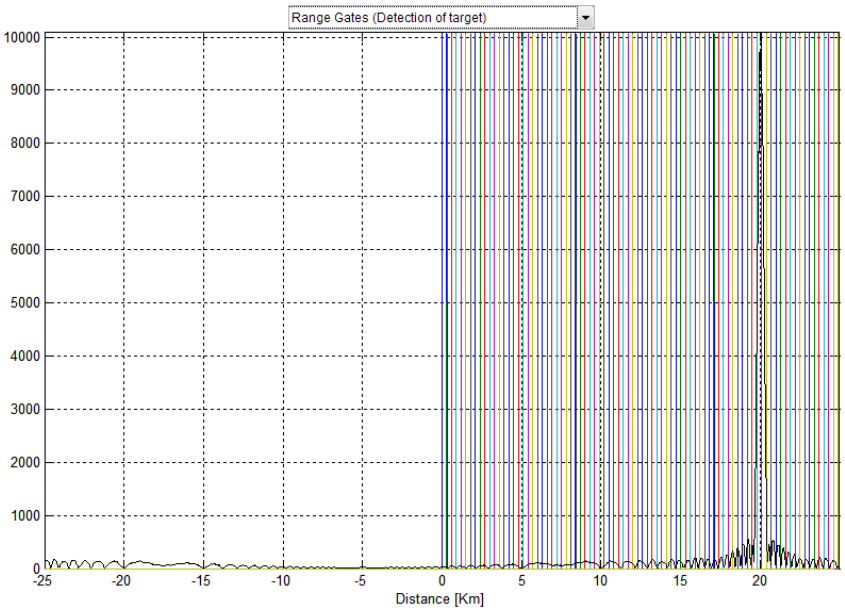


**Fig A.-15: Example 3. Results II.**

Note that low frequency information appears in Fig A.-14. However, in Fig A.-15, the clutter component has been suppresseA. Note to that the compressed pulse is too wide due to the mismatched filtering.

## A.4. Example 4: Pulse Compression by using Custom FM law

This example is for proving how to compress a pulse by using FM Laws. First push "Load Configuration". Next mark the "FM Law" box, then next elements will appear. We are proving how to enter our own FM Law, thus, select "Custom FM Law" as Fig A.-16 shows.

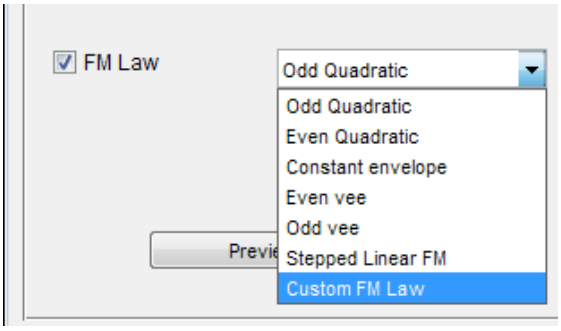


**Fig A.-16: Example 4. Setting the Simulation Configuration I.**

After selecting "Custom FM Law", the command window will ask to enter our FM Law, you can use either one code line or an external variable to enter the FM Law. We are using the FM Law shown in Fig A.-17.

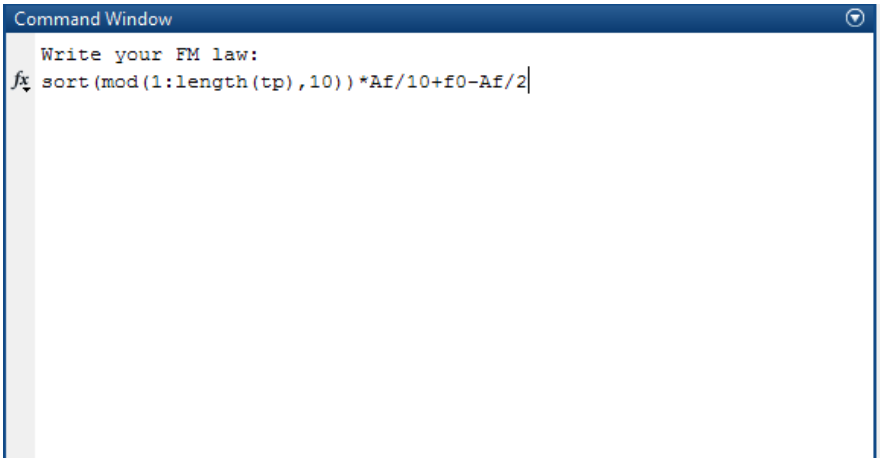


**Fig A.-17: Example 4. Setting the Simulation Configuration II.**

Once the FM Law has been entered correctly, we can observed the FM Law before simulating by pushing “Preview Fm Law” (Fig A.-18 and A.-19).

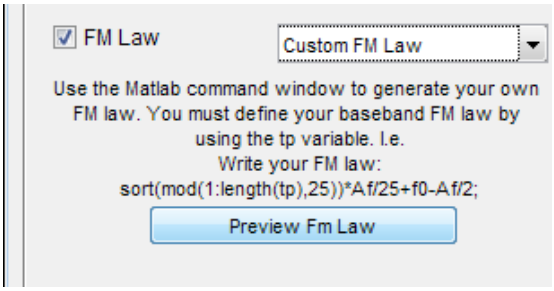


**Fig A.-18: Example 4. Setting the Simulation Configuration III.**

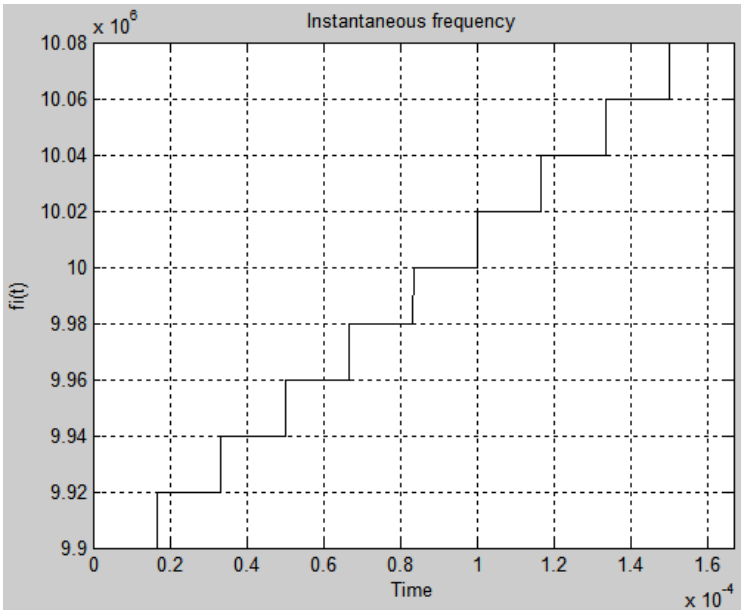


**Fig A.-19: Example 4. Stepped Linear FM.**

Note that the FM Law entered is a Stepped Linear FM with ten steps. Next push “Confirm Settings”, and simulate the results. We can observe that the signal spectrum differs from the preceding cases (Fig A.-20) and that the compressed signal presents several high sidelobes (Fig A.-21).

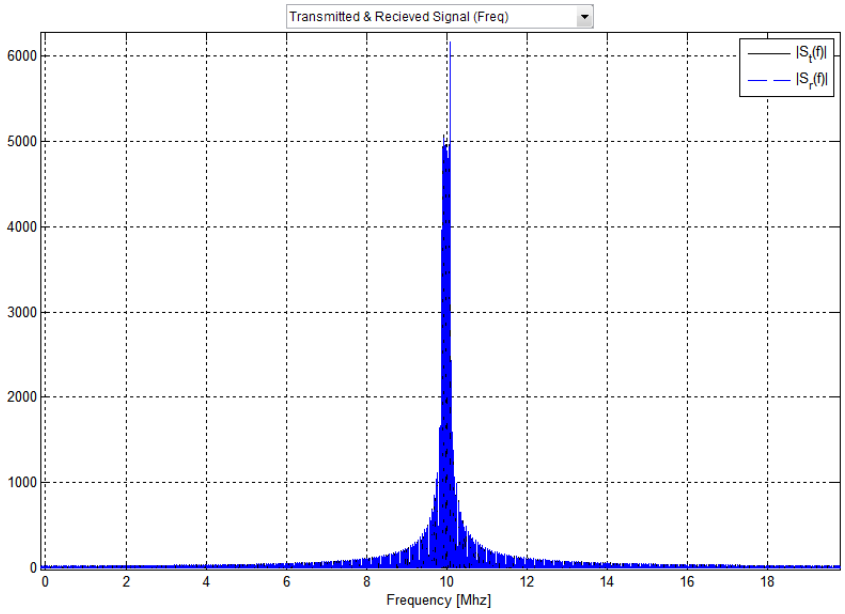


**Fig A.-20: Example 4. Results I.**

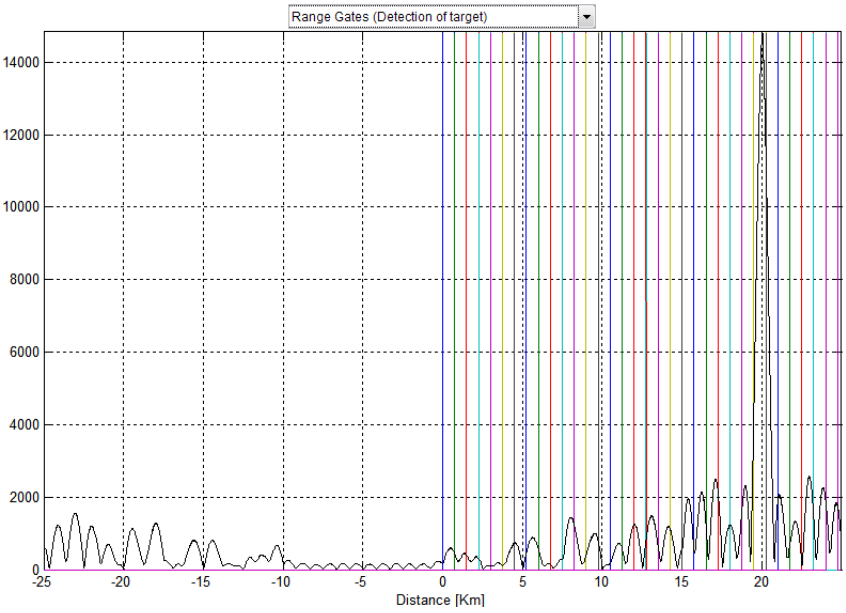


**Fig A.-21: Example 4. Results II.**

# Appendix B. Matlab´s Functions description

This appendix provides information about the implemented functions to perform the study of pulse compression techniques and to build the Matlab´s GUI. The functions are describe from Table B.-1 to Table B.-9.

| ***Table B.-1: chirp_lineal.m*** | |
|---|---|
| ***Description*** | *This function is for building the CHIRP pulse.* |
| ***Input arguments*** | *f0 is the carrier frequency.*<br>*dt is the duty cycle. It is closed between 0.1 a 1.*<br>*Af is the modulation index.*<br>*Np is the number of pulse replicas transmitted.*<br>*Prf is the pulse repetition frequency.*<br>*fs is the sample frequency.* |
| ***Output arguments*** | *s2 is the pulse chirp vector.*<br>*t is the time vector.*<br>*f is the frequency vector.* |

| ***Table B.-2: fm_law.m*** | |
|---|---|
| ***Description*** | *This function is for building the fm modulated pulse.* |
| ***Input arguments*** | *f0 is the carrier frequency.*<br>*dt is the duty cycle. It is closed between 0.1 a 1.*<br>*fi is the instantaneous .*<br>*Np is the number of pulse replicas transmitted.*<br>*Prf is the pulse repetition frequency.*<br>*fs is the sample frequency.*<br>*Tp is the time vector where the pulse is defined.* |
| ***Output arguments*** | *s2 is the modulated pulse vector.* |

| ***Table B.-3: target.m*** | |
|---|---|
| ***Description*** | *This function simulates a target effect.* |
| ***Input arguments*** | *alfa is the radar equation in linear.*<br>*R is the range of the target.*<br>*v is the speed of the target.*<br>*f0 is the carrier frequency.*<br>*s is the signal vector that the effects are applied.*<br>*f is the frequency vector.*<br>*t is the time vector.* |
| ***Output arguments*** | *y is the output vector.* |

| ***Table B.-4: hilbert.m*** | |
|---|---|
| ***Description*** | *This function calculates the Hilbert transform.* |
| ***Input arguments*** | *x is the signal vector that the transform is applied.*<br>*f is the frequency vector.* |
| ***Output arguments*** | *y is the output vector.* |

| ***Table B.-5: taylor_truncated.m*** | |
|---|---|
| ***Description*** | *This function is for building a truncated Taylor´s Filter.* |
| ***Input arguments*** | *f is the frequency vector.*<br>*f0 is the carrier frequency.*<br>*Af is the modulation index.*<br>*n is a design parameter (view equation ).*<br>*k is a design parameter (view equation ).* |
| ***Output arguments*** | *y is the transfer function vector of the pulse in frequency domain.* |

| ***Table B.-6: taylorf.m*** | |
|---|---|
| ***Description*** | *This function is for building a Taylor´s Filter.* |
| ***Input arguments*** | *f is the frequency vector.*<br>*f0 is the carrier frequency.*<br>*Af is the modulation index.*<br>*n is a design parameter (view equation ).*<br>*SLL is a design parameter (view equation ).* |
| ***Output arguments*** | *y is the transfer function vector of the pulse in frequency domain.* |

| ***Table B.-7: detect.m*** | |
|---|---|
| ***Description*** | *This function is for detecting a pulse.* |
| ***Input arguments*** | *f is the frequency vector.*<br>*f0 is the carrier frequency.*<br>*alfa is the roll of factor.*<br>*t is the time vector.*<br>*r is the input signal.*<br>*flag is for selecting the detection type.* |
| ***Output arguments*** | *y is the detected signal vector.* |

| Table B.-8: ran_gate.m | |
|---|---|
| **Description** | *This function implements range gates.* |
| **Input arguments** | *t is the time vector.*<br>*width is the width of the ranges gates.*<br>*T is the duration of a full pulse.*<br>*tau is the duration of the transmission time period.* |
| **Output arguments** | *y is a matrix which stores the range gates.* |

| Table B.-9: chirp_lineal.m | |
|---|---|
| **Description** | *This function is for building the CHIRP pulse.* |
| **Input arguments** | *f0 is the carrier frequency.*<br>*dt is the duty cicle. It is closed between 0.1 a 1.*<br>*Af is the modulation index.*<br>*Np is the number of pulse replicas transmitted.*<br>*Prf is the pulse repetition frequency.*<br>*Fs is the sample frequency.* |
| **Output arguments** | *s2 is the pulse chirp vector.*<br>*t is the time vector.*<br>*f is the frequency vector.* |

Other functions are used in the GUI implementation. These functions are shown in Table B.-10.

| Table B.-10: Other functions. | |
|---|---|
| **Name** | **Description** |
| *gui.m* | *This function contains the gui window components.* |
| *config.m* | *This function contains the config window components.* |
| *AF_calB.m* | *This function contains the AF_calc window components.* |
| *load_par.m* | *This function loads the simulation parameters from the config window to variables.* |
| *simulation.m* | *This function performs the simulation.* |

# Bibliography


| | |
|---|---|
| [Peyton Z. Peebles Jr, 1998] | Peyton Z. Peebles, Jr; "Radar Principles" (1998). John Wiley & Sons. |
| [F. Quesada et al., 2010] | Fernando Quesada Pereira, David Cañete Rebenaque, Alejandro Álvarez Melcón; "Sistemas Radares: Detección y Reconocimiento de Blancos" (Primera edición, 2010). Universidad Politécnica de Cartagena. |
| [B. Zrnic et al., 1998] | Bojan Zrnic, Aleksa Zejak, Andrija Petrovic, Igor Simic; "Range Sidelobe Suppression For pulse Compression Radars Utilizing Modified RLS Algorithm"; Spread Spectrum Techniques and Applications, 1998. Proceedings., 1998 IEEE 5th International Symposium on (Volume:3 ); pages 1008-1011. |
| [A. J. Zejak et al., 1991] | A. J. Zejak, E. Zenther, P. B. Rapajic; "Doppler optimized mismatched filters"; Electronics letters, 1991. Vol 21, No. 7; pages 551-560. |
| [A. J. Zejak et al., 1994] | A. J. Zejak, E. Zenther, M. L. Dukic; "Doppler optimized compression filters"; IEEE ISSSTA'94, Finland, 1994; pages 534-538. |
| [S. D. Blunt & K. Gerlach, 2003] | Shannon D. Blunt, Karl Gerlach; "A Novel Pulse Compression Scheme Based on Minimum Mean-Square Error Reiteration"; Radar Conference, 2003. Proceedings of the International; pages 349-353. |
| [S. D. Blunt & K. Gerlach, 2004] | Shannon D. Blunt, Karl Gerlach; "Adaptive Pulse Compression"; Radar Conference, 2004. Proceedings of the IEEE; pages 271-276. |
| [S. D. Blunt et al., 2009] | Shannon D. Blunt, Aaron K. Shackelford, Karl Gerlach, Kevin J. Smith; "Doppler Compensation & Single Pulse Imaging using Adaptive Pulse Compression"; IEEE Transactions on Aerospace and Electronic Systems, 2009, vol. 45; pages 647-659. |
| [D. A. Swick, 1969] | David A. Swick; "A Review of Wideband Ambiguity Functions"; Signal Processing Branch Acoustics Division; 1969. |